Glutathione transferase-derived compounds as potential therapeutic agents

By

RUWANI PUNYAKANTHI HEWAWASAM

BSc (Hon), MPhil (Biochemistry)

A thesis submitted for the degree of Doctor of Philosophy from
The Australian National University

The John Curtin School of Medical Research
The Australian National University
Canberra
Australia

Australian
National
University

THE JOHN CURTIN
SCHOOL OF MEDICAL RESEARCH

August 2011

STATEMENT

This thesis describes the results of research undertaken in the Muscle Research Group, Department of Translational Biosciences, The John Curtin School of Medical Research, The Australian National University, Canberra, Australia, between April 2007 and November 2010. This study was supported by The National Health and Medical Research Council, Australian Postgraduate Awards, John Curtin School of Medical Research supplementary scholarship and The Australian National University miscellaneous scholarship.

All experiments and data analyses presented in this thesis are my own original work accomplished under the supervision of Prof Angela F Dulhunty, Prof Philip G Board and Dr Marco G Casarotto. The information and resources derived from the published or unpublished work of others is acknowledged in the text.

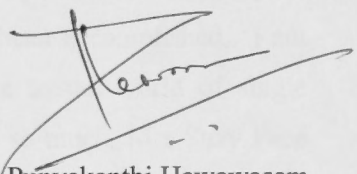

Ruwani Punyakanthi Hewawasam

Muscle Research group

Department of Translational Biosciences

The John Curtin School of Medical Research

College of Medicine, Biology and Environment

The Australian National University

ACKNOWLEDGEMENT

I would like to express my heart-felt gratitude to my main PhD supervisor, Prof Angela Dulhunty, for her guidance, endless support and encouragement provided throughout this journey. Her understanding and patience, especially during the first few years of this learning journey, made this experience a pleasure to remember. Indeed, I have grown up, not only in terms of research but also in so many other aspects of my life. Thank you so much, Angela, for understanding the struggle I had to balance my family life and the research life. I am also grateful to Prof Phil Board for his invaluable guidance and support throughout the last few years. Many thanks again for the valuable comments provided for the preparation of this thesis. I am also heartily thankful to Dr Marco Casarotto, my advisor, for the guidance and support provided, especially for the valuable suggestions provided to analyse results from tryptophan fluorescence quenching experiments.

Dr Dan Liu from the Molecular genetics Group is gratefully acknowledged for her huge contribution to the GST project. Thank you so much for teaching me protein expression and purification and also for providing some peptides for my experiments. Without your help and contribution to the project, this would never have been accomplished. I am always grateful to Prof Esther Gallant, who introduced me to the world of single channel experiments and cardiomyocyte cultures. Thank you so much, Mrs Suzy Pace and Mrs Joan Stivala, for your endless supply of vesicles and all the support you gave me and especially the kindness you have shown all these years. Thank you Suzy, for sharing your knowledge on Ca^{2+} release assays. Dr Yamuna Karunasekara is also acknowledged gratefully for guiding me through the steps of tryptophan fluorescence quenching experiments and also for sharing so many things and helping me in many ways over the last few years. My gratitude also goes to Mrs Cathy Gillespie, at the Microscopy and Cytometry Resource Facility at JCSMR, for introducing me to confocal microscopy and for helping me to set up several new techniques. Thank you so much Dr Hanshen Tae, for the friendship we shared over the last few years and especially for proof reading my thesis. I would like to thank all members of the Muscle Research Group, who have supported me immensely in so many different ways, and made these last few years a pleasure to remember.

All my family members in Canberra, specially my uncle Mr Chandrasiri Perera and his family are also remembered dearly for all the support they have given me from the day we arrived in Australia.

I am also thankful to my brother, sister-in-law (Aruna and Asanka), sister and brother-in-law (Thilini and Udara) for helping me in numerous ways and for everything we shared. We will definitely miss you all, especially Ashvin and Vinuki when we go back. My gratitude also goes to my mother-in-law, who spent several months away from her family to help me and to keep company with the kids.

I am indebted to you, my dearest Aruna, without your encouragement and support; I would never have achieved any of this. Thank you for being so understanding and especially for encouraging me to accept this scholarship although you could not join us at that time. I know very well how hard it was for you to live all alone for two years, especially without kids. My beautiful daughters, Charu and Kimaya, I am so sorry I had to take you away from your thaththa and I know how badly you missed him. I will definitely make up for all the time I stayed away, locked up in a room, writing my thesis. Yes, amma finally finished her studies.

My dearest amma and thaththa; I do not have words to say how lucky I am to have you as my parents and how much you mean to me. You have always been a shadow in my life, loving me unconditionally, supporting me endlessly and encouraging me in each and every step of this journey. I would never have achieved any of this without you and your blessings. I love you both so much and dedicate this thesis to you with gratitude from the bottom of my heart.

ABSTRACT

Glutathione transferases are generally recognized for their role as antioxidant enzymes in phase II detoxification reactions. Recent studies identified a diverse range of other functions which are unrelated to detoxification. One such action is the specific inhibition of cardiac ryanodine receptor Ca^{2+} release channel. It is well documented that excessively active RyR2 channels are partly responsible for low store Ca^{2+} levels and defective Ca^{2+} release in heart failure. Therefore, inhibition of RyR2 is a potential strategy for the treatment of heart failure as it would help to maintain low RyR2 activity during diastole.

Previous studies which examined the effects of truncating GSTM2 on its ability to alter Ca^{2+} release from SR and RyR2 channel activity identified the GSTM2 C terminal domain (GSTM2C) as the region responsible for the inhibitory effect. Although it supported the inhibition of RyR2, it did not support the activation of RyR1 channels which was shown by the full length protein. Activity of smaller fragments from the GSTM2C indicated that the helix 6 in the C terminal domain is critical for the inhibitory effect. Although fragments containing the helix 6 sequences inhibited Ca^{2+} release from cardiac SR and RyR2 channel activity, helix 6 sequence alone was not effective. Structural analysis on circular dichroism spectroscopy revealed the helix 6 sequence to be unstructured which may have explained the lack of activity, if the helical nature of the fragment was essential for its efficacy. On the other hand, the active fragment of GSTM2 responsible for the inhibition of RyR2 activity may involve not only helix 6 but also the flanking helices.

Therefore, the main aims of the thesis were to identify the minimum fragment of GSTM2 which is capable of inhibiting RyR2, to determine the effect of mutations on the inhibitory effect, to confirm the region of RyR2 that interacts with GSTM2 and finally, to determine the effects of GSTM2 fragments on the contractility of ventricular cardiomyocytes.

First, I examined the activity of RyR2 in the presence of two GSTM2C constructs with potentially destabilizing mutations in helix 6. The mutants, F157A and Y160A failed to

inhibit cardiac RyR2 activity in single channel lipid biayer experiments and Ca^{2+} release from cardiac SR. Although they retained the helical structure as indicated in circular dichroism spectroscopy, tryptophan fluorescence indicated changes in folding. Interestingly, wild type GSTM2C inhibited cardiac RyR2 only at positive potentials, which may develop during Ca^{2+} efflux, but not at negative potentials. This further suggested that therapeutics mimicking the structure of GSTM2C may reduce excess Ca^{2+} release during diastole, which can lead to fatal arrhythmias.

Previous experiments carried out in our laboratory also showed that H5678 fragment of GSTM2C (containing helices 5,6,7 and 8) is capable of binding to the DR3 region of RyR2 which explains the isoform specific activity of GSTM2. Tryptophan fluorescence quenching experiments that I performed confirmed the binding between H5678 and 22 amino acid fragment (1869-1890) of DR3 region, which further narrowed down the GSTM2 binding site in cardiac RyR2. Consistent with previous results, binding between the two proteins was weak with dissociation constants in micro molar range. Since DR3 is located in the clamp region of the 3D structure of RyR2, specific binding of GSTM2C to RyR2 could dramatically influence the gating of the channel.

I investigated the effect of GSTM2C and the mutants, F157A and Y160A on the contractility of neonatal cardiomyocytes. Consistent with the results obtained with single channel lipid bilyer experiments and Ca^{2+} release assays, the mutants failed to reduce the contractility of cardiomyocytes. Ability of GSTM2C to inhibit RyR2 activity hence Ca^{2+} release from SR was further indicated when the contractility of cardiomyocytes was reduced significantly in the presence of GSTM2C. A new property of GSTM2C was identified when the GSTM2C was shown to be capable of entering into cardiomyoctytes without a carrier cell penetrating peptide.

The overall results presented in this study identify GSTM2C as a potential therapeutic for the treatment of heart failure. The helix 6 sequence in the GSTM2C and its flanking helices played a major role in stabilizing the molecule and in binding to the DR3 region of RyR2. Due to the voltage dependent activity, GSTM2C could be used during diastole to reduce the abnormal Ca^{2+} leak through ryanodine receptors. Thus, GSTM2C could be the only isoform specific, endogenous inhibitor of cardiac ryanodine receptor activity reported so far.

PUBLICATIONS ARISING FROM THIS THESIS

PAPERS

1. D Liu , R Hewawasam , SM Pace , EM Gallant , MG Casarotto , AF Dulhunty , PG Board . (2009) Dissection of the inhibition of cardiac ryanodine receptors by human glutathione transferase GSTM2. **Biochemical Pharmacology**. 77(7):1181-93.

2. R Hewawasam , D Liu , MG Casarotto , AF Dulhunty, PG Board (2010) The structure of the C-terminal helical bundle in glutathione transferase M2-2 determines its ability to inhibit the cardiac ryanodine receptor. **Biochemical Pharmacology**. 80(3): 381-88.

3. A F Dulhunty, R Hewawasam , D Liu , MG Casarotto , PG Board (2011) Regulation of cardiac muscle ryanodine receptor by glutathione transferases. **Drug Metabolism Reviews**. 43(2): 236-52.

4. D Liu , R Hewawasam , MG Casarotto , AF Dulhunty , PG Board. (2011) The inhibitory GSTM2 binding site is located in divergent region 3 of the cardiac ryanodine receptor. **Journal of Biological Chemistry** (Under review).

CONFERENCE ABSTRACTS

1. D Liu, R Hewawasam, SM Pace, EM Gallant, MG Casarotto, AF Dulhunty, PG Board. Structural dissection of the inhibition of cardiac ryanodine receptorby human glutathione transferase GSTM2. **ComBio 2008** (Joint conference of the Australian Society for Biochemistry & Molecular Biology, the Australian Society of Plant Scientists and the Australia and New Zealand Society for Cell and Developmental Biology) . 21-25 sept 2008. Canberra, Australia

2. R Hewawasam, D Liu, PG Board, AF Dulhunty. Effect of mutations on the modulation of the activity of ryanodine receptor by GSTM2. **32nd annual meeting of the Australian Society for Biophysics.** 28th Sept-1st Oct 2008.Canberra, Australia.

3. R Hewawasam, D Liu, PG Board, MG Casarotto, AF Dulhunty. F157A and Y160A substitutions in the helix 6 region of GSTM2C terminus reduces the

inhibitory action of helix 6 on RyR2 channels. **Australian Physiological Society Meeting**, Melbourne, Australia.30th Nov- 3rd Dec 2008.

4. R P Hewawasam, D Liu, M G Casarotto, P G Board, A F Dulhunty. Destabilization of the interaction between helix 6 and cardiac ryanodine receptor reduces the inhibitory action of GSTM2. **Curtin Conference on Ion Channels and Transporters**. Canberra, Australia. 15th-17th April 2009.

5. R P Hewawasam, D Liu, M G Casarotto, P G Board, A F Dulhunty. Activity of GST M2-2 C terminus and it's mutants on cardiac ryanodine receptor calcium channels in the presence and absence of ATP. **Gordon Research Conference on Muscle: EC coupling**. 14th-19th June 2009. Boston, USA.

6. R P Hewawasam, M G Casarotto, P G Board, A F Dulhunty GSTM2C terminus modulates the contractility of cultured rat ventricular cardiomyocytes. **Australian Physiological Society Meeting**, Adelaide, Australia. 28th Nov- 1st Dec 2010.

7. R P Hewawasam, M G Casarotto, P G Board, A F Dulhunty. GSTM2C terminus alters the cardiac function by reducing Ca^{2+} release through RyR2 in field stimulated ventricular cardiomyocytes. **55th Annual meeting of Biophysical Society**, Baltimore, Maryland, USA. 5th -9th March 2011.

8. R P Hewawasam, M G Casarotto, P G Board, A F Dulhunty. Effect of GSTM2C terminus and its mutants (F157A and Y160A) on cardiomyocyte function. **Gage Conference on Ion Channels and Transporters**. Canberra, Australia. 18th-20th April 2011.

ABBREVIATIONS

ANOVA	analysis of variance
ANU	Australian National University
APS	ammonium persulphate
ATP	adenosine triphosphate
BAPTA	1,2-bis(2-aminophenoxy)ethane-N,N,N',N'-tetra-acetic acid
BSA	bovine serum albumin
CD	circular dichroism
CICR	Ca^{2+}-induced Ca^{2+} release
CLIC	chloride intracellular channel
CPP	cell penetrating peptide
CPVT	catecholaminergic polymorphic ventricular tachycardia
Cryo-EM	cryo-electron microscopy
DDH_2O	distilled deionised water
DHPRs	dihydropyridine receptors
DTT	dithiothreiotol
E. Coli	Escherichia coli
EC coupling	excitation-contraction coupling
FCS	foetal calf serum
GST	glutathione transferase
GSTM2C	glutathione transferase C-terminal domain
I'	mean current
I'_F	fractional mean current
IPTG	Isopropyl β-D-1-thiogalactopyranoside
JCSMR	The John Curtin School of Medical Research
kDa	kilo Dalton

MH	malignant hyperthemia
nm	nanometers
OD	optical density
OG	Oregon Green fluorophore
PAGE	polyacrylamide gel electrophoresis
PBS	phosphate buffered saline (140 mM NaCl; 50 mM sodium phosphate to ~ pH 7.0)
PDB	protein data bank
P_o	open probability
rpm	revolutions per minute
RR	ruthenium red
RyRs	ryanodine receptors
SDS	sodium dodecyl sulphate
SEM	standard error of the mean
SERCA	sarcoplasmic/endoplasmic reticulum Ca^{2+} ATPase
SR	sarcoplasmic reticulum
TA	the transmembrane assembly (of RyRs)
TEMED	N,N,N,N-Tetramethylethylenedianime
TES	N-Tris[hydroxymethyl]methyl-2-animoethanesulfonic acid
T_o	mean open time
TRIS	Tris-[hydroxymethyl]aminomethane
T-tubule	transverse tubule
V	voltage
VICR	voltage-induced Ca^{2+} release

Table of Contents

Chapter 1 General Introduction

1.1 Muscle tissues

There are three types of muscle tissues.

Skeletal muscle tissue - Muscle fibers in this tissue are the longest muscle fibers which attach to and cover the bony skeleton. They have striations and act voluntarily. Skeletal muscle is responsible for overall body mobility.

Cardiac muscle tissue - This occurs only in the heart where it constitutes the bulk of the heart walls. Cardiac muscle is also striated but involuntary. Cardiac muscle usually contracts at a rate set by the heart's pacemaker, but neural control allows the heart to speed up for brief periods.

Smooth muscle tissue - This muscle tissue is found in the walls of hollow visceral organs such as the stomach, urinary bladder and respiratory passages. These are non striated and involuntary muscle fibers.

1.1.1 Cardiac muscle

Cardiac muscle is the involuntary striated muscle found in the walls of the heart. The cells that comprise cardiac muscle are called cardiomyocytes. Cardiac muscle cells are adapted to be highly resistant to fatigue. They have a large number of mitochondria, enabling continuous aerobic respiration via oxidative phosphorylation, numerous myoglobins and a good blood supply, which provides nutrients and oxygen to the muscle cells. The heart is so tuned to aerobic metabolism that it is unable to pump efficiently under ischemic conditions.

1.1.2 Cardiac muscle structure

Several types of cardiac myocytes are found in the adult human heart (Fig 1.1). The most numerous are working myocytes of the atria and ventricles that are specialized for

contraction. Atrial myocytes are smaller in diameter than those of ventricles. Purkinje fibres are found in the AV bundle, bundle branches and ventricular endocardium and are specialized for rapid conduction. Nodal cells in the SA and AV nodes are responsible for pacemaker activity and an atrioventricular conduction delay respectively (Katz, 2006).

Cardiac muscle shares similarities with skeletal muscle with regard to its striated appearance and contraction mechanisms, with both mechanisms differing significantly from those in smooth muscle fibers. However, in contrast to the long, cylindrical, multinucleated skeletal muscle fibers, cardiac cells are generally short, fat, uninucleate branching cells that fit together tightly at unique junctions called intercalated discs (Fig 1.2a). Each fiber contains one or at most two large, pale, centrally located nuclei.

The intercellular spaces are filled with a loose connective tissue matrix (endomysium) containing numerous capillaries. This delicate matrix is connected to the fibrous skeleton, which act as a tendon, giving cardiac cells an insertion to pull on and exert their force against. Skeletal muscle fibers are independent of one another both structurally and functionally. In contrast, the plasma membranes of adjacent cardiac cells interlock at dark-staining junctions which are the intercalated discs mentioned above. These discs contain anchoring desmosomes and gap junctions (Fig 1.2b). The desmosomes prevent adjacent cells from separating during contraction and the gap junctions allow ions to pass from cell to cell, transmitting current to generate action potentials throughout the entire heart. Because cardiac cells are electrically coupled by the gap junctions, myocardium behaves as a single coordinated unit or functional syncytium (Marieb EM, 2010). Large mitochondria account for 25-35% of the volume of cardiac cells, compared with only 2% in the skeletal muscle (Powers *et al.*, 2007). This gives cardiac cells a high resistance to fatigue. Most of the remaining volume is occupied by myofibrils that form typical sarcomeres. The sarcomeres have Z discs, A bands and I bands that reflect the arrangement of the thick (myosin) and thin (actin) filaments composing them.

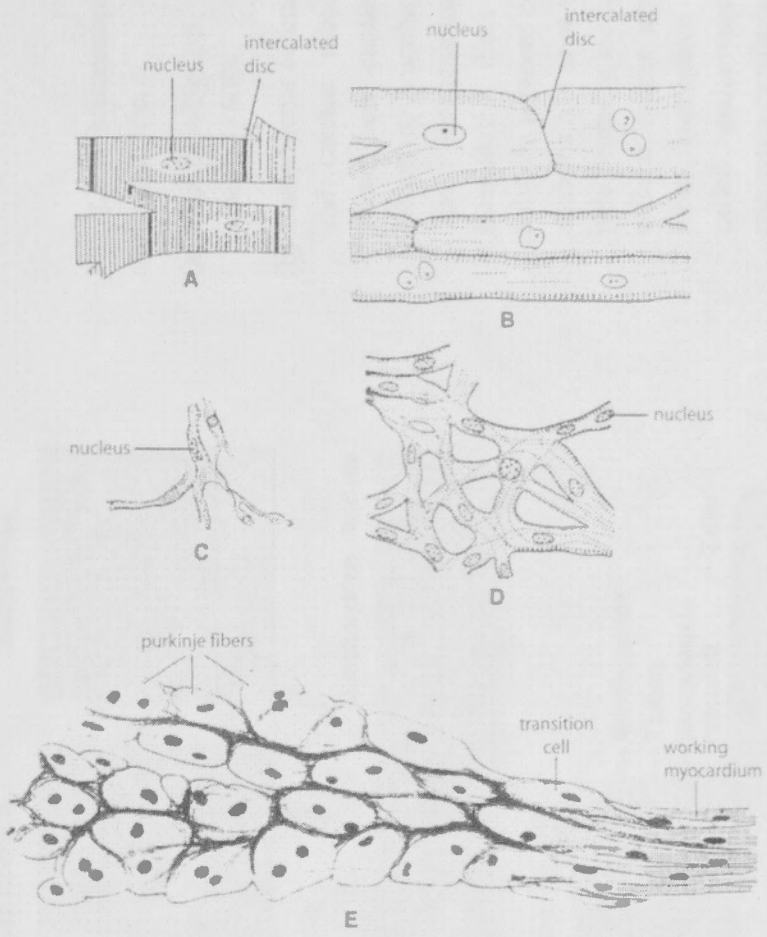

Fig 1.1: Human cardiac myocytes. A: Working ventricular myocytes containing cross striations, central nuclei and intercalated discs. B: Purkinje fibers which are large, poorly staining cells with sparse cross striations. The SA node (C) and AV node (D) are networks of small, sparsely cross striated cells. E: Transition cells are seen where purkinje fibers (left) impinge on the working myocardium (right). (Katz, 2006)

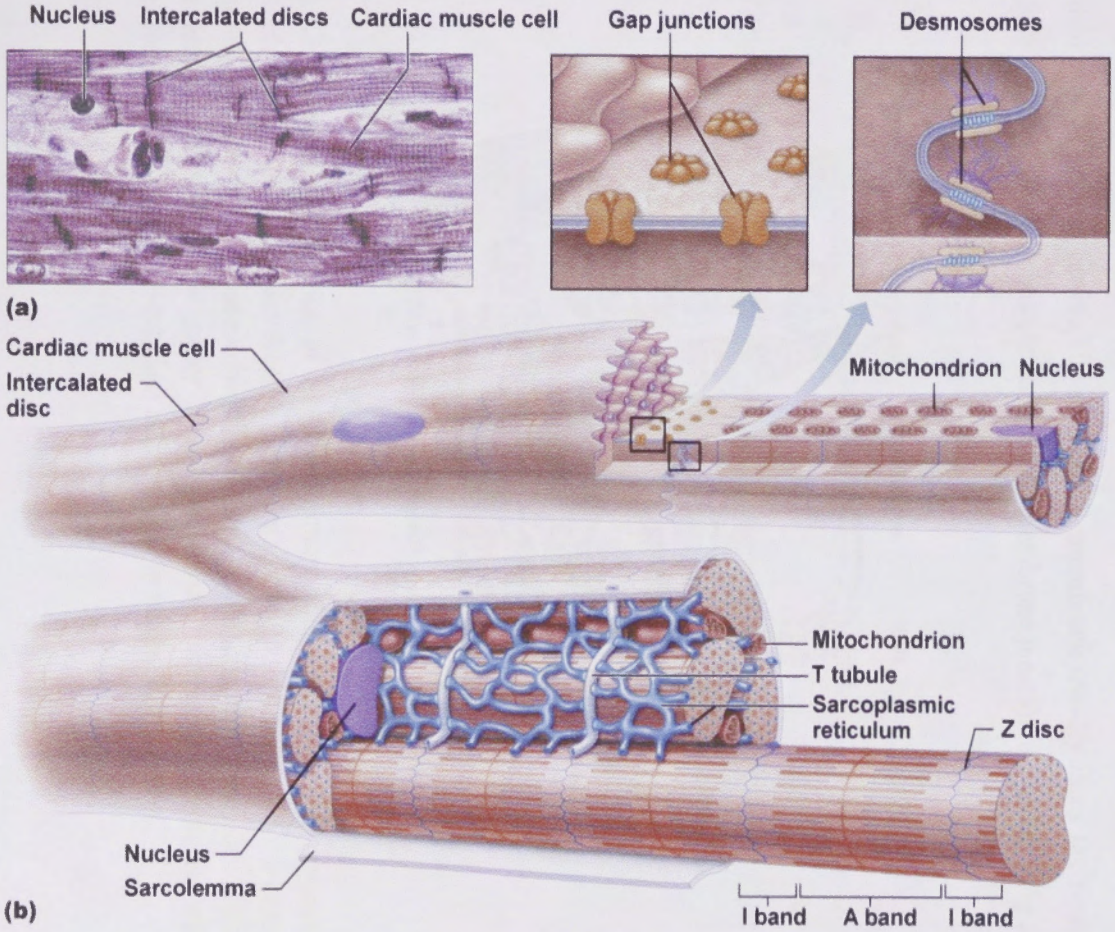

Fig 1.2: Microscopic anatomy of cardiac muscle.

(a) Photomicrograph of cardiac muscle (×600)

(b) Components of intercalated discs, and cardiac muscle fibers. As shown here, cardiac muscle cells are short, branched and striated. The dark-staining areas are intercalated discs or junctions, between adjacent cells. Each fiber contains one or at-most two large, pale centrally located nuclei. Inter cellular spaces are filled with a loose connective tissue matrix called endomysium containing numerous capillaries (Marieb EM, 2010).

1.1.2.1 Cardiac and skeletal muscle has fundamental differences

In contrast to skeletal muscle, myofibrils of cardiac muscle cells vary greatly in diameter and branch extensively, accommodating the abundant mitochondria that lie between them. This difference produces a banding pattern in heart cell that is less defined than that seen in the skeletal muscle.

The system for delivering Ca^{2+} for contraction is also less elaborate in cardiac muscle cells. The T tubules are wider and fewer than in skeletal muscle and they enter the cells once per sarcomere at the Z discs. In skeletal muscle, T tubules invaginate twice per sarcomere at the junction of the A-band and I-band. The cardiac sarcoplasmic reticulum is simpler and lacks the large terminal cisternae seen in skeletal muscle. Few triads are seen in cardiac muscle fibers. The cardiac SR membrane usually faces the t-tubule or surface membrane on one side, to form a two-membrane junction or "dyad" (Fig 1.3).

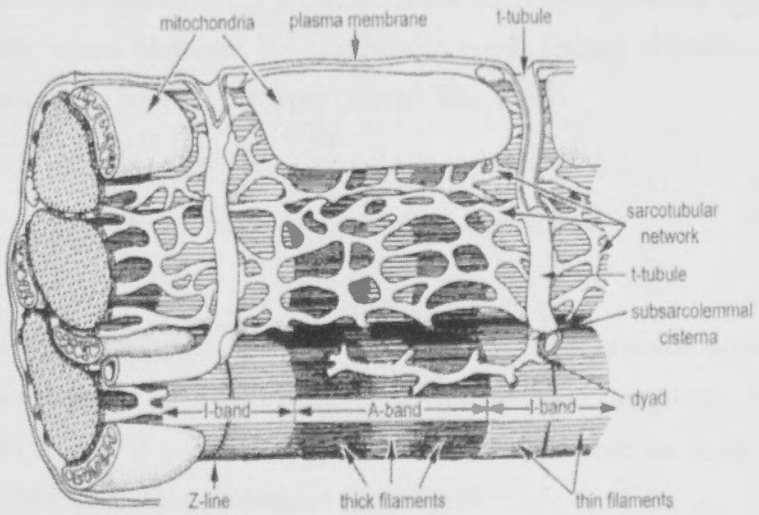

Fig 1.3: Schematic illustration of the ultrastructure of a working cardiac myocyte. The sarcoplasmic reticulum, an intracellular membrane system that surrounds the contractile proteins, consists of the sarcotubular network at the centre of the sarcomere and sarcolemmal cisternae. The latter form specialized composite structures with the transverse tubular system (T-tubules) called dyads or triads (Katz, 2006).

Skeletal muscle fibers must be stimulated to contract by an action potential delivered by nerves ending at a neuromuscular junction. In contrast, some specialized cardiac muscle cells (1%) are self-excitable. These cells initiate spontaneous rhythmical depolarization that is transmitted to the rest of the heart. This is called automaticity or autorhythmicity. The bulk of heart muscle, however, is composed of contractile muscle fibers responsible for the hearts pumping activity. In skeletal muscle, all cells of a given motor unit are stimulated and contract at the same time. Impulses do not spread from cell to cell. In cardiac muscle, the healthy heart either contracts as a unit or does not contract at all. This coordinated action occurs because gap junctions electrically tie all cardiac muscle cells together into a single contractile unit capillaries (Marieb EM, 2010). Consequently, the depolarization wave travels across the heart from cell to cell via ion passage through the gap junctions. In cardiac muscle cells, the absolute refractory period or the unexcitable period when Na^+ channels are still open or inactivated lasts approximately 250ms, nearly as long as a contraction. In contrast, skeletal muscle fiber has a short refractory period of 1-2ms in which contraction lasts for 15-100ms. The long cardiac refractory period normally prevents tetanic contractions, which would stop the hearts pumping action. However, the sequence of events leading to muscle contraction is generally similar in both muscle types (Marieb EM, 2010).

1.1.2.2 Microscopic anatomy of cardiac muscle fiber

The contractile proteins which make up almost half of the volume of working cardiac myocytes are organized in a regular array of cross-striated myofibrils. Most of the remaining cell volume is occupied by mitochondria that generate the large amounts of chemical energy required for contraction (Katz, 2006).

Striations, a repeating series of dark and light bands, are evident along the length of each myofibril (Fig 1.4a). In an intact muscle fiber, the dark A bands (A for Anisotropic) and light I bands (I for isotropic) are nearly perfectly aligned with one another, giving the cell as a whole its striated appearance. Each dark A band has a lighter region in its mid section called the H zone (H for helle; "Bright"). Each H zone is bisected vertically by a dark line called the M line (M for middle) formed by molecules of the protein myomesin. The light I bands also have a midline interruption, a

darker area called the Z disc (or Z line) (Fig 1.4b). A sarcomere is the smallest contractile unit of the muscle fiber, the functional unit of the skeletal or cardiac muscle. The average sarcomere length is ~2 μm. The sarcomere is the region of a myofibril between two successive Z discs. In other words, it cantains an A band flanked by half an I band at each end. Within each myofibril, sarcomeres are aligned end to end (Marieb EM, 2010).

The banding pattern of a myofibril at the molecular level arises from an orderly arrangement of two types of even smaller structures within the sarcomeres. These smaller structures are the muscle equivalents of the actin and myosin containing microfilaments. The central thick filaments containing myosin extend the entire length of the A band. The more lateral thin filaments containing actin extend across the I band and partway into the A band. The Z disc, a coin shaped sheet composed largely of the protein alpha actinin, anchors the thin filaments (Fig 1.4c). Intermediate (desmin) filaments (not illustrated) extending from the Z disc connect each myofibril to the next throughout the width of the muscle cell. The cross sectional view shows clearly that each thick filament is surrounded by a hexagonal arrangement of six thin filaments, and each thin filament is enclosed by three thick filaments (Fig 1.4d, Marieb EM, 2010).

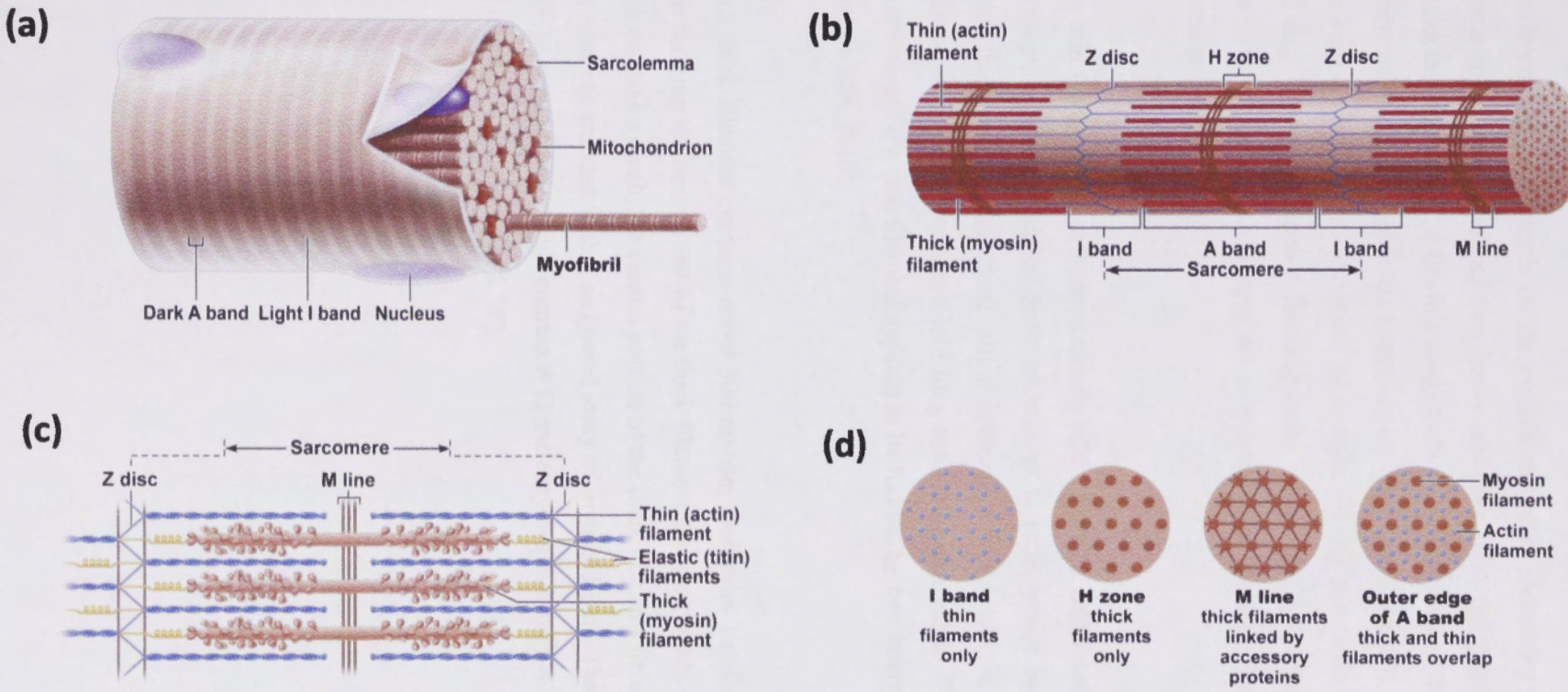

Fig 1.4: Microscopic anatomy of striated muscle fiber. a) Diagram of a part of a muscle fiber showing the myofibrils. One myofibril is extended afrom the cut end of the fiber. b) A small part of one myofibril enlarged to show the myofilaments responsible for the banding pattern. Each sarcomere extends from one Z disc to the next. c) Enlargement of one sarcomere (sectioned lengthwise). Notice the myosin heads on the thick filaments. d) Cross sectional view of a sarcomere cut through in different sections. (Marieb EM, 2010)

Muscle contraction depends on the myosin and actin containing microfilaments. Each myosin molecule consists of two heavy and four light polypeptide chains and has a rodlike tail attached by a flexible hinge to two globular heads. The tail consists of two intertwined helical polypeptide heavy chains. The globular heads, each associated with two light chains, are the active end of myosin. During contraction, they form the thick and thin filaments, together forming cross bridges and swivel around their point of attachment. These cross bridges act as motors to generate the tension developed by a contracting muscle cell.

The thin filaments are composed chiefly of the protein, actin. Actin has kidney-shaped polypeptide subunits, called globular actin or G actin, which bear the active sites to which the myosin heads attach during contraction (Fig 1.5A). In the thin filaments, G actin subunits are polymerized into long actin filaments called fibrous or F actin. The backbone of each thin filament appears to be formed by two intertwined actin filaments (Marieb EM, 2010).

Each thick filament contains about 300 myosin molecules bundled together with their tails forming the central part of the thick filament and their heads facing outward and at each end. As a result, the central portion of the thick filament (in the H zone) is smooth, but ends are studded with a staggered array of myosin heads. The heads bear actin and ATP binding sites and also contain ATPase enzymes that split ATP to generate energy for muscle contraction (Fig 1.5B).

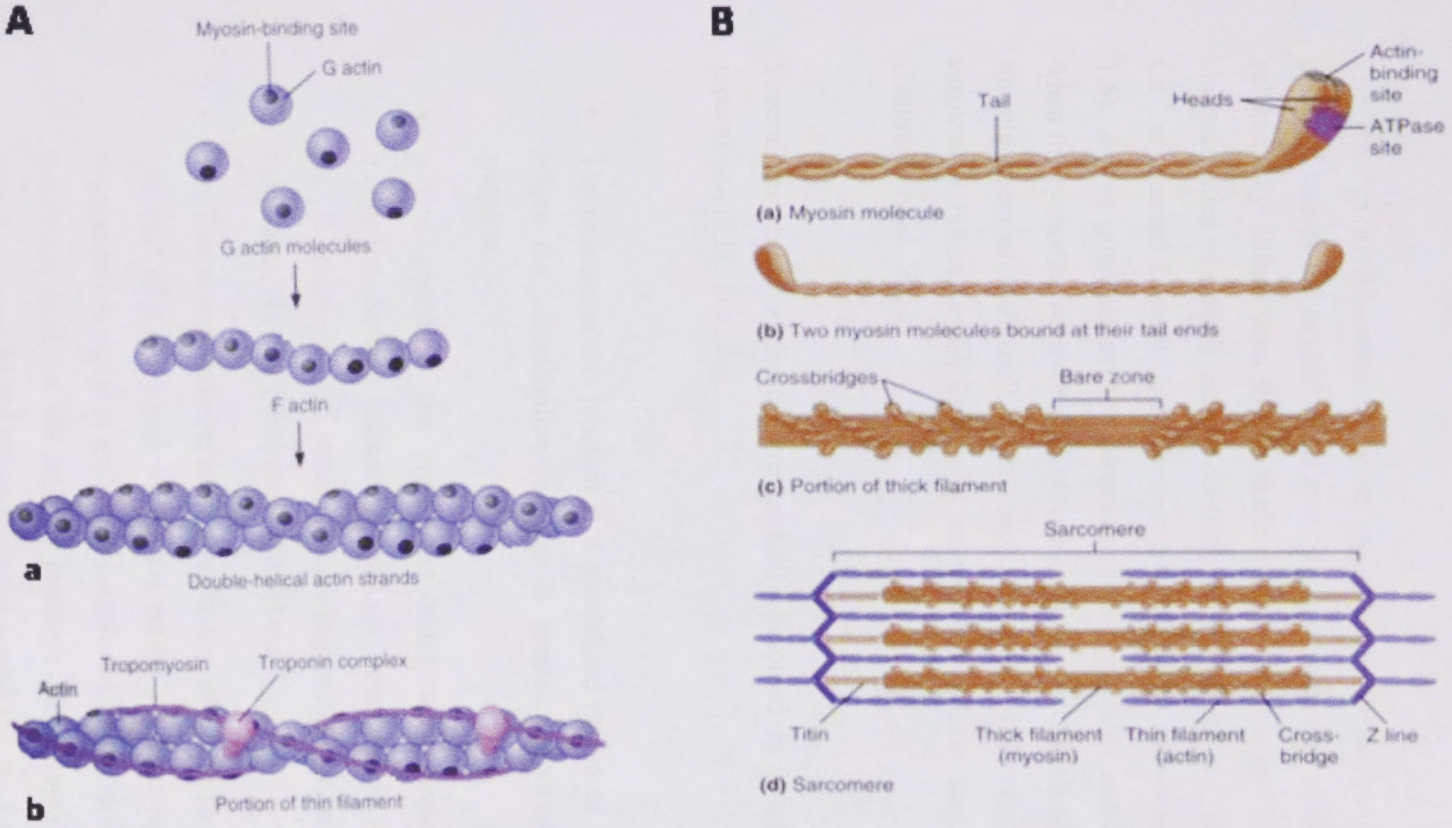

Fig 1.5: **A**: Structure of a thin filament; (a) the backbone of a thin filament consists of two strands of polymerized actin molecules wound together to form a double helix. Dark dots represent myosin binding sites. (b) A portion of a thin filament showing troponin and tropomyosin in their normal resting positions on the actin strands. Actin's myosin binding sites are covered by tropomyosin when a muscle cell is at rest. **B**: Structure of a thick filament. (a) A myosin molecule, a dimer of two subunits wound together. (b) Two myosin molecules joined by tail to tail. (c) A portion of a thick filament showing cross bridges at either end but not in the middle. (d) A detailed view of sarcomere showing relative positions of thick and thin filaments and titin, which anchors thick filaments in place (Germann WJ, 2005).

1.1.3 Cardiac excitation-contraction (EC) coupling.

The term "excitation-contraction coupling" refers to the mechanism by which the action potential causes the myofibrils of muscle to contract. EC coupling in cardiac muscle substantially differs from that in skeletal muscle and it has important effects on the characteristics of cardiac muscle contraction. In both tissues, contraction occurs when Ca^{2+} is released from the SR in response to a surface membrane action potential (Fig 1.6). Action potential evoked (depolarization-dependent) contraction does not occur when the ryanodine receptor Ca^{2+} release channel (RyR) is absent in RyR1-null skeletal muscle fibers or RyR2-null cardiac myocytes. RyR1-null animals die at birth due to respiratory failure, while RyR2-null animals die at birth due to oxygen deprivation (Dulhunty *et al.*, 2011).

Several membrane structures are critically involved in initiating the EC coupling process and in EC coupling.

- The neuromuscular junction is a specialized region of the surface membrane, where the acetylcholine receptor is located, opposing to the motor nerve endplate.
- Action potentials are propagated along the sarcolemma or the surface membrane. Several critical proteins are embedded in the membrane, such as Na^+, K^+ channels, Ca^{2+} pumps that are responsible for the extrusion of Ca^{2+} from cytoplasm, Na^+-Ca^{2+} exchanger (NCX) etc.
- The T tubular membrane is an invagination of the surface membrane and forms one half of a dyad and carries the action potential into the cell so that the depolarization signal is uniformly distributed throughout the cell. The T tubular membrane contains the voltage sensitive dihydropyridine receptors (DHPR) whose response to the action potential constitutes the first step in EC coupling. Cardiac DHPRs are much fewer in number and not organized in regular arrays of tetrads (in which four DHPRs are located so that each can interact with one

subunit of the RyR tetramer in skeletal muscle) and are not well-aligned with RyRs (Sun *et al.*, 1995, Felder and Franzini-Armstrong, 2002).

- Sub sarcolemmal cisternae are flattened structures that form the dyad with the plasma membrane (Katz, 2006). This cardiac junctional SR releases calcium via RyR channels from the SR into the cytosol in response to the plasma membrane depolarization. The capacity of cardiac junctional SR is smaller than skeletal terminal cisternae because the cardiac SR does not form expanded terminal cisternae at the junction.

The tissue specific mechanism of EC coupling may be partially due to the substantial sequence heterogeneity between skeletal (RyR1) and cardiac RyRs (RyR2), although the 3-D profiles of the RyR1 and RyR2 are similar. The divergent regions in the RyR sequence may encompass the Ca^{2+} / Mg^{2+} inhibition sites (Du *et al.*, 2000, Hayek *et al.*, 1999) which contributes to the VICR in skeletal muscle but not to the CICR in cardiac muscle.

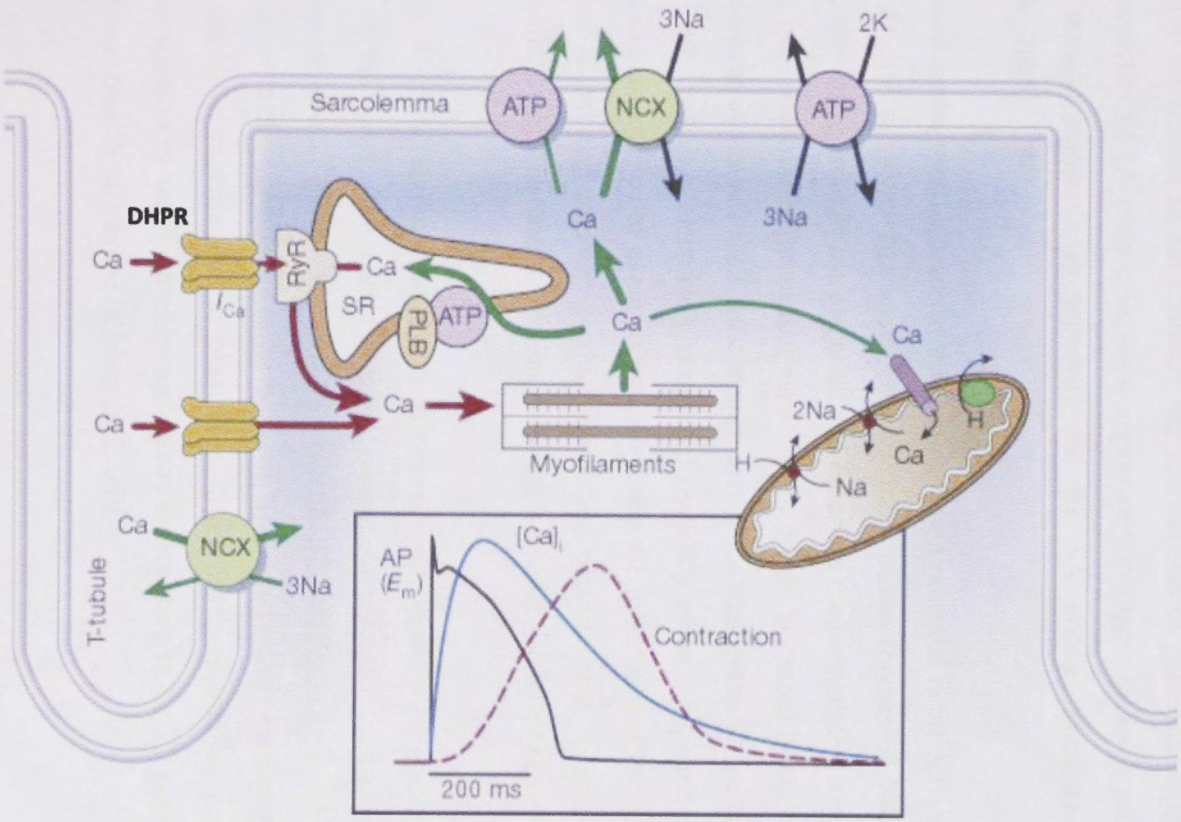

Fig 1.6: EC coupling in cardiac muscle. Figure shows the Ca^{2+} transport pathways in ventricular myocytes with the inset showing the time course of an action potential, Ca^{2+} transient and contraction measured in a rabbit ventricular myocyte at 37°C. NCX- Na^{+}/Ca^{2+} exchanger, ATP- Ca^{2+} ATPase, PLB- Phospholamban, SR-sarcoplasmic reticulum. DHPR-dihydropyridine receptor. RyR-Ryanodine receptor. Adapted from (Bers, 2004).

1.1.3.1 Cardiac action potential

The cardiac action potential differs significantly in different regions of the heart and this reflects the different electrical characteristics in different regions of the heart. For instance, the specialized conduction tissue of the heart has the special property of depolarizing without any external influence i.e. automaticity (defined above, section 1.1.2.1).

There are important physiological differences between nodal cells and ventricular cells. The specific differences in ion channels and mechanisms of polarization give rise to unique properties of SA node cells, most importantly the spontaneous depolarisations (cardiac muscle automaticity) necessary for the SA node's pacemaker activity (Klabunde, 2005).

The standard model used to describe the cardiac action potential is the action potential of the ventricular myocyte. This action potential has 5 phases (numbered 0-4, Fig 1.7). Phase 4 is the resting membrane potential, and describes the membrane potential when the cell is not depolarized. The resting membrane potential is caused by the difference in ionic concentrations and their conductance across the membrane of the cell during phase 4. Once the cell is electrically stimulated (typically by an ionic current from an adjacent cell), a sequence of events begins involving the influx and efflux of multiple cations and anions that together produce the action potential that is, propagated to adjacent cells. In this fashion, an action potential is conducted, to all the cells of the heart.

This phase 4 of the action potential is associated with diastole (relaxation) of the chamber of the heart. The normal resting membrane potential in the ventricular myocardium is about -85 to -95 mV. This potential is determined by the selective permeability of the cell membrane to various ions. The membrane is most permeable to K^+ and relatively impermeable to other ions. The resting membrane potential is therefore dominated by the K^+ equilibrium potential according to the K^+ concentration gradient across the cell membrane (Klabunde, 2005).

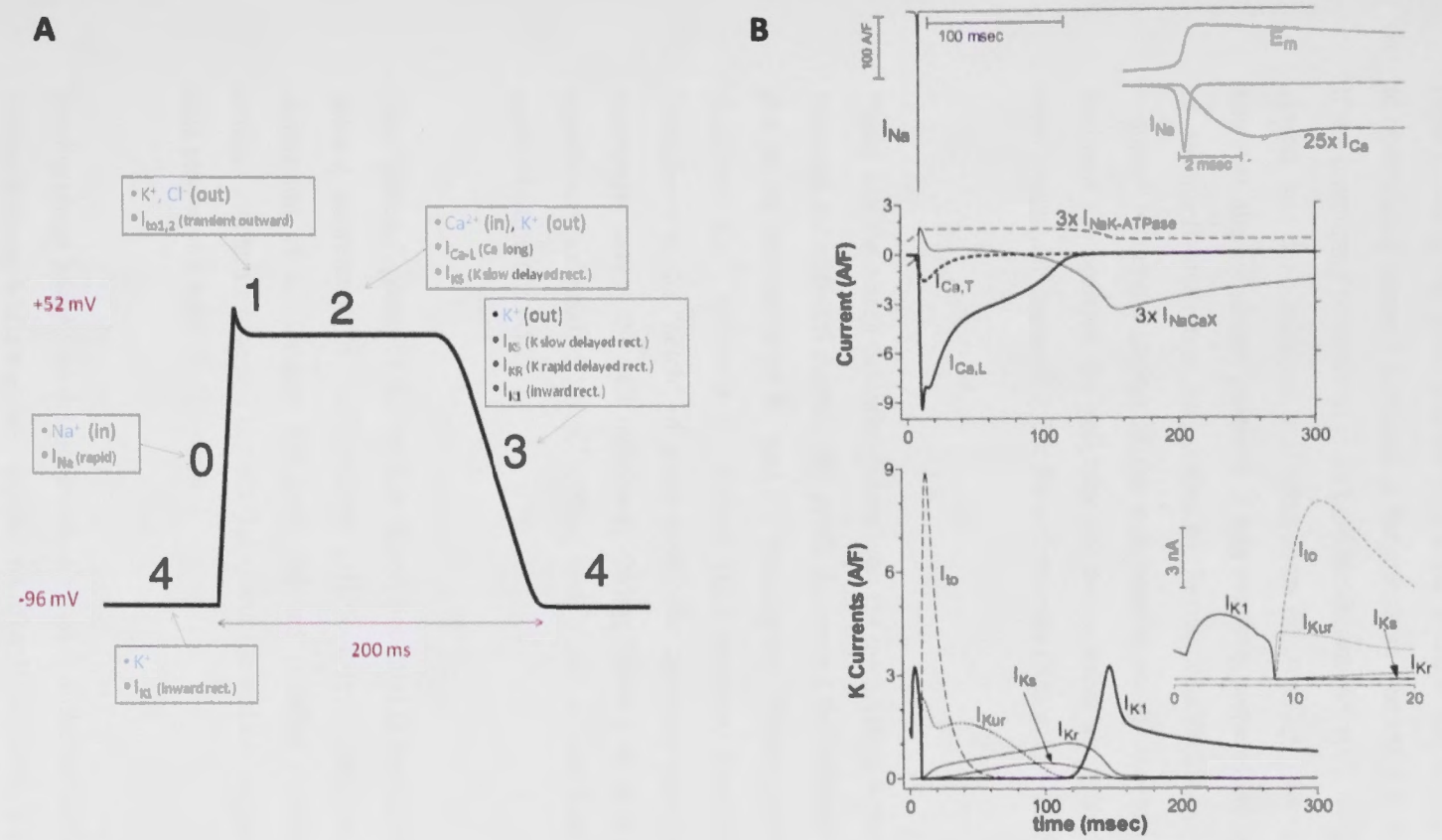

Fig 1.7: A: Phases of a ventricular myocyte action potential. Five phases are shown. Phase 4: resting membrane potential when the cell is quiescent. Phase 0: the rapid depolarization phase due to rapid influx of Na^+ ions. Phase 1: inactivation of fast Na^+ channels and a transient net outward current due to movement of K^+ and Cl^- ions causes the downward deflection. Phase 2: Plateau is due to the movement of Ca^{2+} in through DHPR and K^+ out. Phase 3: rapid repolarization when L-type Ca^{2+} channels close while slow delayed rectifier K^+ channels are still open. This causes a net outward current. B: Major ionic currents superimposed during the action potential. I_{Na} is shown in an expanded time scale. K currents are shown separately. I_{Na}: Na^+ current; $I_{Ca,L}$: L type Ca^{2+} current; $I_{Ca,T}$: T type Ca^{2+} current; I_{NaCaX}; Na/Ca exchanger; I_{to}: transient outward currents; I_{KS}: slow delayed rectifier K^+ channels; I_{Kr}: rapid delayed rectifier K^+ channels; I_{K1}: inward rectifier current; I_{Kur}: ultra rapid outward current (Bers,2001).

Phase 0 is the rapid depolarization phase. This phase is due to the opening of the fast Na^+ channels causing a rapid increase in the membrane conductance to Na^+ and thus a rapid influx of Na^+ ions into the cell; a Na^+ current. The ability of the fast Na^+ channels to open during phase 0 is related to the membrane potential at the moment of excitation. If the membrane potential is at its baseline (about -85 mV), all the fast Na^+ channels are closed, and depolarization will open them all, causing a large influx of Na^+ ions. If, however, the membrane potential is less negative, some of the fast Na^+ channels will be in an inactivated state insensitive to further depolarization, thus causing a lesser response to depolarization of the cell membrane. If the resting membrane potential becomes too positive, the cell may not be excitable and conduction through the heart may be delayed, increasing risk for arrhythmias (Klabunde, 2005).

Phase 1 of the action potential occurs with the inactivation of the fast Na^+ channels. The transient net outward current (the small downward deflection of the action potential) is due to the movement of K^+ and Cl^- ions, carried by the transient outward K^+ current (I_{to1}) and Ca^{2+} activated Cl^- current (I_{to2}) currents, respectively. I_{to1} in particular contributes to the "notch" of some ventricular cardiomyocyte action potentials. Cl^- ion movement across the cell membrane during Phase 1 is as a result of the change in membrane potential, from K^+ efflux, and is not a contributory factor to the initial repolarization ("notch").

The "plateau" phase of the cardiac action potential is sustained by a balance between inward movement of Ca^{2+} through DHPR L-type calcium channels and outward movement of K^+ through the slow delayed rectifier potassium channels, I_{Ks}. The sodium-calcium exchanger current, $I_{Na,Ca}$ and the sodium/potassium pump current, $I_{Na,K}$ also play minor roles during phase 2.

During phase 3 (the "rapid repolarization" phase) of the action potential, the L-type Ca^{2+} channels close, while the slow delayed rectifier K^+ channels are still open. This ensures a net outward current, producing a negative change in membrane potential, thus

allowing more types of K^+ channels to open. These are primarily the rapid delayed rectifier K^+ channels and the inwardly rectifying K^+ current, I_{K1}. This net outward, current (reflecting loss of positive charge from the cell) causes the cell to repolarize. The delayed rectifier K^+ channels close when the membrane potential is restored to about -80 to -85 mV, while I_{K1} remains conducting throughout phase 4, contributing to set the resting membrane potential (Klabunde, 2005).

1.1.3.2 Pacemaker action potential

Spontaneous depolarization underlying automaticity is due to the plasma membranes of specific cells within the heart that have reduced permeability to potassium (K^+) but still allow passive transfer of calcium ions, allowing a net charge to build. Of the cells that can undergo spontaneous depolarization, the fastest are the primary pacemaker cells of the heart, which set the heart rate. Therefore, automaticity is most often demonstrated in the sinoatrial node, the so called "Pacemaker of the Heart". Abnormalities in automaticity result in rhythm changes. Electrical activity that originates from the SA node is propagated to the rest of the heart. The fastest conduction of electrical activity is via the electrical conduction system of the heart.

The pacemaker potential (also called the pre potential and generated by the pacemaker current) is the slow, positive change in voltage across the cell's membrane that occurs between the end of one action potential and the beginning of the next action potential (Fig 1.8). This depolarization reaches the threshold potential for an action potential and consequently fire the next action potential (Robert, 2004). The pacemaker potential drives the rhythmic firing (automaticity) of pacemaker cells, and the rate of change (i.e., the slope) of the pacemaker potential determines the timing of the next action potential and thus the intrinsic firing rate of the cell. Because the pacemaker potential occurs during the non-contracting time between heart beats (diastole), it is also called the diastolic depolarization (Klabunde., 2005, Katz., 2006).

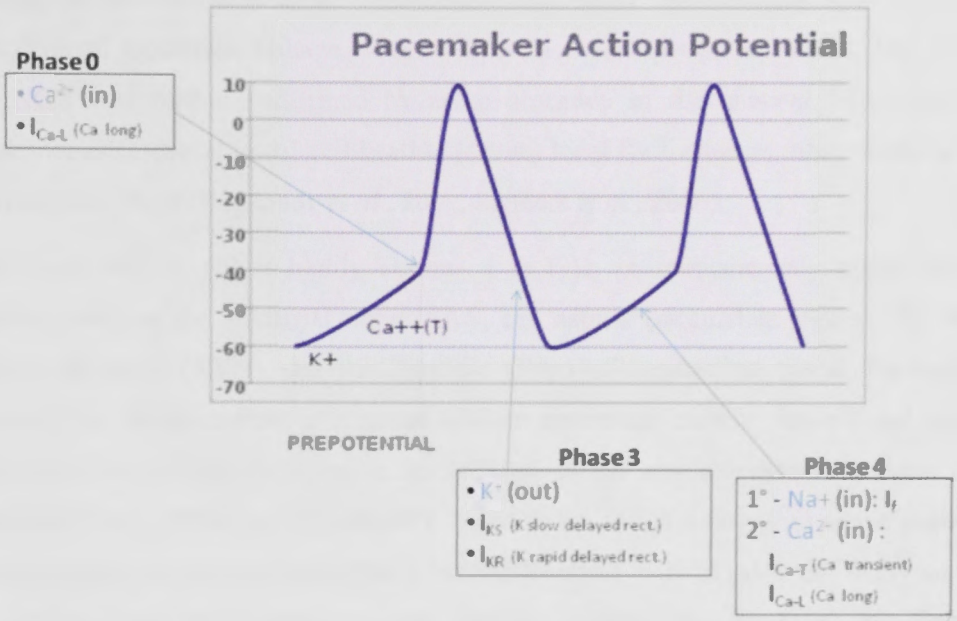

Fig 1.8: Action potential of the pacemaker cells. Funny currents (I_f) generated by both K^+ and Na^+ conductances are responsible for the pre potential. These channels in the SA node cells causes the membrane potential to slowly become more positive (depolarize). Next, opening of T or transient channels further depolarize the cell until eventually the L or long lasting Ca^{2+} channels are activated and an action potential is initiated.

Evidence in support of the active presence of K^+, Ca^{2+}, Na^+ channels and Na^+/Ca^{2+} exchanger (NCX) during the pacemaker phase have been variously reported in the literature, but several indications point to the "funny" current as one of the most important (DiFrancesco, 2006). There is now substantial evidence that also SR Ca^{2+}-transients participate to the generation of the diastolic depolarization via a process involving the NCX (Lai *et al.*, 1989). Most recent discoveries over the past decade made possible by simultaneous sub membrane Ca^{2+} imaging and membrane potential or current recordings with cell attached patch electrodes, have shown that timed Ca^{2+} releases occur during diastolic depolarizations and activate NCX, causing an inward Ca^{2+} influx so that the late diastolic depolarization to exponentially increase, driving the membrane potential to the threshold for the rapid upstroke of the next action potential. As suggested by Lakatta and Difrancesco, such rhythmic spontaneous intracellular

cycling can be referred to as an "intracellular Ca^{2+} clock" that interacts with the classic sarcolemmal membrane voltage clock to form an overall pacemaker clock. The role of the NCX was further confirmed by acute blockade of the channel which stopped spontaneous sinoatrial nodal cell beating leaving local Ca^{2+} releases intact (Lakatta and DiFrancesco, 2009, Bogdanov *et al.*, 2001, Sanders *et al.*, 2006).

The funny current (I_f) is highly expressed in cells in spontaneously active cardiac regions, such as the sinoatrial node (SAN, the natural pacemaker region), the atrio-ventricular node (AVN) and the Purkinje fibres of conduction tissue. Particularly unusual, the funny current is a mixed sodium-potassium current, inward and slowly activating during hyperpolarization to voltages in the diastolic range in these cells (normally from -60/-70 mV to -40 mV). When at the end of a sinoatrial action potential the membrane repolarises below the I_f threshold (about -40/-50 mV), the funny current is activated and the resultant inward current, initiates the onset of the diastolic depolarization; by this mechanism, the funny current can control the rate of spontaneous activity of sinoatrial myocytes, hence the cardiac rate (Verkerk *et al.*, 2007).

1.1.3.3 The intrinsic conduction system

The intrinsic cardiac conduction system consists of noncontractile cardiac cells specialized to distribute impulses throughout the heart, so that it depolarizes and contracts in an orderly, sequential manner. Therefore, the heart beats as a coordinated unit.

Autorhythmic cardiac cells are also found in the atrioventricular bundle, right and left bundle branches and ventricular walls as Purkinje fibers. Impulses pass throughout the heart in order from SA node, AV node, AV bundle, right and left branches to Purkinje fibers (Fig 1.9A, Marieb EM, 2010). SA node, located at the right atrial wall generates impulses about 75 times every minute, in humans.

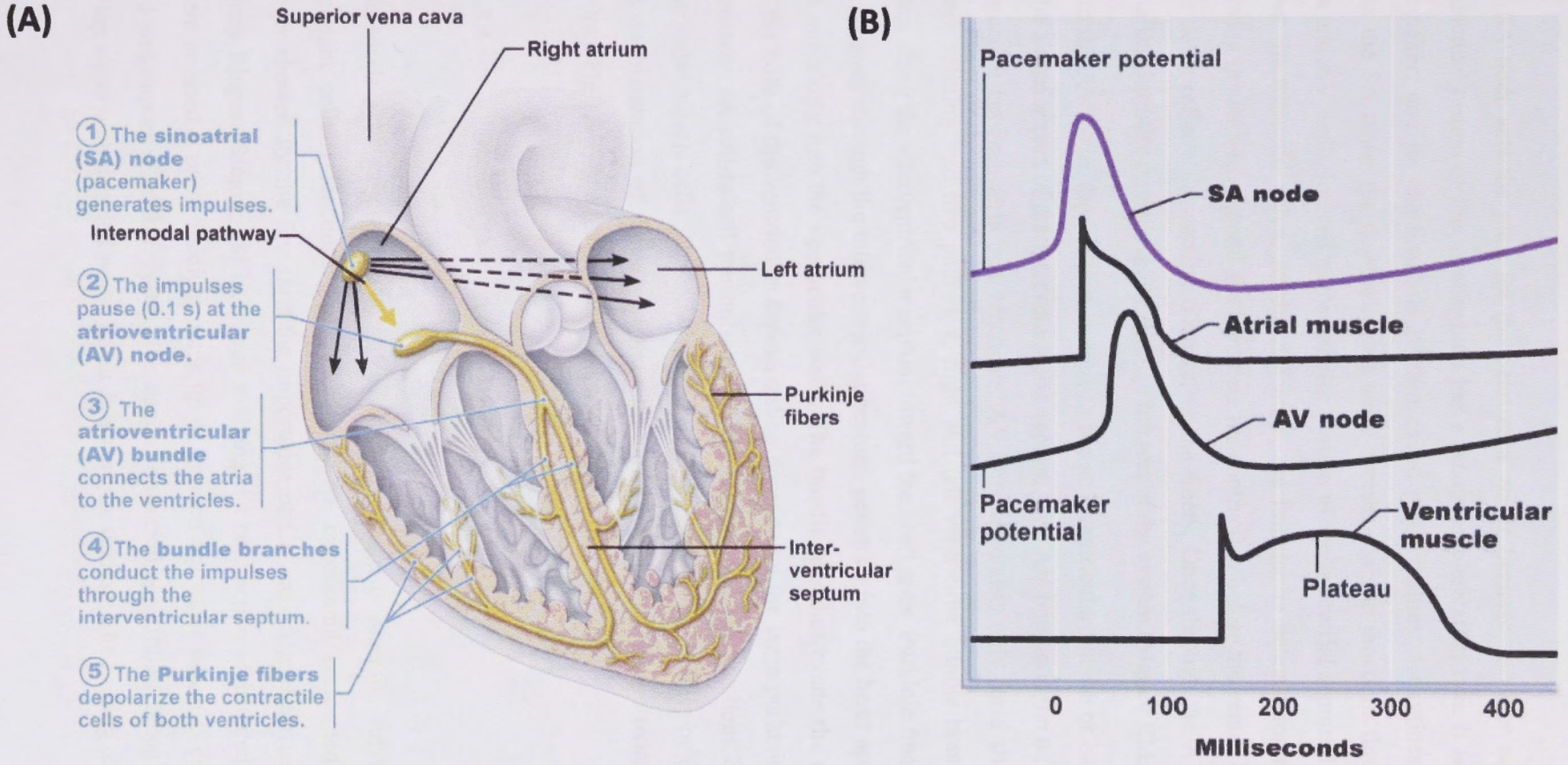

Fig 1.9: (A) Anatomy of the intrinsic conduction system showing the sequence of electrical excitation. **(B)** Comparison of action potential succession during one heart beat at various locations (Marieb EM, 2010).

The SA node sets the pace for the heart as a whole because no other region of the conduction system or the myocardium has a faster depolarization rate. It is the heart's pacemaker, and its characteristic rhythm called sinus rhythm, determines heart rate. From the SA node, the depolarization wave spreads via gap junctions throughout the atria and AV node, located in the inferior portion of the interatrial septum immediately above the tricuspid valve. At the AV node, the impulse is delayed for about 0.1 s, allowing the atria to respond and complete the contraction before the ventricles contract. This delay reflects the smaller diameter of the fibers. Once through the AV node, the signalling impulse passes rapidly through the rest of the system (Marieb EM, 2010).

From the AV node, the impulse sweeps to the atrioventricular bundle or bundle of His in the superior part of the interventricular septum. The AV bundle is the only electrical connection between atria and ventricles. AV bundle persists only for a short distance before splitting into two pathways, right and left ventricular bundle branches which course along the interventricular septum toward the heart apex. Purkinje fibers complete the pathway through the interventricular septum, penetrate into the heart apex and then turn superiorly into the ventricular walls. The bundle branches excite the septal cells, but the bulk of the ventricular depolarization depends on the large purkinje fibers and ultimately, on cell-to-cell transmission of the impulse via gap junctions between the ventricular muscle cells. The total time between initiation of an impulse by the SA node and depolarization of the last of the ventricular muscle cell is approximately 0.22s (220ms, Fig 1.9B) in a healthy human heart (Marieb EM, 2010).

1.1.3.4 Role of calcium (Ca^{2+})

Calcium is a ubiquitous carrier of cellular signals and is essential for most of the important cellular reactions (Carafoli, 2005). An experiment performed by Sidney Ringer showed for the first time the importance of Ca^{2+} as a signal carrier in muscle. Sidney Ringer (Ringer, 1883a,b) was studying the contraction of isolated frog hearts where he used a saline medium made up of London tap water which is considered as hard and impure (Carafoli, 2005). The hearts contracted beautifully. When he replaced the tap water with distilled water, he made a startling finding: The beating of the hearts

became progressively weaker, and stopped altogether after about 20 min. Adding Ca^{2+} salts to the suspension medium maintained the contraction. Therefore, Ringer found a novel function of Ca^{2+} in a tissue that has nothing to do with bone or teeth. Since then, Ca^{2+} is considered as a molecule which controls a wide range of cellular processes (Carafoli, 2005).

Ringer's discovery did not attract any attention for years. In 1946, L V Heilbrunn did an experiment in which he applied Ca^{2+} salts to either ends of a frog muscle fiber and concluded that Ca^{2+} could diffuse from the cut ends to the contractile elements to initiate a contraction (Heilbrunn *et al.*, 1946). Later, K Bailey showed that the ATPase activity of myosin was activated by Ca^{2+} but not by Mg^{2+} and suggested the presence of Ca^{2+} in the vicinity of myosin controlled the contraction of the muscle (Bailey, 1942). Internal Ca^{2+} store in the muscle fiber, the SR was discovered in 1960s which was very important to explain the mechanism of muscle contraction (Ebashi, 1961, Ebashi and Ebashi, 1962).

Today, cardiac muscle contraction is believed to be initiated by the calcium induced calcium release mechanism from the cardiac RyR located on the SR membrane (Ebashi and Endo, 1968, Endo *et al.*, 1970). Calcium induced Calcium release in cardiac muscle fiber increases the concentration of cytosolic Ca^{2+} from a typical resting concentration of approximately 100 nM to micromolar levels (1-10 μM) usually at a rate of 100 μM/ms. This 10-100 fold elevation of cytosolic Ca^{2+} mediates contraction as a result of the interaction of Ca^{2+} with a regulatory subunit of troponin and results in the release of contractile proteins, actin and myosin (Stokes and Wagenknecht, 2000). These contractile proteins interact via myosin cross-bridges and cross bridge cycling allows the sarcomere to shorten and generate force which is proportional to the concentration of cytosolic Ca^{2+}. Once the contraction is completed, relaxation commences with the cessation of Ca^{2+} release from SR and commencement of Ca^{2+} uptake into the SR (Stokes and Wagenknecht, 2000). The sarcolemma repolarises and concentration of cytosolic Ca^{2+} concentration is restored to resting levels. Unlike the Ca^{2+} release, Ca^{2+} reuptake into the SR is active and requires energy from ATP hydrolysis to activate the Ca ATPase machinery (SERCA pump) located in the SR membrane. Reuptake of Ca^{2+} into the SR generates a thousand-fold concentration gradient of Ca^{2+} across the SR membrane in the resting muscle. At the molecular level, this pumping is $\sim 10^5$ times

slower than release, reflecting the mechanical constraints of energy coupling (Stokes and Wagenknecht, 2000).

Ca^{2+} is bound to the main SR Ca^{2+}-binding protein, calsequestrin 2 (CSQ2) which is widely regarded as the principal Ca^{2+} buffering molecule present within the SR in adult cardiac muscle cells, though other Ca^{2+} binding proteins are also present. CSQ2 is the sole CSQ isoform present in the SR in cardiac muscle (Murphy *et al.*, 2010, Cala *et al.*, 1990, Campbell *et al.*, 1983) and is thought to be predominantly localized to the junctional SR. (Murphy *et al.*, 2010). The force generated by the shortening of the sarcomere terminates when the concentration of the cytosolic calcium is reinstated to resting levels equivalent to those maintained prior to the depolarization of the sarcolemma. Thus, calcium is the driving force of muscle contraction (Stokes and Wagenknecht, 2000).

1.1.3.5 The mechanism of force generation in muscle

EC coupling is the sequence of events by which transmission of an action potential along the sarcolemma leads to the sliding of myofilaments. The action potential is brief and ends well before contraction starts. The events of excitation-contraction coupling occur during the latent period, between action potential initiation and the beginning of mechanical activity. Obviously, the electrical signal does not act directly on the myofilaments. Instead, it causes the rise in intracellular Ca^{2+} concentration that allows the filaments to slide (Marieb, 2010).

When physiologists first discovered the presence of actin and myosin in myofibrils, they thought that muscle contractions were caused by shortening of the proteins themselves. As advances in microscopy occurred, researchers discovered that during muscle cell contraction the A band does not change in length, but the I band and the H zone shorten. Since A band spans the length of the thick filaments in a sarcomere, this means the thick filaments do not change length when the muscle cell contracts. Later, it was discovered that the shortening of the I bands occurred not because thin filaments contract, but because they slide past the thick filaments, moving deeper into the H zone and decreasing its width. As this occurs, adjacent A bands move closer together and thus the

sarcomere shortens. This was called the sliding-filament theory (Huxley and Hanson, 1954, Huxley and Niedergerke, 1954). During muscle contraction, the mechanism that drives the sliding of thick and thin filaments past one another is called cross bridge cycle (Fig 1.10, Marieb EM, 2010).

Cross bridge formation or attachment of myosin heads to actin requires Ca^{2+}. Tropomyosin is a filamentous protein arranged parallel to the actin filament (Fig 1.5a). Troponin on the other hand is a globular protein complex with three subunits; troponin inhibitory component (TN-I), tropomyosin binding component (TN-T) and Ca^{2+} binding component (TN-C). The TN-T subunit binds the troponin complex to tropomyosin at gaps along the actin filament. During the resting state where the concentration of Ca^{2+} is around 100 nM, tropomyosin molecules block the myosin binding sites on actin, thus inhibiting the interaction of actin and myosin (Germann WJ, 2005, Marieb EM, 2010). With the release of Ca^{2+} from SR during the initiation of muscle contraction the concentration of Ca^{2+} peaks at about 1 μM and at this level, Ca^{2+} binds to TN-C and triggers a conformational change in TN-I which allows the tropomyosin to move so that the myosin-binding sites on actin are exposed. To activate its group of seven actins, a troponin must bind to two Ca^{2+} ions, change shape, and then roll tropomyosin into the groove of the actin helix, away from the myosin-binding sites. In short, the tropomyosin "blockade" is removed when sufficient Ca^{2+} is present. Once the myosin binding sites are exposed, the events of the cross bridge cycle occur in rapid succession (Marieb EM, 2010).

The sliding of thin filaments continues as long as the Ca^{2+} signal and adequate ATP are present. In skeletal muscle, when nerve impulses are delivered rapidly, intracellular Ca^{2+} levels increase greatly, due to successive "puffs" or rounds of Ca^{2+} released from the SR (Marieb EM, 2010) .

1)

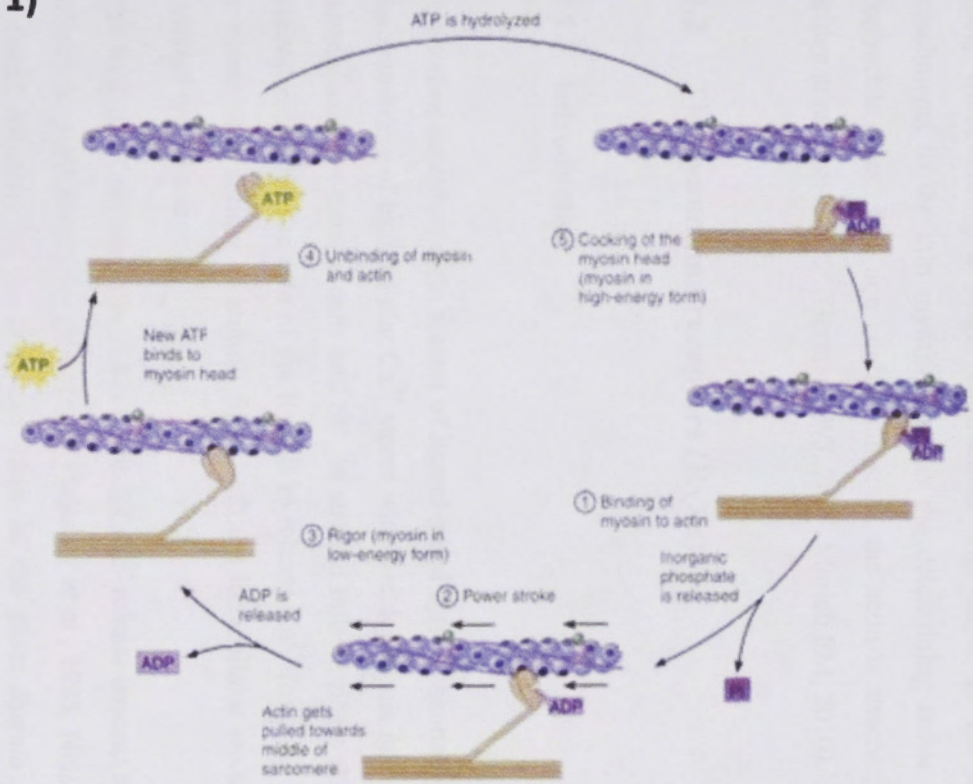

2)

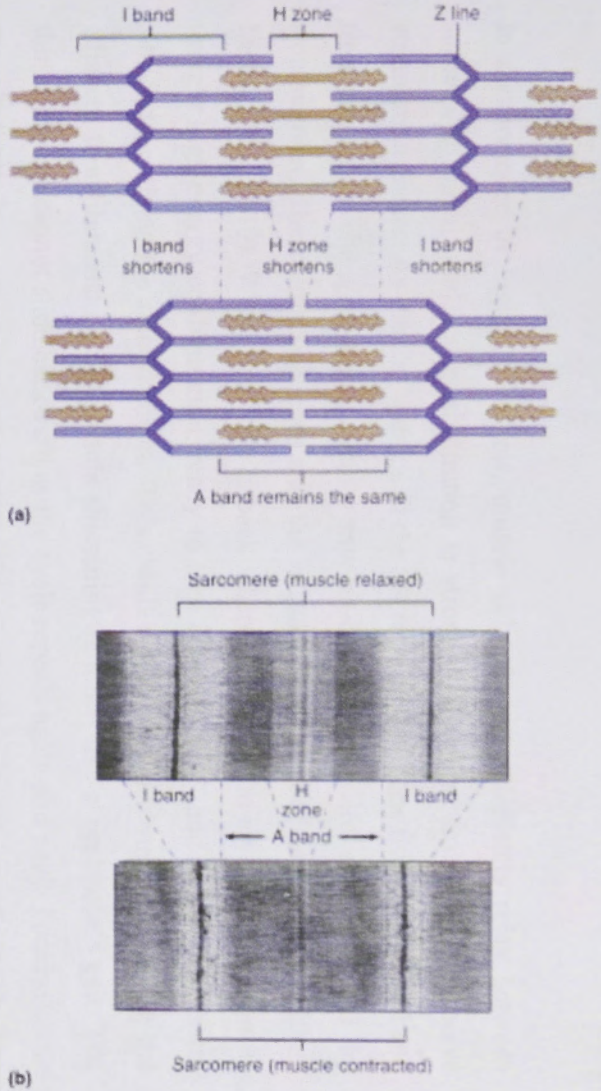

Fig 1.10: 1) The cross bridge cycle. 2) Sliding filament model of muscle contraction. (a) A schematic drawing. (b) A photomicrograph showing the relative positions of the thick and the thin filaments in sarcomeres in a relaxed muscle(top) and a contracted muscle (bottom). Adapted from (Germann WJ, 2005).

In the presence of high Ca^{2+} levels, muscle cells do not completely relax between successive stimuli and Ca^{2+}concentration is stronger and more sustained until nerve stimulation ceases. As the Ca^{2+} pumps of the SR reclaim Ca^{2+} ions from the cytosol and troponin again changes shape, actin's myosin-binding sites are again covered by tropomyosin. The contraction ends and the muscle fiber relaxes (Germann WJ, 2005, Marieb EM, 2010). When the cycle is back where it started, the myosin head is in its upright high-energy configuration, ready to take another "step" and attach to an actin site farther along the thin filament. This "walking" of the myosin heads along the adjacent thin filaments during muscle shortening is much like a centipede's gait. The thin filaments cannot slide backward as the cycle repeats again and again because some myosin heads are always in contact with actin. Contracting muscles routinely shorten 30-35% of their total resting length, so each myosin cross bridge attaches and detaches many times during a single contraction. The angle of the myosin cross bridge attachments to the thin myofilaments is the determining factor in the generation of contractile force. In a non contracting state, the actin is attached to the myosin cross bridge at an angle of 45° (Germann WJ, 2005, Marieb EM, 2010).

1.2 The ryanodine receptors (RyRs).

1.2.1 Introduction

Ryanodine receptors form a class of ligand-gated cation channels that are embedded in the membrane of intracellular Ca^{2+} stores within endoplasmic reticulum (ER) in smooth muscle and non-muscle cells and SR in striated muscle fibers (Dulhunty *et al.*, 2002, Meissner, 2002). The role of the RyR is to release Ca^{2+} from the intracellular stores in response to a variety of stimuli from both the intracellular environment and/or from external environment.

The RyR was first named in 1980s as the SR Ca^{2+} release channel because of its specific affinity to plant alkaloid – ryanodine. (Fleischer *et al.*, 1985, Nelson, 1987) Ryanodine is found naturally in the stem and roots of the plant *Ryania speciosa*. Ryanodine alkaloid was first isolated as a potential insecticide (Elison and Jenden, 1967, Jenden and Fairhurst, 1969) and its potent paralytic action on skeletal and cardiac muscles was

immediately evident. (Fairhurst, 1973, Nayler *et al.*, 1970) The ryanodine alkaloid was shown to inhibit SR Ca^{2+} release by binding with high affinity to a protein present in the SR membrane. The ryanodine binding protein was purified and existed in a tetrameric complex (Lai *et al.*, 1989, Dulhunty *et al.*, 2002) whose shape was subsequently visualized using electron microscopy (Lai *et al.*, 1989). Interestingly, the size and shape of the ryanodine binding protein complex was similar to that of the "feet" structures, which appear to physically link the T-tubule and SR membranes.

RyRs were initially isolated from rabbit skeletal muscle SR terminal cisternae (Inui *et al.*, 1987) and their activity was later demonstrated using native RyRs reconstituted in artificial lipid bilayers allowing their identification as the Ca^{2+} release channel of the SR (Lai *et al.*, 1988, Smith *et al.*, 1988, Coronado *et al.*, 1992, Hymel *et al.*, 1988). Incorporation of the ryanodine binding protein complex into artificial planar lipid bilayers revealed that this protein was an ion channel (Hymel *et al.*, 1988). The RyR channel is a poorly selective Ca^{2+} channel (selectivity Ca^{2+}/K^{+} ~6) with very high conductance (~700pS when K^{+} is charge carrier and ~100 pS when Ca^{2+} is charge carrier). The channel is regulated by Ca^{2+}, ATP, Mg^{2+} and caffeine. Interestingly, application of the ryanodine alkaloid locks the channel in a slow-gating sub conductance state. Openings of the ryanodine bound channel are long-lived and have smaller unit current ~1/3 or ~ 1/2 of control amplitude. Interestingly, at levels of 100 μM or more, the channel is irreversibly inhibited in a concentration and time-dependent manner with low affinity. This action of ryanodine on single RyR channel function is quite distinctive and is now often used to functionally identify the channel (Meissner, 1986, Feher *et al.*, 1988).

RyRs can be co-expressed with inositol 1, 4, 5- trisphosphate (IP_3) receptors, which form a second class of Ca^{2+} release channels found principally in smooth muscle and non-muscle cells, but are also present in the heart and skeletal muscle fibers. Both share structural similarities; high homology at the carboxy terminal sequences that form the channel pore, and functional similarities including Mg^{2+}, Ca^{2+} and ATP regulation. RyRs however, have higher conductance than IP_3Rs. Therefore, they are employed in situations that require fast release of larger quantities of calcium such as muscle EC coupling (Foskett *et al.*, 2007, Koulen and Thrower, 2001).

1.2.2 Isoforms of ryanodine receptors

Three isoforms of RyRs encoded by distinct genes have been identified in mammals with distinct tissue distribution. There is a 67-70% average amino acid sequence homology among the three RyR isoforms (Takeshima, 1993, Nakai *et al.*, 1990). RyR1, which is predominantly expressed in the skeletal muscle, was the first to be reported and it was fully sequenced in 1989 (Marks *et al.*, 1989). It has also been reported in some parts of the brain; most predominantly in purkinje cells of the cerebellum (Kuwajima *et al.*, 1992, Mori *et al.*, 2000), smooth muscle (Fritz *et al.*, 2007, Li *et al.*, 2009) and human dendritic cells (Uemura *et al.*, 2007). RyR2 is the dominant form in cardiac muscle (Yano *et al.*, 2006). It also has a higher distribution in the brain than the other isoforms (Giannini *et al.*, 1995). RyR3 was first identified in the brain (Hakamata *et al.*, 1992), but is ubiquitously distributed in smooth muscle and non-muscle cells (Ogawa *et al.*, 2000) and in small amounts in skeletal muscle, particularly in neonatal muscle (Bertocchini *et al.*, 1997).

The high amino acid sequence identity mentioned above is observed particularly in their C-terminal membrane spanning regions. Major sequence differences however do exist in three regions, which are known as divergent regions DR1, DR2, and DR3. (Zhang *et al.*, 2003). The DR1 region is between RyR2 residues 4210–4562 (or RyR1 residues 4254–4631); the DR2 region is between RyR2 residues 1353–1397 (or RyR1 residues 1342–1403) and the DR3 region is between RyR2 residues 1852–1890 (or RyR1 residues 1872–1923) (Fig 1.11). These divergent regions are likely to be responsible for some of the major functional differences between the three mammalian RyR isoforms. The three isoforms of the RyR, along with three isoforms of the IP_3 receptor (also products of 3 separate genes), are expressed in various combinations in a tissue specific and developmentally regulated manner (Mikoshiba, 2007, Bezprozvanny, 2005). In smooth muscle and in the central nervous system for example, the isoform combinations of IP_3 receptors and RyRs are highly region specific. In addition there are numerous splice variants of each of the three IP_3R and RyR genes, which are also expressed in a developmentally regulated and tissue specific manner and can have specific functional characteristics that differ widely between variants (Kimura *et al.*, 2005). Therefore there is enormous variety in the characteristics of Ca^{2+} release from intracellular stores and the Ca^{2+} release process can be fine tuned for the specific functional requirements of different tissues at different stages of development.

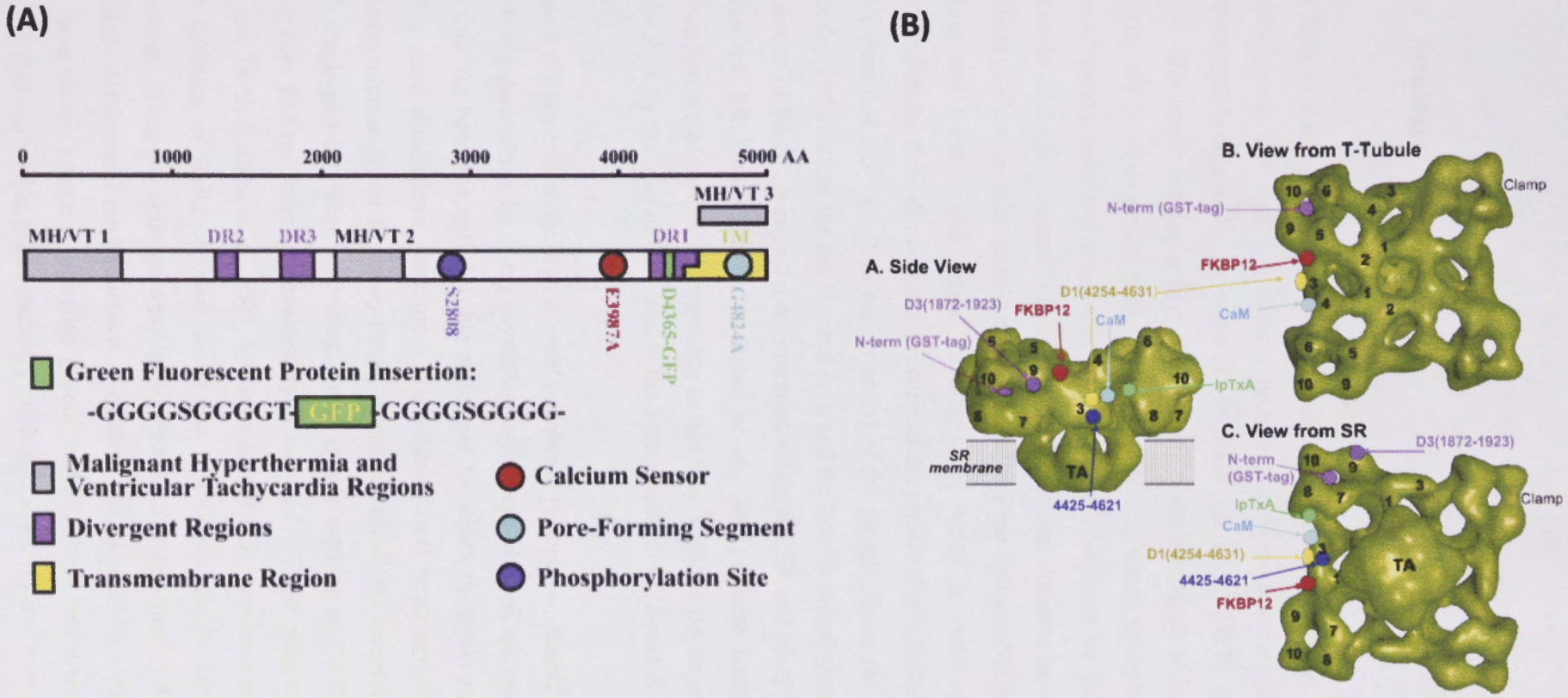

Fig 1.11: **(A)** Divergent regions of cardiac ryanodine receptor, DR1, DR2 and DR3 (Liu *et al.*, 2002). **(B)** Three dimentional structure of the skeletal ryanodine receptor, with some key sites for protein interactions. D1 (DR1) and D2 (DR2) indicate divergent regions between RyR1 and RyR2 (Bers, 2004).

1.2.3 Structure

The RyR is the largest ion channel protein identified to-date with a single cation-selective pore. The RyR ion channel protein is a homotetramer composed of four subunits each with a molecular mass of ~560KDa (Liu *et al.*, 2002). The protein spans the SR membrane and has a huge cytoplasmic assembly which is formed by the N-terminal 4/5 (~ 4000 amino acids) of the protein and which contains a multitude of ligand binding sites and regulatory domains that co-operate to control the gating properties of the ion channel (Fig 1.11B). Ten structural domains have been identified in the cryo-electron microscopic reconstructions of the cytoplasmic assembly in each subunit and these provide ligand binding sites, which in many cases have been identified on the three dimensional structure of the protein (Fig 1.12B, Liu *et al.*, 2002). The C-terminal $1/5^{th}$ (~ 1000 amino acids) of the protein forms the trans-membrane assembly and contains the ion channel pore and the tiny "luminal" domain which faces the lumen of the SR, senses the environment within the SR and binds to other proteins within the SR lumen (Fig 1.12, Beard *et al.*, 2009). These luminal sensors and interactions are of particular importance in that they facilitate the ubiquitous regulation of the RyR by the load of Ca^{2+} ions in the intracellular store (Beard *et al.*, 2009, Laver, 2007).

Since RyRs are extremely large integral membrane proteins, an atomic structure has not yet being determined by X-ray crystallography. Cryo-electron microscopy (cryo-EM) has thus far been the only feasible technique by which to obtain information about RyR's three dimensional structures. Three-dimensional structures were obtained by electron microscopy of frozen-hydrated, detergent-solubilized receptors in conjunction with single-particle image processing. Three groups working on the structure of RyR1 using cryo EM spectroscopy revealed RyR1 maps of different resolutions, 9.6°A, 10.3 °A and 14 °A (Ludtke *et al.*, 2005, Samso *et al.*, 2005 & Serysheva *et al.*, 2005). Cryo EM structure of RyR2 reported so far has a lower resolution compared to RyR1 structures. Wang and colleagues published the cryo EM structures of RyR2 in 2011 and the three dimentional reconstructions were estimated to be 27 °A (Wang *et al.*, 2011). All three of the known mammalian genetic isoforms have two major components; a large, 4-fold symmetric, prism-shaped, cytoplasmic assembly that accounts for greater

than 80% of the receptor's mass (290A° x 290A° x 130A°) and is composed of at least 10 discrete, loosely packed domains, and a transmembrane region (120A° x 120A° x 70A°) whose dimensions lead us to conclude that very little of RyR's protein mass is present on the luminal side of the sarco/endoplasmic reticulum (Fig 1.12, Liu *et al*, 2004).

It is not clear why higher resolution has not been attained by cryo-EM for RyR2, but it is suspected that there is some inherent instability in RyR2's structure following detergent solubilization and purification away from its natural membrane environment (Liu *et al*., 2004).

According to the cryoelectron microscopic model, DR2 and DR3 should be located in the cytoplasmic assembly, which is known to interact with regulatory ligands such as calmodulin, FK506 binding protein and dihydrophyridine receptor on the plasma membrane (Fig 1.11B and 1.12A). Previous results from many groups predict that DR1 contain one of the membrane traversing segments of RyR in all of the proposed models of the transmembrane topology (Liu *et al*, 2002, Takeshima *et al*., 1989, Zorzato *et al*., 1990, Otsu *et al*., 1990, Nakai *et al*., 1990) specifically residues 4499-4519 in RyR2.

Recently published studies employed GFP insertion strategy to map the DR1 region to the handle in sub-region 3 of RyR2 (Liu et al., 2002). DR2 and DR3 regions were mapped to the cytoplasmic clamp sub region domains 6 and 9 (Liu et al., 2004, Zhang et al., 2003).

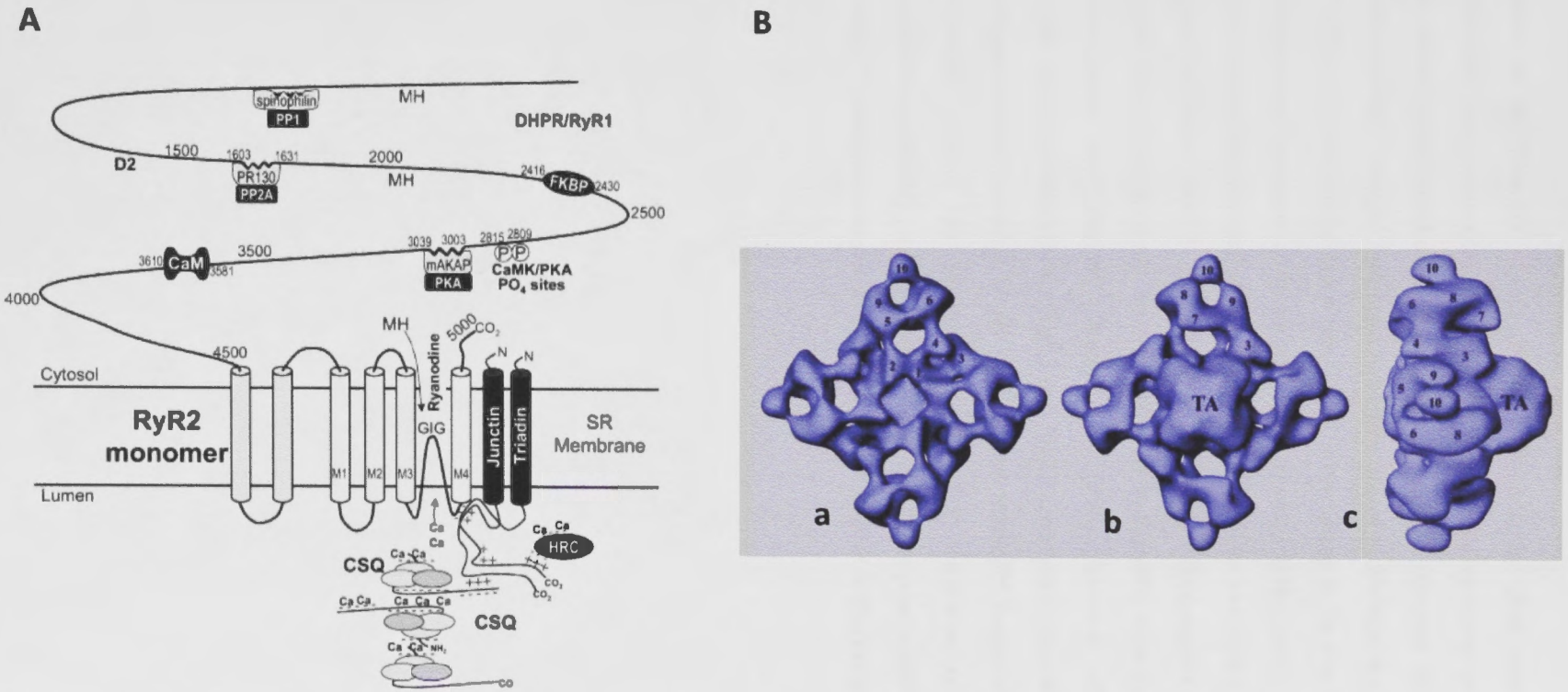

Fig 1.12: A) Cardiac RyR with interaction sites of some associated proteins. M1-M4 indicate the four transmembrane domains with a putative pore region (GIG).(Bers, 2004).The intra SR and transmembrane domains are the apparent sites of interaction of triadin and junction. Most other ligands, calmodulin (CAM), Ca2+, FK-506 binding protein (FKBP), protein kinase A (PKA), phosphatises 1 & 2A (PP1 &p PP2A) and imperatoxin A bind to the molecular mass between the SR and sarcolemmal membrane. B) Three-dimensional structures of RyR2 presented in three different views, a: Top view from cytoplasmic surface that interacts with the transverse tubule; b: Bottom view from sarcoplasmic reticulum lumen; c: side view which shows that RyR2 has a small transmembrane assembly (TA) and a large cytoplasmic assembly. Numerals on the cytoplasmic assembly indicate the distinguishable domains (Liu *et al*; 2002).

Sharma *et al* (Sharma *et al.*, 1998) published the first report on cryo electron microscopy and image analysis of the cardiac ryanodine receptor in 1998 in which the three dimentional structure of the cardiac ryanodine receptor was compared with the skeletal muscle isoform. Averaged two dimentional projection images for RyR2, as well as RyR1, prepared under same conditions, were found to be nearly identical in overall dimentions and appearance at the resolution attained at that time, ~30 °A. A difference image formed by subtracting the RyR1 average from the RyR2 image showed some regions of both positive and negative differences (presence or absence of certain regions) in density between the two isoforms specifically near corners of the receptor referred to as "clamp region" (Sharma *et al.*, 1998). The most striking feature observed was the similarity between the RyR1 and RyR2 reconstructions. Both consist of a trans-membrane assembly and a larger cytoplasmic assembly comprising multiple domains (numbered in Fig 1.13). Differences appeared in the corner (clamp) regions of the cytoplasmic assembly where domains 8,9 and 10 appear somewhat larger, whereas domain 7 is somewhat smaller in RyR2 relative to RyR1(Sharma *et al.*, 1998).

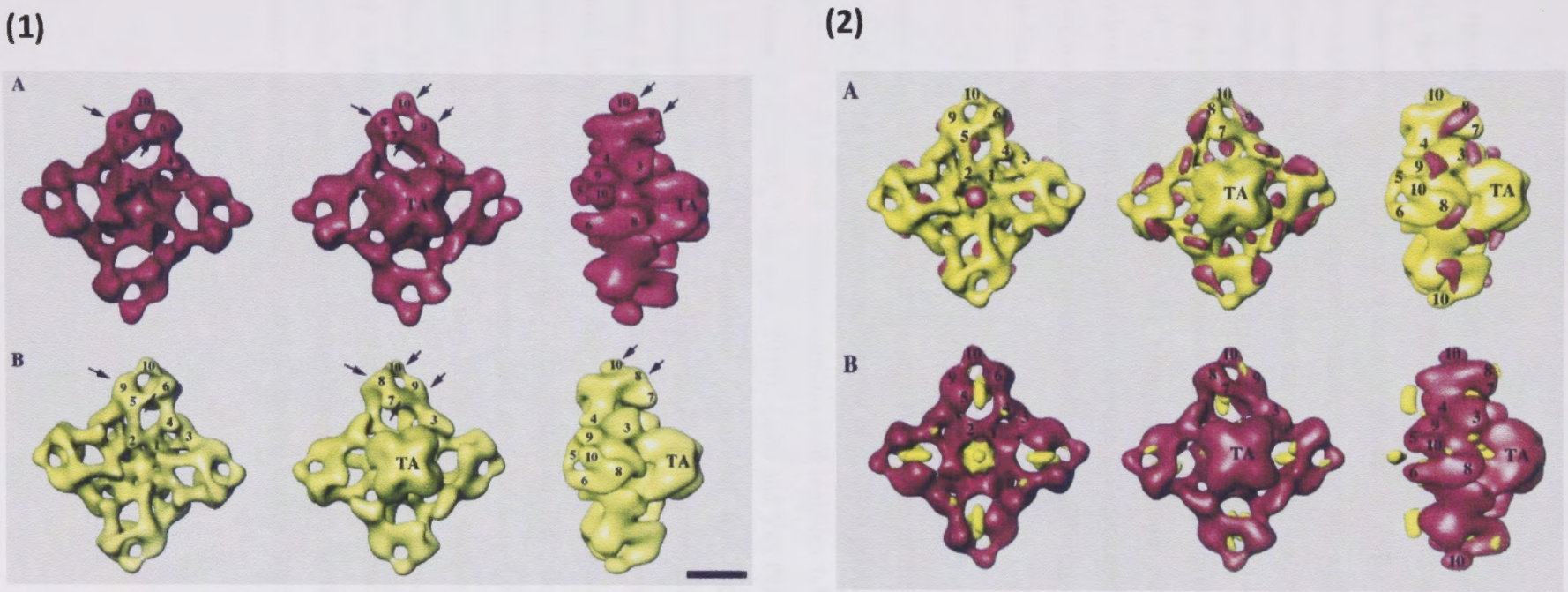

Fig 1.13. **(1)** Three-dimensional surface representation of RyR2 (*A*) and comparison with RyR1 (*B*). Leftmost figure is the surface that would face the cytoplasm and the apposing transverse tubule in a dyad-triad junction. The *middle* group face the sarcoplasmic reticulum, and the rightmost group shows RyR2 and RyR1 in a side view. *Arrows* point to obvious differences between RyR2 and RyR1. **(2)** Differences between RyR1 and RyR2 from three-dimensional reconstructions. The three-dimensional reconstructions were subtracted and contoured to show the largest differences in density between the two. *A*, the RyR1 reconstruction (*yellow*) is shown with the differences corresponding to extra density in RyR2 superposed in *rose*. *B*, the RyR2 reconstruction with the differences corresponding to excess density in RyR1 superposed in *yellow*. The putative structural domains are labeled with numerals *1–10*. *TA*, transmembrane assembly. *Scale bar,* 100 Å. (Sharma *et al*., 1998)

The region between domains 5 and 6 appears to be connected by a bridge of density in RyR1 that is absent or weaker in RyR2. Fig 1.13 shows the RyR1 reconstruction with differences attributable to extra density present in RyR2. Fig 1.13(2B) shows RyR2 superimposed with differences corresponding to additional density in RyR1. Furthermore, the regions within each clamp showing the greatest differences in the two-dimensional projection averages (images not shown here) of RyR1 and RyR2 correlate well in position, with the differences in the three-dimensional reconstructions (Sharma *et al.*, 1998). Interestingly, the clamp regions are thought to interact with the dihydropyridine receptor in skeletal muscle (Wagenknecht *et al.*, 1996). Therefore, differences in these regions may contribute to the differing mechanisms of EC coupling in skeletal and cardiac muscle.

Amador *et al* in 2009 reported the crystal structure of the N-terminal 210 residues of RyR1 at 2.5 °A resolution while Tung *et al* in 2010 published the crystal structure of regions of RyR1 which encompass amino acid residues 1-559 also at 2.5 °A resolution (Amador *et al.*, 2009, Tung *et al.*, 2010). Lobo and Van Petegem (2009), also published the crystal structure of N-terminal domain of RyR2 (residues 1-217) at 2.55°A resolution (Fig 1.14). The crystal structure contains two chains in the asymmetric unit. Central in the N terminal domain structure is a β-trefoil core, consisting of 12 β strands, folded into three similar β-β-β-loop-β (trefoil) units which is held together through extensive hydrophobic packing (Lobo and Van Petegem, 2009). Although, several differences were noted, these studies indicated that both RyR1 and RyR2 have the same overall fold and relative orientation of the helix to the β-trefoil core in the N-terminal domain (Song *et al*, 2011). This crystal structure of the N-terminal domain of RyR2 is only a step closer towards the understanding of the structure of the complete RyR2 structure. Therefore, a higher resolution structure of the full length RyR2 structure is necessary to understand the largest ion channel known todate.

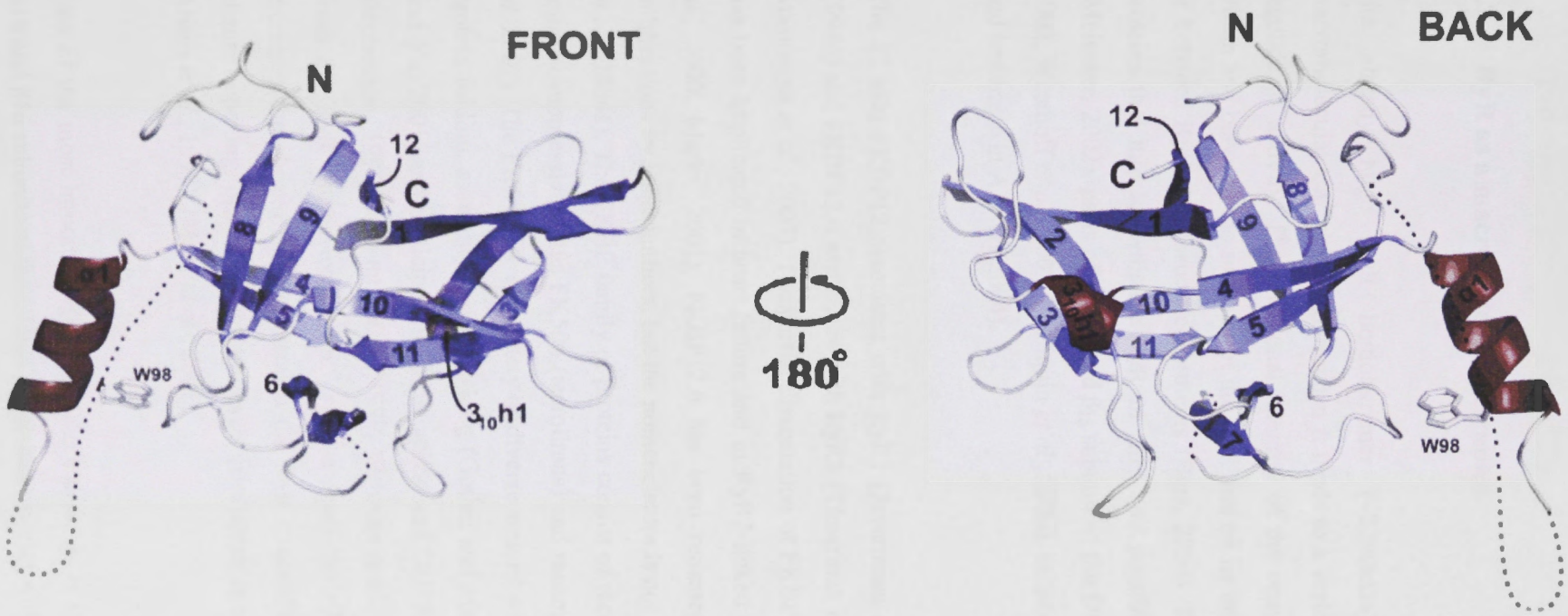

Fig 1.14: Overall structure of the RyR2 N-terminal domain showing α helix (α1) and 3_{1o} helix (3_{1o}h1) in red, β strands in blue and loops in white. Amino acids in a 3_{1o} helix are arranged in a right-handed helical structure, each amino acid corresponds to a 120° turn in the helix Amino acids in a 3_{1o} helix are arranged in a right-handed helical structure, each amino acid corresponds to a 120° turn in the helix and the N-H group of an amino acid forms a hydrogen bond with the C=O group of the amino acid three residues earlier. This repeated i+3 → i hydrogen bonding defines a 3_{1o} helix. Two views, front and back rotated at 180° around vertical axis are shown. Loops present in the construct but not modelled are shown as dotted lines. W98 in the α1- β5 loop is shown in stick representation. This tryptophan residue, and the loop to which it belongs, are unique to RyR2. (Lobo and Van Petegem, 2009)

1.2.4 RyR as a macromolecular complex

The already huge RyR homotetramer (~2200kDa) forms the even larger macromolecular Ca^{2+} release unit when it binds to a variety of associated proteins that regulate its activity. The functional integrity of the complex depends on interactions within and between the subunits of the RyR and on its interaction sites within the RyR or between RyR and associated proteins (Bers, 2004). There are several cytoplasmic proteins that interact with the RyR *in vitro* and possibly *in vivo*; the FKBP family (Meissner, 2002), parts of the α_1 and β_{1a} subunit of the DHPR and Homer (Feng *et al.*, 2002, Westhoff *et al.*, 2003, Pouliquin *et al.*, 2006), calmodulin 1, phosphatases 1 & 2A and imperatoxin A (Bers,2004).

The 12 kDa FKBP12 associates with RyR1 (Jayaraman *et al.*, 1992, Brillantes *et al.*, 1994a) and FKBP12.6 associates with RyR2 (Timerman *et al.*, 1996, Barg *et al.*, 1997, Masumiya *et al.*, 2003). The partial dissociation of FKBP12.6 from the RyR2 complex has been implicated in heart failure and in RyR2-linked cardiac arrhythmias (Yano *et al.*, 2000, Marks, 2001). FKBP12.6 has been renamed calstabin2 in some recent publications by some authors, but the nomenclature is not generally accepted. (Wehrens *et al.*, 2004a). The FKBP family of proteins consist of receptors for the commonly used immunosuppressive drugs FK506 (tacrolimus) and rapamycin (sirolimus) (Dulhunty *et al*, 2007). The FKBPs have a variety of diverse actions which also include assistance in protein folding, assembly and trafficking (Gothel and Marahiel, 1999, Schiene-Fischer and Yu, 2001) and participate in EC coupling and DHPR-RyR interactions (Lamb and Stephenson, 1996, Dulhunty *et al.*, 1999, Wehrens *et al.*, 2003). Dissociation of FKBP from the RyR causes excess Ca^{2+} release from the SR (McCall *et al.*, 1996) and increases the current flowing through the RyR channel by enhancing the duration of channel opening, often to substate levels (Brillantes *et al.*, 1994b, Ahern *et al.*, 1994, Ahern *et al.*, 1997), (Marx *et al.*, 2001).

One of the most important RyR regulatory proteins is the DHPR. In skeletal muscle, α1S and β1a subunits of the DHPR physically interact with RyR1 (Tanabe *et al.*, 1990,

Nakai *et al.*, 1998a,b), (Coronado *et al.*, 2004, Kugler *et al.*, 2004). This physical "skeletal" type of EC coupling is vastly different from EC coupling in the heart, in that

there is no requirement for external Ca^{2+} ions to enter and activate the RyR1 channel whereas cardiac EC coupling is absolutely dependent on the entry of external Ca^{2+} (Fig.1.6). Although there is no physical connection between the RyR and DHPR in the heart, the cardiac isoform of the RyR can interact with parts of the DHPR α1 subunit *in vitro* (Dulhunty *et al.*, 2005a, Dulhunty *et al.*, 2005b).

Homer is a cytoplasmic protein that binds to and regulates the cardiac RyR (Westhoff *et al.*, 2003, Pouliquin *et al.*, 2006). It is an adaptor protein which has been implicated in Ca^{2+} signalling because it can physically couple metabotropic glutamate receptors to inositol 1,4,5-trisphosphate receptors (IP3R) in intracellular Ca^{2+} stores and thereby regulate the IP3R Ca^{2+} channel activity (Tu *et al.*, 1998, Xiao *et al.*, 2000, Ango *et al.*, 2001).

The RyR macromolecular complex extends into the SR lumen. Luminal proteins associated with the complex include CSQ, the main luminal Ca^{2+} binding protein and triadin and junctin, the anchoring proteins for CSQ, retaining CSQ in vicinity of RyRs. There are several other Ca^{2+} binding proteins and small molecules which may or may not bind to the RyR, but play a role in RyR regulation and intracellular Ca^{2+} homeostasis. These are JP-45, sarcalumenin (SLM), calreticulin, calumenin and CSQ-like proteins (Beard *et al*, 2004, Anderson *et al*, 2006).

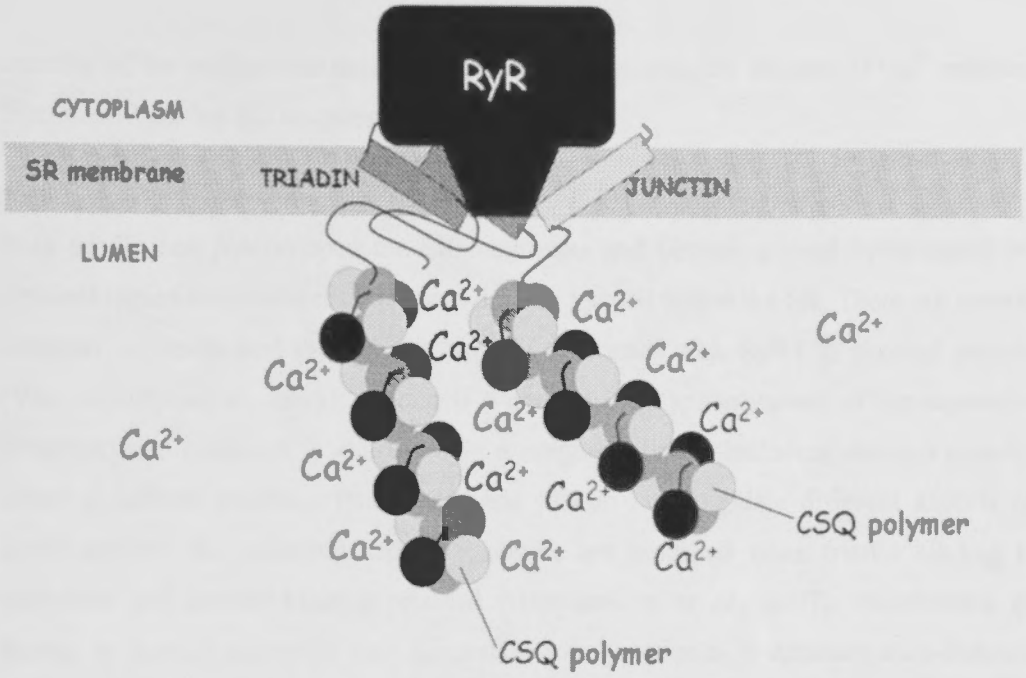

Fig. 1.15: An illustration of the interaction between RyR, CSQ polymers, triadin and junctin. The RyR, triadin and junctin span the SR membrane, while junctin binds only to the luminal residues. The C-terminal tails of both the anchoring proteins bind to the CSQ polymer. Adapted from (Dulhunty *et al.*, 2007).

The main Ca^{2+} binding protein in the SR is CSQ. CSQ is homologous with the endoplasmic reticulum Ca^{2+} binding protein, calreticulin. CSQ1 is predominantly expressed in fast twitch skeletal muscle. Whereas, CSQ2 is predominantly expressed in slow-twitch skeletal and cardiac muscle (Dulhunty *et al*, 2007). CSQs are acidic glycoproteins that constitute 27% of junctional SR protein content. CSQ does not only bind Ca^{2+} but also regulates Ca^{2+} release from the SR by communicating with the RyR via two other key proteins, triadin and junctin (Fig. 2). There is evidence that CSQ may be able to bind directly to the RyR and regulate its activity in the absence of triadin and junctin (Herzog *et al.*, 2000). CSQ in muscle is essential for normal Ca^{2+} signalling since mutations in CSQ can lead to arrhythmias and sudden cardiac death (Lahat *et al.*, 2001, Viatchenko-Karpinski *et al.*, 2004, Terentyev *et al.*, 2006). Wei *et al* (Wei *et al.*, 2009) speculated that CSQ2 facilitated high rates of Ca^{2+} release through RyR2 during systole while CSQ1 inhibited RyR1 activity. These interactions between CSQ and the RyR are mediated by triadin and junctin (Beard *et al.*, 2002, Terentyev *et al.*, 2003). All of these studies indicate that both CSQ1 and CSQ2 not only determines the Ca^{2+} storage

capacity of the cardiac and skeletal SR, but also regulates the amount of Ca^{2+} released from the SR during EC coupling.

Both triadin and junctin span the SR membrane and contain a short cytoplasmic N-terminal region and a longer C-terminal domain located within the SR. There are several isoforms of triadin and the 95 kDa isoform associates with RyR1 in skeletal muscle (Vassilopoulos *et al.*, 2005). Junctin is a non-catalytic splice variant of the aspartate-β-hydroxylase gene and is expressed in a range of tissues including skeletal muscle. There is indirect evidence that triadin and junctin may regulate different aspects of RyR1 activity. EC coupling and Ca^{2+} release are modified when triadin binding is abolished and junctin binding retained (Goonasekera *et al.*, 2007). Knockdown of triadin in skeletal myotubes also suggests a role for triadin in depolarisation-induced Ca^{2+} release, while knockdown of junctin suggests that it has a separate role (Wang *et al.*, 2009). Triadin overexpression stimulates cardiac EC coupling and arrhythmias in transgenic mice in some studies (Kirchhof *et al.*, 2007, Terentyev *et al.*, 2005). In contrast, junctin overexpression or its down-regulation in myocytes indicates that junctin suppresses RyR2 activity (Kirchhefer *et al.*, 2003, Yuan *et al.*, 2007).

1.2.5 Ryanodine receptor regulation

RyR channels are modulated by numerous factors, including a number of physiological agents (e.g., Ca^{2+}, ATP and Mg^{2+}, calmodulin, S100A etc), various cellular processes (e.g., phosphorylation, oxidation, etc) and several pharmacological agents (e.g., ryanodine, caffeine, ruthenium red etc) (Fill *et al*, 2002). The intrinsic properties of the RyR channel include activation by 1-100 μM cytoplasmic Ca^{2+}, adenine nucleotides and caffeine, and inhibition by <1 μM or >100 μM (RyR1) to 1 mM (RyR2) cytoplasmic Ca^{2+}, and by Mg^{2+}, ryanodine and ruthenium red. Formation of such a complex, and interactions with other ligands in the cytoplasm and SR lumen, provides a multi-faceted regulation of the RyR which sets the background activity of the Ca^{2+} release channel

(Fill *et al*, 2002). The structure and function of the main regulatory ligands and components of the RyR complex are briefly reviewed below.

1.2.5.1 Regulation of RyR by Ca^{2+}

Ca^{2+} ions are by far the most important modulators of the RyR2. In the absence of other modulators such Mg^{2+} and ATP, a bell-shaped Ca^{2+} activation/inactivation curve was first obtained using SR vesicle-Ca^{2+} efflux measurements (Meissner and Henderson, 1987) and later using ^{3}[H] ryanodine binding and measurement of single channel bilayers (Meissner *et al.*, 1997). Both RyRs are activated by increasing [Ca^{2+}] from 100 nM to 1-10 μM and inhibited by a further increase to 500 μM (RyR1) or to 10 mM Ca^{2+} (RyR2) (Meissner *et al.*, 1986a, Laver *et al.*, 1997b) The bimodal dependence of RyR2 activity on the physiological activator Ca^{2+} suggests the presence of high affinity activating and low affinity inhibitory Ca^{2+} binding sites. It is generally accepted that these are located on the large cytosolic foot region of the RyRs. In addition, in single channel measurements SR luminal Ca^{2+} regulated RyR2 either by binding to luminal channel sites (Sitsapesan and Williams, 1997, Gyorke and Gyorke, 1998) or by luminal Ca^{2+} gaining access to cytosolic Ca^{2+} activation and inactivation sites (Xu and Meissner., 1998, Xu and Meissner., 2004). This was explained in detail by Laver, 2009, where he suggested that four hypothetical divalent cation sites (I_1, I_2, A and L) may regulate the gating activity of RyR2 (Fig 1.16). This article discussed the possibility that the process involved two independent mechanisms. First, Ca^{2+} binding to the L-site located in the luminal side initiates channel openings, then luminal Ca^{2+} flows through to the cytoplasmic A-site which prolongs the openings. When Ca^{2+} binds to the I_2-site, the channel is inactivated (Laver, 2009). Bhat *et al* first suggested that the activation site might be in the membrane domain (Bhat *et al.*, 1997a).

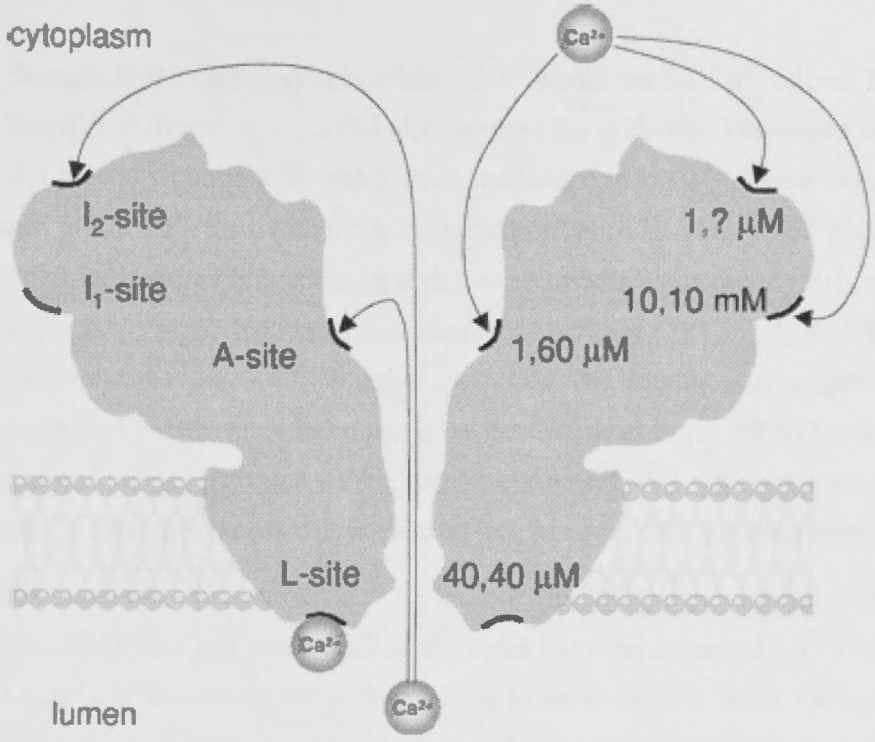

Fig 1.16: Hypothetical locations of four Ca^{2+} and Mg^{2+} regulatory sites which explain Ca^{2+} and Mg^{2+} regulation of the gating of the cardiac RyR2 are shown here. The names given to these sites are included on the left hand side and Ca^{2+} and Mg^{2+} affinities of corresponding sites are indicated on the right. Mg^{2+} affinity of the I_2 site remains unknown (?). Accessibility of cytoplasmic or luminal Ca^{2+} on these sites are shown by arrows (Laver, 2009).

The total $[Ca^{2+}]$ within the SR lumen is estimated to be ~20 mM (Fryer and Stephenson, 1996) but, with functional buffering by CSQ and other Ca^{2+} binding proteins in the SR, the free $[Ca^{2+}]$ is maintained at around 1 mM (Fryer and Stephenson, 1996, Szegedi *et al.*, 1999). This is the "resting" physiological free $[Ca^{2+}]$ and creates a strong Ca^{2+} concentration gradient between the SR lumen and the cytoplasm (with 100 nM Ca^{2+}) which ensures efficient Ca^{2+} release. Small fluctuations in free luminal $[Ca^{2+}]$ that occurr with Ca^{2+} release, could be compensated for by rapid Ca^{2+} dissociation from CSQ located in the lumen adjacent to the RyR pore (Park *et al.*, 2004). Wei *et al* (Wei *et al.*, 2009) compared the properties and regulation of RyR1 and RyR2 by CSQ1 and CSQ2 respectively. They reported that there are major differences between the two isoforms in which CSQ1 inhibits RyR1, but CSQ2 activates RyR2 and the Ca^{2+} binding to CSQ2 is 50% lower than CSQ1. They speculated that CSQ2 might facilitate high rates of Ca^{2+}

release through RyR2 during systole while CSQ1 would reduce Ca^{2+} release through RyR1. Beard *et al* (Beard *et al.*, 2009) also reported the molecular interaction of CSQ, triadin and junctin with the RyR which modulated changes in Ca^{2+} release in response to changes in the Ca^{2+} load within SR in the striated muscle. They noted triadin and junctin exert independent influences on RyR1 where triadin alone modify EC coupling while junctin alone supported functional interactions between CSQ and RyR (Wei *et al*, 2009, Goonasekera *et al*, 2007, Wang *et al*, 2009). The authors also suggested that CSQ, triadin and junctin relay information on the Ca^{2+} load in the SR to the RyR, so that resting and voltage activated Ca^{2+} release can be modified in response to changes in store load. To serve this purpose, physical coupling was suggested between proteins.

The loaded Ca^{2+} store is a prerequisite for normal SR Ca^{2+} release. Studies in skinned skeletal muscle fibres and intact cardiac myocytes show an enhanced Ca^{2+} release as luminal $[Ca^{2+}]$ is increased, but a decrease in channel activity when Ca^{2+} store is depleted (Lamb *et al.*, 2001, Lukyanenko *et al.*, 1999). As suggested by Rios *et al* (Rios *et al.*, 2006), in skeletal muscle store depletion after an action potential is minimal (50% in cardiac muscle compared to 15% in skeletal) and reduction in store Ca^{2+} does not appear to inhibit Ca^{2+} release. Therefore, it was concluded that free SR Ca^{2+} does not mediate physiological termination of Ca^{2+} release in the skeletal muscle. Launikonis *et al* hypothesized that Ca^{2+} ions adsorbed to linear polymers of CSQ constitute a proximate store (Launikonis *et al*, 2006). Building on that hypothesis Rios *et al* propose that depletion of the proximate store contributes to the robust signal needed for channel closure, and the effect is mediated by depolymerisation of CSQ (Rios *et al*, 2006).

1.2.5.2 ATP and Mg^{2+}

Cytosolic ATP is an effective RyR channel activator (Copello *et al.*, 2002,Coronado *et al.*, 1994, Smith *et al.*, 1985, Sonnleitner *et al.*, 1997, Xu *et al.*, 1996). Cytosolic Mg^{2+} is a potent RyR channel inhibitor (Copello *et al.*, 2002, Coronado *et al.*, 1994, Laver *et al.*, 1997a, Smith *et al.*, 1985, Xu *et al.*, 1996). The cytosol of most cells contains ~5 mM total ATP and ~1 mM free Mg^{2+}. This means that most ATP is in its Mg^{2+}-bound form. Free ATP (~300 μM in the cytosol) is the fraction that binds to and activates the RyR

channel (Sonnleitner *et al.*, 1997). The action of ATP and Mg^{2+} on single RyR channel function is RyR-isoform specific. Free ATP is a much more effective activator of the RyR1 channel than the RyR2 channel (Copello *et al.*, 2002, Coronado *et al.*, 1994, Smith *et al.*, 1985), (Xu *et al.*, 1996). The RyR3 channel is also less ATP sensitive than the RyR1 channel (Chen *et al.*, 1997, Jeyakumar *et al.*, 1998) The action of Mg^{2+} on single RyR channels is complex (Copello *et al.*, 2002, Laver *et al.*, 1997a). First, Mg^{2+} competes with Ca^{2+} at the Ca^{2+} activation site, shifting the Ca^{2+} sensitivity of the channel (Copello *et al.*, 2002, Coronado *et al.*, 1994, Laver *et al.*, 1997a, Xu *et al.*, 1996). Second, Mg^{2+} competes with Ca^{2+} at the low affinity Ca^{2+} inhibition site (Copello *et al.*, 2002, Laver *et al.*, 1997a). The low affinity Ca^{2+} inhibition site does not discriminate between different divalent cations, although cytoplasmic Ca^{2+} does not reach 0.2 to 10 mM levels *in vivo*. The RyR1 channel is substantially more sensitive to this action of Mg^{2+} than the RyR2 or RyR3 channels (Copello *et al.*, 2002, Jeyakumar *et al.*, 1998). In the presence of physiological levels of Mg^{2+} and ATP, RyR1 channels require less Ca^{2+} to activate than RyR2 or RyR3 channels (Copello *et al.*, 2002) (Rousseau *et al.*, 1992, Takeshima *et al.*, 1995, Xu *et al.*, 1996).

1.2.5.3 Oxidation and nitrosylation.

RyRs contain 80–100 cysteines per monomer with approximately 25–50 in the reduced state with free –SH groups (Xu *et al.*, 1998b). An additional six to eight are considered hyper-reactive, making them susceptible to modification by oxidation (Xu *et al.*, 1998b). Oxidation of critical sulfhydryls located on the cytoplasmic side of RyR affects both the gating properties of the channel and responsiveness to channel modulators, such as adenine nucleotides, caffeine, and affects Ca^{2+} and Mg^{2+} sensitivity; the channel's ability to bind calmodulin (Zhang *et al.*, 1999) and calstabin (FKBP12.6) are also affected (Aracena *et al.*, 2005). Reactive oxygen species increase Ca^{2+} efflux from cardiac SR vesicles, and calmodulin functions as a mediator of reactive oxygen species-triggered Ca^{2+} release through the RyR (Kawakami and Okabe, 1998). Endogenous nitric oxide modulates the nitrosylation of RyR and alters the channel activity. Hence, it is suggested as the physiological modulator of RyR redox state. (Xu *et al.*, 1998b). Wang *et al* suggested that SR Ca^{2+} release channel is an end target of neuronal nitric

acid synthase (NOS1) signalling (Wang *et al*, 2010). They investigated the mechanism of NOS1 modulation of RyR2 activity and found that NOS-/- myocytes displayed a decreased fractional SR Ca^{2+} release and reduced RyR2-S-nitrosylation levels. They also observed that knockout of NOS1 led to a decrease in [^{3}H] ryanodine binding to RyR2 and Ca^{2+} spark frequency. In this study, NO donor and nitrosylating agent SNAP (*S*-nitroso-*N*-acetylpenicillamine) reversed the depressed open probability of RyR2 activity and the reduced spark frequency in NOS1-/- myocytes suggesting that NOS1 signalling increases RyR2 activity via a S-nitrosylation, which contributes to the NOS-1 induced positive inotropic effect (Wang *et al.*, 2010).

The redox state of RyR2 is altered in heart failure leading to enhanced RyR2 activity, which presumably contributes to decreased SR Ca^{2+} content and induces other Ca^{2+} release abnormalities observed in heart failure (Donoso *et al.*, 2011). Heart failure is accompanied by increased oxidative stress resulting from formation of reactive oxygen species (eg, superoxide anion, hydrogen peroxide, and hydroxyl radical).(Terentyev *et al.*, 2008, Belch *et al.*, 1991, Sawyer *et al.*, 2002) (Cesselli *et al.*, 2001, Giordano, 2005) These compounds react with reactive cysteines (ie, free thiols susceptible to redox-based modifications), causing changes in RyR2 function. Sulfhydryl oxidation by various oxidizing agents has been shown to increase RyR2 open probability (Eager, 1999, Meissner, 2002, Hidalgo *et al.*, 2002, Zima and Blatter, 2006).

1.2.5.4 Phosphorylation

Phosphorylation and dephosphorylation play a key role in regulating the function of many ion channels, including RyRs. The Ca^{2+} release channel is a target protein for several kinases (including cAMP-dependent protein kinase A (PKA), protein kinase C (PKC), cGMP-dependent protein kinase (PKG) and calmodulin-dependent protein kinase II (CaMK II)) and protein phosphatases (PP1, PP2A). Ser^{2809} and Ser^{2815} in RyR2 (substrates for PKA and CaMKII) and Ser^{2843} in RyR1 (a substrate for PKA, PKG and CaMKII, (Suko *et al.*, 1993, Varsanyi and Meyer, 1995, Xu *et al.*, 1998a, Kushnir and Marks, 2010, Marx *et al.*, 2000, Wehrens *et al.*, 2004b) are the specific

phosphorylation sites identified to date. Although multiple phosphorylation sites are predicted by several groups (Hain *et al.*, 1995, Takasago *et al.*, 1991), studies using site-directed mutagenesis of RyR2 have demonstrated that PKA specifically phosphorylates Ser^{2809} (Marx *et al.*, 2000, Wehrens *et al.*, 2006, Wehrens *et al.*, 2004b) and CaMKII specifically phosphorylates Ser^{2815} (Kushnir *et al.*, 2010, Wehrens *et al.*, 2004b).

PKA phosphorylation of RyR2 activates the channel (Valdivia *et al.*, 1995), at least in part by increasing the sensitivity of RyR2 to cytosolic Ca^{2+} (Marx *et al.*, 2000). It has been proposed that PKA phosphorylation of RyR2 causes dissociation of calstabin2 (FKBP12.6) from the channel complex as a result of steric repulsion between the negatively charged phosphate group that is covalently linked to RyR2 and Asp37 on calstabin2 (Huang *et al.*, 2006, Marx *et al.*, 2000). Supporting this hypothesis, a mutant RyR2 engineered with aspartic acid in place of Ser^{2808} (RyR2-S2808D, murine RyR2) has reduced binding of calstabin2 and increased P_o at diastolic $[Ca^{2+}]$ (Wehrens *et al.*, 2006). The observation that calstabin2 depleted channels have increased P_o which can be further enhanced by PKA phosphorylation (Wehrens *et al.*, 2003) supports the proposal that PKA phosphorylation of RyR2 also enhances RyR2 activity independent of calstabin2 depletion. CaMKII phosphorylation of RyR2 at Ser^{2815} increases the P_o of RyR2 by sensitizing the channel to cytosolic Ca^{2+}, though unlike PKA this does not dissociate calstabin2 from the channel (Wehrens *et al.*, 2003).

1.2.5.5 Calmodulin

CaM is a ubiquitously expressed, highly conserved, 17 kDa protein that contains four Ca^{2+}-binding EF hands, two on each end of the protein. CaM preferentially inhibits RyR2 at $[Ca^{2+}] < 10$ mM by binding to a region on RyR2 comprising amino acids 3583–3603 (Yamaguchi *et al.*, 2003). CaM may assist in closing RyR2 after Ca^{2+} release from SR in EC-coupling (Xu and Meissner, 2004). Supporting this hypothesis, cardiomyocytes isolated from mice engineered with RyR2 lacking the CaM-binding site have prolonged Ca^{2+} transients (Yamaguchi *et al.*, 2007).

1.2.5.6 Calstabin 2 (FKBP12.6)

Calstabin2 (FKBP12.6) is a 12.6 kDa immunophilin originally identified by its ability to bind to FK506, a common immunosuppressant used in organ transplantation. FKBP12.6 has peptidyl-prolyl cis/trans-isomerase (rotamase) activity that is highly conserved among all FKBP isoforms (Marks, 1996). FKBP12 and FKBP12.6 have been renamed by some authors as calstabin1 and calstabin2 reflecting their roles as RyR1 and RyR2 Ca^{2+} channel stabilizers, respectively (calcium channel-stabilizing binding proteins) (Wehrens and Marks, 2003).

FKBP12.6 was first shown to colocalize with RyR2 in the heart (Timerman *et al.*, 1994) and dissociating FKBP12.6 from RyR2 enhanced channel Po (Kaftan *et al.*, 1996, Xiao *et al.*, 1997). Genetic deletion of FKBP12.6 enhanced SR Ca^{2+} release in isolated cardiomyocytes (Xin *et al.*, 2002). The location of the FKBP12.6-binding site on RyR2 is controversial. Using yeast two-hybrid and site-directed mutagenesis Ile2427 and Pro2428 were identified as the peptidyl–prolyl bond to which FKBP12.6 binds (Marx *et al.*, 2000). Others have challenged the findings that FKBP12.6 stabilizes the closed state of RyR2 (Timerman *et al.*, 1996, Xiao *et al.*, 2007). Chen and colleagues observed that ryanodine binding to cell lysates of HEK293 cells expressing RyR2 was similar whether or not RyR2 was co-expressed with FKBP12.6 (Chen *et al.*, 2010). Additionally, the P_o of recombinant RyR2 reconstituted in planar lipid bilayer was similar in the absence and presence of FKBP12.6 (Xiao *et al.*, 2007). Methodological differences between single channel studies including the use of different charge carriers (K^+ vs. Ba^{2+} vs. Ca^{2+}), absence or presence of a voltage across the bilayer membrane, [ATP] and [Mg^{2+}], [Ca^{2+}] in the *cis* and *trans* compartments may partially explain these conflicts. On the other hand, many other studies now suggest that FKBP12.6 modulates RyR2 activity (Chen *et al.*, 2010, Gellen *et al.*, 2008, Hu *et al.*, 2010, Noguchi *et al.*, 2008, Zhang *et al.*, 2008, Zhang *et al.*, 2009).

1.2.5.7 Ruthenium red

Ruthenium red (RR) is a potent inhibitor of SR Ca^{2+} release (Zucchi and Ronca-Testoni, 1997). It is a polycationic dye with a linear structure consisting of three ruthenium atoms with a net valence of 6. The addition of 1-10 μM RR to the cytoplasmic side of

reconstituted RyR1 and RyR2 channels in lipid bilayers induces prolonged channel closure (Rousseau *et al.*, 1996, Smith *et al.*, 1985). Multiple mechanisms are suggested for this action. RR inhibition is more effective at increasing channel close times when RyRs are less activated by cytoplasmic Ca^{2+} or ATP. In a fully activated channel in the bilayer, both cytoplasmic and luminal application of RR induces multi-level substates (but not a complete channel closure) that depended on the holding potential (Xu *et al.*, 1999). This observation led to the possibility that RR may enter the conductance pathway of the RyR from both luminal and cytoplasmic side and multiple RR molecules and binding sites may be involved in this effect (Xu *et al.*, 1999). RR may also block ryanodine-modified RyR channels in a voltage-dependent manner by binding to multiple binding sites in the conductance pore (Takeshima, 1993). RR binding sites on the RyR have been localized to sequences 1862-2094 and 3657-3776 using fragments of RyR1 with RR overlay assay (Chen and MacLennan, 1994). There is evidence suggesting that the sensitive domains for calmodulin, Ca^{2+}, and ruthenium red on the RyR1 may be adjacent or overlap, so that close interactions between these molecules can exert a coordinated effect on RyRs (Chen and MacLennan, 1994).

1.2.5.8 Ryanodine

Ryanodine is the plant alkaloid that was used to identify the Ca^{2+} release channel, and after which the RyR is named (Fill and Coronado, 1988). It binds preferentially to RyR channels in their open state with high affinity (8 nM) and locks the channels open to a substate level, while inhibiting the channel at higher concentrations (K_d 3-5 μM) (Lai and Meissner, 1989, McGrew *et al.*, 1989) and locking the RyR into a closed state. The high affinity ryanodine-binding site has been localized to the C-terminal domain of RyR1 (residue 4475-5037) (Callaway *et al.*, 1994), the region of the protein which

contains the pore (Bhat *et al.*, 1997a). The binding site on RyR2 has been identified in a smaller segment containing residues 4820-4829 (Chen *et al.*, 2002).

1.2.5.9 Dantrolene

Dantrolene is a hydantoin derivative commonly used for the treatment of the genetic disorder, malignant hyperthermia, which is caused by inherited mutations in RyR1. Importantly, dantrolene represents the only drug targeting RyR that is currently approved for acute clinical use because it is hepatotoxic in the long term (Krause *et al*, 2004). In skeletal muscle, 10–100 μM dantrolene inhibits abnormal Ca^{2+} release from the SR (Kobayashi *et al.*, 2005). The inhibition of SR Ca^{2+} release through RyR2 was also observed in cardiac muscle, but the sensitivity to dantrolene was lower than in the skeletal muscle. Recently, it has been demonstrated that dantrolene can stabilize domain–domain interactions within the RyR complex (Kobayashi *et al.*, 2005). Taken together, these data suggest that dantrolene might exert therapeutic effects in heart failure by preventing an abnormal SR Ca^{2+} leak (Wehrens and Marks, 2004). The principal disadvantages of dantrolene are its hepatotoxicity, poor water solubility and difficulties in rapidly preparing a suitable solution for intravenous administration. In hospital settings, dantrolene solutions should be warmed to improve water solubility, and an intravenous line with a blood filter system should be administered during emergency situations (Krause *et al*, 2004). Recent therapeutic developments have been suggested but none of them have yet been introduced into the clinical treatment of human MH syndrome. Dantrolene is also associated with multiple side effects and possible drug interactions and can not be used in people with many medical conditions. A lot of contradictory evidence has been published in the past about the dantrolenes binding site and its mechanism of action. Azumolene, a derivative of dantrolene which is 30 times more soluble, is a safe compound for long-term administration, but does cause a mild, reversible reaction in skeletal muscle and kidney (do Carmo *et al*, 2010). Therefore, there is a high demand for a more specific drug which has minimum side effects and drug interactions.

1.2.5.10 Glutathione-S-transferase

The glutathione transferases (GSTs) are a family of phase II detoxification enzymes that utilize glutathione in reactions contributing to the detoxification of a wide range of exogenous and endogenous compounds. These include chemical carcinogens,

therapeutic drugs and products of oxidative stress. GSTs are the subject of my investigations. Previous experiments conducted in our lab have suggested that GSTs may have a therapeutic potential in cardiac therapy. The muscle specific glutathione transferase GSTM2 inhibits the activity of cardiac ryanodine receptor (RyR2) calcium release channels with reasonably high affinity and activates skeletal RyR (RyR1) channels with lower affinity. This study addresses the effect of GSTM2 on the cardiac RyR in detail.

1.2.6 Ryanodine receptors as pharmacological targets for heart disease

Clinical and experimental studies over the past decade have provided a lot of evidence that intracellular RyR calcium release channels play a major role in the development of cardiac arrhythmias and heart failure. There are a large number of rare point mutations in RyR1 and RyR2 which disrupt the function of the ion channel and lead to abnormal Ca^{2+} homeostasis and disrupted contractile function. These point mutations are responsible for debilitating skeletal myopathies and arrhythmias in the heart, both of which can be fatal (Betzenhauser and Marks, 2010). RyR2 function can be severely compromised in heart failure and the consequential changes in RyR2 function contribute further to the severity of heart failure (Gyorke, 2009). In the majority of cases, mutations of RyR channels causes an increase in channel activity under resting conditions and this leads to higher than normal diastolic cytoplasmic Ca^{2+} concentration. Due to its central involvement in striated muscle function and the specific roles of RyR2 in the heart, the RyR is an obvious target for therapeutic intervention in cardiac disorders whether they are genetic or acquired (Dulhunty *et al*, 2011). Consequently, there is a strong desire to identify and/or develop novel pharmacological agents that may target these Ca^{2+} signalling pathways.

Of the pharmacological reagents known to directly modulate RyR channel activity, dantrolene, is routinely employed for manipulation of these channels under acute clinical circumstances (Table 1). Limitations on available drugs for therapeutic manipulation of RyR channels include (Mackrill, 2010): (1) low membrane permeability: RyRs are intracellular targets so drugs must be able to either diffuse across membranes, or be imported by cellular transporters, in order to act on these channel complexes; (2) low solubility in aqueous solutions for membrane-permeant drugs, such as dantrolene; (3) lack of specificity: for example, caffeine and local anaesthetics act on multiple systems; (4) poor selectivity between RyR subtypes; no available drug acts on just one RyR isoform; (5) low potency: for example, caffeine stimulates RyR gating in the millimolar range; (6) toxicity via direct action on RyRs: for example, effects of ryanodine on RyR gating can be complex, displaying both biphasic dose–response relationships (activating then inhibiting channel opening) and 'use-dependence' (only binding to open channels); (7) indirect toxicity: for example, dantrolene metabolites might be hepatotoxic via a mechanism independent of RyR gating: however, this hepatic toxicity is a matter of controversy, since it is not detectable in isolated hepatocytes (Krause *et al.*, 2004). Consequently, future therapeutic interventions targeting RyRs could include: discovery of novel drugs acting directly, selectively and efficaciously on single RyR isoforms; molecular genetic approaches, which might be of limited scope for RyR associated pathologies that display developmental aetiologies; and development of drugs targeting tissue-specific RyR interacting proteins.

Recent discovery by Watanabe *et al* suggested that flecainide inhibited cardiac ryanodine receptor-mediated Ca^{2+} release and prevented arrhythmias in a mouse model of CPVT. It was reported to be directly targeting the underlying molecular defect. CPVT in two human subjects who were highly symptomatic on conventional drug therapy were completely prevented by the administration of flecainide, indicating that this currently available drug is a promising mechanism-based therapy for CPVT (Watanabe *et al.*, 2009). The data published on the drug JTV519 (K201) in stabilizing FKBP/RyR interactions and improving cardiac muscle function in heart failure in mice has also shown that RyR is an effective therapeutic target for heart failure in animal models (Liu *et al.*, 2006). Another drug, Carvedilol and its new analogs also suppressed

arrhythmogenic store overload-induced Ca^{2+} release (SOICR). Carvedilol is the only beta blocker tested that effectively suppresses SOICR by directly reducing the open duration of the cardiac ryanodine receptor (Zhou et al., 2011).

Common name	Chemical nature	Effect on channel activity			Concentration range	Clinical or pharmaceutical use	Off-target or side-effects
		RyR1	RyR2	RyR3			
Ryanodine	Alkaloid	+/-	+/-	+/-	nM to mM	Unsuitable	Toxic
4-chloro-meta-cresol (CmC)	Chlorinated phenol	+	+	0	μM to mM	Fungicide Preservative	Environmental toxin, Activates respiratory burst in neutrophils
Caffeine (and congeners)	Methylxanthine	+	+	+	mM	Stimulant Food ingredient	Phosphodiesterase inhibitor, adenosine receptor antagonist.
Dantrolene(and congeners)	Hydantoin derivative	-	0	-	μM	Treatment of malignant hyperthermia, muscle spasticity, neuroleptic malignant syndrome and ecstasy intoxication.	Hepatotoxic. Peural effusion. Central nervous system and gastrointestinal side effects.
Procaine and tetracaine	Amino ester	-	-	-	μM to mM	Local anesthetic	Voltage gated sodium channel antagonists. NMDAR and 5-HT3R antagonists. Biphasic effects on GABA(A)R.
Ruthinium red	Polycationic dye	-	-	-	nM to μM	Currently none. (membrane impermeant)	Modifies TRP cation channels and mitochondrial calcium transporters.

Table 1. Pharmacological reagents that influence RyR gating directly. Such substances bind directly to motifs present within RyR monomers, or in ryanodine, to sites that are only formed in the tetrameric state. '-' indicates a decrease in open probability, '+' signifies an increase and '0' signifies no effect (Mackrill, 2010).

1.3 Glutathione transferases

The glutathione transferases (EC 2.5.1.18) have historically been called glutathione S-transferases, and it is this name that gives rise to the widely used abbreviation, GST. These enzymes contribute to the phase II detoxification pathway and form glutathione conjugates by catalysing the nucleophilic attack by reduced glutathione (GSH) on nonpolar compounds that contain an electrophilic carbon, nitrogen, or sulphur atom. Their substrates include halogenonitrobenzenes, arene oxides, quinones, and α,β-unsaturated carbonyls (Keen and Jakoby, 1978, Hayes and Pulford, 1995, Armstrong, 1997, Hayes and McLellan, 1999, Sheehan *et al.*, 2001). However, it is becoming increasingly apparent that the GSTs have a range of other functions that continue to be elucidated. GSTs have been implicated in the modulation of cell signaling kinases such as JUNK and ASK-1 (Adler *et al.*, 1999, Cho *et al.*, 2001) (Wu *et al.*, 2006), the synthesis of steroid hormones (Johansson and Mannervik, 2001), the catabolism of tyrosine (Blackburn *et al.*, 1998) (Fernandez-Canon *et al.*, 1999) and in the activation of interleukin 1β (Laliberte *et al.*, 2003). They are also implicated in the binding, sequestration and transport of hydrophobic compounds (Hayes and Pulford, 1995). Our laboratory first discovered the ability of members of GST structural family to modulate ryanodine receptor calcium release channels from cardiac and skeletal muscle. This will be discussed in detail in section 1.3.3.2.

Three major families of proteins that are widely distributed in nature exhibit glutathione transferase activity. Two of these, the cytosolic and mitochondrial GSTs form soluble enzymes that are only distantly related (Ladner *et al.*, 2004, Robinson *et al.*, 2004). The third family containing microsomal GST is now referred to as membrane-associated proteins in eicosanoid and glutathione (MAPEG) metabolism (Jakobsson *et al.*, 1999). In humans there are six MAPEG family proteins; two enzymes involved in leukotriene biosynthesis (leukotriene C4 synthase and 5-lipoxygenase activating protein), and four microsomal proteins (MGST1, MGST1-L1,MGST2, MGST3), three of which demonstrate both glutathione transferase and glutathione peroxidase activities (Jakobsson *et al.*, 1999). A further distinct family of transferases exists, represented by

the bacterial fosfomycin resistance proteins FosA and FosB (Armstrong, 2000); Only the soluble GSTs will be discussed further.

1.3.1 Soluble GSTs

1.3.1.1 Classification and nomenclature

A unifying nomenclature for the human GSTs and their corresponding genes extendable to other mammalian species has been introduced (Mannervik *et al.*, 1992). The soluble GSTs are subdivided into classes based on sequence identity where the sequence identity within a class is higher than 50% (Mannervik *et al.*, 1985). The seven mammalian classes known to date are designated by the Greek letters: Alpha, Mu, Pi, Theta, Omega, Sigma and Zeta, (Fig 1.17) and are abbreviated, Alpha (GSTA), Mu (GSTM), Pi (GSTP), Theta (GSTT), Omega (GSTO), Sigma (GSTS), and Zeta (GSTZ) (Board *et al.*, 1997, Board *et al.*, 2000, Hussey and Hayes, 1992). The subunits within a class are numbered using Arabic numerals in order of their discovery. For example, GST A3-3 is a member of the Alpha class and is a homodimer of two GSTA3 subunits. The gene for the Alpha class subunit 3 is written GSTA3. A lower case letter added as prefix can be used to specify from which species the GST comes, *e.g.*, hGSTA3-3 for the human enzyme. If allelic variants exist these are distinguished by letters. For example, the GST M1-1 variant with Lys in position 173 is called GST M1a-1a and the gene encoding this allelic variant is denoted GSTM1*A.

All these sub classes share a similar tertiary structure known as the 'GST-fold' (described in more detail in Section 1.3.1.3.) which forms the basis of a structural superfamily. Outside of this homologous group lies the Kappa class of GSTs. GST Kappa is found within the mitochondria (Jowsey *et al.*, 2003) (Pemble *et al.*, 1996) and perixosomes (Morel *et al.*, 2004) of cells, and is excluded from the cytoplasm. In contrast to cytoplasmic GSTs, the structure of the Kappa class varies from the canonical GST-fold.

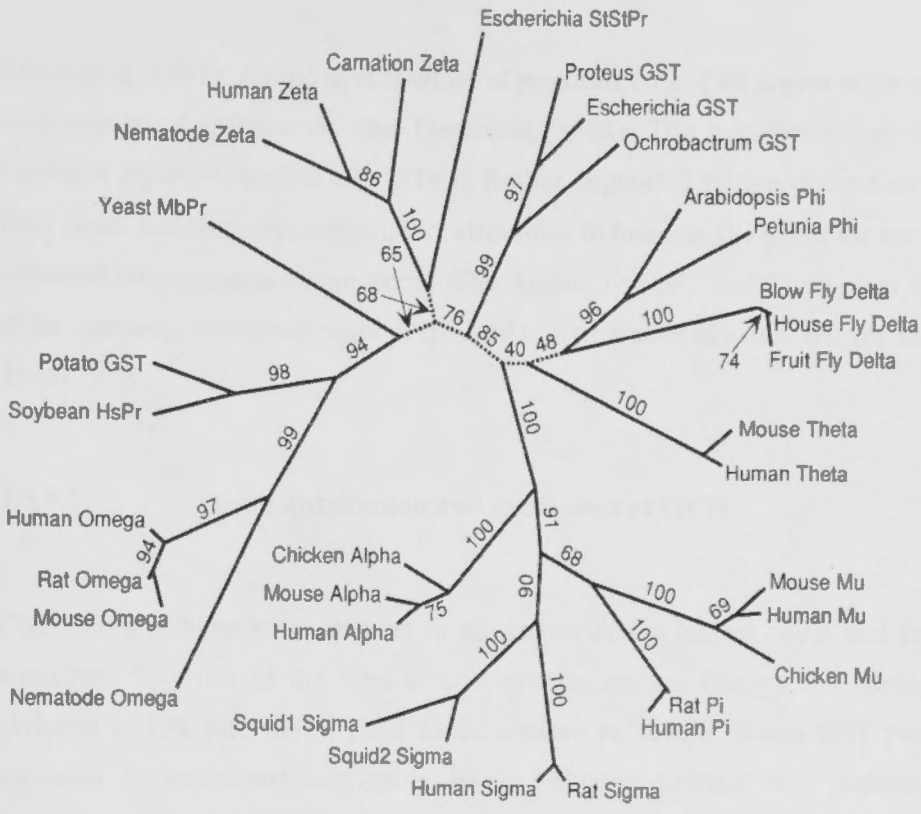

Fig 1.17: An unrooted phylogeny showing the most likely relationship between representative GST and GST-like amino acid sequences (Board *et al.*, 2000).

There are no clearly established criteria concerning the extent of sequence similarity required for placing a GST in a particular class. As mentioned before, it is generally accepted that GSTs share greater than 50% identity within a class, and those with less than 30% identity are assigned to separate classes. Much emphasis tends to be placed on the primary structure of the N-terminal domain because, within the classes, this region tends to be better conserved than others, as it includes the active site. The N-terminal region contains a catalytically essential tyrosine, serine or cysteine residue that interacts with the thiol group of GSH (Dirr *et al.*, 1994, Liu *et al.*, 1992, Atkins *et al.*, 1993). In addition, substrate and inhibitor specificity, as well as tertiary and quaternary structural properties, are considered to classify GSTs (Mannervik *et al.*, 1985, Sheehan *et al.*, 2001). Each subfamily may include as many as five separate, highly homogeneous, polypeptides, which may share greater than 90% identity (Hayes and Pulford, 1995,

Rowe *et al.*, 1998). Amino acid residues at positions 60 and 80 appear to be particularly well conserved (Mannervik and Danielson, 1988). The hypothesis that the classes represent separate families of GSTs is further supported by the distinct structures of their genes and their chromosomal localizations. In humans, the genes for each class are clustered on a separate chromosome. The Alpha-, Mu-, Pi- and Theta-class GST genes differ markedly from each other in size and in intron/exon structure (Hayes and Pulford, 1995).

1.3.1.2 Tissue distribution and expression of GSTs

GST enzymes have been detected in all tissues of the human body, and in the liver constitute 5 - 10% of the total soluble protein content (Hayes and Strange, 2000) (Whalen and Boyer, 1998). Each tissue appears to have a unique GST profile, with variation in isoenzyme expression levels between different cell populations. For example in the liver, GSTP1 is limited to epithelial cells, GSTM1 to hepatocytes (Strange *et al.*, 1989) and GSTT1 to bile duct epithelial cells and the nucleus of hepatocytes (Strange *et al.*, 1989). The cellular distribution of GST isoenzymes is thought to reflect the xenobiotic challenge potentially faced by a specific cell population. The pi-class enzyme is the most widely distributed isoenzyme and usually the most abundant. The expression of the different isoenzymes is highly tissue-specific. For example, the alpha class enzyme is the major isoenzyme in the human liver and kidney, whereas the pi-class enzyme is predominant in placenta, erythrocytes, breast, lung and prostate. GSTM2 (previously termed GST4) is specifically expressed in human heart and skeletal muscle (Board *et al.*, 1988). GSTs appear to be fairly ubiquitous amongst aerobic organisms (Wilce and Parker, 1994).

1.3.1.3 The structure of GSTs

The first crystal structure of a GST was published in 1991 (Reinemer *et al.*, 1991). Today, crystal structures are available for all of the soluble GST classes. The three-dimensional structure of human GST has been determined for GST A1-1

(Sinning *et al.*, 1993), GST A4-4 (Bruns *et al.*, 1999), GST M1a-1a (Patskovsky *et al.*, 1999b), GST M2-2 (Raghunathan *et al.*, 1994), GST M3 -3 (Patskovsky *et al.*, 1999a), GST O1-1 (Board *et al.*, 2000), GST P1-1 (Reinemer *et al.*, 1992), GST T2-2 (Rossjohn *et al.*, 1998), GST Z1-1 (Polekhina *et al.*, 2001) and hGSTK (Li *et al.*, 2005). The crystal structures of GSTs are shown in Fig 1.18.

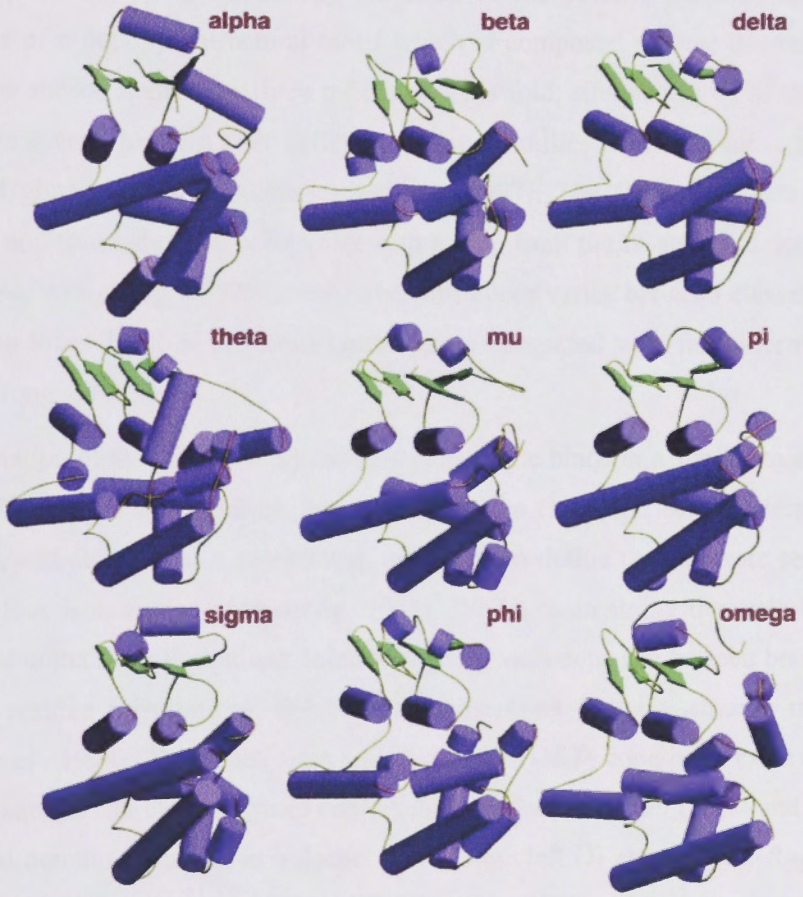

Fig 1.18: Arrangement of secondary structures of members of the GST superfamily. Adapted from (Board *et al.*, 2000). Coordinates of all nine structures were superimposed and then pulled apart for clarity. Helices are represented as cylinders, and β-strands are represented as arrows.

The cytoplasmic GST classes are comprised of around 200 to 240 amino acids, ranging in molecular weight from 17 to 28 kDa (Mannervik and Danielson, 1988). Despite the relatively low sequence similarity between GST classes, each protein shares the same fundamental structure consisting of two domains connected by a short linker region which present a V-shaped interface. Despite large differences among the amino acid sequences of different soluble GSTs, less than 10% being strictly conserved, all isoenzymes have a similar protein fold consisting of two domains. The N-terminal domain, making up approximately one-third of the protein, contains the G-site and consists of a βαβαββα structural motif which is composed of four β–strands arranged into two sheets, flanked by three α-helices. This fold, similar to that of thioredoxin, is found in several proteins from different enzyme families which appear to have evolved to bind glutathione or cysteine (Armstrong, 1997). The C-terminal domain is all α-helical and forms the H-site, together with a loop from the N -terminal domain (Dirr *et al.*, 1994, Armstrong, 1997). The number of helices varies between classes, in keeping with the lower level of sequence conservation compared with the N-terminal domain (Armstrong, 1997).

Examination of the structures shows that glutathione binds in a similar manner to all of the different GSTs. In contrast, the structure of the H-site varies considerably between classes, and also within a given class, and helps to define the substrate selectivities of the various isoenzymes (Armstrong, 1997). Whilst maintaining the overall N- and C-terminal domain configurations, minor structural variations can be seen between classes due to residue substitutions, deletions and insertions in the β–strands and α–helices (Dirr *et al.*, 1994). The Alpha class and Theta class GSTs contain an extra C-terminal α -helix, and the Mu class enzymes contain an extra loop between the β2 and α2 in the N-terminal domain, resulting in a deeper active site cleft (Ji *et al.*, 1992, Raghunathan *et al.*, 1994, Wilce and Parker, 1994). GST Omega is distinguished by an extra stretch of proline-rich amino acids in the N-terminal domain and two extra helices in the C-terminal domain (α9 and α10) which create a more open active site and a relatively large and polar H-site (Board *et al.*, 2000). All of these structural elements are located close to the substrate-binding sites and seem to contribute to a more constricted active site of the Alpha, Mu and Theta enzymes compared to enzymes from the Pi and Sigma families (Armstrong, 1997, Rossjohn *et al.*, 1998).

1.3.1.4 GSTM2

The tertiary and quaternary structure of GSTM2 is quite similar to that of classes pi and alpha. GSTM2 is a homodimer in which the two subunits are related by a 2-fold rotation. Each monomer has a glutathione binding domain and a hydrophobic substrate binding domain. As mentioned earlier, the secondary structure of the glutathione binding domain consists of a βαβαββα motif while the hydrophobic binding site is primarily α-helical. The tertiary structure of the glutathione binding domain is similar to that observed in other enzymes that bind glutathione (Sinning *et al.*, 1993). Class mu enzymes have an additional loop that covers the glutathione binding site. These additional peptide segments in the class mu enzymes partially occlude the active site and may affect catalysis by reducing rates of product release. Studies conducted by Raghunathan *et al* (1994) on class mu enzymes found predominantly in human muscle tissue indicated that extensive changes in protein structure do not occur as a result of ligand binding. However, it was clear that a number of local changes in structure and dynamics occurred as a consequence of ligand binding (Penington and Rule, 1992b, Penington and Rule, 1992a).

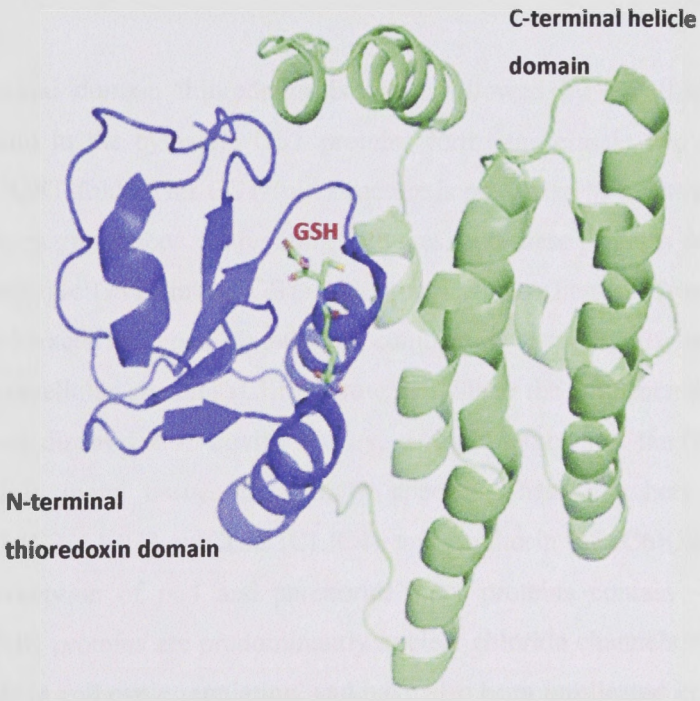

Fig 1.19: Crystal structure of GSTM2 adapted from the Protein Data Base (PDB) entry 1XW5 (Raghunathan *et al.*, 1994) with N terminal thioredoxin domain shown in blue and the C-terminal helicle bundle shown in green. GSH in the active site is shown in stick format and CPK colour code.

Three different crystal forms of GSTM2 have been obtained, one of which contains a monomer in the asymmetric unit and diffracts to 1.85 °A. The remaining two crystal forms contain two (3.5 °A) and four (3.0 °A) monomers per asymmetric unit (Asymmetric unit is the smallest part of a crystal which can be used to produce the entire crystal. It may contain a whole molecule, a portion of a molecule or multiple molecules which may not be the functional unit) (Raghunathan *et al.*, 1994). The tertiary structure of residues 1-202 is similar to that of the corresponding region in the class mu isoform of glutathione transferase from rat, GST3-3 (Ji *et al.*, 1992). However, significant differences in the conformation of the two enzymes have been observed in the region of the active site that binds hydrophobic substrates. These differences include a 2°A shift in the carboxy terminus of a helix, and significant heterogeneity in the conformation of the last 15 residues of the carboxy terminus. The conformation and degree of disorder of the last 15 residues correlates with the extent of protein-protein contacts within the unit cell (Raghunathan *et al.*, 1994).

1.3.2 Proteins with the GST-fold

The N-terminal domain thioredoxin-like fold followed by an all-helical C-terminal domain found in the cytosolic GST proteins forms the classic two domain structure termed the 'GST-fold'. This GST-fold structure is possessed by a few proteins which do not function as glutathione conjugating enzymes, and these proteins are included along with the cytosolic GSTs into a GST-fold structural superfamily (Cromer *et al.*, 2007). The best characterised non-glutathione conjugating superfamily members are the chloride intracellular channel (CLIC) proteins. Since the first member of CLIC, p64 (CLIC5), was discovered in bovine kidney, several members of the CLIC family have been found in many tissues from many species. These members include NCC27 (CLIC1), CLIC2, CLIC3, mtCLIC (CLIC4), and parchorin (CLIC6)(Meng *et al.*, 2009). With the exception of p64 and parchorin, these proteins contain ~240 amino acid residues. CLIC proteins are predominantly nuclear chloride channels which are thought to play a role in cell cycle regulation, and have also been implicated in the regulation of calcium release through the ryanodine receptor (Cromer *et al.*, 2007, Dulhunty *et al.*, 2001, Dulhunty *et al.*, 2005c, Tonini *et al.*, 2000, Valenzuela *et al.*, 2000). CLIC1 and

CLIC2 have significant sequence and structural homology with the soluble GST Omega, including an active site cysteine residue (Board *et al.*, 2004, Dulhunty *et al.*, 2001,Harrop *et al.*, 2001). In addition, CLIC proteins are also capable of membrane integration and ion channel (pore) formation (Cromer *et al.*, 2002, Harrop *et al.*, 2001). Due to their ability to convert from soluble protein to membrane channel, CLIC proteins are referred to as Janus proteins, after the Roman two-faced god. The structural reconfiguration of the soluble CLIC protein for channel function appears to be pH dependent, and may involve tetramer formation (Warton *et al.*, 2002). Two potential membrane-spanning helices have been located in CLIC1, in the N- and C-terminal domains (Cromer *et al.*, 2002, Harrop *et al.*, 2001). The activity of the CLIC proteins on the RyR activity will be discussed in 1.3.3.3.

1.3.3 Regulation of RyR by members of glutathione transferase superfamily

During the last few years, members of our laboratory have discovered that several isoforms of the glutathione transferase structural family, which are present in the cytoplasm of the skeletal and cardiac muscle, are novel modulators of RyR activity (Board *et al.*, 2004, Dulhunty *et al.*, 2001, Dulhunty *et al.*, 2005c). As mentioned earlier, the predominant GST expressed in human skeletal and cardiac muscle is hGSTM2, a member of the Mu class (Suzuki *et al.*, 1987, Board *et al.*, 1988, Hussey *et al.*, 1991). GSTO1-1 is also present in skeletal and cardiac muscle (Board *et al.*, 2000). In the following sections, the specific effects of three members of GST structural family from the Omega (GSTO1-1), Mu (GSTM2) and CLIC (CLIC2) classes on the activity of ryanodine receptor are discussed.

1.3.3.1 GSTO1-1

Dulhunty *et al* (2001) reported that 1 μM GSTO1-1 added to the cis (cytoplasmic) solution in lipid bilayer experiments, reduced RyR2 activity by ~50%. Covalent modification (oxidation) of the RyR complex by GSTO1–1 was not responsible for the

inhibition, because channel activity recovered and was even potentiated above control levels when GSTO1–1 was washed out. Addition of polyclonal anti-GSTO1–1 antiserum restored normal channel activity with potentiation of activity above control levels (Dulhunty *et al,*2001). These changes in channel activity were a specific effect of the antibody on GSTO1–1 because recovery was not seen when pre-immune serum lacking antibody was added to channels whose activity was depressed by GSTO1–1. Two other kinds of experiments indicated that inhibition of RyR2 activity by GSTO1–1 is related to its thiol transferase activity. First, when GSTO1–1 was treated with *N*-ethylmaleimide (GSTO1–1-M), it lost both its enzyme activity and its ability to inhibit RyR2 activity (Dulhunty *et al,*2001). Channel activity was increased by GSTO1–1-M. GSTO1-1 alone (control) was then applied, and channel activity was reversed. The depression may have been less than expected because inactive GSTO1–1-M was occupying some of the inhibition sites and preventing GSTO1–1 binding. In another set of experiments, GSTO1–1 with a Cys-32 to Ala mutation that removed enzyme activity lost its ability to cause depression of RyR2 activity. Indeed, RyR2 channel activity was increased by the mutated GSTO1–1(Dulhunty *et al,*2001). An increase in RyR2 activity to levels that was greater than before exposure to GSTO1–1 after washout of the enzyme was also seen after addition of antibody and after addition of *N*-ethylmaleimide-treated enzyme, suggesting that an activating action of GSTO1–1 was unmasked when the inhibitory effect was removed or was not present. Only an excitatory effect of GSTO1–1 was seen in skeletal muscle RyR1 channels, and this was not reversed within 5 min of removing GSTO1–1(Dulhunty *et al,*2001., Dulhunty *et al*, 2011).

Results of Dulhunty *et al* (2001) study clearly indicated that GSTO1–1 is able to either inhibit or potentiate RyR calcium channel activity. The results also suggested that the inhibition observed does not depend on an oxidation reaction, but require an active enzyme conformation, and that the inhibition is seen only in RyR2. Activation of RyRs was shown to be independent of enzyme activity and was seen in both RyR1 and RyR2. Dulhunty *et al* (2001) suggested that RyR2 has two binding sites for GSTO1–1 and that enzyme binding to one site activates the channel, whereas enzyme binding to the second site inhibits the channel. Recent data published by the laboratory contradicted this conclusion as the inhibitory action of the GSTs is located in the C-terminal helical bundle. The C-terminal domain strongly inhibits RyR2 when expressed alone in a

construct in which the N-terminal thioredoxin fold domain containing the glutathione binding site had been deleted. The inhibitory activity is dependent on the native conformation of helix 6 in the C terminal domain (Liu *et al.*, 2009). The observations that the inhibitory action of GSTO1-1 on RyR2 was lost after NEM treatment of the GST and after the Cys-32 → Ala substitution in its catalytic site might be explained if both the NEM treatment and the mutation had in fact altered the accessibility of helix 6, perhaps altering the conformation or flexibility of the protein so that helix 6 became buried in C-terminal helical bundle (Dulhunty *et al*, 2011).

1.3.3.2 GSTM2

The main GST of interest of my PhD study is GSTM2 isoform (previously known as GST4) which is considered as the most physiologically important GST in muscle as it is specifically expressed in human skeletal and cardiac muscle (Board *et al.*, 1988). Abdellatif *et al* (Abdellatif *et al.*, 2007) reported the presence of a similar protein in rabbit skeletal muscle and sheep heart in the order of concentrations 17-93 μM (Fig 1.20).

The results shown in Fig 1.20B indicate that there is a small amount of Pi class GST in the affinity purified fraction from sheep heart. The intensity of staining and thickness of the bands in Fig.1.20 suggests that the predominant GST in both muscle preparations is closely related to human GSTM2. Previous studies showed a modulation of RyR1 and RyR2 channel activity by GSTO1-1 and GSTA1-1 within the ~1-30 μM range of concentrations. Abdellatif *et al* (Abdellatif *et al.*, 2007) also reported that 1-30 μM recombinant human GSTM2 and GSTM2 like protein isolated from rabbit muscle reduced the activity of cardiac RyR2 channels. GSTM2 would reduce RyR2 activity and lead to the accumulation of Ca^{2+} in the cardiac SR and thus lower cytoplasmic Ca^{2+} concentration during diastole. On the other hand, GSTM2 increased the open probability of RyR1 channels primarily followed by an activation dependent secondary decline in activity in some cases.

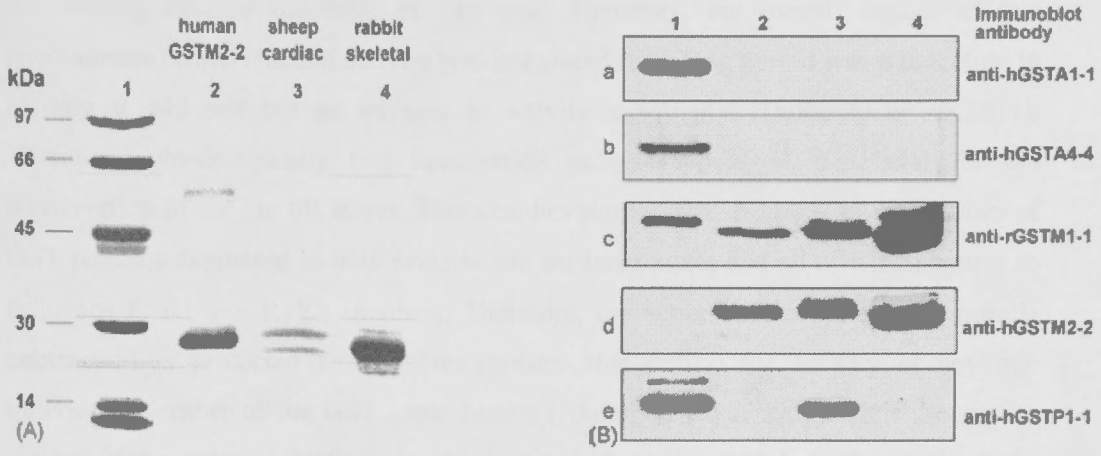

Fig 1.20: GSTs, including an hGSTM2-like protein, are present in the cytosol of rabbit skeletal and sheep cardiac muscle fibres. (A) Coomassie Blue stained SDS-PAGE gel: lane 1, molecular size markers; lane 2, recombinant hGSTM2; lane 3, glutathione affinity purified GST fraction from homogenised sheep cardiac muscle fibres; lane 4, glutathione affinity purified GST fraction from homogenised rabbit skeletal muscle fibres. (B) Western blots using different antibodies to identify GSTs of different classes present in the glutathione affinity purified fraction obtained from rabbit skeletal and sheep cardiac muscle fibres. Lane 1, recombinant human GSTA1-1, A4-4, M1-1 and P1-1 proteins as positive controls in panel a, b, c, and e, respectively, and blank as a negative control in panel d; lane 2, recombinant hGSTM2; lane 3, GST proteins affinity purified from sheep cardiac muscle cytosol; lane 4, GST proteins affinity purified from rabbit skeletal muscle

RyR1 channels with low and high activity behaved differently in the presence of GSTM2. GSTM2 altered the activity of very active RyR1 channels in a manner that differed from the activation of rabbit skeletal RyR1 channels by GSTO1-1 (Dulhunty *et al*, 2011). Channels with low activity were activated by GSTM2 in the same way as GSTO1-1. But channels with a higher activity showed an activation-dependent

inactivation. In these channels, channel openings were turned off or inactivated when the activity became too high at +40 mV. Therefore, the overall impact of this phenomenon, when channel activity was integrated for a long period was a reduction in activity at +40 mV but an increase in activity at -40 mV (Dulhunty *et al*, 2011). Therefore, physiologically this inactivation process would be beneficial for the conservation of Ca^{2+} in SR stores. These studies showed that there are several classes of GST proteins expressed in both skeletal and cardiac muscle and all of which appear to influence RyR1 and RyR2 channels. Therefore, the action of the proteins on muscle contraction is protected from polymorphisms that reduce the activity of any one individual member of the GST super family (Abdellatif *et al*, 2007). Thus the similar actions of the different GSTs on the Ca^{2+} release channel, particularly the cardiac RyR, means that function is conserved even if one member of the class is disabled (Abdellatif *et al*, 2007). The activity of GSTM2 on cardiac ryanodine receptor (RyR2) is further investigated in this study.

1.3.3.3 CLIC2

As discussed previously, CLIC proteins are a class of soluble and membrane bound proteins that have been grouped together on the basis of their sequence similarity. The proteins were named CLIC because the first members of the family to be characterized formed intracellular chloride channels (Heiss and Poustka, 1997). CLIC proteins are found in the membranes of nucleus, secretary vesicles, endoplasmic reticulum, trans golgi vesicles and large dense core vesicles (Board *et al.*, 2004) and are widely distributed in tissues including heart and skeletal muscle. Our laboratory discovered that CLIC2 is a member of the GST structural family and an inhibitor of cardiac RyR2 activity (Dulhunty *et al.*, 2001, Dulhunty *et al.*, 2005c, Jalilian *et al.*, 2008). As discussed in 1.3.2, six CLIC proteins have been identified in humans (CLICs 1-6) and the GST-like structure of CLIC1, CLIC2, CLIC3 and CLIC-4 has been confirmed by X-ray crystallography (Cromer *et al.*, 2007, Littler *et al.*, 2005, Harrop *et al.*, 2001, Littler *et al.*, 2004, Li *et al.*, 2006). The structures of GSTM2 and CLIC2 are compared in Fig 1.21. As discussed in Dulhunty *et al* (Dulhunty *et al*, 2011), a major structural

difference between GST and CLIC proteins is that CLIC proteins are monomers and they have no known catalytic activity. Otherwise, they have a strong structural resemblance to Omega class GSTs. Structural studies indicate a strong effect of the redox condition on the CLIC proteins. Approximately one quarter of the 80-100 cysteines in each RyR subunit (depending on the isoform) contain free –SH groups, many of which are available to sense redox potential (Dulhunty *et al.*, 2000) (see section 1.2.5.3 above). Similarly, there are several free –SH groups apparent in the structure of CLIC2 (Cromer *et al.*, 2007). Jalilian *et al* (2008) reported addition of cytoplasmic CLIC2 inhibited RyR2 with oxidizing redox potentials, but activated RyR2 under reducing conditions, presumably depending on the response of redox sensors that are present in CLIC2 and RyR2. Since cardiac ischemia involves a destructive Ca^{2+} overload that is partly due to oxidation-induced increase in RyR2 activity, Jalilian *et al* (2008) speculated that the properties of CLIC2 place it in an ideal position to limit ischemia-induced cellular damage in cardiac muscle.

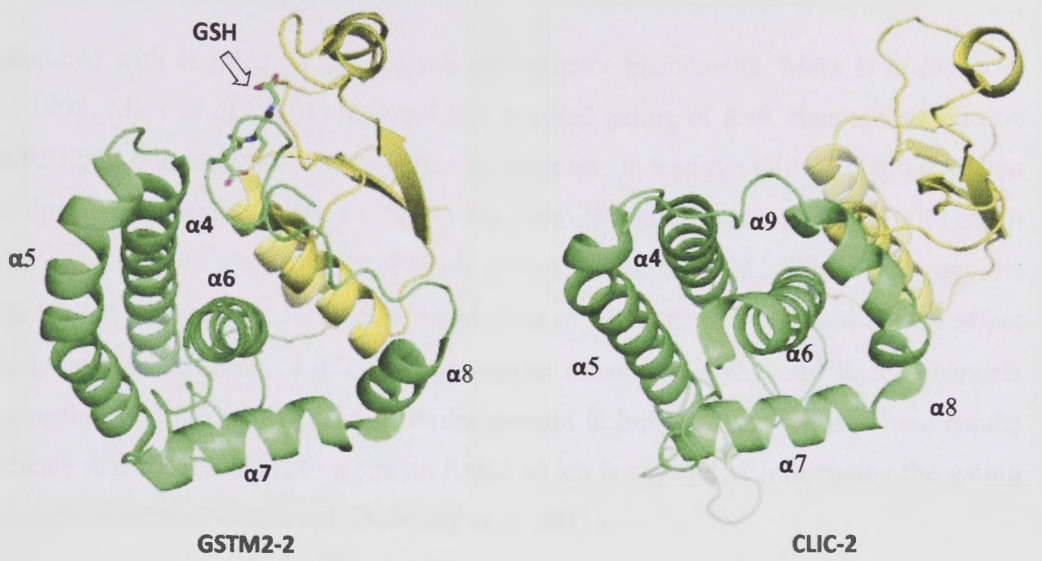

Fig 1.21: A comparison of the structures of GSTM2 from PDB entry 1XW5 (Raghunathan *et al.*, 1994) and CLIC2 PDB entry 2R5G (Cromer *et al.*, 2007). GSH is bound to the catalytic site of GSTM2 but not to the CLIC2 which does not have a catalytic site. Figure was adapted from Dulhunty *et al* (2011).

Effect of CLIC2 on RyR2

CLIC-2 interacts with the cytoplasmic side of cardiac RyR2 channels in lipid bilayers and inhibits Ca^{2+} release from cardiac SR vesicles in spectrophotometric studies (Dulhunty *et al*, 2005). As with the GSTs, the inhibition of RyR channels is easily reversed by removing CLIC-2 from the solution or by adding an anti-CLIC-2 antibody (Board *et al.*, 2004). CLIC2 showed a stronger effect on RyR2 channels when added in the presence of activating cytoplasmic Ca^{2+} concentrations of 10-100 μM where it reduces the P_o by ~90%. In the presence of sub activating concentrations of 100 nM Ca^{2+}, P_o was reduced only by ~60%. CLIC2 is active in the same range of concentrations as the GSTs, with maximal inhibition is seen with concentrations of ~5 μM. Although the number of channel openings to all levels was reduced, the fraction and duration of openings to sub state levels were increased after the exposure to CLIC2. It also increased coupled gating which enabled several RyR2 channels to open synchronously (Dulhunty *et al.*, 2005c). Both FKBP12 and FKBP12.6 have been

associated with coupled gating and sub conductance phenomena. Marx *et al* (Marx *et al.*, 1998, Marx *et al.*, 2001) reported that coupled gating of RyR channels depend on FKBP12/12.6 association with the channel complex. Indeed the CLIC2 binding site on the three dimensional structure of RyR1 has been determined (Meng *et al.*, 2009) and it is close to the site where FKBP12 binds to RyR1 (Samso *et al.*, 2006). This suggests that CLIC2 may be able to modify the binding of FKBP12 to RyR1 which may affect the gating mechanism. CLIC2 showed similar effects on RyR1 and RyR2 channels suggesting that it might bind to a similar domain in both RyR isoforms. These results indicate that CLIC2 binds to a site on RyR2 which is capable of influencing the gating mechanism of the ion channel (Dulhunty *et al*, 2011).

Effect of CLIC2 on RyR1

In contrast to the action of GSTs on RyR1, CLIC2 inhibits both RyR1 and RyR2 activity (Board *et al.*, 2004). In contrast to the GSTM2 induced inhibition on skeletal RyR1 which is dependent on the level of activation of RyR1, CLIC2 showed a "simple" inhibition on both RyR1 and RyR2 (Dulhunty *et al*, 2011). CLIC2 also depressed the Ca^{2+} release from skeletal SR vesicles. Meng *et al* (2009) reported that CLIC2 facilitated the [^{3}H] ryanodine binding to skeletal SR and purified RyR1 which indicated that the channel open probability is increased in the presence of CLIC2. Since ryanodine binds to the open conformation of the channel, its binding increases when the open probability of the RyR channel increases. A similar effect where CLIC2 inhibits the RyR2 activity but increases the ^{3}[H] ryanodine binding, was observed by Dulhunty *et al* (Dulhunty *et al.*, 2005c) in the presence of RyR2. This contradictory result will be explained by the cryo electron microscopy localization of the CLIC2 binding site on skeletal ryanodine receptor (Meng *et al*, 2009) in the next section.

CLIC2-RyR1 interaction and structural characterization by cryo-electron microscopy

Meng *et al* (2009) reported the first study in which the cryo EM and 3D image reconstruction methods were used to determine the binding site of CLIC2 on RyR1. Their analysis revealed that CLIC2 bound to the surface of the cytoplasmic assembly of RyR1 which faces the T-tubular membrane between domains 5 and 6 in the clamp region of the protein (Fig 1.22). When CLIC2 is bound to the domains 5 and 6 of RyR1, they suggested that it might strengthen the interaction between these two domains, thus stabilizing the closed state of the RyR1 channel with limited access to the pore (Meng *et al* ,2009). This stabilization may explain the inhibitory effect observed on Ca^{2+} release from the SR and single channel activity in lipid bilayers. The study also showed that CLIC2 binding causes a conformational change in a different part of the clamp region, with a marked separation of domains 9 and 10 (Fig 1.22). A separation in domains 9 and 10 was earlier reported in the "open" confirmation of RyR but not in the "closed' conformation (Serysheva *et al.*, 1999). In other words, the CLIC2 bound RyR1 clamp structure resembles the clamp structure of the "open" confirmation of RyR1. (Serysheva *et al.*, 1999) reported that cryo-EM study of the "open" structure of RyR1 showed an opening in the central region of the tetramer that indicated enhanced access to the channel pore. However, this central opening does not appear after CLIC2 is bound to RyR1, so that the channel resembles the "closed" RyR1 confirmation. Meng *et al* suggest that the observed increase in ^{3}[H] ryanodine binding to RyR1-CLIC2 complex and increase in binding affinity may be due to the fact that CLIC2 when bound to the closed RyR1 channel induces a conformational change in the clamp region which resembles the "open" confirmation (Meng *et al*, 2009).

As mentioned earlier, the coupled gating and sub conductance activity shown by the RyR1-CLIC2 complex can be explained by the Meng *et al* cryo EM study (Meng *et al*, 2009). The FKBP12 binding site is formed by the intersection of the domains 3,5 and 9 which is on the upper surface of the cytoplasmic assembly of RyR1 (Samso *et al.*, 2006). The separation of domains 9 and 10 observed in the CLIC2-RyR1 complex may affect the binding between FKBP12 and domains 3,5 and 9 in RyR1, consequently channel sub conductance and gating properties.

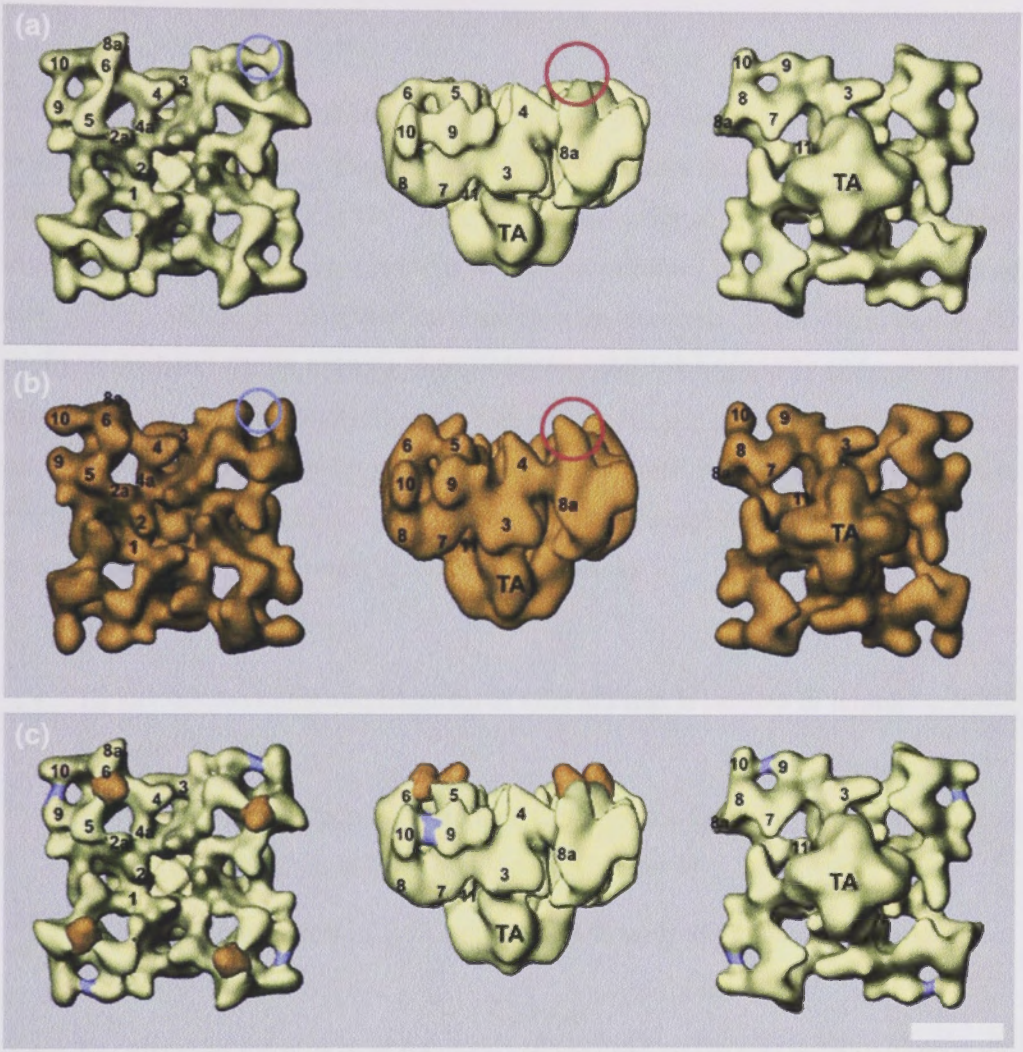

Fig. 1.22: Three-dimensional surface representations of RyR1 and the RyR1–CLIC2 complex, and the 3D difference map. The 3D reconstruction of RyR1 is shown in yellow (a) and the RyR1–CLIC2 complex (b) is shown in orange. (c) The difference map (RyR1–CLIC2 minus RyR1) shown in orange is superimposed on the 3D reconstruction of RyR1 alone (yellow), another minor negative difference (RyR1 minus RyR1–CLIC2) shown in blue-violet, is also superimposed. The 3D reconstructions are shown in three views: left, top view from the cytoplasmic surface, which in situ would face the transverse tubule; middle, side view; right, bottom view showing the surface that would face the SR lumen. The numerals 1–11 on the cytoplasmic assembly indicate the distinguishable domains, according to our earlier nomenclature. The scale bar represents 100 Å. Adapted from (Meng *et al.*, 2009, Dulhunty *et al*, 2011).

1.4 Project aims

Preliminary data from our laboratory suggested the potential of GSTM2 as a template for the development of new drugs in the treatment of heart failure. Among a variety of factors, abnormal intracellular Ca^{2+} handling, in particular abnormal Ca^{2+} release from the sarcoplasmic reticulum via cardiac RyR2, plays a crtitical role in the pathogenesis of heart failure. Although inhibitory mechanisms are essential to maintain low RyR2 activity in the heart during diastole, few are known and they are poorly understood. This project provides an opportunity to close that knowledge gap and to characterize a new drug target which could be developed to specifically inhibit RyR2 activity in cardiac arrhythmias and heart failure. To further explore the therapeutic potential of GSTM2, my contribution to the following aims will be addressed.

- To identify the minimum fragment of GSTM2 that is capable of inhibiting RyR2 (Chapter 3)
- To determine the effects of mutations that alter the flexibility of the C-terminal domain of GSTM2c and helix 6 sequence (Chapter 4).
- To identify the region of RyR2 that interacts with the minimum component of GSTM2 (Chapter 5).
- To determine the effects of fragments of GSTM2 on the contractility of neonatal ventricular cardiomyocytes (Chapter 6).

Chapter 2 Materials and Methods

2.1 Introduction

Materials and methods routinely used throughout this project are described in this chapter. On the other hand, specific procedures are described in each result chapter. All chemicals used were of analytical grade unless otherwise stated and were obtained from several sources as given in 2.2. Unless otherwise stated, all solutions and chemicals were dissolved or diluted in Milli-Q water, obtained from Milli-Q plus ultra pure water system (Millipore, MA, USA). The composition of each of the buffers and solutions used for each experiment is given with the respective procedure. Experimental techniques such as bacterial culture, protein purification, cardiomyocyte culture were carried out in PC2 certified laboratories at The John Curtin School of Medical Research (JCSMR), ANU. Protein purification was performed in the Molecular Genetics group, JCSMR. Intrinsic tryptophan quenching spectroscopy was carried out using general JCSMR facilities. Field stimulation of cardiomyocytes and confocal microscopy were performed at the Microscopy and Cytometry Resource Facility (MCRF), JCSMR. Circular Dichroism Spectroscopy experiments were carried out at the Research School of Chemistry, ANU. All other experiments were performed in the Muscle Research Group laboratories, JCSMR, ANU.

2.2 Materials

No	Name of Chemical	Manufacturer
1	1,2-bis(o-aminophenoxy) Incethane-N,N,N',N'-tetraacetic acid (BAPTA)	Sigma-Aldrich
2	2-trishydroxymethylmethylamino-1-ethanesulfonic acid (TES)	Sigma-Aldrich
3	4-(2-Aminoethyl) benzene sulfonyl fluoride hydrochloride (AEBSF)	MP Biomedicals
4	4-(2-hydroxyethyl)-1-piperazineethanesulfonic acid (HEPES)	Life Technologies
5	Acetic acid glacial, 99.8%	Scharlau
6	Adenosine-5'-triphosphate, di sodium salt	Sigma Chemical Co
7	Alexa fluor 568, Goat anti mouse IgG	Molecular Probes
8	Ammonium persulfate (APS)	W W R International
9	Ampicillin	Sigma-Aldrich
10	Antipyrylazo III	Sigma-Aldrich
11	Anti-α-actinin	Sigma-Aldrich
12	Benzamadine	Sigma-Aldrich
13	Beta mercaptoethanol, 99.00%	BDH chemicals
14	Bis;acrylamide, 30%	BioRad Laboratories
15	Bovine serum albumin	Sigma-Aldrich
16	Ca^{2+} ionophore (A23187)	Sigma-Aldrich
17	Caesium chloride	Merck
18	Caesium hydroxide	Sigma-Aldrich
19	Caesium methane sulfonic acid- Na salt (CH_3SO_3Na)	Aldrich Chemical Co
20	Caffeine	Sigma Chemical Co
21	Calcium chloride	Msllinckrodt Inc
22	Collagen-Vitrogen 50	Cohesion
23	Collagenase	Worthington Biochem coop
24	Coomassie ® brilliant blue R 250	BioRad Laboraties
25	Dithiothreitol (DTT)	MP Biochemicals

	Di-Sodium hydrogen ortho phosphate	Ajax Finechem
26	Dulbecco's modified Eagle's medium (DMEM)	Gibco- Invitrogen
27	Ethylene glycol tetraacetic acid	Sigma-Aldrich
28	Foetal calf serum	Sarana Australia animal serum manufacturers
29	Glucose	BDH Chemicals
30	Glutamine	Media- JCSMR
31	Glycerol	BDH Chemicals
32	Glycine	Bacto laboratories
33	Hank's Buffered Salt Solution ($HBSS^{+}$)	Media- JCSMR
34	Imidazole	Sigma-Aldrich
35	Isopropyl β-D-1 thiogalactopyranoside (IPTG)	Sigma-Aldrich
36	Leuopeptin	Sigma-Aldrich
37	Luria broth	Media-JCSMR
38	Magnesium chloride	BDH Chemicals
39	Magnesium sulphate	BDH Chemicals
40	Mannitol	Scharlau
41	Mercaptoethanol,β	Thermo Scientific
42	Methanol, 99.00%	Ajax Finchem
43	n-Decane, 99.00%	Sigma-Aldrich
44	Oregon green dye	Molecular Probes
45	Paraformaldehyde	Mallinckrodt Chem
46	Penicillin	CSL biosciences
47	Pepstatin A	Sigma-Aldrich
48	Phenyl methane sulfonyl fluoride (PMSF)	Sigma-Aldrich
49	Potassium chloride	APS Chemicals Ltd
50	Potassium dihydrogen phosphate	Mallinckrodt Chem
51	Ruthinium red	Sigma-Aldrich
52	Slow fade Gold, antifade reagent	Molecular Probes
53	Sodium azide (NaN_3)	Ajax Chemicals
54	Sodium bicarbonate	M&B Australia
55	Sodium Chloride	Chem Supply Pvt

		Ltd
56	Sodium dihydrogen ortho-phosphate	Merck Pty Ltd
57	Sodium dodecyl sulphate (SDS)	Sigma-Aldrich
58	Sodium hypochloride	Northfork
59	Streptomycin sulfate	Sigma-Aldrich
60	Sucrose	Sigma-Aldrich
61	Tetramethylethylenediamine (TEMED), 99.00%	Sigma-Aldrich
62	Thapsigargin	Sigma-Aldrich
63	Tris, 99.80%	BioRad Laboratories
64	Triton-X-100	Sigma Chemicals
65	Trypsin	Media, JCSMR

Table 2.1: List of materials

2.3 Methods

2.3.1 SR vesicle preparation

Native skeletal sarcoplasmic vesicles were isolated from muscles dissected from the back and leg muscle of the New Zealand white rabbit. Rabbits were dissected by Prof. Angela Dulhunty, Muscle Research group, JCSMR. Experimental procedures 2.3.1.1 and 2.3.1.2 were carried out by Mrs Suzy Pace and Mrs Joan Stivala, JCSMR, ANU, Canberra, Australia.

2.3.1.1 Skeletal muscle RyR-enriched vesicle preparation

RyR-enriched heavy SR vesicles from the terminal cisternae were prepared according to (Saito *et al.*, 1984), with minor modifications (Ahern *et al.*, 1997, Ahern *et al.*, 1994). New Zealand white rabbits were killed by captive bolt and drained of blood. Back and leg muscle (predominantly fast twitch muscle) was removed and rinsed in phosphate buffered saline, containing: 137 mM NaCl, 7 mM Na_2HPO_4, and 2.5 mM $NaH_2PO_4 \cdot H_2O$, with 2 mM EGTA, pH 7.4. Once excess fat was removed, the tissue was diced and snap-frozen in liquid nitrogen and stored at -70 °C in 100 g aliquots until required for experiments. For the preparation of SR vesicles, 100 g of tissue was homogenized in a Waring blender (Waring Products Div., Connecticut, USA) for 4 x 15 s on high in a SR homogenizing buffer, containing: 5 mM imidazole, 300 mM sucrose, pH 7.4. In all cases, pH was adjusted using a TPS digital pH meter (Bacto Laboratories; Lane Cove, Australia). The homogenate was centrifuged at 11,000 x g in a Beckman J2-21 centrifuge, JA-14 rotor (Beckman Instruments, Gladesville, Australia) for 20 min. The resultant pellet was resuspended in the same homogenizing buffer and then rehomogenized and centrifuged as above. After filtering the supernatant through 4 layers of cotton gauze, the sample was centrifuged at 110,000 x g in a Beckman L8-70 centrifuge, Ti-45 rotor for 1-2 h. The pellet, considered to contain crude SR was collected and resuspended in a total volume of 42 ml of SR homogenizing buffer in a Dounce Teflon homogenizer (Edwards Instrument Company; Narellan, Australia).

seven ml of this microsomal fraction was loaded onto a discontinuous sucrose density gradient, composed of 4 ml of 45%, 7 ml of 38%, 7 ml of 34%, 7 ml of 32%, and 4 ml of 27% (w/v) sucrose layers. Sucrose solutions were prepared in an SR diluting buffer containing: 5 mM imidazole, pH 7.4, plus a standard protease inhibitor solution: 1 mM benzamadine, 0.5 mM Phenyl Methane Sulfonyl Fluoride (PMSF) and 2.2 μM leuopeptin, 1 μM pepstatin-A. Centrifugation of the gradients at 70,000 x g in a Beckman SW-28 rotor for 16 h allowed the sub-fractionation of crude SR vesicles. The sucrose density bands appearing at the 34/38% (Band3, B3) and 38/45% interface (Band 4,B4) were collected and diluted with at least 2 volumes of diluting buffer. Following centrifugation of the diluted fractions at 125,000 x g in a Beckman Ti-45 rotor for 1 h, the final pellet was resuspended in 1 ml of SR homogenizing buffer and SR diluting buffer to a final concentration of approximately 20mg/ml. Aliquots of 15 μl were snap frozen and stored at -70 °C.

2.3.1.2 Cardiac crude SR preparation

Crude cardiac SR was prepared as described by (Chamberlain and Fleischer, 1988, Laver *et al.*, 1995). Sheep hearts were collected in ice cold phosphate buffered saline (PBS) with 2 mM EGTA and then rinsed several times to remove blood. Fat was trimmed from the ventricles and the atria were removed. The ventricles were cut to small pieces in Petri dishes in homogenizing buffer containing 0.29 M sucrose, 10 mM imidazole, 0.5 mM DTT and 3 mM NaN_3, pH 6.9, and homogenized in a Waring blender 3 x 10 s on high. The homogenate was centrifuged at 11,000 x g in a Beckman JA-14 rotor for 20 min. The resultant supernatant was filtered through four layers of cotton gauze, followed by a further high speed centrifugation in a Beckman Ti-45 rotor for 2 h at 110,000 x g. The pellet was then resuspended in 60 ml of buffer A (homogenizing buffer with 0.65 M KCl, plus standard protease inhibitor cocktail) in a Potter homogeniser (Edwards Instrument Company; Narellan, Australia). The homogenate was set on ice for 30 min and centrifuged at 7,000 x g in Beckman a JA-20 rotor, to remove insoluble particles. The supernatant was then centrifuged at 180,000 x g in a Beckman Ti-70 rotor for 100 min. The crude SR pellet was finally suspended in

15 ml of buffer A, snap frozen in 15 µl or 1 ml aliquots and stored at -70 °C or in liquid nitrogen.

2.3.2 Recombinant protein production

The DNA fragments of the GSTM2 gene were obtained by PCR using plasmid pKKGSTM2 (Ross and Board, 1993). All proteins used in this study were cloned into an in-house histidine ubiquitin expression vector, pHUE (Catanzariti *et al.*, 2004). Mutagenesis was undertaken by overlapping PCR and the presence of the desired mutations and the absence of additional mutations was confirmed by DNA sequencing. The numbering of residues mutated in the C-terminal domain is based on the whole GSTM2 subunit. All pHUE vectors carrying GSTM2C and mutants F157A and Y160A were transformed into E. coli BL21 (DE3). Mutagenesis, cloning and preparation of the ubiquitin-fused-C terminal domain peptides and mutatnts were performed by Dr Dan Liu at the Molecular Genetics group, JCSMR, ANU. All proteins were purified by nickel agarose affinity chromatography. These methods are outlined below, with protein expression conditions and purification methods modified slightly according to specifications in the literature available for GST enzymes. The GSTM2C-terminal domain and mutants were expressed as His-ubiquitin fusion proteins. Proteins were engineered to carry an 8 kDa tag (hexa-his tag) which contains six histidine residues followed with an ubiquitin specific proteolytic site which was located immediately to the N terminal end of the proteins. The hexa-his tag is useful in assisting protein purification as it has high selectivity for nickel coated agarose beads. The poly His-ubiquitin tag used for the affinity chromatography was subsequently cleaved by digestion with a catalytic fragment of the deubiquitylating enzyme mouse Usp2 as described in (Catanzariti *et al.*, 2004). Following cleavage, the polyhistidine-ubiquitin tag was removed by a further round of nickel agarose chromatography. The wildtype GSTM2C-terminal domain and C-terminal domain mutants were prepared in the same manner. Proteins expressed in this system have no additional purification tag residues remaining after purification.

2.3.2.1 Protein expression

A single bacterial colony was picked to inoculate 40 ml of LB containing 100 μg/ml ampicillin, and were grown overnight at 37 °C while shaking. The overnight culture was then diluted in (1:100) 2 L of pre-warmed LB+Ampicillin and grown at 37 °C until an OD_{600} of 0.6-0.8 was reached (typically about 3 h). Induction of protein expression was achieved by addition of IPTG to a final concentration of 0.1 mM and incubation was continued for another 4 h at 37 °C before the cells were harvested. Cells were collected in 500 ml Drypin bottles (Du Pont Instruments, USA) then pelleted using a SLA1500 rotor (Sorval RC-5C refrigerated super speed centrifuge, Dupont Instruments, USA) at 6000 rpm for 15 min at ~4°C. Pellets were frozen overnight at –20 °C.

2.3.2.2 Protein purification

Pellets were thawed slowly on ice and then resuspended in ~75 ml of cold buffer A (50mM Sodium phosphate buffer, 0.3 M NaCl, 10% Glycerol, pH 7.0), 10 mM imidazole and 1.2 mM of AEBSF (4-(2-Aminoethyl) benzene sulfonyl fluoride hydrochloride). To lyse cells, a FRENCH pressure cell (Thermo IEC, USA, 1500 psi) was used. The cell lysate was then centrifuged at 15000 rpm for 20 min at 4 °C in SS34 rotor (Sorval RC-5C refrigerated super speed centrifuge, Dupont Instruments, USA). Supernatant was transferred into 2, 50 ml falcon tubes containing nickel agarose beads (total 1.5 ml). Beads were equilibrated in Buffer A prior to use. Incubation was carried out in a rotating wheel overnight at 4 °C. The beads were then spun down at 1500 rpm in a benchtop centrifuge (Eppendorf centrifuge Model 5810R, Eppendorf, USA) at 4 °C for 5 min. The supernatant was discarded and beads were washed in a filter funnel continuously with buffer A (~ 400 ml) until the $OD_{280} < 0.01$. After the final wash, the beads were transferred into an elution column. The column was then washed with 100 ml of buffer A and 50 mM imidazole. Recombinant proteins were eluted from the beads using the elution buffer (500 mM imidazole, buffer A). The hexa-His tag was removed by exposing the recombinant protein to ubiquitin specific protease (USP41) digestion in the presence of 1mM DTT. The USP41 to protein ratio was either 1:15 (v:v) or 1:20 depending on the concentration of the protein. The mixture was incubated for 3 h in a heating block at 25 °C. Overnight dialysis was carried out at 4 °C in buffer A and 10%

glycerol to get rid of DTT and imidazole. The excised hexa-his tag was removed by incubating the digested recombinant protein with 1.5 ml of nickel coated agarose beads for 2 h on a rotating wheel at 4 °C. The beads were spun down at 1500 rpm for 5 min at 4 °C using a bench top centrifuge (Eppendorf centrifuge Model 5810R, Eppendorf, USA) The supernatant obtained was dialysed in 50mM HEPES buffer (50 mM HEPES, 200 mM KCl, 10% Glycerol, pH 7.4) at 4 °C prior to storage at -20 °C.

2.3.2.3 Polyacrylamide gel electrophoresis (PAGE)

Cell extracts and purified proteins were resolved on 'self-cast' denaturing polyacrylamide gels. BenchMark protein ladders (Invitrogen) were used for protein molecular weight and size references.

A self-cast gel of 12% was prepared of 1.5 mm thickness.

- Resolving gel: 3.6 ml of 30% bis:acrylamide, 2.25 ml of resolving gel buffer (1.5 M Tris with HCl and 0.4% SDS, pH 8.8), 33 µl of 10% APS, 11.25 µl TEMED.
- Stacking gel: 0.3 ml of 30% bis:acrylamide, 0.5 ml of stacking gel buffer (0.5 M Tris with HCl, 0.4% SDS, pH 6), 7.5 µl of 10 % APS and 3.8 µl of TEMED.
- Running buffer: 25 mM Tris, 192 mM glycine and 0.1% SDS. (pH 8.3)
- Loading dye: 10% stacking buffer, 20% SDS, 5% beta mercapto ethanol, 10% glycerol

Loading dye was added to each sample at protein:dye ratio of 5:1 and boiled for 5 min to denature. Samples were briefly centrifuged before loading. Gels were run at 150 V for approximately 30-40 min using the Mini-PROTEANTM 3 Electrophoresis Cell apparatus (BioRad).

2.3.2.4 Protein visualization: Coomasie blue staining

Non-specific detection of proteins in polyacrylamide gels was done by Coomassie ® brilliant blue R 250 stain. Stain was prepared by dissolving 0.25 g of Coomassie brilliant blue stain in 90 ml of methanol:H_2O (1:1 v/v) and 10 ml of glacial acetic acid. The solution was filtered through Whatman No 01 filter to remove any particulate matter. At the end of electrophoresis, gels were placed in Coomassie blue staining solution. Staining was done on a platform shaker with gentle agitation overnight. Gels were removed and washed with RO water to remove excess stain. Gel was then destained with five to ten gel volumes of detaining solution (20% methanol, 10% acetic acid) with slow agitation on a platform shaker.

2.3.2.4 Quantification of protein concentration

Absorbance of proteins at 280 nm was determined by the micro-volume spectrophotometer, Nanodrop (Thermo, model ND-1000) for approximate quantification of concentration of proteins. At the end of protein purification, colorimetric detection and quantification of total protein was done by Pierce Bicinchoninic acid (BCA) protein assay according to the instructors manual (Pierce, Thermo Scientific, USA). This method combines the well known reduction of Cu^{2+} to Cu^{+} by protein in an alkaline medium (Biuret reaction) with the highly sensitive and selective colorimetric detection of the cuprous cation (Cu^{+}) using a unique reagent containing bicinchoninic acid. The purple coloured reaction product of this assay is formed by the chelation of two molecules of BCA with one cuprous ion. This water soluble complex exhibits a strong absorbance at 562 nm that is nearly linear with increasing protein concentrations over a broad working range (Smith *et al.*, 1985).

2.3.3 Protein fluorescent labelling

The glutathione transferase C terminal domain was fluorescently labelled with Oregon Green according to the instructions of the manufacturer (Molecular Probes, Invitrogen).

As fluorophores were generally conjugated to primary amine groups, proteins were dialysed into PBS (which is free of ammonium ions and primary amines) prior to labelling. Following labelling, the protein samples were separated from unconjugated fluorophore by chromatography through G-25 medium Sephadex PD10 columns and dialysis against PBS. The absorbance of labelled proteins at 280 nm and at the fluorophore absorbance maxima were measured on a Nanodrop (ND1000) spectrophotometer (Nanodrop technologies), and the protein concentration and degree of fluorescence labelling calculated using the following equations.

$$\text{Fluorescent protein concentration (M)} = \frac{[A_{280} - A_{max} \times CF]}{\varepsilon \times \text{pathlength}}$$

A_{28o} – Absorbance at 280 nm

A_{max} – Maximum absorbance

Where CF is the correction factor for fluorophore absorbance at 280 nm (0.12 Oregon Green) as provided by the manufacturer and ε is the extinction coefficient of the protein.

$$\text{Degree of labelling} = \frac{A_{max} \times \text{MW protein}}{[\text{protein}] \times \varepsilon_{dye}}$$

The extinction coefficient of fluorophores (ε_{dye}) was provided by the manufacturer and was 70000 for Oregon Green.

2.3.4 Intrinsic tryptophan fluorescence quenching spectroscopy

Experiments were performed on a LS50B luminescence spectrophotometer (Perkin Elmer, USA) using an excitation slit width of 10 nm and an emission slit width of 9 nm. An A_{290} cut-off filter was used for the study. Protein samples (5 μM protein) were placed in a quartz cuvette (Spectrosil Far UV Quartz windows cuvette, Starna Cells Inc, USA) .Quenchers were titrated into the cuvette whilst mixing by pipetting the solution. The fluorescence signal was measured by exciting the sample at 280 nm and monitoring

the emission from 290-450 nm. The maximum fluorescence intensity at 340 nm was monitered and used to determine the dissociation constant (*Kd*). The fluorescence values were corrected for dilution effect and the fluorescence arising from the quenchers. Data was analysed using GraphPad Prism software. Nonlinear regression curve was generated with the relative fluorescence intensity at 340 nm (F340) as a function of quencher concentration (μM). The equilibrium binding constants (Kd) were estimated using equation mentioned below.

$$Y = F_0 - \frac{F_0 - Fs}{2E_0}\left[E_0 + X + K_d - \sqrt{(E_0 + X + K_d)^2 - 4E_0X}\right]$$

X – Titrant concentration

Y – Relative fluorescence

F_o - Initial fluorescence of protein without the quencher

F_s - Final fluorescence of the protein

E_o - Concentration of protein to be quenched

K_d - Dissociation constant.

2.3.5 Circular Dichroism (CD) Spectroscopy

Circular dichroism was used to monitor the absorbance of a protein or peptide over a wavelength range of 180 – 260 nm (near UV spectral region), which provides information on the basic structural content of the sample when compared with reference spectra. Alpha helix, beta sheet and random coil structures each give rise to a characteristic shape and magnitude of CD spectrum. The Fig 2.1 shows spectra for poly-lysine, a reference amino acid in these three different conformations. Some of these reference absorbance characteristics include:

Alpha helices – maximum at 192 nm, and minima at 208 nm and 222 nm;

Beta pleeted sheets- a peak at 189 nm and a minimum at 200 nm;

Random coil – minima at 197 nm and 222 nm ; (Johnson, 1990).

Protein and peptide samples were prepared at 1 mg/ml concentration in 10 mM sodium phosphate buffer (pH 8.0), and absorbance was measured in a 1 mm path length quartz cuvette using a Chirascan circular dichroism spectrometer (Applied Photophysics, UK) at 20 °C.

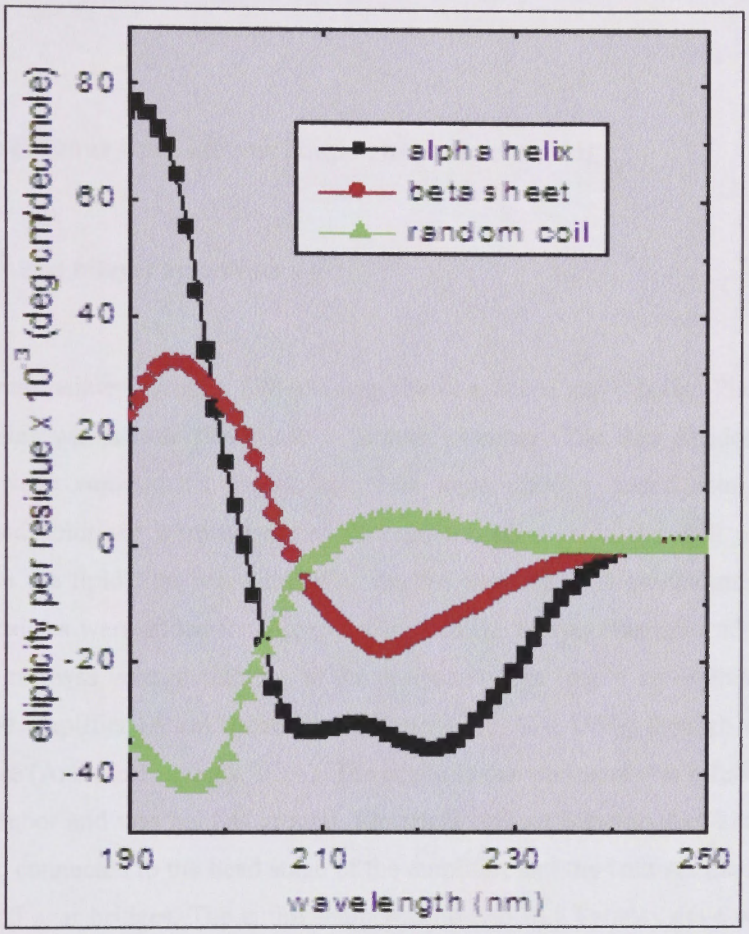

Fig 2.1: Standard curve for poly lysine which shows the characteristic spectra for an α helix, β sheet and a random coil which are acquired at different pH levels.

Ten measurements were recorded for every sample, scans were averaged, normalised to a baseline of buffer alone and a smoothing function was applied. Data was analysed using Pro-Data software, and the absorbance measure was converted to units of molar ellipticity (degrees × cm^2 × $dmol^{-1}$× 10^6) based on sample concentration and cuvette path length.

2.3.6 Artificial Planar lipid bilayer single channel recording

2.3.6.1 Lipid bilayer system set up

Lipid bilayers were painted across a 150 μM aperture in a delrin cup (Caillac Plastics, Seaford, Australia) which was fitted into a bilayer chamber. The cup divided the chamber into two compartments. Stock solutions were directly added into both compartments and solutions were connected through the aperture in the wall of the delrin cup before the lipid film was painted across the aperture. The compartment to which the SR vesicles were added for incorporation into the bilayer was referred to as the *cis* chamber and was voltage clamped to the desired voltage (e.g. + or - 40mV) by an Axopatch 200 amplifier (Axon instruments, Foster City, CA, USA) through a CV 203BV head stage (Axon instruments, USA). The opposite compartment was referred to as the *trans* chamber and was held at ground. Electrical contact between AgCl coated silver electrodes, connected to the head stage of the amplifier and the bath solution was via 250 mM CsCl agar bridges. The entire setup was housed in a Faraday cage with a sliding front cover to reduce electrical noise during the recording process. The delrin cup aperture was illuminated using a fibre optic light (Fiberoptic Illuminator Model 15001, Fibre optic light Guides, Sydney, Australia) and the aperture was viewed through a light microscope (HWF 20x/11, Koyawa, Tokyo). Current was sampled at a bandwidth of 5 kHz and filtered at 1 kHz on a computer using a Continuous Analog/Digital display program 1.0 (BLM data transfer). The signal was filtered at 1 kHz with a low pass 8-pole Bessel filter (Rockland Systems Corporation, Model 432 dual hi/lo filter) before being displayed on a Hitachi VC 6023 digital storage oscilloscope, or digitally filtered for viewing directly on a computer screen. Experiments were carried out at 23 ± 2 °C.

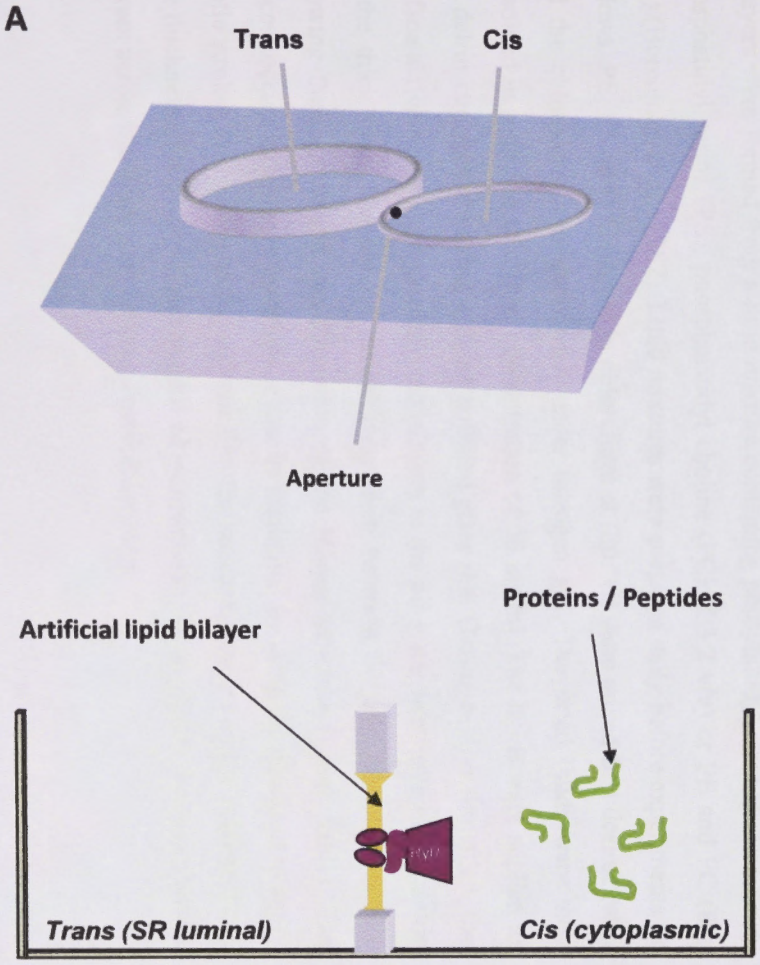

Fig 2.2: A) The bilayer set up consist of the cis and trans chambers separated by an aperture across which the artificial bilayer is painted. Cardiac/ skeletal SR vesicles containing RyR2/RyR1 are added to the cis chamber and the solution stirred until a channel incorporated into the lipid bilayer. Proteins/ peptides are added to the cis/ cytoplasmic chamber. B) The procedure for incorporating ion channels form the sacroplasmic reticulum (SR; RyR in this case) into lipid bilayers. Vesicles of the SR membrane (approximately 0.1 μm diameter) are isolated from muscle tissues using differential centrifugation methods. The SR vesicles containing ion channels are added to the bath near the lipid bilayer. Fusion of the vesicles with the bilayer carries ion channels into the bilayer membrane. B was Adapted from (Laver, 2001)

2.3.6.2 Preparation of agar bridges and silver chloride coated Ag electodes

Silver wires cut to the desired length were lightly sanded and then immersed in 12.5% sodium hypochloride for 1 h. Once the electrode was coated with silver chloride (became black in colour), they were wiped and inserted into brass connectors. Both electrodes were connected to the CV 203BV head stage. Agar bridges were used between the electrodes and the bath solution to reduce junction potential effects. To prepare agar bridges, 1% (w/v) mixture of agar powder in 250 mM CsCl was warmed on a hotplate and injected into 20-30 cm length of 1.47 mm laboratory tubing (Dow Corning Corperation, MI, USA). Once the agar set, the tubing was cut into 1.5 cm pieces and stored in 250 mM CsCl at 4 °C.

2.3.6.3 Formation of lipid bilayers

Bilayers were formed from a lipid mixture containing phosphatidyl ethanolamine (PE), phosphatidyl serine (PS), phosphatatidyl choline (PC) (5:3:2 v/v) or PE and PC (8:2 v/v) (Borchman *et al.*, 1982). Lipid mixtures were prepared daily before experiments as follows. PE, PS and PC (stored in chloroform at -20 °C) were mixed in a desired ratio and the chloroform was evaporated under nitrogen gas. The dried lipids were then dissolved in *n*-decane to a final concentration of 50 mg/ml. The lipids were applied to the delrin cup aperture using a flame polished glass rod. During bilayer formation, the surface active lipids aggregate into monolayers at the oil-water interfaces on each side of the thick film. The solvent drains away from between the two monolayers, thus allowing their apposition and formation of the bilayer structure (Laver, 2001). The process occurs either spontaneously or can be facilitated by using the glass rod to apply gentle strokes to the edge of the solvent film (to increase pressure on the solvent film). The thickness of the bilayer was monitored by observing the amplitude of the capacitive current across the bilayer in response to a voltage ramp.

The capacitance is proportional to the area (A) of the capacitor divided by the thickness (T) of the capacitor plates (i.e. the bilayer)

$C \alpha A / T$

The current flowing across the capacitor (Borchman *et al,* 1982) is equal to capacitance (C) times the rate of change of voltage (dV/dt)

Ic = C x dV/dt

If dV/dt is 1 (e.g 1V/s), then

Ic = C x 1/T

The bilayer current and channel incorporation (2.3.6.4) were monitored using an Axopatch 200 amplifier (Axon Instruments, CA).

2.3.6.4 Vesicle fusion

SR vesicles from cardiac or skeletal preparations (10 μg/ml of protein) were added to the *cis* solution and stirred vigorously, with the potential difference across the bilayer held at +40 mV. Vesicle fusion was detected by channel openings sometimes superimposed by a step increase in leak current. Vesicle fusion was aided by the osmotic gradient of 250 mM *cis* Cs^+ versus 50 mM *trans* Cs^+. After channel fusion, the *cis* chamber was perfused with a perfusion solution containing 10 μM Ca^{2+} using a back-to-back syringe with five chamber volumes of perfusion solution, to remove vesicles and to prevent further vesicle incorporation. The *trans* Cs^+ concentration was raised to 250 mM with the addition of 200 mM $CsCH_3O_3S$. Two mM ATP was added to the cytoplasmic side of RyR to activate the RyR channel in the presence of low concentrations (nM) of Ca^{2+}. In addition, cytoplasmic ATP elicits persistent channel activation at high (μM) concentrations of Ca^{2+} (Meissner, 1986, Smith *et al.*, 1988). The

orientation of the incorporated vesicle has been shown to be such that the cytoplasmic side faces the *cis* chamber, whilst the luminal side faces the *trans* chamber in 99% of cases (Miller and Racker, 1976). The characteristic response of RyRs to the agonists Ca^{2+} and ATP or to the antagonist ruthenium red was used to confirm that the RyR had the correct orientation. Only channels responding appropriately were analysed.

The following solutions were made prior to the experiment.

- *Cis* solution: 20 mM CsCl, 230 mM CsMS, 5 mM $CaCl_2$, 10 mM TES, 500 mM Mannitol, pH 7.4.
- *Trans* solution: 20 mM CsCl, 30 mM CsMS, 1 mM $CaCl_2$, 10 mM TES, pH 7.4
- Perfusion solution: 2 mM BAPTA, 1.9 mM $CaCl_2$, 20 mM CsCl, 230 mM CsMS 10 mM TES, pH 7.4

2.3.6.5 Experimental setup

All solutions were made from analytical grade reagents using DDH_2O and were pH adjusted to 7.4 with CsOH or HCl. Free [Ca^{2+}] in the solution was monitored by a Radiometre Analytical ISE25Ca Ca^{2+} electrode (Villeurbanne Cedex, France).

Approximate concentrations of BAPTA or Ca^{2+} ions required to adjust the free Ca^{2+}in the solution to the desired level were calculated by the BAD program and amounts fine tuned using the Ca^{2+} electrode. Cesium ions were used as the current carrier in bilayer experiments for several reasons. 1) Ca^{2+} is an endogenous RyR ligand that regulates channel activity-thus to use Ca^{2+} in a physiological range to modulate activity and see an analysable current, it is preferable to use a different charge carrier. Ca^{2+} would inhibit RyR1 activity if used at concentrations required to detect a measurable Ca^{2+} current. 2) Cs^+ conductance of the RyR is higher in symmetric 250 mM Cs^+ (525 pS) than Ca^{2+} (Smith *et al.*, 1988, Laver *et al.*, 1995). The higher Cs^+ conductance improves the signal to noise ratio, allowing more accurate measurements of channel gating. 3) Cs^+ is a very much weaker regulator of RyR than Ca^{2+} (Laver *et al.*, 1997a); 4) the K^+ channel which is enriched in muscle is blocked by Cs^+ (Coronado *et al.*, 1992),

therefore use of Cs^+ tensuring that K^+ channel activity was not recorded. $CH_3O_3S^-$ was used as the major anion to minimize the current through SR anion channels as all identified SR anion channels so far identified have a low permeability to $CH_3O_3S^-$ (Rychkov *et al.*, 1998). The solutions contained 20 mM Cl^- to reduce the junction potentials between the solution and AgCl electrodes. Agar bridges were also used to reduce junction potentials on AgCl electrodes that might have developed with solution changes. At the end of each experiment, ruthenium red was applied at 1mM concentrations to the *cis* chamber, to specifically block the RyR channel (Smith *et al.*, 1988).

2.3.6.6 Channel recording

Once vesicle incorporation was detected, channel activity was recorded using the Axopatch 200 amplifier (Axon Instruments, CA). The voltage was applied to the *cis* chamber while the *trans* chamber was held grounded. All potentials are expressed according to standard physiological convention as the voltage in the cytoplasmic solution relative to luminal solution, V_{cis} -V_{trans} ($V_{cytoplasm}$ - V_{lumen}) and changed every 30s between +40mV and -40mV. All recordings were performed in symmetrical solutions (with respect to Cs^+, Cl^- and $CH_3O_3S^-$). Proteins/peptides were added to the *cis* chamber to desired concentrations whilst stirring and currents were recorded for at least 5 min under each condition.

2.3.6.7 Single channel analysis

Single channel parameters were obtained using an in house program, Channel 2 (Developed by P.W. Gage and M. Smith, John Curtin School of Medical Research, Canberra, Australia). Thirty second recordings were used to measure the following:

Open probability (P_o) = T_{open}/T_{total} (1)

Mean open time (T_o; ms) = T_{open}/n (2)

Fractional mean current (I'_F) = I'/I_{max} (3)

In the above equations, T_{open} is the sum of all channel open times; T_{Total}, the total time of analysed record; n, the number of events; I', mean current, an average of all data points obtained during a recording period and I_{max}, maximal current during channel opening in the experiment. In this study, the open probability (P_o) of channels was assessed in two ways, either as T_{open}/T_{Total} (equation 1) where an open threshold discriminator was set above the baseline noise at ~20% of maximal current, while close threshold was above the base line noise or halfway in between open threshold and baseline (The threshold discriminator was used where only one channel opened, and includes only substate openings >2 pA). When more than one channel opened in the bilayer, the open probability was also approximated by I'_F, (equation 3) which is the mean current divided by the maximum channel current recorded when all channels opened simultaneously. The accuracy of the I'_F measurement depends on the noise level being equally distributed above and below the baseline, so that mean current is close to zero when the channel is inactive. Therefore fluctuations in baseline levels were corrected with the program Baseline (Developed by Dr D. R. Laver, University of Newcastle, Australia). I'_F is approximately equal to the P_o measured by threshold discrimination when most of channel openings are to the maximum conductance so that $P_o \sim I'_F$. When test data is normalized to control data relative P_o = relative I'_F. Therefore, regardless of whether P_o was measured directly or as I'_F, all test data is normalized to control data and expressed as relative P_o.

2.3.6.8 Statistics

Average data are presented as mean ± SEM. Statistical significance was evaluated using paired or unpaired Student's T-test as appropriate or ANOVA. To reduce effects of variability in control open probability (P_oc), and to evaluate test parameters after protein addition (Fredj *et al,* 2005), data were expressed as the difference between the $\log_{10} P_o$t and $\log_{10} P_o$c for each channel (eg $\log_{10} P_o$t - $\log_{10} P_o$c). The difference from control was assessed with a paired t-test applied to $\log_{10} P_o$t and $\log_{10} P_o$c. The difference between each concentration was assessed using ANOVA on $\log_{10} P_o$t - $\log_{10} P_o$c at each concentration with the multidimensional Mahalanobis test. The difference between

$\log_{10} P_o t$ - $\log_{10} P_o c$ at +40 mV and at -40 mV at each concentration was assessed using the Students T-test. A P value of <0.05 was considered significant for all tests.

2.3.7 Ca^{2+} release from SR

A Cary 3 spectrophotometer was used to monitor extravesicular Ca^{2+} at 710 nm, using the Ca^{2+} indicator antipyrylazo III .Cardiac SR vesicles (200 μg/ml of protein) were added to a solution containing 100 mM KH_2PO_4, 0.5 μM antipyrylazo III, 1 mM Na_2ATP and 4 mM $MgCl_2$ controlled at a temperature of 25 °C and magnetically stirred. A calibration curve of optical density change in response to four sequential additions of 12.5 mM $CaCl_2$ was constructed in the absence of vesicles. Cardiac SR was then added to the cuvette, causing an increase in extravesicular [Ca^{2+}] which then declined as Ca^{2+} was taken up by the Ca^{2+} ATPase which was activated by the MgATP in the solution (Fig 2.3A). An increase in optical density indicates an increase in extravesicular [Ca^{2+}] detected by antipyrylazo III. The SR was then loaded with four additions of 7.5 μM Ca^{2+} (Fig 2.3A). Thapsigargin (2.25 μM) was added to block the Ca^{2+}-ATPase so that the rate of Ca^{2+} release through the RyR was not contaminated by Ca^{2+} uptake, and then 5 mM caffeine for cardiac SR or 0.5 mM caffeine for skeletal SR was added to activate the RyR. Next, 5 μM ruthenium red was added to confirm that Ca^{2+} release was through the RyR and finally Ca^{2+} ionophore (A23187) was added to release Ca^{2+} remaining in the SR. The recordings show optical density as a function of time after vesicle addition (Fig 2.3A). The SR vesicles were incubated for 20 min prior to the start of the experiment with the GSTM2Construct in vehicle buffer or with vehicle buffer alone. The same concentrations of GSTM2Construct in vehicle buffer or with vehicle buffer alone were added to the cuvette solution prior to vesicle addition. The initial rate of caffeine-induced Ca^{2+} release was measured (Fig 2.3).

An ATP regenerating system was not used. The protocol followed in these experiments was tightly controlled, so, the ATP concentration would have been the same during drug exposure in each experiment, and ATP would have been utilized at the same rate and varying with time in the same way from experiment to experiment. Since the rate of

Ca^{2+} uptake during loading was the same in the first and fourth loading step (Fig 2.3) it was assumed that ATP was not severely depleted (Hewawasam *et al*, 2010). Ca^{2+} release (the rate of caffeine induced

Ca^{2+} release minus the rate with thapsigargin, Fig 2.3B) was calculated as nmoles of Ca^{2+} per mg of SR vesicles per min. Average data were presented as caffeine-stimulated Ca^{2+} release rate in the presence of GSTM2C construct relative to the Ca^{2+} release rate in the presence of vehicle alone (Timerman *et al*., 1993).

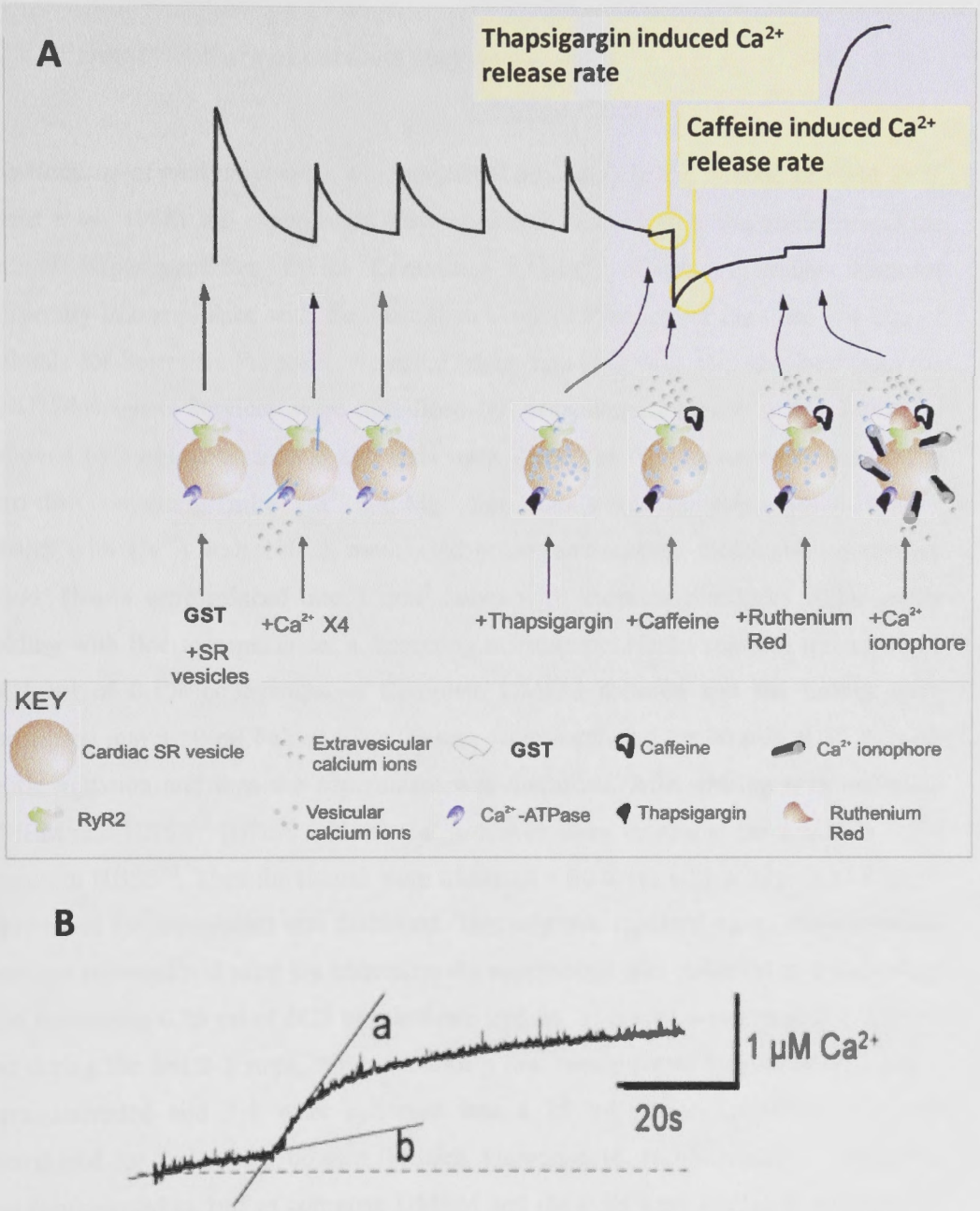

Fig 2.3: A) A typical Ca^{2+} release experiment (with GST) showing a record of optical density as a function of time. (Jalilian *et al.*, 2008) B) X and Y expansion of the baseline release in thapsigargin and the caffeine release transient. The line labeled (b) indicates the baseline Ca^{2+} release rate after addition of thapsigargin, while the line labeled (a) indicates the initial rate of Ca^{2+} release after caffeine addition. The lines are included to indicate where the measurement was taken. The rate was calculated from the derivative of the points in that region of the curve.

2.3.8 Primary culture of cardiomyocytes

The isolation of cardiomyocytes was conducted according to the method of Field *et al.* (Field *et al.*, 1988). All experiments were carried out according to the guidelines of the Animal Experimentation Ethics Committee (AEEC) of the Australian National University in compliance with the Australian Code of Practice for the Care and Use of Animals for Scientific Purposes. Neonatal wistar rats (1-2 days old) obtained from the ANU Bioscience Services were sacrificed by decapitation. Hearts were aseptically removed by surgical dissection and atria were discarded. Ventricles were placed in a petri dish containing 1ml of Ca^{2+} and Mg^{2+} free Hank's balanced salt solution $HBSS^{(+)}$ (HBSS with Ca^{2+}) with 10FCS mentioned below and washed thoroughly to remove blood. Hearts were minced into 1 mm^3 cubes with iridectomy scissors while gently holding with fine forceps, under a dissecting microscope. Hanks solution was replaced by 1 ml of 0.1% collagenase in Complete DMEM solution and the tissues were transferred into a 50 ml Falcon tube. Tissues were incubated for 30 min at 37 °C with gentle agitation and then the supernatant was discarded. After rinsing with complete DMEM and $HBSS^{(-)}$ (HBSS without Ca^{2+}), tissues were incubated for 5 min in 0.1% trypsin in $HBSS^{(-)}$. Then the tissues were triturated ~ 20 times with a large bore Pasteur pipette and the supernatant was discarded. This step was repeated once. The incubation step was repeated and after the trituration the supernatant was collected to a microfuge tube containing 0.25 ml of FCS to inactivate trypsin. This step was repeated 3-5 times and during the last 2-3 steps, triturated with a fine bore pipette. Supernatants, 1 and 2 were discarded and 3-8 were collected into a 15 ml sterile centrifuge tube and centrifuged for 5 min at 1500 rpm (Hettich, Universal 16, HD Scientific). The pellet was resuspended in 1ml of complete DMEM and the cells were seeded at a density of 1×10^6 cells/ml. The cells were incubated for 1 h at 37 °C and rinsed with $HBSS^{(+)}$. After gently flooding the dish with 2 ml of complete DMEM, cells were incubated in a dual chamber water jacketed incubator (Forma Scientific Inc, Marietta, OH) at 37 °C in an atmosphere of 5% CO_2 and 95% air. Approximately 3-4 h after plating, the dishes were washed again in 1.5 ml of $HBSS^{(+)}$ with bicarbonate and replaced with 1.5 ml of complete DMEM. Within 24 h of initial culture, cardiomyocytes start to exhibit spontaneous rhythmic contractions. The cell preparation contained over 95% of

cardiomyocytes as judged by spontaneous contractions and morphology. Culture medium was routinely renewed every 2 days.

Following solutions were made in advance;

Complete DMEM (cDMEM): further supplemented with 0.1M glutamine, 1M glucose, 0.6M mercaptoethanol, 100units/ml Penicillin and 7mM Streptomycin.

cDMEM 10FCS: cDMEM with 10% fetal calf serum

cDMEM 5FCS: cDMEM with 5% fetal calf serum

HBSS$^{(+)}$ with calcium: Obtained from Media and Wash up, JCSMR, ANU. 1 L of media contains NaCl 100 g, KCl 5 g, $MgSO_4.7H_2O$ 1.25 g, $MgCl_2.6\ H_2O$ 1.25 g, $CaCl_2$ 1.4 g, Glucose 12.5 g.

HBSS$^{(+)}$ 10FCS: HBSS(+) with 10% fetal calf serum

HBSS$^{(-)}$ without calcium and magnesium: Obtained from Media and Wash up, JCSMR, ANU. 1 L of media contains NaCl 100 g, KCl 5 g, $Na_2HPO_4.2H_2O$ 0.75 g, KH_2PO_4 0.6 g, 1M glucose.

HBSS$^{(+)}$ 10FCS, HBSS$^{(-)}$ solutions were treated with $NaHCO_3$ prior to the experiment. 0.1% Collagenase in cDMEM and 0.1% trypsin in HBSS$^{(-)}$ were also prepared. Collagen was coated on 10mm or 28mm coverslips as required.

2.3.9 Immunostaining of cultured cardiomyocytes

Cultured cardiomyocytes were stained by an indirect immunostaining method modified from (Fredj *et al.*, 2005). Cells were fixed for 20 min with 4% paraformaldehyde at

room temperature and washed three times with phosphate buffered saline (PBS^{++}, PBS containing 0.9 mM $CaCl_2$, 0.52 mM $MgCl_2$ and 0.16 mM $MgSO_4$). They were then permeabilized for 10 min with 0.1% Triton-X-100 in PBS^{++}, washed three times with PBS^{++} and blocked for 15 min in PBS-BSA (PBS^{++} containing 1% BSA). PBS-BSA was used to block non-specific binding sites before labelling with specific antibodies. A monoclonal anti-α-actinin (sarcomeric) antibody in 1:200 dilution was used to characterize cardiomyocytes as this antibody is specific for α skeletal muscle actinin and α cardiac muscle actinin. It stains Z lines in skeletal and cardiac muscle but not the non-sarcomeric muscle elements such as fibroblasts. Primary antibodies were applied for 1 h in PBS-BSA with 0.1% triton-X-100. After washing the cells thoroughly three times in PBS^{++}, secondary antibody, alexa fluor 568, goat anti mouse IgG was added in 1:100 dilution. Cells were incubated for 30 min in dark. Cells were washed again in PBS^{++} three times and coverslips were mounted up side down in mounting solution (90% glycerol and 10% PBS, Slow Fade Gold antifade reagent) and air dried for 30 min in the dark. In control experiments, the incubation steps with primary antibody were omitted.

2.3.10 Field stimulation of cardiomyocytes.

On day 4 of culture, the cardiomyocytes were stimulated using a Digitimer constant voltage isolated stimulator (DS2A-Mk.II, Digitimer Ltd, UK). Following method was optimized by trial and error to achieve optimal stimulation of the cardiomyocytes. Live beating cardiomyocytes seeded on a 29 mm coverslips were placed on a micro-incubator (Harvard Apparatus, MA, USA, model PDMI-2) in serum free complete DMEM media. Cells were maintained at 37 °C in the presence of reticulated CO_2/air 5%/95% on a temperature controller (Model TC-202A, Harvard Apparatus, MA, USA) installed on the microscope stage. A field of view was selected with a high population of cells and the cells were field stimulated with a pair of platinum wires placed on opposite sides of the cells and connected to the stimulator which delivered pulses of 1 Hz, 3 V and 2 ms duration. These pulse parameters were optimized by increasing the

voltage slowly until a contraction was observed. Then cells were stimulated at a voltage 5% (in V/cm) higher than the threshold. The gap between the two electrodes was 2 mm. The polarity of the stimulating electrodes was reversed at every fifth pulse to avoid build up of electrolyte by-products. Cell beating was recorded using a JVC video camera KY/F550 attached to Nikon TE2000-U microscope at the Microscopy and Cytometry Resource Facility (MCRF) at the John Curtin School of Medical Research, ANU. The GST protein was added to the cells at the appropriate concentration and cells were incubated on the microscopic stage for 2 h without changing the field of view. At the end of the incubation period, cells were stimulated again using the above parameters and cell beating was recorded. Still frames of systolic (most contracted) and diastolic (most relaxed) cardiomyocytes were captured using I Movie application (3.0.3, Apple Computers, Inc). Images were analysed using Image Pro plus 6.2 software and the percentage cell shortening of the control cells were measured as the difference between diastolic (D) and systolic (S) length divided by diastolic (D) length presented as a percentage (i.e. (D-S)% / D).

2.3.11 Confocal microscopy

Confocal microscopy was performed on cells grown on no.1 (~ 0.15 mm thick) glass coverslips (HD Scientific Pty Ltd, Australia) using a Leica SP5 confocal microscope (Leica, Mannheim, Germany). Cells were usually viewed live in serum free complete DMEM or immunostained with anti α actinin. When viewing cell uptake of GSTM2C tagged with Oregon green dye in live cardiomyocytes, cells were washed thoroughly with control media prior to the viewing.

Fluorescence excitation of different fluorophores was performed using the following laser lines and emission filter settings:

· Argon 488 nm, 495 – 551 nm (Oregon Green).
· He/Ne 561 nm, 576 – 652 nm (AlexaFluor568).

Laser excitation was performed sequentially when using multiple fluorophores to avoid channel bleed-through, and images overlayed to obtain merged data. Laser power and gain settings were manipulated to optimise signal-to-noise ratio, however iris settings (pinhole diameter) were maintained at the objective numerical aperture (1.4 N.A. for both 20X and 60X oil immersion objectives) so that confocal optical slice thickness was maintained. A series of images were taken through the z-plane to show the location of protein within the cardiomyocytes. Control experiments using single fluorophore-treated cardiomyocytes were also conducted to ensure the absence of fluorophore bleed-through into subsequent channels.

Chapter 3 Dissection of human GSTM2 to determine the region responsible for the modulation of ryanodine receptor activity.

3.1 Introduction

As mentioned in the chapter 1, members of the GST structural family are endogenous RyR modulators which produce strong inhibition of the cardiac RyR2, but not skeletal RyR1 channels. This activity has been observed with GSTO1-1 and the muscle specific GSTM2.

As outlined in the General Introduction, a strong, highly significant inhibition of cardiac RyR2 activity was observed in the presence of 1 μM GSTO1-1 whereas a smaller but significant activation was observed in the presence of 10 μM GSTO1-1 with skeletal RyR1 activity (Dulhunty *et al.*, 2001a). Dulhunty *et al* also reported that addition of GSTO1-1 antibody to the bilayer bath reversed the inhibition of RyR2. Also, when GSTO1-1 was treated with N-ethylmaleimide (NEM), it lost both enzymatic activity and its ability to inhibit RyR2 channel activity. When Cys 32 present in the active site of GSTO1-1 was substituted to Ala, it also removed both the proteins enzymatic activity and the ability to inhibit RyR2 channels. All these observations suggested that the enzymatic activity of GST proteins may play a major role in the inhibition of cardic rynodine receptor activity.

Recombinant GSTA1-1 also interacted with RyR2 channels isolated from sheep heart (Dulhunty *et al.*, 2011). The results showed effects on RyR2 channels, very similar to those obtained for GSTO1-1, although higher concentrations of GSTA1-1 were required. Ten μM of GSTA1-1 added to the *cis* solution which bathes the cytosolic side of RyR2 channels, reduced the relative open probability to <50% of control. However, lower concentrations of GSTA1-1 did not inhibit the ryanodine receptor activity.

Also as outlined in the General Introduction, the CLIC2 (chloride intracellular channel 2) protein, which is also expressed in the heart, is also an endogenous inhibitor of RyR2. Previous studies conducted in Professor Phil Board's laboratory showed that it

had a strong structural resemblance to GSTO1-1 but differed from the GSTs as it exists as a monomer and has an atypical enzyme activity (Board *et al.*, 2004). CLIC-2 also interacts with the cytoplasmic side of the RyR2 channels in lipid bilayers and inhibits Ca^{2+} release from cardiac SR vesicles. Consistent with the results obtained for GSTs, the inhibitory effect could be easily reversed by removing CLIC-2 from the solution or by adding anti-CLIC-2 antibody to the bath. It also showed a stronger inhibitory effect when added in the presence of activating cytoplasmic Ca^{2+} concentrations of 10-100 μM (~90%) compared to sub activating cytoplasmic concentrations of 100 nM Ca^{2+} (~60%, (Dulhunty *et al.*, 2011, Dulhunty *et al.*, 2005c). As with the GSTO1-1, GSTA2-2 and GSTM2, the effect of CLIC-2 protein on RyR2 is also influenced by the conserved Cys 30 residue in the N-terminal thioredoxin motif (Board *et al.*, 2004).

In contrast to the actions of GSTs on RyR1, CLIC-2 inhibits both RyR1 and RyR2 channels (Board *et al.*, 2004). However, this inhibition is not complex and is unlike the complex activation dependent inactivation of RyR1 observed for GSTM2. As mentioned in 1.3.3.2, Abdellatif *et al* (Abdellatif *et al.*, 2007) first reported the distribution and the ability of GSTM2 to interact with skeletal and cardiac RyR. The different actions of GSTM2 and CLIC-2 indicate that the proteins may interact with different sites on RyR1. Meng *et al* also reported in 2009 (Meng *et al.*, 2009) that CLIC-2 can interact with RyR1 and modulate its channel activity. CLIC-2 depressed Ca^{2+} efflux from skeletal SR vesicles and depressed single RyR1 channel activity.

Following the observations of RyR modulation by GSTO1-1, GSTA1-1 and CLIC2, the effect of GSTM2 was investigated because, its specific expression in muscle suggested that it would be the most likely GST to play a significant role in the modulation of RyRs. The selective inhibition of cardiac RyR2 by the muscle specific GSTM2 suggested that the active region of GSTM2 which interacts with RyR2 may be a potential therapeutic agent in the treatment of heart failure. But it would be less useful if the action of the GST depended on its enzymatic activity. The region of GSTM2 that interacts with RyR and the mechanism of action of GSTM2 on cardiac and skeletal ryanodine receptors remained unknown. Therefore, the human GSTM2 was dissected and the region responsible for the modulation of ryanodine receptor activity was

determined. It was also hoped that, in addition to revealing the basic mechanism of action, defining the structure of the interacting region may eventually lead to the design of a specific compound which alter the ryanodine receptor activity.

To investigate whether the RyR-active residues of the GSTM2 protein are located in the N or C-terminal domains, deletion constructs were designed containing either the N or C-terminal halves of GSTM2. As mentioned earlier, the Cys32-Ala substitution in the catalytic site of GSTO1-1 had prevented the inhibitory action of GST on RyR2 (Dulhunty *et al.*, 2001a). Therefore, it was expected that the inhibitory action of GSTM2 might depend on the thioredoxin fold and thus be located in the N-terminal domain which contain the first three α helices and the four β strands (Fig 1.19). Unfortunately, despite being cloned into the pHUE (Histidine-tagged Ubiquitin Expression) vector for enhanced solubility and ease of purification (Catanzariti *et al.*, 2004), the N-terminal domain proved to be insoluble during recombinant expression (Liu *et al*, 2009). Therefore, its actions on cardiac and skeletal ryanodine receptor activity could not be explored. The C terminal domain of GSTM2 was soluble. Therefore, the effect of GSTM2C (GSTM2C) and smaller C-terminal domain fragments on the cardiac and skeletal ryanodine receptor activity was investigated in detail in comparison to the full length GSTM2 molecule (Liu *et al*, 2009).

3.1.1 Region responsible for RyR2-specific activity of GSTM2 is unambiguously located in the C terminal helical bundle.

As it was expected that the C terminal domain of the protein would be inactive, it was a surprise to find that GSTM2C at 30 μM was as effective as the full length protein at 30μM in inhibiting caffeine-induced Ca^{2+} release from cardiac SR and single channel lipid bilayer activity (Liu *et al.*, 2009).

GSTM2C inhibited caffeine-induced Ca^{2+} release from cardiac SR with similar efficacy to the full length protein. But, the GSTM2C was inactive when applied to the skeletal SR preparation. An activation of caffeine-induced Ca^{2+} release from skeletal SR was observed in the presence of 30μM full length protein. In contrast, the rate of Ca^{2+}

release was not altered significantly with GSTM2C. Similar results were observed in single channel lipid bilayer experiments (Liu *et al.*, 2009). GSTM2C inhibited the single cardiac RyR2 channel significantly more than the full length protein. GSTM2C did not activate or alter skeletal RyR1 activity in contrast to the full length protein which triggered an increase in the relative open probability (P_o).

The results reported by Liu *et al* (2009) clearly indicate that the inhibitory effect of GSTM2C on cardiac ryanodine receptor activity is fully supported by the C terminal helical bundle while the activation of skeletal ryanodine receptor activity is not supported at all. Since the full length protein activates skeletal ryanodine receptor activity both in single channel lipid bilayer experiments and Ca^{2+} release assays, it could be assumed that N-terminal half of the protein is responsible for the activation of RyR1 channels.

It was concluded that the C terminal half of GSTM2 is highly specific for RyR2. The active site for GST enzyme activity and GSH binding site are located in the N-terminal half of GSTM2. Pharmacologically, it is advantageous that the C- terminal half of the protein is active as it could be administered without any side effects that might be associated with its enzymatic action or its action on RyR1 in skeletal muscle.

3.1.2 Fragments of GSTM2C do not affect Ca^{2+} release from skeletal SR

As described in the chapter 1, GSTM2C consists of five α helices. Therefore, to determine which part of GSTM2C was responsible for inhibition of RyR2, constructs were designed (Fig 3.2), with various combinations of these helices.

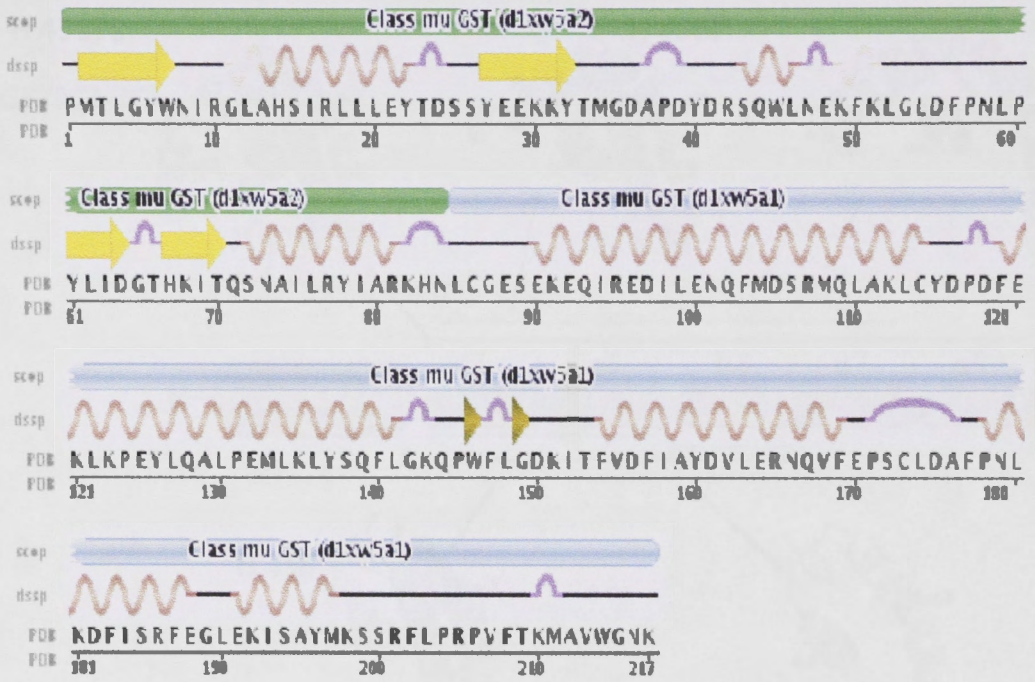

Figure 3.1: Schematic illustration of the secondary structure of GSTM2 from RCSB Protein Data Bank website (http://www.rcsb.org) using PDB file 1xw5. Green bars indicate the thioredoxin-like domain and blue bar indicates the alpha helical domain. Yellow arrows indicate extended strands, brown arrow heads indicate isolated beta ridges, purple curves indicate hydrogen bonded turns and red spirals indicate alpha helices.

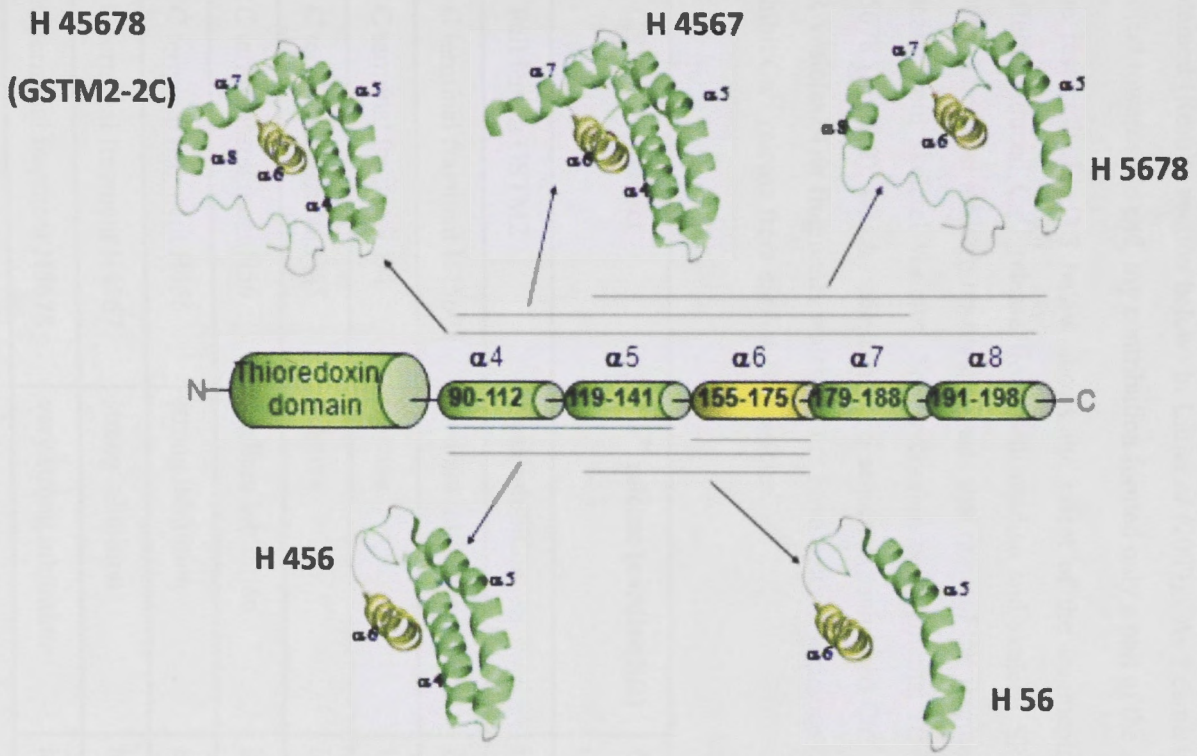

Fig 3.2: An illustration of the different constructs of the C-terminal regions used (Liu *et al*, 2009). The linear structure of GSTM2C is shown in the centre. The helices are numbered sequentially from α4 to α8. The structures of the fragments shown here have been predicted from the complete crystal structure (PDB entry 1XW5) of (Raghunathan *et al*., 1994) and have not been independently determined. Therefore, the precise structure of the fragments may differ in the absence of constraints imposed by the complete molecule. Combination of helices in each fragment are named as H456 (e.g. helices 4,5 and 6) respectively. Figure adapted and modified from (Dulhunty *et al*., 2011).

The constructs were named according to the numbers of the helices that they contained. Thus, H456 for example contain sequences helices 4, 5 and 6. The results described here (in the Introduction) were carried out by Dan Liu, Esther Gallant and Suzy Pace. This data is presented in some detail because it was combined with the results that I obtained (Results section below) in Liu *et al* (2009). As I came into this aspect of the project towards the end, my contribution formed only a part of the study.

The results in Fig 3.3 below shows the effect of the fragments from GSTM2C on caffeine-induced Ca^{2+} release from both cardiac and skeletal SR vesicles (Liu *et al*, 2009). The most striking observation was that none of the fragments reduced the Ca^{2+} release from skeletal vesicles. Four recombinant fragments, H56, H456, H4567 and H5678 (Fig 3.2), which contain helix 6 sequence, inhibited Ca^{2+} release from cardiac SR vesicles. The fragments which do not have helix 6 sequence (H4 & H45) failed to inhibit Ca^{2+} release from cardiac SR vesicles.

GSTM2Construct	**Ca^{2+} release (cardiac SR)**	**Ca^{2+} release (skeletal SR)**
Full length GSTM2	weak inhibition	inactive
C terminal fragment H45678	medium inhibition	inactive
C terminal fragment H4	inactive	inactive
C terminal fragment H45	inactive	inactive
C terminal fragment H56	medium inhibition	inactive
C terminal fragment H456	strong inhibition	inactive
C terminal fragment H4567	strong inhibition	inactive
C terminal fragment H5678	very strong inhibition	inactive

Table 3.1: A summary of the effect of GSTM2 and its fragments on Ca^{2+} release from cardiac and skeletal SR vesicles (Liu *et al.*, 2009).

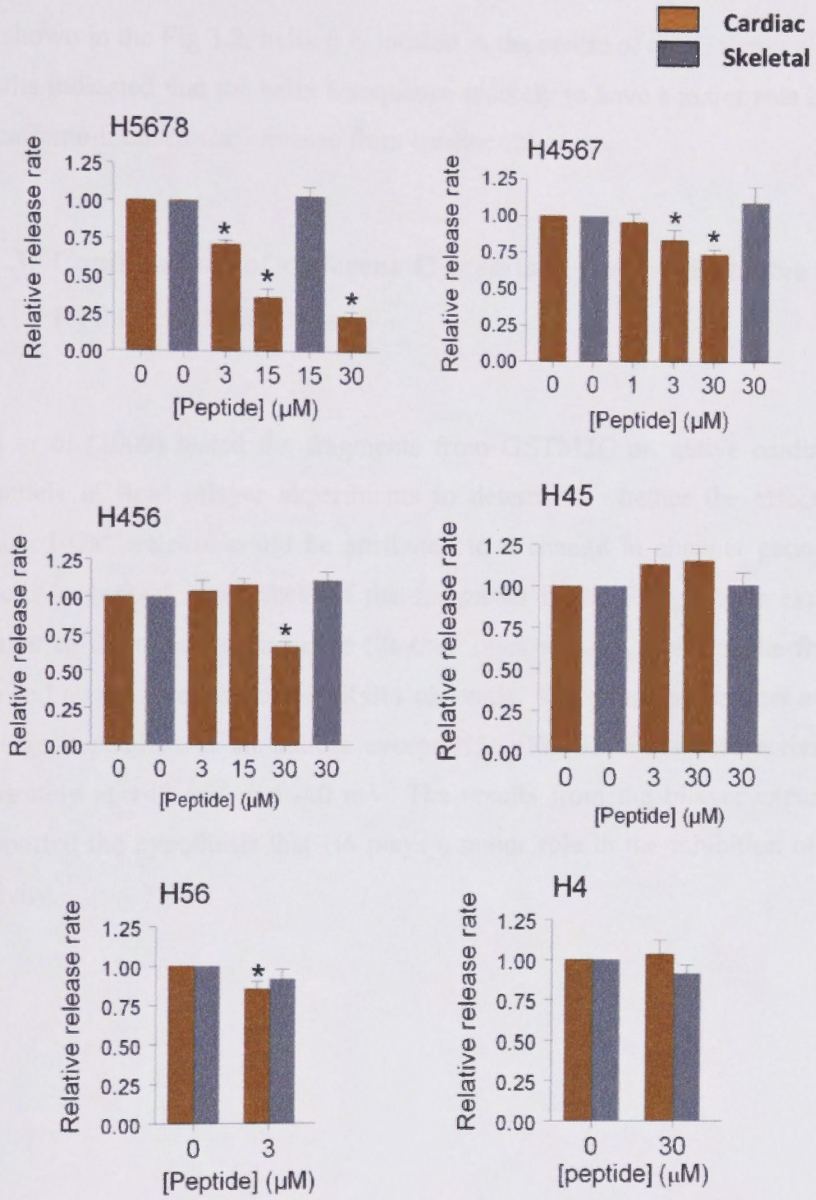

Fig 3.3: Average relative rates of Ca^{2+} induced Ca^{2+} release from cardiac (brown bins) and skeletal (grey bins) SR vesicles that had been incubated with fragments H4 (A), H45 (B), H56 (C), H456 (D), H4567 (E) and H5678 (F). The concentration of each fragment used is indicated on the X axis in each graph. GSTM2C constructs containing the H6 sequence inhibit Ca^{2+} release from cardiac vesicles, but do not affect Ca^{2+} release from skeletal SR vesicles. (*) indicates a significant difference from control values. N≥5 for each data set (Liu *et al.*, 2009).

As shown in the Fig 3.2, helix 6 is located in the centre of the C terminal domain. These results indicated that the helix 6 sequence is likely to have a major role in the inhibition of caffeine-induced Ca^{2+} release from cardiac SR.

3.1.3 Contribution of different C terminal fragments to the inhibition of RyR1/RyR2 channels

Liu *et al* (2009) tested the fragments from GSTM2C on native cardiac and skeletal channels in lipid bilayer experiments to determine whether the effects on caffeine-induced Ca^{2+} release could be attributed to a change in channel gating or to a pore block. In general, the effects of the fragments in the lipid bilayer experiments were similar to the effects seen in the SR Ca^{2+} release assay. None of the fragments tested showed an inhibitory effect on RyR1 channels. The effect on channel activity was not voltage dependent in all helices except H56 (Fig 3.4 E), where activity was shown separately at +40 mV and -40 mV. The results from the bilayer experiments further supported the hypothesis that H6 plays a major role in the inhibition of cardiac RyR2 activity.

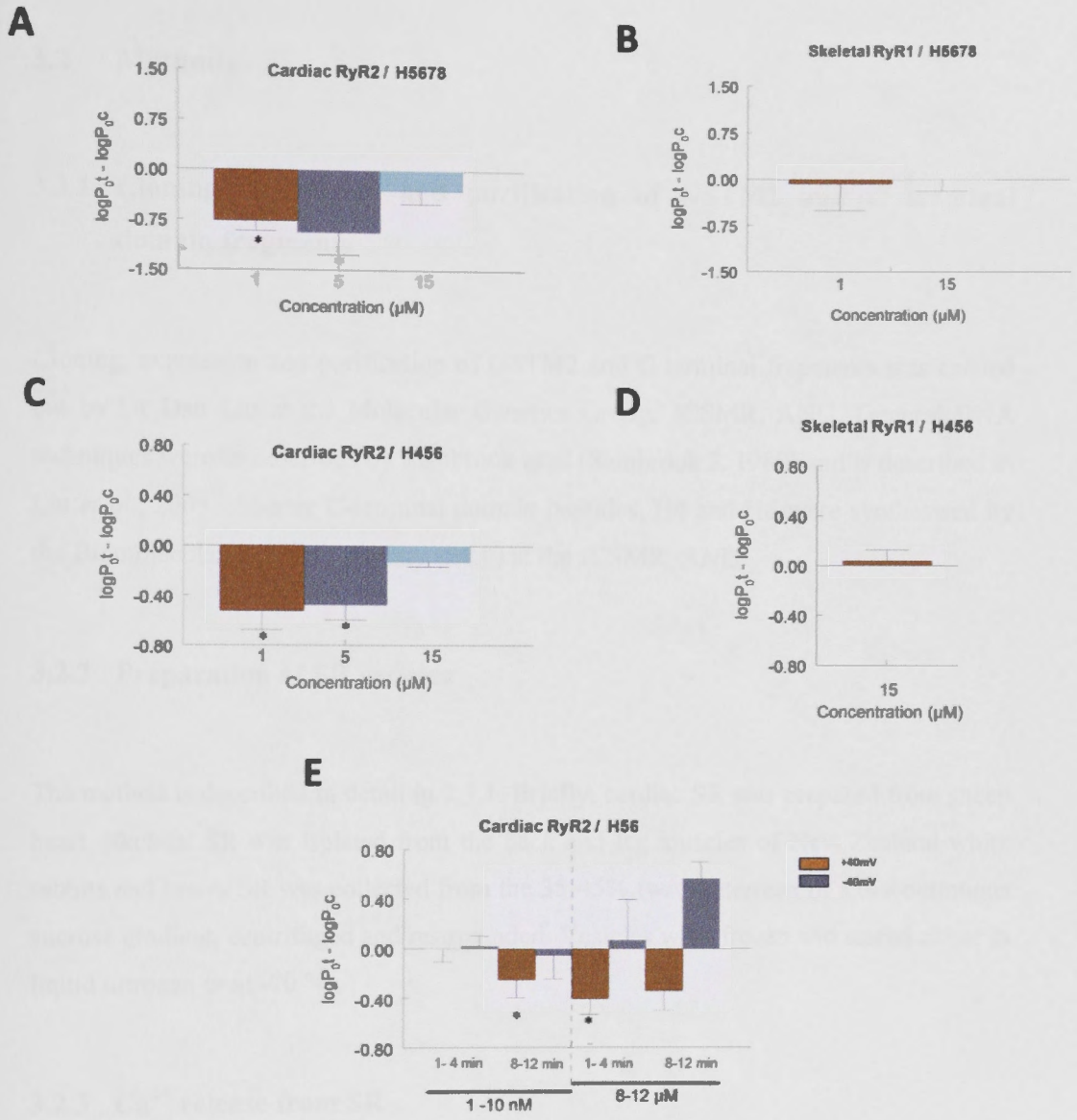

Fig 3.4: Effect of GSTM2C fragments H5678, H456 and H56 on cardiac RyR2 channels and skeletal RyR1 channels are summarized. A, C & E show graphs of average relative open probability (average of the log P_ot- log P_oc values for each individual channel, where P_oc is the internal control for that channel) obtained in the presence of the indicated concentrations of each construct for cardiac RyR2. Both H5678 (B) and H456 (D) did not affect skeletal RyR1 activity. Due to the complex action of H56, data is shown separately for +40 and -40mV and is shown between 1-4 min and between 8-12 min after the addition of two different ranges of concentrations of H56. (*) indicates a significant difference from control values (Liu *et al.*, 2009).

3.2 Methods

3.2.1 Cloning, expression and purification of GSTM2 and C terminal domain fragments

Cloning, expression and purification of GSTM2 and C terminal fragments was carried out by Dr Dan Liu at the Molecular Genetics Group, JCSMR, ANU. General DNA techniques were as described by Sambrook *et al* (Sambrook J, 1989) and is described in Liu *et al.*, 2009. Shorter C-terminal domain peptides, H4 and H6 were synthesised by the Biomolecular Resource Facility (BRF) at the JCSMR, ANU.

3.2.2 Preparation of SR vesicles

The method is described in detail in 2.3.1. Briefly, cardiac SR was prepared from sheep heart. Skeletal SR was isolated from the back and leg muscles of New Zealand white rabbits and heavy SR was collected from the 35-45% (w/v) interface of a discontinuous sucrose gradient, centrifuged and resuspended. Vesicles were frozen and stored either in liquid nitrogen or at -70 °C.

3.2.3 Ca^{2+} release from SR

Cardiac or skeletal SR vesicles were incubated with peptides in vehicle buffer for 20 min prior to the start of the experiment. The same concentrations of GSTM2Constructs were added to the cuvette solution prior to vesicle addition. The baseline rate of Ca^{2+} release after addition of thapsigargin and the initial rate of caffeine-induced Ca^{2+} release were measured. A calibration curve of optical density changes with four additions of 12.5 μM $CaCl_2$ was constructed (Fig 3.5). The calibration curve was not altered by the presence of GSTM2, caffeine or ruthenium red. The method is detailed in 2.3.7.

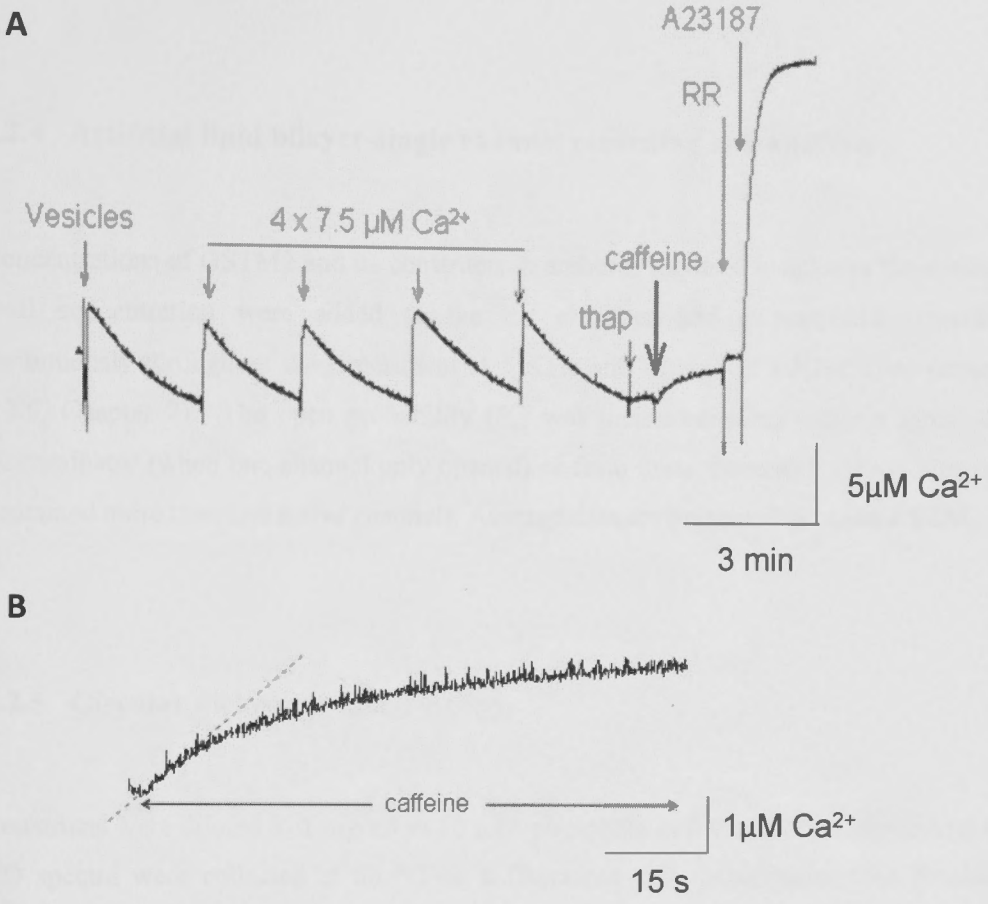

Fig 3.5: Measurement of caffeine-induced Ca^{2+} release from SR vesicles. The record in (A) shows an entire typical experiment measuring Ca^{2+} release from cardiac SR vesicles. [Ca^{2+}] was monitored with antipyralazo III absorbance. SR vesicles were added to the cuvette and loaded with Ca^{2+} added in four aliquots of 7.5 μM. The added Ca^{2+} was transported into the vesicles by the SR Ca^{2+} ATPase which was subsequently blocked by thapsigargin (thap). Ca^{2+} release was then initiated with 5mM caffeine (or 0.5mM caffeine with skeletal SR). Ruthenium red (Murray and Ohlendieck, 1997) was added to confirm that release was through RyR2. Remaining Ca^{2+} was released by the ionophore A23187, showing that a large non-caffeine releasable pool of Ca^{2+} remained in the SR preparation and that antipyralazo was not saturated with Ca^{2+} during the caffeine-induced response. (B) The caffeine transient was expanded and the initial rate of release (broken line) measured. Vesicles were equilibrated with the H6 construct (or buffer in control experiments) for 20 min on ice before the experiment commenced.

3.2.4 Artificial lipid bilayer-single channel recording and analysis

Concentrations of GSTM2 and its constructs in amounts required to achieve the desired final concentration were added to the *cis* chamber and current was recorded continuously throughout the experiment at 5 KHz and filtered at 1 KHz. (See section 2.3.6, Chapter 2). The open probability (P_o) was measured using either a threshold discriminator (when one channel only opened) or from mean current, I' (when bilayers contained more than one active channel). Average data are presented as mean ± SEM.

3.2.5 Circular dichroism spectroscopy

Constructs were diluted to 1 mg/ml in 10 mM phosphate buffer and pH adjusted to 8.0. CD spectra were collected at 20 °C on a Chirascan CD spectrometer (See detailed method, 2.3.5 in Chapter 2). Ten spectra were collected, averaged and subjected to a smoothing function.

3.3 Results

3.3.1 Control experiments: Effect of ATP and ruthenium red on RyR incorporated on artificial lipid bilayers.

Isolated, native SR vesicles were added to the *cis* chamber in the single channel lipid bilayer experiments described here. Correct orientation and identification of RyR in the bilayer set up was determined by monitoring the response of RyR to the cytoplasmic RyR modulators, ATP and ruthenium red (RR).

More than 99% of incorporated channels responded to specific agonist, ATP, indicating that incorporated RyR were correctly orientated, cytoplasmic side facing the *cis* chamber and luminal side facing the *trans* chamber. ATP promotes channel activity in two ways, either by binding to the RyR directly in a Ca^{2+}-independent manner (Meissner *et al.*, 1986b, Laver *et al.*, 2001) or by mediating RyR phosphorylation through hydrolysis (Dulhunty *et al.*, 2001a). ATP (2 μM) was added to the *cis* chamber in the presence of 10 μM *cis* Ca^{2+}, both to increase RyR activity and to determine the correct orientation of the incorporated channel. Application of ATP led to a 2.3-fold increase in activity in a majority of channels, increasing fractional mean current (I'f) from 0.17± 0.01 to 0.40 ±0.02 at both -40 mV and +40 mV (Fig. 3.8). Some channels showed as much as 3-4 fold increase in channel activity within 1-2 min and the activity remained constant up to ~15 min in almost all channels analysed.

According to Ma (1993), the blocking effect of RR is dependent on the side of the membrane to which it was added and is highly asymmetric and strongly voltage dependent. RR applied at sub micromolar concentrations to the *cis* side induces an all or none flicker block of ryanodine activated channels and the blocking effect is strongly voltage dependent and reduces the open probability of the channel. According to the author, *trans* RR produces a different blocking effect where the overall open probability is not altered. However, RR reduces single channel currents from the luminal side (current flow from *trans* to *cis* at negative potentials). The highly asymmetric block of RyR by RR produces an additional way of identifying the orientation of the bilayer. A channel with a normal *cis*-cytoplasmic, *trans*-luminal SR orientation channel will

respond to the addition of sub micromolar concentration of RR to the *cis* side with a fast flicker gating, an inversely orientated channel will respond with a reduction in single channel current amplitude (Ma, 1993).

As mentioned in the Chapter 1, micro molar concentrations of RR, added to the *cis* chamber dramatically decreases P_o, producing a long term channel closure that is substantially irreversible (Zucchi and Ronca-Testoni, 1997, Xu *et al.*, 1999, Ashley and Williams, 1990). In this study, addition of 10 μM RR in the *cis* chamber induced an almost complete inhibition of the RyR channel (Fig. 3.8A) with only rare and very brief openings. An activity drop was seen within 1 min after completion of chamber stirring, followed by total channel closure within 2 min, under conditions used in this study. Therefore, RR was used as a tool at the end of each experiment to confirm that the channel was a RyR and was oriented correctly.

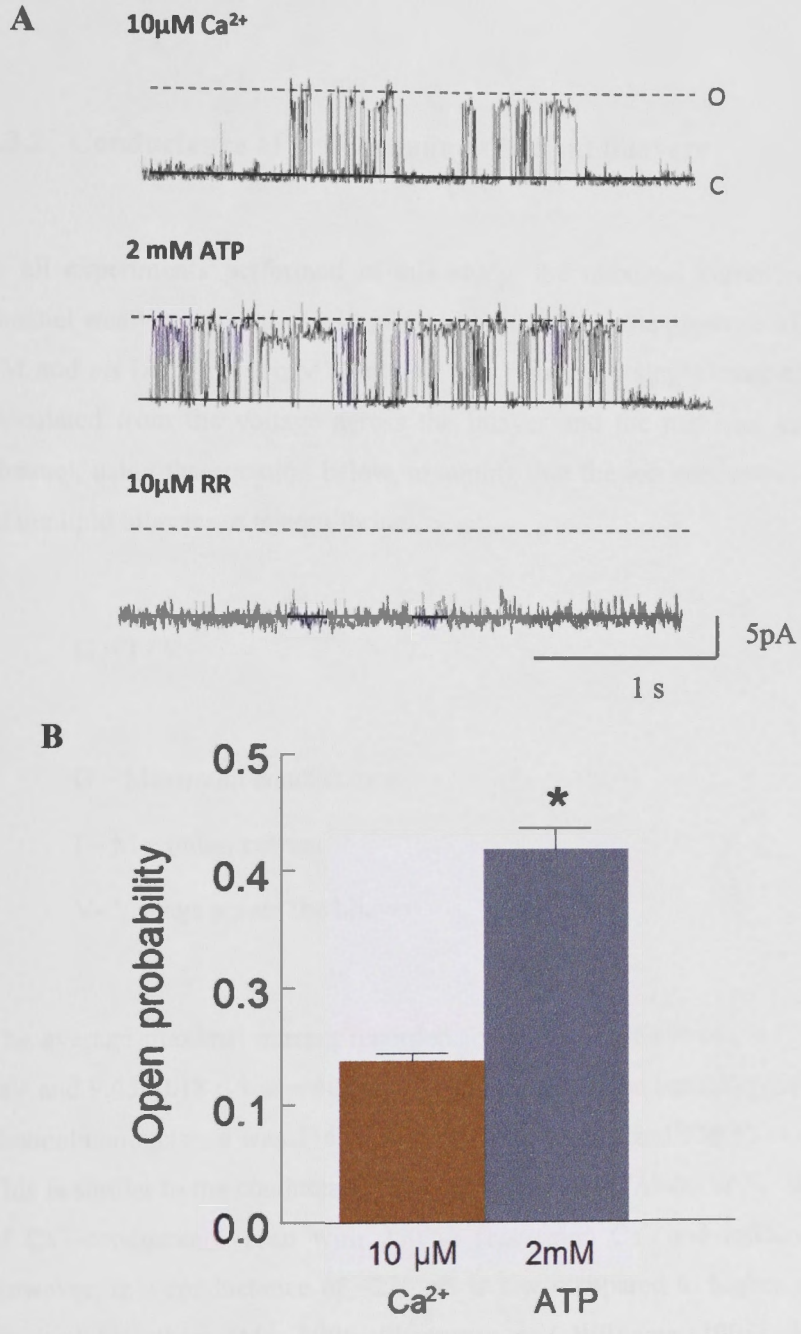

Fig 3.6: Effect of ATP and RR on RyR2. A) Activity of RyR in the presence of 10 μM *cis* Ca^{2+} concentration (control), 2 mM ATP and 10 μM ruthenium red. Records of 3 s of channel activity at +40 mV are shown. Single channel opening is upward from zero current (c, continuous line) to maximum open conductance (o, broken lines). Activation of the RyR by ATP, showing an increase in activity after ATP addition (lower trace) compared with the control is followed by a complete closure of the channel in the presence of 10 μM ruthenium red. B) Average open probability of the RyR2 channel in the presence of 10 μM *cis* Ca^{2+} and 2 mM ATP (*) indicate average values significantly different from control.

3.3.2 Conductance of RyR2 channels in lipid bilayers

In all experiments performed in this study, the maximal current of a single RyR2 channel was very similar at +40 mV and – 40 mV, in the presence of a *cis* [Ca^{2+}] of 10 μM and *cis* [ATP] of 2 mM (Fig 3.7). The maximum single channel conductance was calculated from the voltage across the bilayer and the maximal current through the channel, using the equation below, assuming that the ion concentrations on either side of the lipid bilayer are in equilibrium.

$$G = I / V$$

G – Maximum conductance

I – Maximum current

V- Voltage across the bilayer

The average maximal current recorded for RyR2 channels was 9.39±0.26 pA at + 40 mV and 9.45±0.18 pA at – 40 mV. When applied to the equation above, average single channel conductance was 234.65±6.54 pS at + 40 mV and 236.35±4.41 pS at – 40 mV. This is similar to the conductance reported previously (Ahern *et al.*, 1997) and is typical of Cs^+ conductance seen with 250/50 (*cis/trans*) Cs^+ and millimolar *trans* [Ca^{2+}]. However, this conductance of ~230 pS is low compared to higher values of ~500 pS reported by others (Ma, 1995, Sitsapesan and Williams, 1995). This is due to the presence of 1 mM Ca^{2+} in the *trans* solution which competes with Cs^+ for the binding sites in the channel pore and reduces the Cs^+ current (Tinker *et al.*, 1992). According to Ahern, (1994), channels showed a conductance of ~ 480 pS when the *trans* [Ca^{2+}] was reduced to 1μM (Ahern *et al.*, 1994).

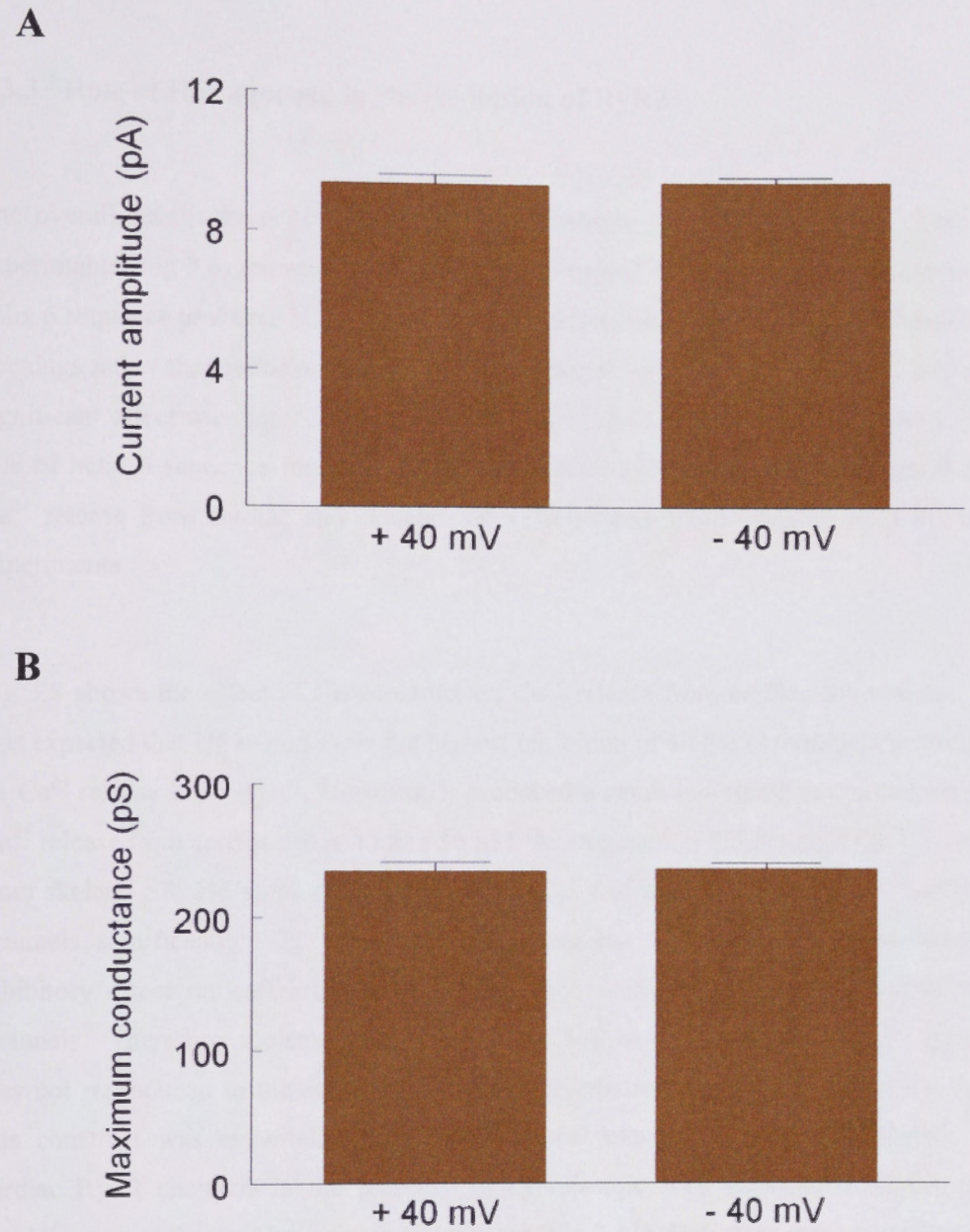

Fig 3.7: Single channel current amplitude (A) and maximaum conductance (B) for +40 and -40 mV. The single current amplitude (pA) is the distance from zero to maximal open current, using a *cis* solution with 10 μM [Ca^{2+}] and 2 mM ATP, and voltage clamped at either +40 or -40 mV. Maximal conductance as calculated by equation,

G= I / V. n = 10 channels.

3.3.3 Role of H6 sequence in the inhibition of RyR2

The overall results from caffeine-induced Ca^{2+} release (Fig 3.3) and single channel experiments (Fig 3.4) showed clearly that the C terminal domain constructs containing helix 6 sequence produced strong inhibition of RyR2 by reducing the number of channel openings rather than reducing the single channel conductance (Liu *et al.*, 2009). But no significant effect was observed in the skeletal RyR1 (Liu *et al.*, 2009). To explore the role of helix 6 sequence further, the effect of helix 6 (H6) alone was investigated on Ca^{2+} release from cardiac and skeletal SR vesicles and single channel lipid bilayer experiments.

Fig 3.8 shows the effect of H6 construct on Ca^{2+} release from cardiac SR vesicles. It was expected that H6 would show the highest inhibition of all the C-terminal constructs on Ca^{2+} release from RyR2. However, it produced a small but significant reduction in Ca^{2+} release from cardiac SR at 15 and 30 μM. As expected, it did not alter Ca^{2+} release from skeletal SR. H6 alone did not alter the activity of either cardiac or skeletal RyR channels significantly (Fig 3.9 and 3.10). Only the fragments which showed an inhibitory effect on caffeine-induced Ca^{2+} release were tested on RyR1 and RyR2 channels. Therefore, the smaller inhibition observed in caffeine-induced Ca^{2+} release was not reproduced in the single channel experiments reinforcing the conclusion that this construct was essentially inactive. Additional experiments were performed on cardiac RyR2 channels in the presence of cytoplasmic ATP (2 mM) to mimic the conditions used for the Ca^{2+} release experiment (Fig 3.11). However, these experiments also failed to show any significant effect of H6.It can be concluded from the Ca^{2+} release and single channel experiments, that C terminal constructs containing H6 sequence plus sequences corresponding to two or more neighbouring helices are essential for a stronger inhibition of cardiac RyR2. The results from my experiments and studies of each of the other fragments (Liu *et al.*, 2009) indicate that H6 sequence is essential for inhibition of RyR2 channels, but either that its structure requires stabilization by the flanking helices or that the flanking helices contribute to the interaction with RyR2.

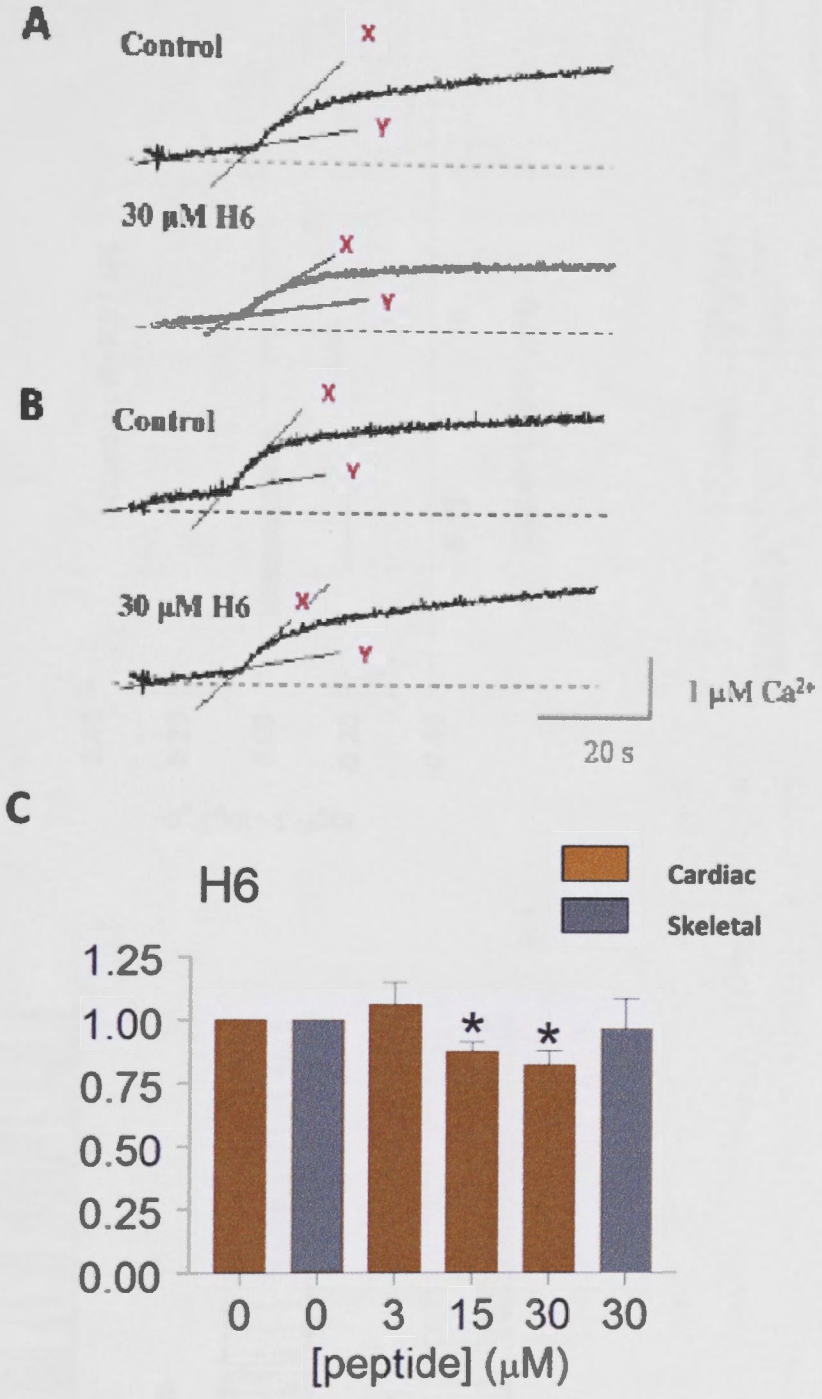

Fig 3.8: H6 produced a small but significant reduction in caffeine-induced Ca^{2+} release from cardiac SR but not from skeletal SR. A) Baseline release with thapsigargin (slope of line Y) and initial rate of Ca^{2+} release after caffeine addition (slope of line X) from cardiac vesicles (A) and skeletal vesicles (B). (C) shows average relative rates of caffeine-induced Ca^{2+} release from cardiac (brown bins) and skeletal (grey bins) SR vesicles that had been incubated with different concentrations of H6. (*) indicates a significant difference from control values.

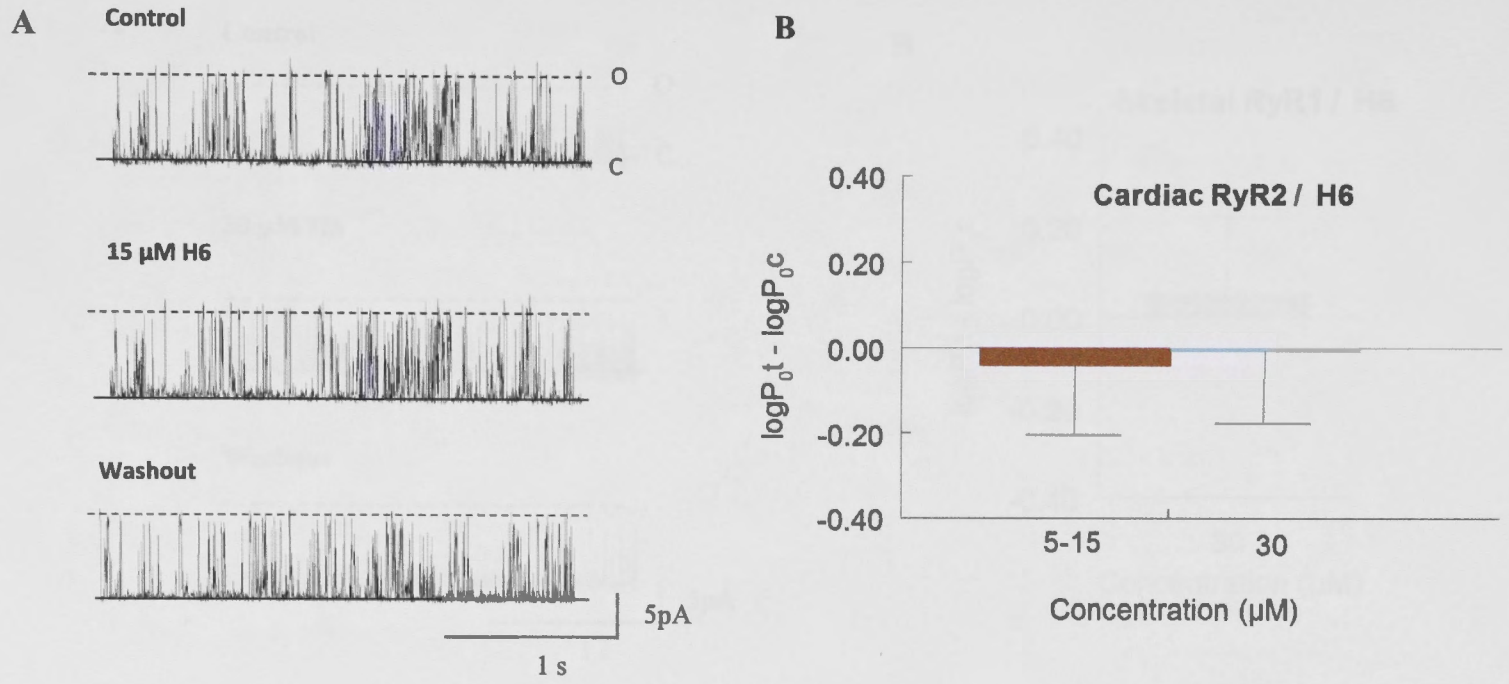

Fig 3.9: H6 alone at 15 µM did not modulate cardiac RyR2 activity significantly. (A) Shows 3 s recordings of representative channel activity at +40 mV. Channel opening is upward from the closed level (c) to open levels (o). (B) Results are presented as average relative P_o (i.e. the average of log $P_{ot} - P_{oc}$) for + 40 mV and -40 mV. Relative P_o values are also presented in the table below the figure.

	Control	5-15 µM	30 µM
Relative P_o	1.0	1.0183	1.2832
SEM	-	0.3833	0.3675

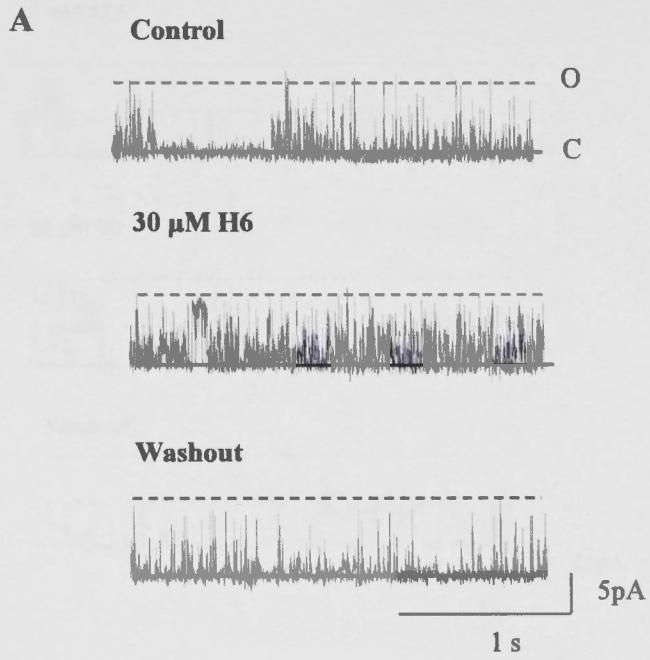

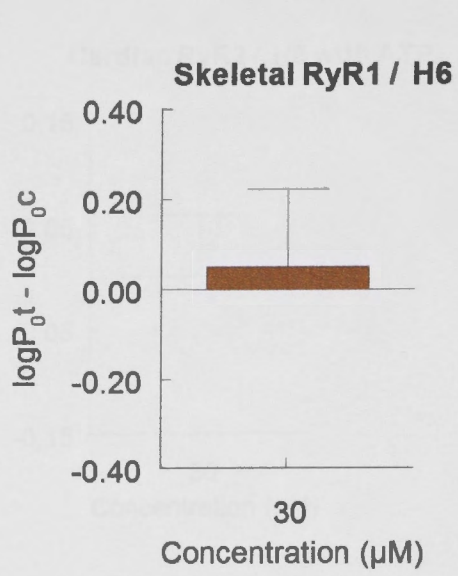

Fig 3.10: H6 alone at 30 μM did not modulate skeletal RyR1 activity significantly. (A) Shows 3 s recordings of representative channel activity at +40 mV. Channel opening is upward from the closed level (c) to open levels (o). (B) Results are presented as average relative P_o (i.e. the average of log $P_{ot} - P_{oc}$) for + 40 mV and - 40 mV. Relative P_o values are also presented in the table below the figure.

	Control	30 μM
Relative P_o	1.0	1.42761
SEM	-	0.6062

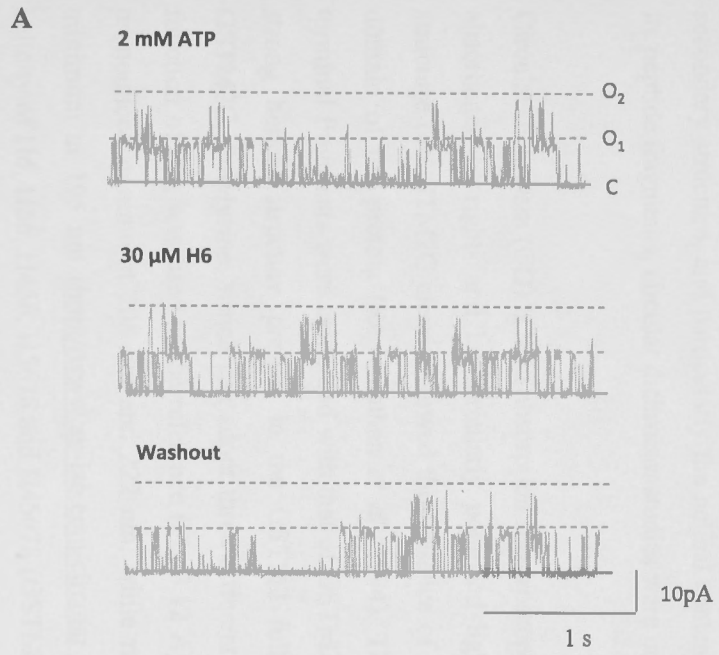

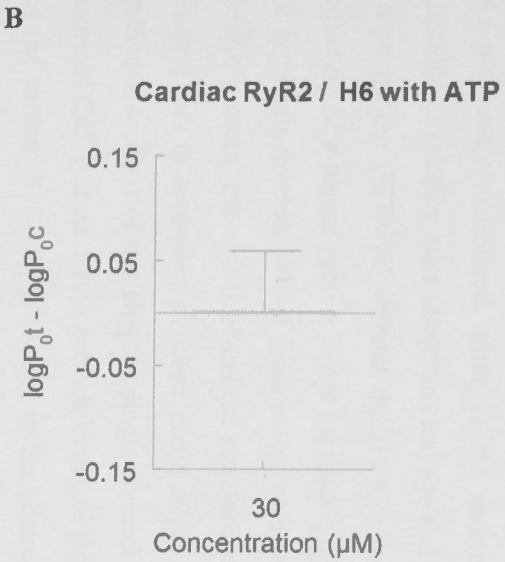

Fig 3.11: H6 alone at 30 µM in the presence of ATP did not modulate cardiac RyR2 activity significantly. (A) Shows 3 s recordings of representative channel activity at +40 mV. Channel opening is upward from the closed level (c) to open levels (o). (B) Results are presented as average relative P_o (i.e. the average of log $P_{ot} - P_{oc}$) for + 40 mV and -40 mV. Relative P_o values are also presented in the table below the figure.

	Control	**30 µM**
Relative P_o	1.0	1.126155
SEM	-	0.428949

3.3.4 A comparison of the helical content of C-terminal constructs

As previously mentioned, some of the shorter C-terminal domain fragments were unstable in solution after ubiquitin cleavage and were not used in this study. An attempt to purify the GSTM2C without the H6 also failed. This instability indicated that the structure of a parent protein is not necessarily retained when the protein is fragmented or segments deleted. Whilst these amino acid sequences may adopt helices in the full-length protein, the extent of helical structure retained in peptide form is not known. Such a loss in secondary structure could affect peptide solution stability. As shown in previous sections of this chapter, single channel lipid bilayer experiments and caffeine-induced Ca^{2+} release assays provide evidence for the importance of H6 in the inhibition of the cardiac RyR. H6 is located in the centre of GSTM2C with several interactions with nearby helices which may be disrupted or altered with removal of the helices, causing structural changes. Thus there may be a correlation between the structure of C-terminal constructs and the inhibitory action on RyR2. In order to ascertain the overall secondary structure, and particularly the helical content, of the C-terminal domain and its peptide fragments, circular dichroism studies were undertaken.

Circular dichroism (CD) is light absorption spectroscopy that measures the difference in absorbance of right- and left-circularly polarised light by a substance. The crystal structure of GSTM2C clearly showed the presence of five α helices in the C terminal domain of the protein (Raghunathan *et al*, 1994). Therefore, CD spectra of the C-terminal fragments were compared with that of GSTM2C. Fig 3.12 B confirms that the strong helical structure present in the GSTM2 full-length protein is retained by GSTM2C. Polylysine, which can adopt three different secondary structure forms as a function of pH, was used as the reference (Fig 3.12 A). Alpha helical proteins display pronounced minima at 208 nm and 222 nm, while random coil structures display a minimum at 195 nm (http://www.ap-lab.com/circular_dichroism.htm). The degree of helicity of H6, H56, H456, H5678 and H45678 (GSTM2C) was assessed and compared by the analysis of their CD profile.

The spectra in Fig 3.12 indicate that there is a high degree of helical content in GSTM2C, H5678, H456 and H56, while the peptide with the H6 sequence is unstructured. When the profiles were compared with GSTM2C, a small left shift was

noted in the 208 nm minimum for the H456 and H56 with a pronounced difference in the 222 nm minimum indicating a reduction in helical content in these two constructs. In contrast, H5678 showed a slight increase in its overall helical content. H6 did not show minima at 208 nm or 222 nm, but a minimum was observed at 195 nm suggesting the presence of a random coil structure. The results show that the fragments containing the sequence of two or more α helical regions are largely helical in structure. The observations further indicate that absence of inhibitory effect of the H6 sequence on RyR channels and the reduced inhibitory effect on caffeine-induced Ca^{2+} release may be due to the lack of α helical structure of the residues in isolation from the surrounding helices.

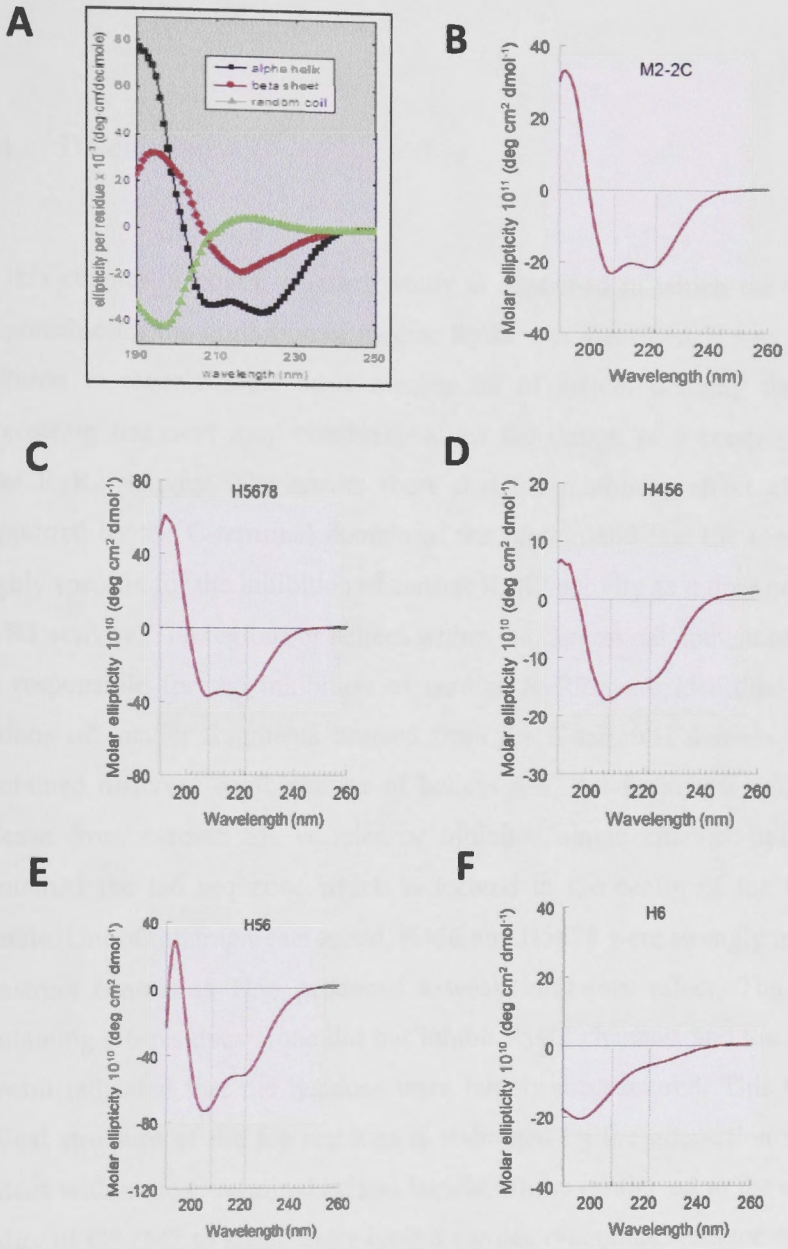

Fig 3.12: Graph A shows a reference profile for poly-lysine which changes its secondary structure from α helix, β pleated sheet to random coil when the pH of the solution changes from 11.0 to 6.5 (Ma *et al*, 2009). Graphs B-E shows CD spectra of each of the constructs, as indicated. GSTM2C (B), H5678 (C), H456 (D) and H56 (E) show a high degree of helical content while H6 is unstructured. Molar ellipticity (deg cm^3 $dmol^{-1}$) is plotted against wavelength in nm. Vertical dotted lines correspond to wavelengths of 208 nm and 222 nm where minima are formed by an ideal alpha helix.

3.4 Discussion

In this chapter, a novel structural study is described in which the region of GSTM2 responsible for the inhibition of cardiac RyR2 was identified. It was also hoped that, in addition to revealing the basic mechanism of action, defining the structure of the interacting fragment may eventually allow the design of a compound to specifically alter RyR2 activity. The results show that the inhibitory effect of GSTM2 is fully supported by the C-terminal domain of the protein and that the C-terminal domain is highly specific for the inhibition of cardiac RyR2 activity as it does not alter the skeletal RyR1 activity. The regions or helices within the C-terminal domain of GSTM2 that may be responsible for the inhibition of cardiac RyR2 were identified by exploring the actions of smaller fragments derived from the C-terminal domain. These fragments contained different combinations of helices 4-8. All fragments which inhibited Ca^{2+} release from cardiac SR vesicles or inhibited single channel lipid bilayer activity contained the H6 sequence which is located in the centre of the C-terminal helical bundle. Out of the fragments tested, H456 and H5678 were strongly inhibitory while the construct containing H56 produced a weak inhibitory effect. The synthetic peptide containing H6 residues alone did not inhibit RyR2 channels and the circular dichroism spectra indicated that the residues were largely unstructured. This suggested that the helical structure of the H6 residues is stabilized by the interaction with neighbouring helices within the C-terminal helical bundle. These results led to the conclusion that the ability of GSTM2 to specifically inhibit cardiac ryanodine receptor activity depends on the structural integrity of the C-terminal part of the protein with helix 6 sequence playing a critical role or on the H6 residues alone when they are contained in a helical structure.

3.4.1 GSTM2, the most physiologically important GST isoform in striated muscle

GSTM2, which was initially known as GST4, is specifically expressed in the human heart and skeletal muscle (Board *et al.*, 1988). Therefore, it may be the most physiologically important GST isoform in human skeletal and cardiac muscle. Abdellatif *et al* (Abdellatif *et al.*, 2007) also reported a similar protein expressed in the rabbit skeletal muscle and sheep cardiac muscle at concentrations in the order of 17-93 μM. This is within the range of concentrations (1-30 μM) that GSTO1-1 and GSTA1-1 had been shown to be effective in altering RyR1 and RyR2 activity (Dulhunty *et al.*, 2001a, Dulhunty *et al.*, 2011). In the present study, the GSTM2 or its fragments were tested within the same physiological range (1-30 μM) and it was predicted that if added to intact cells, the effective fragments of the GSTM2 might replace the endogenous protein and exert their action on the cardiac RyR2 (Liu *et al*, 2009).

3.4.2 Role of ATP

RyR activity was assessed in two ways in this study. Firstly, by measuring the effect on caffeine-induced Ca^{2+} release from SR vesicles and secondly by examining the activity of single channels incorporated into artificial lipid bilayers. ATP, which is an agonist of the RyR, was used in some lipid bilayer experiments with the aim of reproducing one of the Ca^{2+} release assay and one of the physiological conditions that exist in the cell. The caffeine induced Ca^{2+} release assay can not be carried out without ATP in the medium as ATP is essential for the function of Ca^{2+} ATPase and hence, for Ca^{2+} loading into SR. ATP can alter RyR activity either by directly binding to a specific adenine nucleotide binding site on the cytoplasmic domain of the protein (Meissner, 1984, Chan *et al.*, 2000) or by phosphorylation when it provides a substrate for kinases that are either free in the cytoplasm or anchored to the SR membrane (Wang and Best, 1992, Herrmann-Frank and Varsanyi, 1993, Hain *et al.*, 1994, Sonnleitner *et al.*, 1997). As reported by Dulhunty *et al*, prolonged exposure to ATP causes an irreversible increase in RyR

activity in single channel lipid bilayer experiments, suggesting the presence of endogenous kinases anchored to the RyR protein (Dulhunty *et al.*, 2001b). However, the possibility of having soluble kinases in either the bilayer setting or in the Ca^{2+} release assay used in this study is minimal. Some studies use an ATP generating system, mostly phosphoenol pyruvate and pyruvate kinase, to ensure that ATP concentrations are maintained during the experiment. ADP (adenosine-di-phosphate) formed by hydrolysis of ATP during Ca^{2+} binding during cross bridge cycle will be rephosphorylated to ATP by phosphoenol pyruvate and pyruvate kinase. Creatine phosphate and creatine phosphokinase can also be used as an ATP generating system (Board *et al.*, 2004, Penpargkul, 1979). However, an ATP generating system was not used in these studies. The protocol followed in these experiments was tightly controlled, therefore the ATP concentration would have been the same during the protein/peptide exposure in each experiment, and ATP would have been utilized at the same rate and varying with time in the same way from experiment to experiment. As shown in Fig 3.7A, the rate of Ca^{2+} uptake during loading was the same in the first and the fourth loading step, therefore, it was assumed that ATP was not severely depleted.

3.4.3 Non releasable Ca^{2+} pool and K^+ and Cl^- channels

The SR also contains a substantial Ca^{2+} pool that does not respond to caffeine and the fraction of SR occupied by this pool is shown clearly by the release in the presence of the ionophore in the caffeine-induced Ca^{2+} release assay. This pool is due to the presence of longitudinal SR which lacks RyR channels, but contains K^+ and Cl^- channels. Such channels were not seen in lipid bilayer experiments which were performed in the presence of $CsCH_3O_3S$. K^+ channels are impermeable to Cs^+ and Cl^- channels are impermeable to $CH_3O_3S^-$. In addition, the lack of K^+ ions and high [Cs^+] ions inhibit the SR Ca^{2+} ATPase (SERCA) (Kargacin *et al.*, 2005) which are also present in the SR vesicles used in these studies. Therefore, the presence of these channels and the ATPase did not contribute to the currents recorded in the lipid bilayer study.

3.4.4 Sensitivity of Caffeine-induced Ca^{2+} release assay and bilayer experiments

Higher concentrations of proteins/peptide were required to see effects (inhibition or activation) on caffeine-induced Ca^{2+} release than on singe RyR channels in lipid bilayers. A similar difference between the two techniques has been observed previously (Dulhunty *et al.*, 1999, Lu *et al.*, 1994). The difference may in part reflect the lower resolution of the Ca^{2+} release experiments. The reduced inhibition at higher concentrations seen in bilayer experiments was not seen in caffeine-induced Ca^{2+} release. As shown in Fig 3.3 and 3.4, a higher concentration of the respective C terminal fragment was needed to see an inhibitory effect in the Ca^{2+} release assay but the cardiac RyR2 activity was inhibited significantly in the presence of lower concentrations of the protein in single chnnel lipid bilayer experiments. This may have been because higher concentrations are required to see the effects in Ca^{2+} release experiments. However, it may also be that higher concentration effects were specific to the bilayer situation where the channel is in a less physiological environment than in the vesicle study.

3.4.5 Interaction between GSTM2C and RyR2

A consistent feature of all lipid bilayer experiments in this study was that the effects were easily reversible when the GSTM2 or fragments were washed out of the solution. This reversibility may be a common feature for all members of the GST structural family, as the activity of GSTO1-1, GSTA1-1 and CLIC-2 could be reversed when the proteins were perfused from the bilayer solutions (Dulhunty *et al.*, 2001a, Board *et al.*, 2001, Dulhunty *et al.*, 2011). This reversibility indicated that the reaction between RyR and the GST proteins depended on reversible ligand binding rather than the formation of a disulfide bond. As discussed above and in Liu *et al*, the weak nature of the interaction between the GSTs and RyR2 seen in lipid bilayer experiments was also seen in affinity chromatography when the active portion of GSTM2 (H5678) failed to pull down RyR2 (Liu *et al.*, 2009). However, the presence of a physical interaction between the RyR

tetramer and the GSTM2 protein was demonstrated in chemical cross linking experiments shown in Fig 3.13 below (Liu *et al*, 2009).

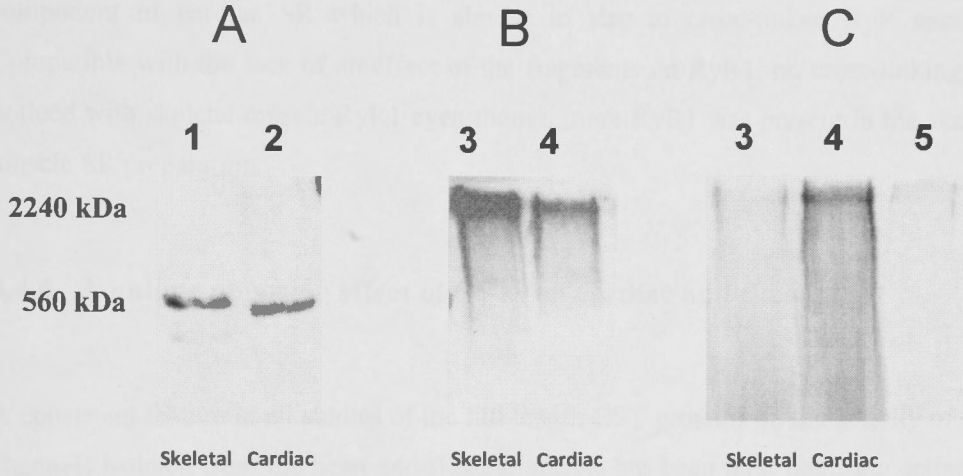

Fig 3.13: Cross-linking analysis of H5678 and RyR interactions. Panel A and B are Western blots immunodetected using anti-RyR antibody. Panel C is [^{35}S] radiography. **Panel A:** Skeletal (lane 1, 2 μg) and cardiac (lane 2, 60 μg) SR that has not been cross-linked. **Panel B:** RyR after the incubation of SR with [^{35}S] methionine labelled H5678 followed by cross linking. Lane 3, 22 μg of skeletal SR + [^{35}S] methionine, lane 4, 62 μg of cardiac SR + [^{35}S] methionine. **Panel C:** Radiograph of SDS-PAGE which shows [^{35}S] methionine labelled H5678 after the incubation with SR and subsequent cross-linking. Lanes 3 and 4 as same as panel B but lane 5 shows [^{35}S] H5678 after the cross linking reaction in the absence of SR (Liu *et al.*, 2009).

RyR monomers show a molecular mass of 560 KDa and the cross linked tetramers are >2200 KDa. Autoradiography (Fig 3.13) shows that the ^{35}S labelled H5678 fragment is co-localized with RyR2 but not with RyR1. The results from this experiment indicate that the sequence containing H5678 from GSTM2C binds to a high molecular weight component of cardiac SR which is similar in size to cross-linked RyR tetramer. Compatible with the lack of an effect of the fragments on RyR1, no cross-linking was noticed with skeletal muscle RyR1 even though more RyR1 was present in the skeletal muscle SR preparation.

3.4.6 A unique opposing effect of GSTs on cardiac and skeletal SR

A consistent feature in all studies of the full length GST proteins on the activity of RyR channels isolated from the heart and skeletal muscle has been their opposing actions in inhibiting cardiac RyR2 channels and in activating RyR1 channels (Board *et al.*, 2004, Liu *et al.*, 2009, Dulhunty *et al.*, 2001a, Dulhunty *et al.*, 2005c). These effects were mild as the channel activity was modulated by the GSTs within a physiological range of open probabilities that allows the channel to maintain its physiological function. Activity of RyR2 was not completely abolished by the GST interaction, but is reduced to 40-60% of the control activity. Similarly, the activity of RyR1 channels was increased by a factor of ~2, so that channels were not fully opened by the GSTs. This leaves the channel in a situation in which it can be further modulated by other endogenous ligands.

As mentioned in the General Introduction, early studies with GSTO1-1 (Dulhunty *et al*, 2001a), GSTA1-1 (Dulhunty *et al*, 2011) and GSTM2-2 (Abdellatif *et al*, 2007) all indicated this opposing effect on skeletal and cardiac RyRs. However, this type of inhibition is not a specific effect of GSTs, since Laver and Lamb, (1998) reported that individual RyR could be inactivated after voltage steps to positive and negative values. These authors further suggested that stepping the membrane potential to positive values would convert the RyR into the activated (+) state and by reversing the potential RyRs would assume the open state rapidly followed by a relatively slow transfer to the

inactivated (-) state (Laver and Lamb, 1998). In contrast to this activation dependent inhibition observed in skeletal RyR, cardiac RyR was inhibited by a "simple" inhibition by GSTM2 in which the channel open probability was reduced similarly at both positive and negative potentials.

3.4.7 Role of the N-terminal domain of GSTM2

Although voltage dependent inactivation of RyR1 was observed with the full length GSTM2, the C terminal constructs did not alter RyR1 activity in a similar manner. This indicated that excitatory action of GTM2 on the skeletal RyR must depend either solely on residues in the N-terminal thioredoxin fold or at least on the presence of some residues in this domain. Despite the overwhelming evidence that the critical site for inhibition of RyR2 is located in the C-terminal half of GSTM2, the N-terminal domain also appears to influence the activity to a certain extent.

The reason why the Cys32 to Ala substitution or N-ethylmaleimide application prevented the inhibitory action of C terminal domain is still not clear, but it is possible that it caused a conformational change in the N-terminal domain, which prevented or limited access to the RyR binding site in the helical bundle. It is also not surprising as some of the C-terminal helices are well buried in the full GSTM2 structure. A similar study presented by Liu *et al* (Liu *et al.*, 2009) also suggested the influence of the active site on the inhibitory effect on RyR2. In that study, a Tyr-7 was replaced by a Phe with the intention of abolishing the enzymatic activity and to alter the structure of the catalytic site. The mutant GSTM2Y7F was tested on cardiac and skeletal RyR and the results were consistent with the previously reported results of GSTO1-1 and suggested the influence of the active site on the modulation of cardiac and possibly skeletal RyR activity. But the results presented in this chapter showed clearly that GSTM2C was more effective than the full length protein in inhibiting both Ca^{2+} release from cardiac SR and single RyR2 channel activity. Unfortunately, the effect of N-terminal domain could not be tested as it was insoluble during recombinant expression.

3.5 Conclusion

Results and discussion presented in this chapter show clearly that the ability of GSTM2 to specifically inhibit the cardiac RyR2 activity depends on the structural integrity of the C-terminal domain of the protein and helix 6, which is located in the centre of the C terminal domain, plays a major role in the inhibition of RyR2. The helix 6 sequence in isolation from surrounding helices was unable to inhibit the cardiac RyR2 activity and structural analysis with circular dichroism spectroscopy revealed that it was unstructured. Therefore, the active region of GSTM2 for the inhibition of the cardiac RyR2 involves the H6 sequence and the helical nature of this region is essential for its activity.

Chapter 4 The structure of the C-terminal helical bundle in GSTM2 determines its ability to inhibit cardiac ryanodine receptor activity.

4.1 Introduction

In Chapter 3, the regions of GSTM2 that interact with RyR2 and inhibit the channel are described. Dissection of the C-terminal domain into smaller fragments revealed that helix 6 located in the centre of the C-terminal helical bundle plays a key role in the inhibition of RyR2, but only when the residues adopt a helical structure. Aceto *et al* have shown that helix 6 plays a key role in the global folding of the cytosolic GST structural family (Aceto *et al.*, 1997). They identified an N-capping box motif (Ser/Thr-Xaa-Xaa-Asp) at the beginning of helix 6, which is strictly conserved in all glutathione-S-transferases and most of the related super family proteins. Their study provided evidence that these capping box residues have an important role in determining the helical conformation of helix 6 in the hydrophobic environment of the protein. However, as discussed in the previous chapter (Chapter 3), circular dichroism spectroscopy revealed that the helix 6 residues alone did not form an α-helix and that this construct was not effective in inhibiting RyR2 activity. In other words, this previous data indicated that the capacity of GSTM2C to inhibit RyR2 was not contained within the non-helical peptide containing the helix 6 sequence. These results suggested that helix 6 and its flanking helices are important for the structural stability of the C-terminal domain and the inhibitory action against RyR2.

The X-ray crystallographic structure of GSTM2 determined by Raghunathan *et al* suggested that helix 6 forms the hydrophobic core of the C-terminal domain and is surrounded by helices 4,5,7, and 8 (Fig 4.1A, (Raghunathan *et al.*, 1994). This helical configuration is also strikingly evident in X-ray crystallographic structures of other GST-fold super family proteins (Figure 4.2) as previously observed for CLIC1. Cromer *et al* reported that there are two regions of significant hydrophobicity in CLICs, as judged by hydrophobicity plots. One region is located in the N-terminal domain and

comprises helix 1 and β-strand 2. The second region is located in the C-terminal domain and comprises most of helix 6 and part of the loop preceding it (Cromer *et al.*, 2002). Both these regions are mostly hydrophobic in all GSTs, as they form the central core of the protein and provide critical interactions in keeping the two domains of the monomer together.

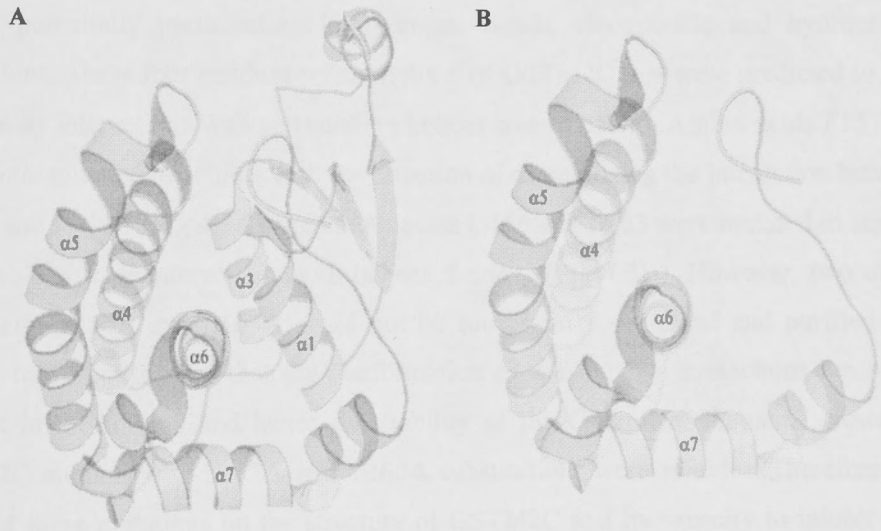

Fig 4.1: The location of helix 6 in the GSTM2 and GSTM2C. A) The crystal structure of GSTM2 prepared from structural coordinates in PDB file 1XW5. B) The predicted structure of GSTM2C after the removal of the N-terminal domain.Adapted from Dulhunty *et al*, 2011.

In GSTM2, helix 6 is connected to the surrounding helices through a series of ionic and hydrophobic interactions. As clearly shown in Fig 4.1B, helix 6 is more exposed in the predicted structure of GSTM2C which is more effective than the full length protein in inhibiting RyR2. This configuration suggests that helix 6 is important for maintaining the fold of the C-terminal domain of GSTM2. It is possible that either the entire fold is responsible for the inhibition of RyR2, or that the helix 6 residues in a helical structure is important for inhibition. An attempt to express the GSTM2C without helix 6 failed

(Dulhunty *et al*, 2011) and this provided additional evidence that helix 6 is essential for the stability of the GSTM2C.

To test this possibility, key contacts between helix 6 and surrounding helices were disrupted. The crystallographic structure of full length GSTM2 protein (RCSB-1XW5,Raghunathan *et al.*, 1994), allowed us to identify four residues within helix 6 that were in close proximity (<5 °A) to amino acid residues located in helices 5, 7 and 8 thereby potentially participating in hydrogen bonds, electrostatic and hydrophobic interactions. These four residues within helix 6 of GSTM2C that were predicted to help stabilize its interactions with surrounding helices were mutated. Amino acids F157 and Y160 were mutated to alanine with the intention of destabilizing the interaction between helix 6 and helix 7 (Fig 4.3A) and amino acids D156 and L163 were mutated to alanine to destabilize their interactions with helices 5 and 7 (Fig 4.3B). However, two of the constructs, D156A and L163A could not be successfully expressed and purified in a soluble form, confirming that the conformation of the helix 6 interactions are a key element in the folding and hence the stability of the C-terminal domain. However, GSTM2C mutants with F157A and Y160A substitutions were soluble. Therefore, the effect of these mutations on the structure of GSTM2C and its capacity to inhibit Ca^{2+} release from cardiac SR and RyR2 channel activity were investigated and results reported in this chapter.

Fig 4.2: Helix 6 is located in the centre of the C-terminal domain of three members of the GST super family. A) GSTO1-1 B) CLIC-2 C) GSTZ1-1. Images were obtained from the PDB entries, 1eem, 2r4v and 1fw1 respectively. Ball and stick models indicate reduced glutathione which binds to each GST isoform.

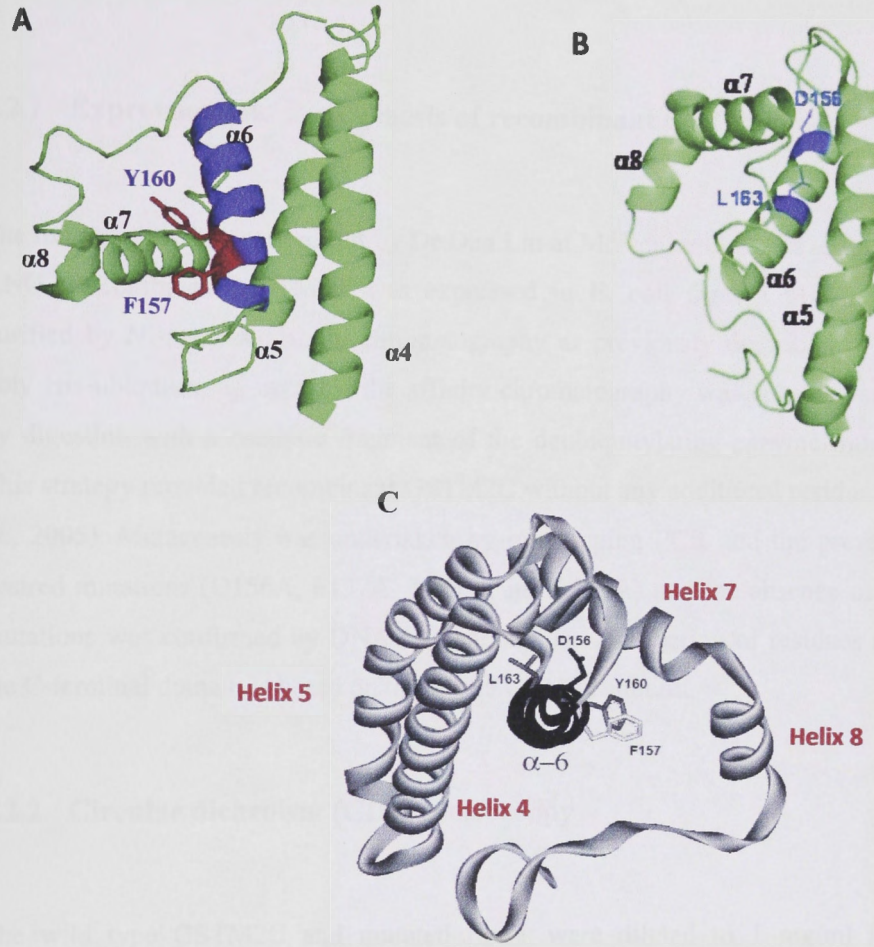

Fig 4.3: Residues in helix 6 of GSTM2C that were predicted to stabilize interactions between helix 6 and surrounding helices. A) Residues Y160 and F157 in helix 6 and their predicted interactions with residues in helix 7. B) Residues D156 and L163 in helix 6 and their predicted interactions with residues in helices 5 and 7. C) Another orientation of GSTM2C which shows clearly the presence of helix 6 in the centre of the molecule and the interaction of residues, Y160, F157, D156 and L163 with other helices.

4.2 Methods

4.2.1 Expression and mutagenesis of recombinant GSTM2C

The mutagenesis was carried out by Dr Dan Liu at Molecular Genetics Group, JCSMR, ANU. Recombinant GSTM2C was expressed in E. coli from a pHUE vector and purified by Ni-agarose affinity chromatography as previously described in 2.3.2. The poly His-ubiquitin tag used for the affinity chromatography was subsequently cleaved by digestion with a catalytic fragment of the deubiquitylating enzyme mouse Usp 2. This strategy provided recombinant GSTM2C without any additional residues (Baker *et al.*, 2005). Mutagenesis was undertaken by overlapping PCR and the presence of the desired mutations (D156A, F157A, Y160A and L163A) and the absence of additional mutations was confirmed by DNA sequencing. The numbering of residues mutated in the C-terminal domain is based on the whole GSTM2 subunit.

4.2.2 Circular dichroism (CD) spectroscopy

The wild type GSTM2C and mutated forms were diluted to 1 mg/ml in 10 mM phosphate buffer and pH adjusted to 8.0. CD spectra were collected at 20 °C on a Chirascan CD spectrometer (Applied Photophysics Ltd, United Kingdom). Ten spectra were collected, averaged and subjected to a smoothing function. Details of the method are described in 2.3.5.

4.2.3 Fluorescence scanning

Experiments were performed on a LS50B Luminescence Spectrophotometer (Perkin Elmer, USA) using an excitation slit width of 10 nm and an emission slit width of 9 nm as described in detail in 2.3.4. Protein samples (5 μM) were placed in a quartz cuvette (Spectrosil Far UV quartz windows cuvette, Starna Cells Inc., USA) and the fluorescence signal was measured by exciting the sample at 280 nm and monitoring the

emission at 290–450 nm. The maximum emission fluorescence intensity was observed at 340 nm.

4.2.4 Ca release from SR vesicles

SR vesicles were prepared from sheep heart as described in 2.3.1.2. The Ca^{2+} release assay was performed as detailed in 2.3.7. The SR vesicles were incubated for 20 min prior to the start of the experiment with the 30 μM wild type or mutant GSTM2C in vehicle buffer or with vehicle buffer alone for control experiments. The same concentrations (30 μM) of GSTM2C construct/mutant in vehicle buffer or with vehicle buffer alone were added to the cuvette solution prior to vesicle addition. Calibration curves of optical density changes with four additions of 12.5 mM $CaCl_2$ to the cuvette solution were constructed in the presence of vehicle or GSTM2C constructs and mutants. None of the proteins, or the presence of caffeine or ruthenium red, affected the calibration curve. The baseline rate of Ca^{2+} release after addition of thapsigargin (slope b, Fig. 4.6B) and the initial rate of caffeine induced Ca^{2+} release (slope a, Fig. 4.6B) were measured.

4.2.5 Determination of single channel activity

Single channel lipid bilayer experiments were performed as described in 2.3.6. Proteins were added to the *cis* chamber at volumes calculated to achieve final concentrations of 5, 15 and 30 μM. Using a 90s trace, average relative open probability was measured from individual channels in the presence and absence of 2 mM ATP at holding potentials +40 mV and –40 mV. Average data were presented as log P_ot- log P_oc.

4.3 Results

4.3.1 Expression and purification of recombinant GSTM2C and mutants, F157A and Y160A

The Expert Protein Analysis System (ExPASY) ProtParam web tool (Swiss Institute of Bioinformatics, Switzerland) estimated that the GSTM2C domain has a theoretical molecular weight of 15450.8. The apparent molecular weight of the purified recombinant GSTM2C, F157A and Y160A after 12% SDS denaturing PAGE (Fig 4.3) was ~ 15 kDa. All three proteins were purified in the same manner and yielded the same molecular weights (Fig 4.4). A faint band with a lower molecular weight appeared below the band for GSTM2C and mutants in all experiments performed. An attempt to separate this band using gel filtration failed and it was assumed to be either an artefact or a different conformation of the protein.

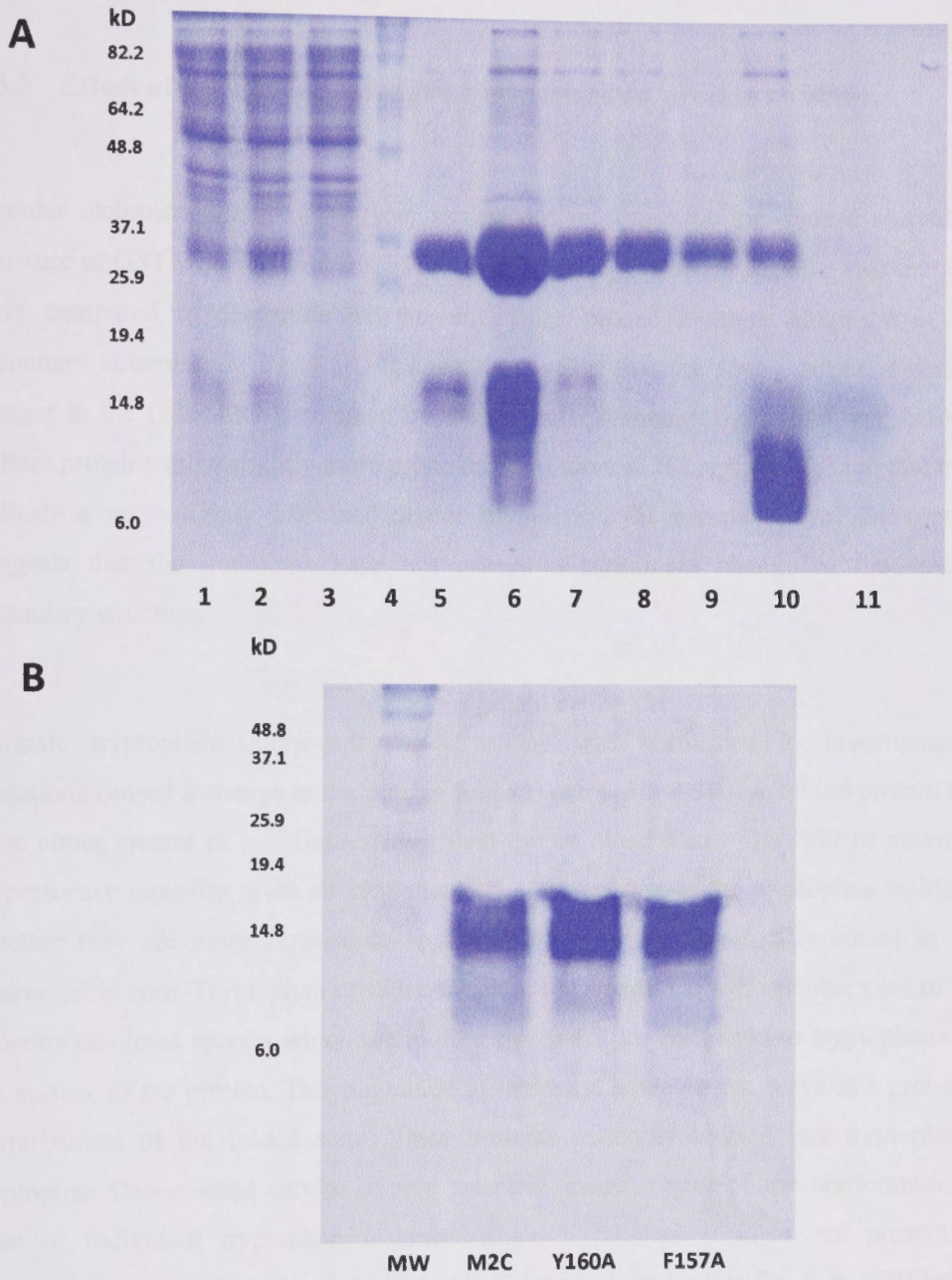

Fig 4.4: SDS PAGE of purified recombinant GSTM2C and mutants. A) Samples from each step in the purification of GSTM2C are shown. Lane 1: total lysate, Lane 2: Supernatant, Lane 3: unbound to Ni-agarose beads, Lane 4: Benchmark protein ladder, Lane 5-9: Eluants 1-5, Lane 10: GSTM2C-ubiquitin specific protease, Lane 11: purified GSTM2C protein, which does not stain very brightly unless very high concentrations were used. Benchmark protein ladder indicate the apparent molecular weight of GSTM2C to be ~14.8 kDa. B) A comparison of purified GSTM2C, Y160A and F157A. According to the protein ladder, molecular weights of GSTM2C and the mutatnts are not significantly different and ~14.8 kDa.

4.3.2 Effect of the F157A and Y160A mutations on protein structure

Circular dichroism spectroscopy was carried out to determine the overall secondary structure of GSTM2C and mutants F157A and Y160A. The spectra for the two mutants were compared to determine whether mutations caused a major alteration in the secondary structure. In Fig 4.5A, the results confirm that the strong helical structure present in the GSTM2C is retained by the mutants. Although the F157A and Y160A mutant proteins show slightly more pronounced minima at 208 nm and 222 nm that may indicate a very slightly increased degree of helicity, the comparison of the spectra suggests that the mutations have not caused a significant change in the overall secondary structure.

Intrinsic tryptophan fluorescence spectroscopy was performed to investigate if mutations caused a change in the protein fold structure (Fig 4.5B). A folded protein can have either greater or less fluorescence than the unfolded form. The shift of maximal fluorescence intensity gives an idea about the environment of the tryptophan residues, whether they are more exposed to an aqueous environment or totally buried in the hydrophobic core. Tryptophan residues which are buried in the hydrophobic core of the proteins can have spectra which are shifted by 10-20 nm compared to tryptophans on the surface of the protein. The magnitude of intensity, however can serve as a probe of perturbations of the folded state. Since proteins generally have a few tryptophans, tryptophan fluorescence can be a very sensitive measurement of the conformational state of individual tryptophan residues. Since tryptophan residues are present at positions 146 in helix 5 and 214 at the C-terminal end of helix 8 in GSTM2C, tryptophan fluorescence could be used to monitor the environment surrounding the residues. Both mutants showed a distinct increase in fluorescence at 340 nm but the increase with the Y160A mutant was particularly striking. These changes in tryptophan fluorescence emission suggest that both mutations have caused changes in the protein conformation that have altered the accessibility and environment of tryptophan residues that occur at positions 146 in helix 5 and 214 at the C-terminal end of helix 8.

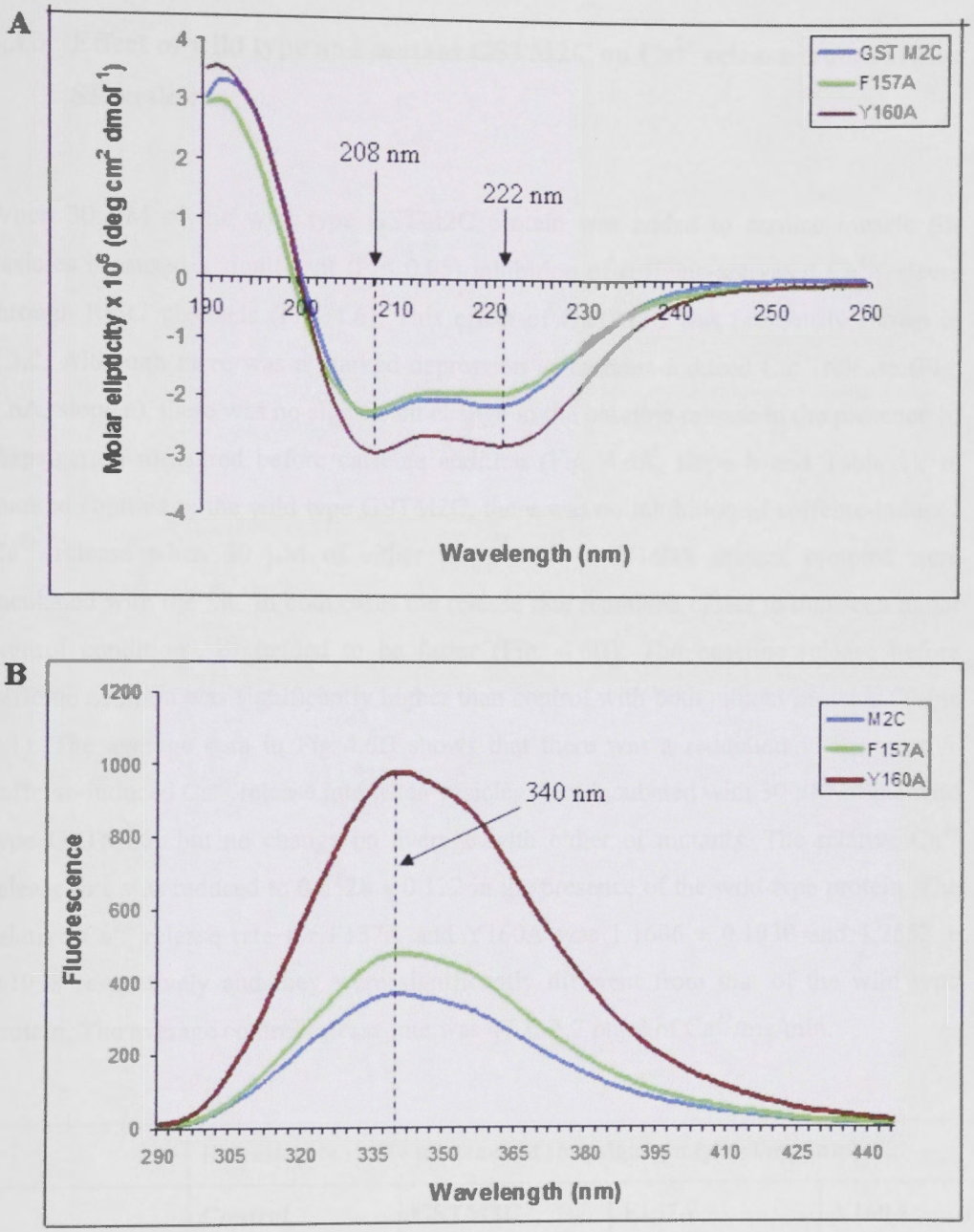

Fig 4.5: Secondary structure and folding of GSTM2C constructs. A) Circular dichroism spectra of GSTM2C and mutants, F157A and Y160A indicate that mutants retained their secondary structure. B) The intrinsic tryptophan fluorescence spectroscopy performed on GSTM2C and the mutants shows that the mutations caused changes in their folding.

4.3.3 Effect of wild type and mutant GSTM2C on Ca^{2+} release from cardiac SR vesicles.

When 30 μM of the wild type GSTM2C protein was added to cardiac muscle SR vesicles it caused a significant ($P < 0.05$) inhibition of caffeine-activated Ca^{2+} release through RyR2 channels (Fig. 4.6). This effect of GSTM2C was previously shown in 3.3.2. Although there was a marked depression of caffeine-induced Ca^{2+} release (Fig. 4.6A, slope a), there was no significant change in the baseline release in the presence of thapsigargin measured before caffeine addition (Fig. 4.6A, slope b and Table 1). In marked contrast to the wild type GSTM2C, there was no inhibition of caffeine-induced Ca^{2+} release when 30 μM of either the F157A or Y160A mutant proteins were incubated with the SR. In both cases the release rate remained closer to that seen under control conditions, or tended to be faster (Fig. 4.6B). The baseline release before caffeine addition was significantly higher than control with both mutant proteins (Table 4.1). The average data in Fig 4.6B shows that there was a reduction in the relative caffeine-induced Ca^{2+} release rate when vesicles were incubated with 30 μM of the wild type GSTM2C, but no change on average with either of mutants. The relative Ca^{2+} release rate was reduced to 0.6528 ± 0.122 in the presence of the wild type protein. The relative Ca^{2+} release rate for F157A and Y160A was 1.1606 ± 0.1930 and 1.2552 ± 0.1998 respectively and they were significantly different from that of the wild type protein. The average control release rate was 47.1±3.7 pmol of Ca^{2+}/mg/min.

	Release rate in the presence of thapsigargin (pmol/mg/min)			
	Control $n = 16$	**GSTM2C** $n = 12$	**F157A** $n = 7$	**Y160A** $n = 7$
Mean ± SEM	6.9 ± 0.72	8.6 ± 0.87	11.3 ± 1.84*	12.7 ± 3.2*

Table 4.1: Rates of unstimulated Ca^{2+} leak after addition of thapsigargin, calculated from slope b (Fig. 4.6A) under control conditions and with the wild type and mutant GSTM2C. * $P < 0.05$.

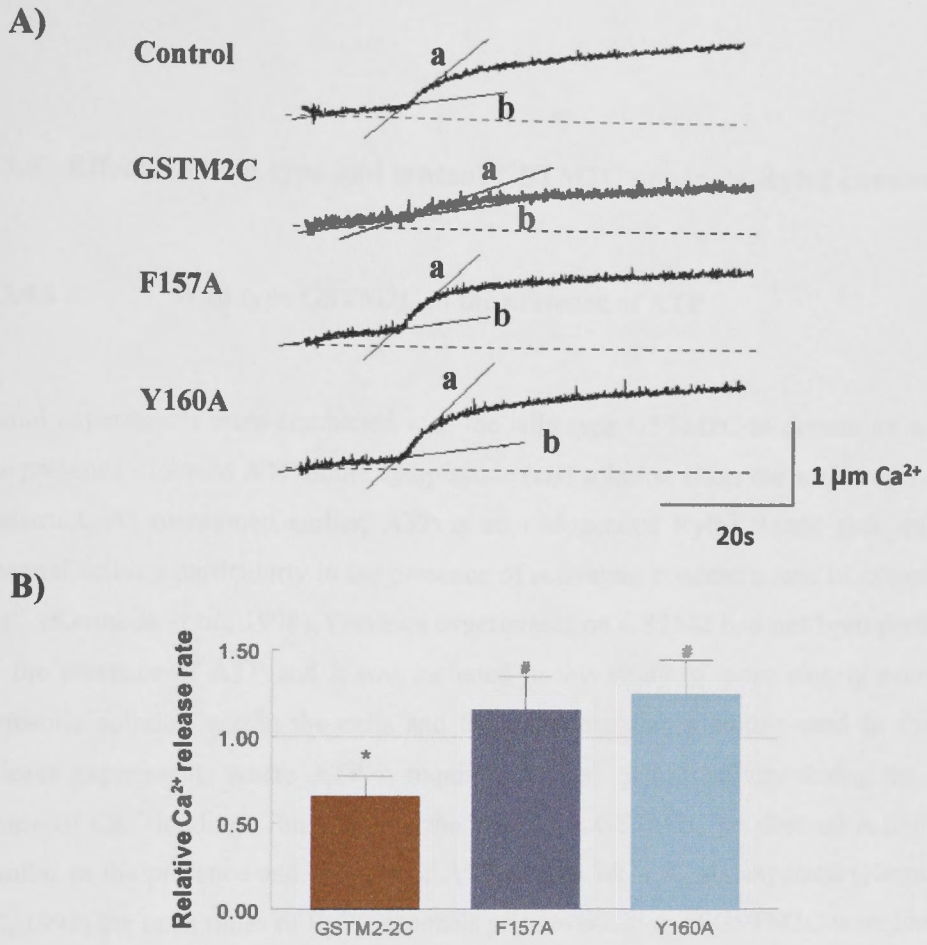

Fig 4.6: Mutation of GSTM2C prevents the protein from depressing the release of Ca^{2+} from the SR through RyR channels. A) Baseline release in the presence of thapsigargin and the caffeine release transient. From the top down: control transient without any GSTM2C construct; in the presence of GSTM2C; F157A; Y160A. The line labelled (b) indicates the baseline Ca^{2+} release rate after addition of thapsigargin and line labelled (a) indicates the initial rate of caffeine induced Ca^{2+} release. These lines indicate where measurement of rate was taken. B) Average data of caffeine-induced Ca^{2+} release rate in the presence of 30 µM GSTM2C construct relative to the Ca^{2+} release rate in the presence of the vehicle alone. * indicates a significant difference compared to the control and # indicates that F157A and Y160A is significantly different from the wild type protein.

n= 12 (GSTM2C), 5 (F157A), 5 (Y160A).

4.3.4 Effects of wild type and mutant GSTM2C on single RyR2 channels

4.3.4.1 Wild type GSTM2C in the presence of ATP

Initial experiments were conducted with the wild type GSTM2C to determine whether the presence of 2 mM ATP in the cytoplasmic (*cis*) solution alters the action of the GST construct. As mentioned earlier, ATP is an endogenous RyR2 ligand that enhances channel activity particularly in the presence of activating concentrations of cytoplasmic Ca^{2+} (Kermode *et al.*, 1998). Previous experiments on GSTM2 had not been performed in the presence of ATP and it was included in this study to more closely mimic the cytosolic solution within the cells and the extravesicular solutions used in the Ca^{2+} release experiments where ATP is required for Ca^{2+} pump activity during the initial phase of Ca^{2+} loading. The effect of the wild type GSTM2C on channel activity was similar in the presence and absence of ATP (Fig. 4.7& 4.8). As expected (Kermode *et al.*, 1998) the open times of RyR2 channels prior to addition of GSTM2C were longer in the presence of 2 mM ATP (control) than in its absence (Fig. 4.7A and 4.8A). The effect of ATP on single channel activity was discussed in 3.3.1. Kermode *et al* examined the mechanism by which ATP activates the sheep cardiac ryanodine receptor and found that adenine nucleotides induce a complex mode of gating and ADP and ATP share a common binding site on the channel. In the presence of cytosolic Ca^{2+}, ATP increases both the frequency and the duration of channel openings and the authors suggested that ATP must bind to both a closed and open state of the channel (Kermode *et al.*, 1998).

The average data in Fig. 4.7B and 4.8B is expressed as relative open probability (i.e. log P_ot - log P_{oc}), to avoid the effects of the well documented variable gating between individual RyR channels under control conditions (Copello *et al.*, 1997). This heterogeneity of gating increases the variability of the average data and biases the average data towards the results obtained in the most active channels. This was observed in both the absence and presence of Mg^{2+} and ATP, which was largely referable to differences in behaviour of the channels and not to experimental error

(Copello *et al.*, 1997). The average ''control'' open probabilities obtained at +40 mV and at -40 mV before addition of the GST constructs are listed in Table 4.2.

It is clear in Table 4.2 that there is no consistent difference between the average control Po values obtained at +40 mV and-40 mV. The effects of the wild type GSTM2C added to the cytoplasmic side (*cis* solution) of RyR2 channels incorporated into lipid bilayers does appear to be voltage-dependent and the voltage-dependence is apparent in both the absence and presence of ATP. There is a strong decrease in channel activity at +40 mV, but little change in activity at -40 mV, and this is apparent in the channel recordings and in the graphs of average relative open probability (Fig. 4.7 & 4.8). The relative open probability was reduced by 32.8, 39.2 and 52.8% in the presence of 5, 15 and 30 μM of GSTM2C respectively. In the presence of 2 mM ATP the relative values at +40 mV were significantly different from those at -40 mV with each GSTM2C concentration used. There was a significant decline in activity at +40 mV but no significant change in activity relative to control at -40 mV (Fig. 4.7B and 4.8B). We have previously shown that the GSTM2C constructs are active within a range of 3–30 μM (Liu *et al.*, 2009). The GSTM2C concentration in the present experiments was increased progressively from 3 to 15 to 30 μM to ensure that the concentrations used were close to saturating. Activity appeared to be the same at each concentration when the experiments were performed in the absence of ATP. When ATP was absent in the *cis* bath solution, the relative open probability was reduced by 28.8, 30.6 and 23.6% in the presence of 5,15 and 30 μM GSTM2C respectively. There was a trend towards a greater decrease in activity in the presence of ATP with 30 μM wild type GSTM2C than with 5 or 15 μM, so that activity may have decreased further had higher concentrations been added. This was not tested as it was not possible to easily concentrate the recombinant GSTM2C constructs further. There was no significant difference between the relative changes in Po in the absence or presence of ATP with 5 or 15 μM of GSTM2C. The decrease in activity with 30 μM GSTM2C was significantly greater in the presence of ATP (Fig. 4.8B) than in its absence. In the context of GSTM2C inhibiting these channels mainly at +40 mV, it is worth noting that a positive membrane potential would tend to develop across the SR membrane during Ca^{2+} efflux when positive charge is dumped onto the cytoplasmic side of the SR membrane. This is significant in the context of the potential use of these compounds as therapeutic agent (Section 4.4.1).

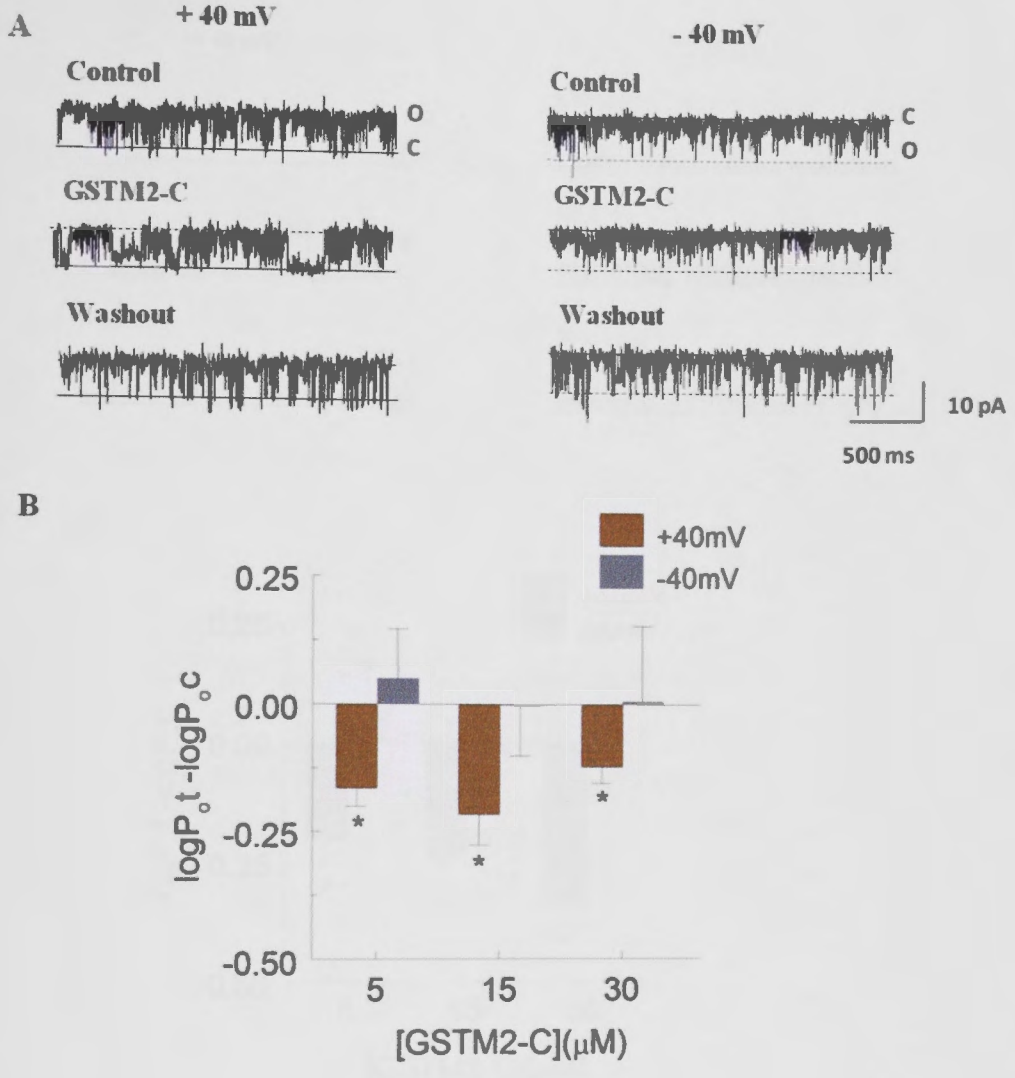

Fig 4.7: Wild type GSTM2C inhibits RyR2 channel activity in lipid bilayers at +40 mV in the absence of 2 mM *cis* ATP. A) shows 3 s recordings of representative channel activity under each condition at +40 mV (left panel) and -40 mV (right panel). Channel opening is upward at +40 mV, from the closed level (solid line, c) to the maximum single channel current (broken line, o). At -40 mV, channel opening is downward from the closed level (c) to open levels (o). The top record in each panel shows control activity before addition of GSTM2C, the middle record shows activity after equilibration for >2 min in 15 μM GSTM2C and the final record shows activity following perfusion of the *cis* chamber to remove GSTM2C. The channel spends more time in the closed state in the presence of GSTM2C than under control conditions or after washout. (B) shows average relative Po (i.e. the average of the Po values for each individual channel relative the internal control for that channel) obtained in the absence of ATP. Data is shown for 5, 15 and 30 μM GSTM2C as indicated, at +40 mV (Brown bins) and -40 mV (Grey bins). (*) indicate values that are significantly different from control. n = 6 (5 μM), 6 (15 μM), 4 (30 μM).

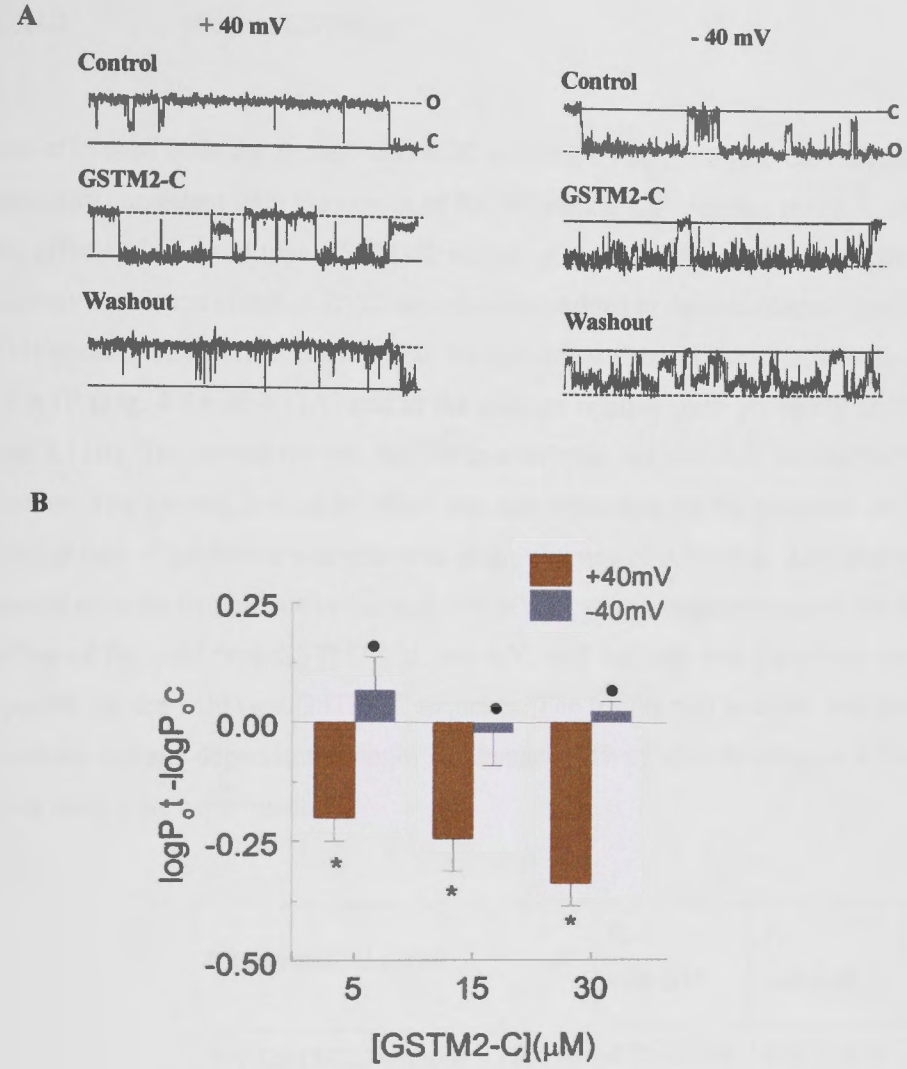

Fig 4.8: Wild type GSTM2C inhibits RyR2 channel activity in lipid bilayers at +40 mV in the presence of 2 mM *cis* ATP. A) shows 3 s recordings of representative channel activity under each condition at +40 mV (left panel) and -40 mV (right panel). Channel opening is upward at +40 mV, from the closed level (solid line, c) to the maximum single channel current (broken line, o). At -40 mV, channel opening is downward from the closed level (c) to open levels (o). The top record in each panel shows control activity with ATP before addition of GSTM2C, the middle record shows activity after equilibration for >2 min in 15 μM GSTM2C and the final record shows activity following perfusion of the *cis* chamber to remove GSTM2C. The channel spends more time in the closed state in the presence of GSTM2C than under control conditions or after washout. (B) shows average relative Po (i.e. the average of the log Pot - log Poc) values for each individual channel, where Poc is the internal control for that channel obtained with GSTM2C in the presence of ATP. Data is shown for 5, 15 and 30 μM GSTM2C as indicated, at +40 mV (brown bins) and -40 mV (grey bins). (*) indicate values that are significantly different from control. (•) indicate values at +40 mV that are significantly different from those at -40 mV at the same GSTM2C concentration. n = 9 (5 μM), 7 (15 μM), 4 (30 μM).

4.3.4.2 Mutant GSTM2C

The effects of both the mutant GSTM2C proteins on single RyR2 Ca^{2+} channels were generally consistent with the results of the SR vesicle Ca^{2+} release study. In contrast to the effects of the wild type GSTM2C, neither of the Y157A or Y160A mutant proteins had any consistent effect on RyR2 activity when added to the cytoplasmic (*cis*) solution. This absence of an effect is evident in the individual channel recordings in the presence of ATP (Fig. 4.9A or 4.11A) and in the average relative open probabilities (Fig. 4.9B and 4.11B). The reason for this decline in activity in the one data set was not explored further. The general lack of an effect was not dependent on the presence of ATP as a similar lack of inhibition was also seen in the absence of ATP (Fig. 4.10 and 4.12). The results with the two mutant proteins at +40 mV serve as a negative control for the strong effect of the wild type GSTM2C at +40 mV, and indicate that the effect on RyR2 is specific for the wild type GSTM2C sequence. The results also indicate that there are no intrinsic voltage-dependent changes in channel activity that develop as a function of time during the experiment.

Experimental series	***n***	P_o **+40 mV**	P_o **−40 mV**
WT GSTM2C without ATP	14	0.27 ± 0.06	0.22 ± 0.03
F157A without ATP	21	0.20 ± 0.02	0.29 ± 0.10
Y160A without ATP	16	0.38 ± 0.14	0.22 ± 0.04
WT GSTM2C with ATP	20	0.42 ± 0.11	0.27 ± 0.07
F157A with ATP	14	0.39 ± 0.06	0.43 ± 0.03
Y160A with ATP	9	0.34 ± 0.04	0.24 ± 0.03

Table 4.2: Average open probability of the internal control is shown for each channel in the particular experiments as listed in column 1. Control values for all three concentrations are included. This data is presented to indicate baseline parameter values of P_o, as average data relative to internal controls is presented in Fig 4.7- 4.12 to illustrate the effects of the GSTM2C constructs on RyR2, to reduce anomalies introduced by the wide range of control values. All values are the mean ± SEM.

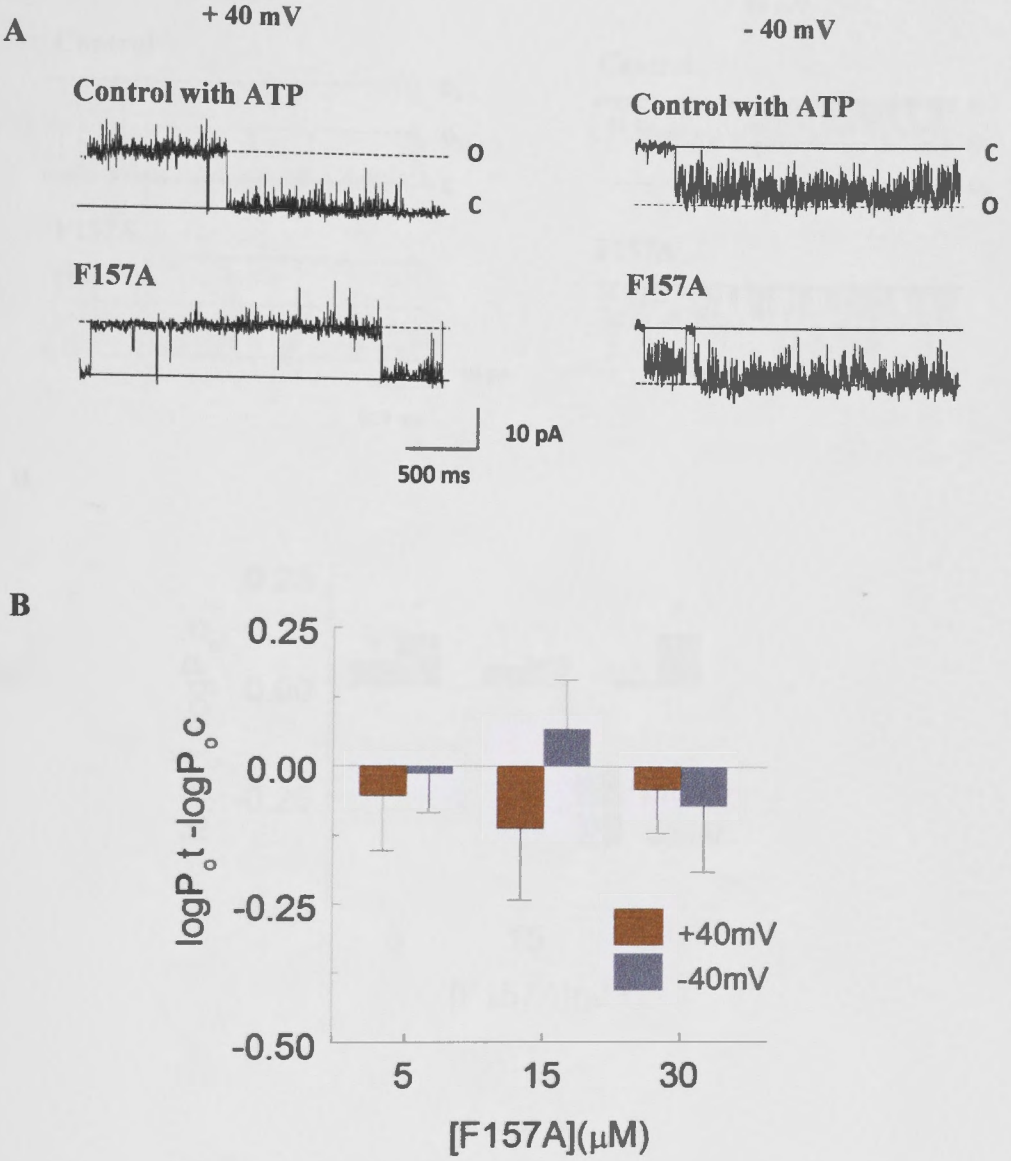

Fig 4.9: F157A mutant does not inhibit RyR2 channel activity in lipid bilayers at +40 mV or -40 mV in the presence of 2mM cis ATP. (A) shows 3 s recordings of representative channel activity under each condition at +40 mV (left panel) and -40 mV (right panel) in the presence of ATP. Channel opening is upward at +40 mV, from the closed level (solid line, c) to the maximum single channel current (broken line, o). At -40 mV, channel opening is downward from the closed level (c) to open levels (o). The top record in each panel shows control activity before addition of F157A, the lower record shows activity after equilibration for >2 min in 30 μM F157A. (B) shows a graph of average relative Po (i.e. the average of the log P_ot - log P_oc) values for each individual channel, where P_oc is the internal control for that channel obtained with F157A. Data is shown for 5 μM, 15 μM and 30 μM F157A as indicated, at +40 mV (brown bins) and -40 mV (grey bins). n = 4 (5 μM), 5 (15 μM), 4 (30 μM).

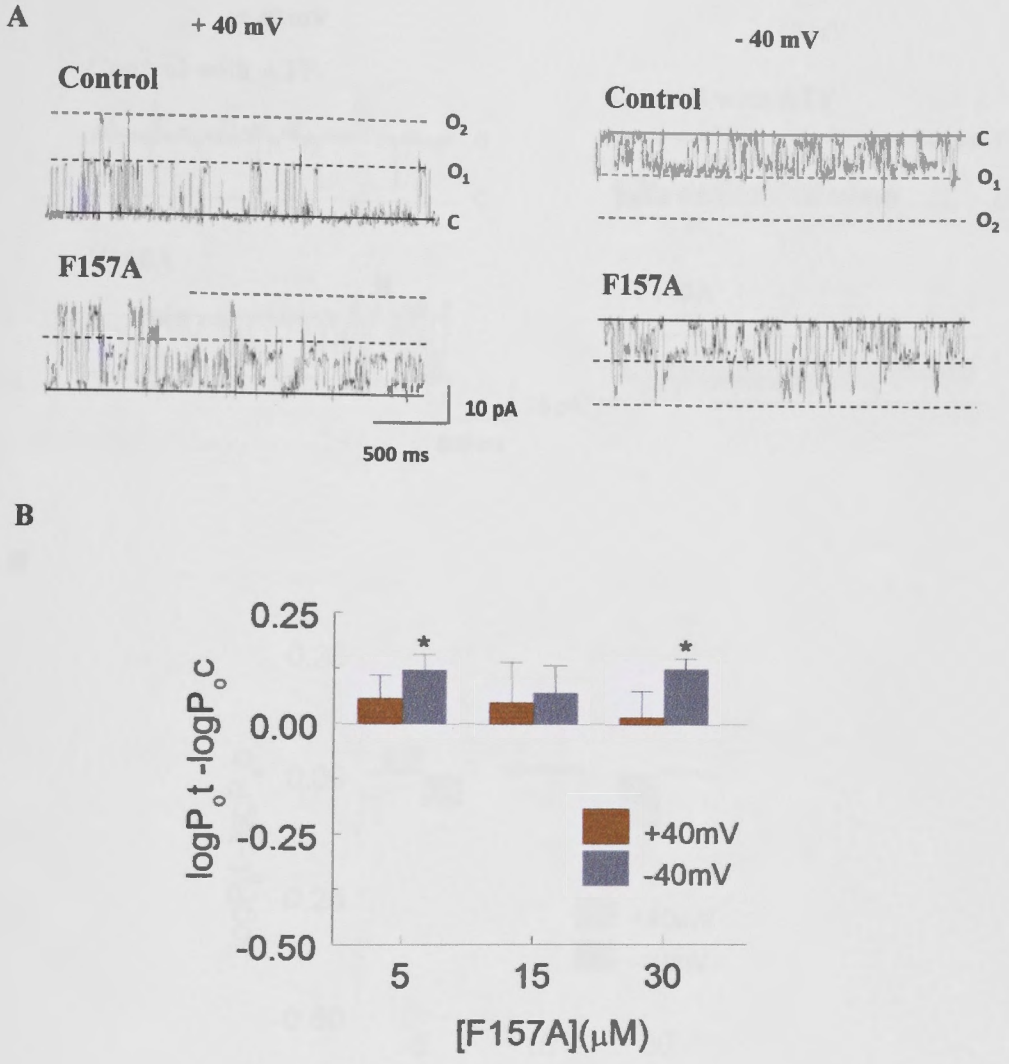

Fig 4.10: F157A mutant does not inhibit RyR2 channel activity in lipid bilayers at +40 mV or -40 mV in the absence of 2mM cis ATP. (A) shows 3 s recordings of representative channel activity under each condition at +40 mV (left panel) and -40 mV (right panel) in the presence of ATP. Channel opening is upward at +40 mV, from the closed level (solid line, c) to the maximum single channel current (broken line, o). At -40 mV, channel opening is downward from the closed level (c) to open levels (o). The top record in each panel shows control activity before addition of F157A, the lower record shows activity after equilibration for >2 min in 30 μM F157A. (B) shows a graph of average relative Po (i.e. the average of the log P_ot - log P_oc) values for each individual channel, where P_oc is the internal control for that channel obtained with F157A. Data is shown for 5 μM, 15 μM and 30 μM F157A as indicated, at +40 mV (brown bins) and -40 mV (grey bins). (*) indicate values that are significantly different from control. n = 6 (5 μM), 6 (15 μM), 4 (30 μM).

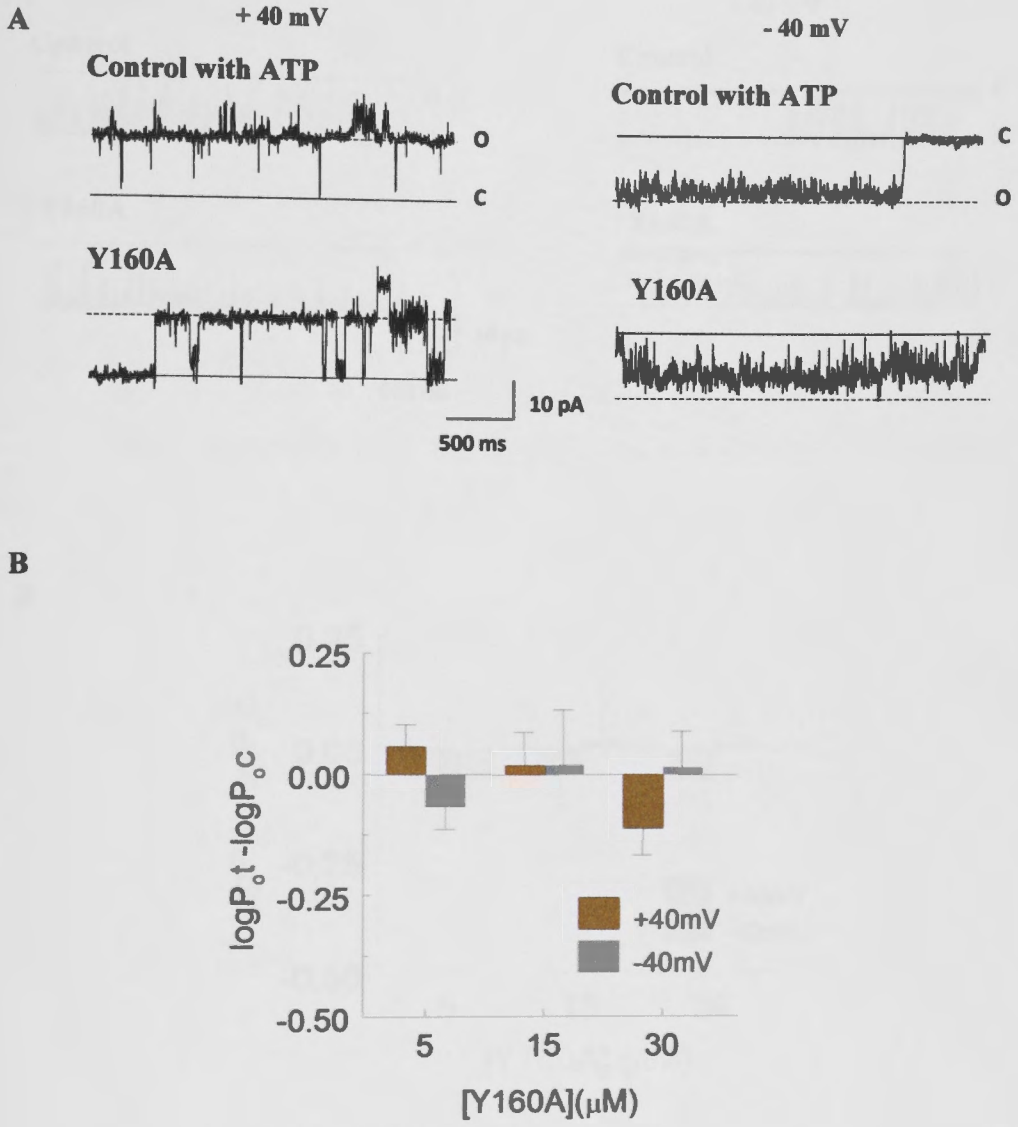

Fig 4.11: Y160A mutant does not inhibit RyR2 channel activity in lipid bilayers at +40 mV or -40 mV in the presence of 2mM cis ATP. (A) shows 3 s recordings of representative channel activity under each condition at +40 mV (left panel) and -40 mV (right panel) in the presence of ATP. Channel opening is upward at +40 mV, from the closed level (solid line, c) to the maximum single channel current (broken line, o). At -40 mV, channel opening is downward from the closed level (c) to open levels (o). The top record in each panel shows control activity before addition of Y160A, the lower record shows activity after equilibration for >2 min in 30 μM Y160A. (B) shows a graph of average relative Po (i.e. the average of the log P_ot - log P_oc) values for each individual channel, where P_oc is the internal control for that channel obtained with Y160A. Data is shown for 5 μM, 15 μM and 30 μM Y160A as indicated, at +40 mV (brown bins) and -40 mV (grey bins). n = 3 (5 μM), 3 (15 μM), 6 (30 μM).

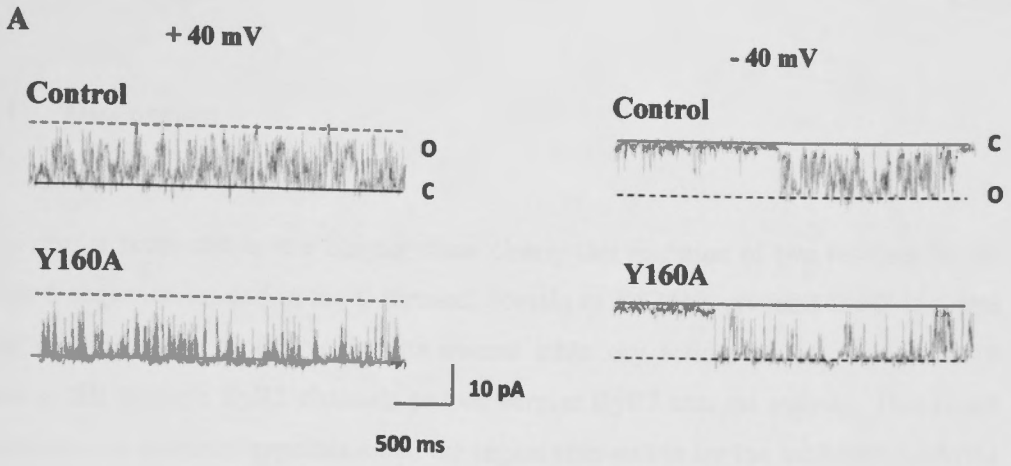

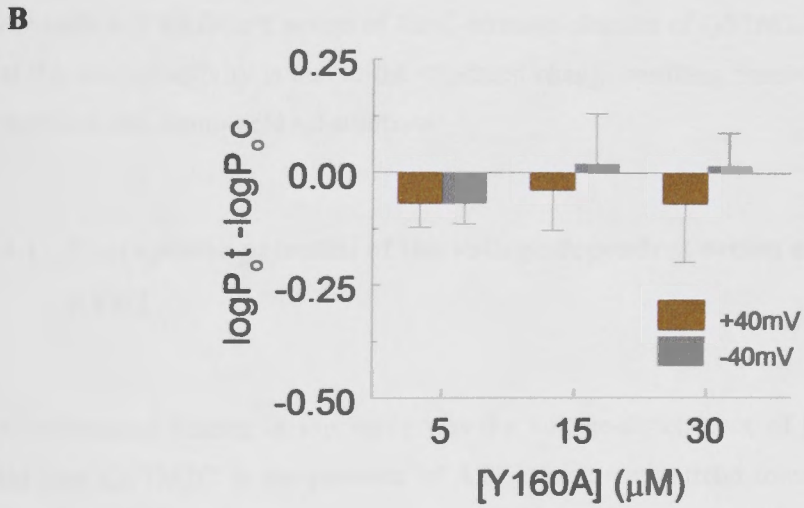

Fig 4.12: Y160A mutant does not inhibit RyR2 channel activity in lipid bilayers at +40 mV or -40 mV in the absence of 2 mM cis ATP. (A) shows 3 s recordings of representative channel activity under each condition at +40 mV (left panel) and -40 mV (right panel) in the presence of ATP. Channel opening is upward at +40 mV, from the closed level (solid line, c) to the maximum single channel current (broken line, o). At -40 mV, channel opening is downward from the closed level (c) to open levels (o). The top record in each panel shows control activity before addition of Y160A, the lower record shows activity after equilibration for >2 min in 30 μM Y160A. (B) shows a graph of average relative Po (i.e. the average of the log P_ot - log P_oc) values for each individual channel, where P_oc is the internal control for that channel obtained with Y160A. Data is shown for 5 μM, 15 μM and 30 μM Y160A as indicated, at +40 mV (brown bins) and -40 mV (grey bins). (*) indicate values that are significantly different from control. n = 5 (5 μM), 5 (15 μM), 5 (30 μM).

4.4 Discussion

The results presented in this chapter show clearly that mutation of two residues in the helix 6 sequence located in the C-terminal domain of GSTM2, prevents the C-terminal half of the protein from exerting its normal inhibitory action on Ca^{2+} release from cardiac SR through RyR2 channels and on cardiac RyR2 channel activity. This result confirms our previous hypothesis that the region responsible for the inhibition of RyR2 is within GSTM2C and it is centered around helix 6 (Liu *et al.*, 2009) and is dependent on the tertiary structure of this region of the GSTM2 protein. The Ca^{2+} release and single channel experiments show that mutation of either F157 or Y160 to alanine eliminates any inhibitory action of the C-terminal domain of GSTM2. It is most likely that the loss of activity is due to the structural change resulting from the substitutions, rather than the amino-acid substitutions.

4.4.1 Therapeutic potential of the voltage dependent action of GSTM2C on RYR2

An unexpected finding in this study was the voltage-dependence of the effect of the wild type GSTM2C in the presence of ATP. There was a trend towards a difference between data at +40 mV and -40 mV in the absence of ATP and this trend became significant when the channel activity was amplified by ATP as it would be in the physiological *in vivo* situation. ATP, which is an endogenous RyR2 ligand, is important for normal channel function and sensitivity to Ca^{2+} induced activation during systole. The effect observed with GSTM2C was not, in any way, equivalent to the enhanced time- and activation-dependent inactivation of RyR1 channels exposed to the full length GSTM2. It was a simple effect in which the open probability of the channel decreased when current was recorded at +40 mV, but not when current was recorded at -40 mV. It is generally agreed that any voltage established across the SR membrane in the intact cell is likely to dissipate rapidly because of the high H^+, K^+, and Cl^- permeability of the SR membrane (Oetliker, 1982). However, a voltage difference across the SR membrane, with the cytoplasmic side positive, would tend to develop during systolic Ca^{2+} release

and during diastole if there was a Ca^{2+} efflux through "leaky" RyR2 channels. A study published in 1984 discussed the relationship between Ca^{2+} release and SR membrane potential and they suggested that SR membrane potential could be a consequence of Ca^{2+} release. They argued that the SR Ca^{2+} release waveform is significantly earlier than any of the possible SR membrane potential signals and the experiments and calculations did not provide evidence in favour of the idea that an SR potential change causes Ca^{2+} release. Theoretical waveforms of SR membrane potential were computed by them using a typical waveform of SR Ca^{2+} release under the assumption that Ca^{2+} crosses the SR membrane as electrical current. Voltage waveforms were calculated using several combinations of electrical parameters for the SR membrane (Bayler *et al.*, 1984). Previous attempts to measure an actual value for the SR membrane potential was not successful as the voltage across the membrane changes constantly and the interference of the surface membrane potential can't be ignored. Therefore, so many assumptions were made in almost all the studies undertaken so far to measure the SR membrane potential. Most of the time, potential waveforms were calculated using the SR Ca^{2+} flux (Baylor *et al*, 1984). Voltage sensitive dyes, which bind to membranes and change their spectral properties in response to the changes in membrane potential, were also used (Antic *et al*, 1999). However, these systems are limited in their capacity for continuous recording since the duration of continuous recording was relatively short, or the number of simultaneous recording sites was limited. Recently, CCD cameras were used for continuous recording over a long-duration with a high spatial resolution. Optical recording systems with a long-duration recording capacity and high spatiotemporal-resolution were also employed for application to spontaneous signals (Hirota and Ito, 2006). However, this method accompanied a new problem. The baseline shift, mainly due to dye bleaching, saturated within a few dozens of seconds. Therefore, scientists are still investigating means of imporving this technique. These methods have been employed in several tissues such as cerebral tissue, neurons etc. In the near future, it might be employed for the measurement of SR membrane potential in skeletal and cardiac tissues and I believe that the method would be fast enough to capture the changes in SR membrane potential.

Any opposing voltage generated by SERCA Ca^{2+} ATPase activity in transporting Ca^{2+} back into the SR would be relatively small, given the very small amplitude of the pump current (Nishie *et al.*, 1990). If a voltage difference appears across the SR

membrane during Ca^{2+} release, they might also be occurring in SR vesicles during caffeine induced Ca^{2+} release assay. Therefore, another possibility is that the voltage dependent blocking effect of GSTM2C may be dependent on the rate of Ca^{2+} release. If the block is dependent on SR membrane potential, the differences between the two functional assays, single channel lipid bilayer experiments and Ca^{2+} release assay, for GSTM2C block of RyR activity would most likely to be due to the differences in membrane potential. The voltage dependence of the inhibitory action of GSTM2C would block the diastolic Ca^{2+} leak, but would not alter the systolic Ca^{2+} efflux. This is because modifications of the RyR activity during systole have only short term effects since there is an autocorrection in the overall Ca^{2+} signalling pathway to maintain a constant systolic Ca^{2+} transient (Trafford *et al.*, 2000). Such autocorrection does not apply during diastole and it is a diastolic Ca^{2+} efflux that is responsible the delayed after depolarisations (DADS) that lead to arrhythmia.

The results suggest that GSTM2C constructs or mimetics based on GSTM2C structure would have little inhibitory effect on the RyR2 channel during diastole in normal heart where there is very little Ca^{2+} efflux. Indeed, when Ca^{2+} efflux is small, there would be a tendency for a negative potential developing across the SR membrane with nett Ca^{2+} influx into the SR. The constructs would be most active during diastole when the RyR

channel is abnormally leaky as in heart failure or with mutations which lead to polymorphic ventricular tachycardia (Dulhunty *et al.*, 2007). These predictions will of course need to be tested in the future in the intact beating heart.

Interestingly, the full length GSTM2 protein did not demonstrate any significant voltage-dependences in its action on RyR2 channels (Abdellatif *et al.*, 2007). Thus an implication of the voltage-dependence of the C-terminal construct is that any therapeutic agent based on its structure would exert an effect on the channel that might differ from the effect of the endogenous protein. The difference may mean that the inhibitory effect during systole would be greater than that during diastole. This would tend to conserve Ca^{2+} in the SR Ca^{2+} store and may help prevent arrhythmias arising from persistent Ca^{2+} release. In the cardiomyocyte, GSTM2C may displace the endogenous GSTs, GSTM1-1, GSTM2-2, GSTP1-1 and CLIC2, and inhibit the cardiac RyR activity. Although CLIC 2 also inhibits RyR2 activity, it has not shown to be

effective during Ca^{2+} release. Also, an activating cytoplasmic concentration of upto 100μM was required for a higher effect with CLIC2.

There was an increase in baseline Ca^{2+} leak from SR vesicles in the presence of the mutants, but no effect on caffeine-induced Ca^{2+} release or on RyR2 activity in bilayers. This effect of the mutants was not explored further, since it did not appear in the activity of the wild type protein. The increase could have been due to a small effect of the mutants on Ca^{2+} leak through the Ca^{2+}-ATPase or on the interaction between thapsigargin and the Ca^{2+}-ATPase. On the other hand it may have been due to a weak non-specific effect of the mutants on unstimulated RyR2 activity since small increases in open probability were seen with the mutants in some cases.

The mechanism by which GSTM2C inhibits the RyR2 is still not clear. It could be explained as a movement of charge in the voltage field during drug binding. An alternative possibility is that drug binding is not voltage-dependent but RyR exists in conformations with different drug binding affinities, the inter conversion between these conformations might be voltage dependent. Further investigation is required to understand the mechanism of action.

4.4.2 Role of helix 6 in GSTM2C

The study presented in the previous chapter (Chapter 3) was designed to identify a minimal region of GSTM2C that was responsible for the inhibition of RyR2. The study suggested that although helix 6 within the C-terminal domain appeared to be a required component in all fragments of GSTM2C that functioned as inhibitors of RyR2 (Liu *et al.*, 2009), a peptide comprised of the helix 6 sequence alone was ineffective as an RyR2 inhibitor. As this individual peptide does not appear to form a helix, it was concluded that the inhibitory properties of the GSTM2C domain and some of its multi helix fragments may be dependent on the conformation of the protein fold that is stabilized by helix 6 or dependent on the helical structure of the helix 6 sequence when

it is stabilized by the surrounding helices (Liu *et al.*, 2009). The data presented in this chapter showed that some single residue substitutions in helix 6 of the C-terminal domain of GSTM2Could destabilize the protein to such an extent that it could not be expressed and purified from E. coli. This confirms that helix 6 plays a central role in stabilizing the folded structure of GSTM2C and is consistent with the previous studies of (Aceto *et al.*, 1997) that indicates that helix 6 contains a conserved motif that contributes to the global folding of GST proteins.

Aceto *et al* identified an N-capping box motif (Ser/Thr-Xaa-Xaa-Asp) which is strictly conserved, at the beginning of the helix 6, in all GSTs and most of the superfamily proteins. Using circular dichroism and peptide remodelling, they demonstrated that these capping box residues have an important role in determining the helical conformation adopted by this fragment in the hydrophobic environment of the protein (Aceto *et al.*, 1997). The results presented in this chapter further support their observation and also explain the significant changes observed in tryptophan

fluorescence in F157A and Y160A. They also speculated that the N-capping residues which are involved in α helix formation in helix 6, also have a role in the folding of the GSTs. The authors discuss that the sequence alignment (shown in grey colour, Fig 4.13) shows a hydrophobic-staple motif (a specific hydrophobic interaction between residues located before the N-cap and the residue located within the helix after N3, I and I+5

interaction), flanking the N-capping box, is also conserved in GST and GST related proteins. It has recently been suggested that these local sequences when simultaneously present at the N-terminal domain of a helix, have an important role in determining the direction of the forming helix with respect to the preceding structural element (Aceto *et al.*, 1997). This relationship between the local structural motifs and the secondary structure formation explains the inability of helix 6 to form an α helix in the absence of flanking helices.

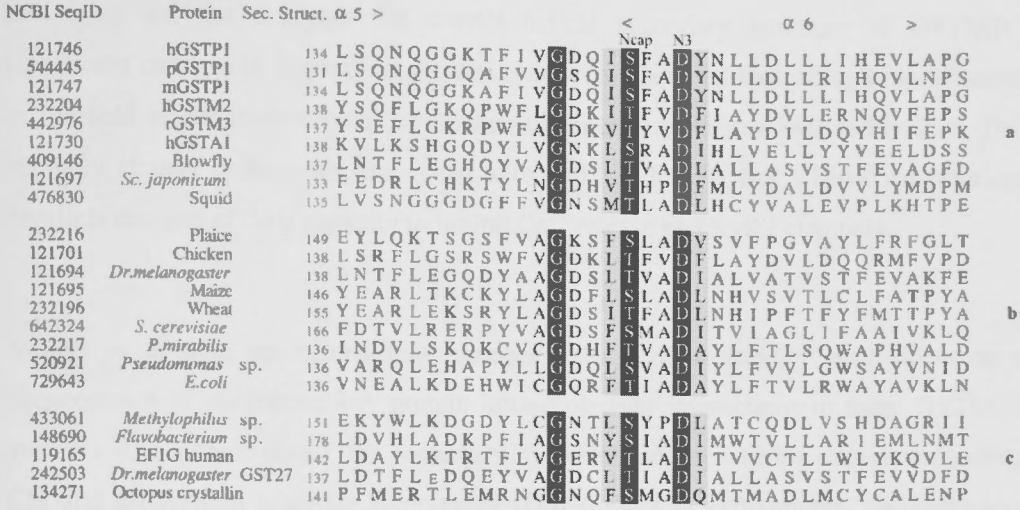

Fig 4.13: Multiple alignment of the amino acid sequences of GST and GST-related superfamily proteins. Helices 5 and 6 of Alpha, Mu, Pi, Theta and Sigma GSTs and the corresponding sequences from distant members of GST and GST-related proteins are shown above. 36 amino acid residues which belong to the secondary structures of the two helices were aligned manually. The position of the first residue shown relative to the full-length protein is indicated at the left of each sequence. The code numbers of the Entrez network service from which these sequences were obtained are shown in the first column. The highly conserved capping box residues are shown in a black box. The Ncap and N3 residues are also indicated at the top of the corresponding column. The highly conserved amino acids residues constituting the hydrophobic staple-motif are shown in a grey box. The highly conserved glycine residue, always located four residues before the Ncap, is shown in a black box. a) Sequences with well known three-dimentional structures. b) Corresponding sequences of GSTs purified from species distant from mammals c) Some of the GST related proteins. Adapted from (Aceto *et al.*, 1997).

4.4.3 Efects of the F157A, Y160A mutations on GSTM2C structure

Lack of an effect on Ca^{2+} release and RyR2 channel activity in the presence of mutants, F157A and Y160A also confirmed that helix 6 plays a central role in maintaining the native fold of the C-terminal domain of GSTM2 or that the helical structure of the helix 6 residues is maintained by the surrounding helices. A recently published CD study also reported that the secondary structure of wild type and mutant GSTM2C variants was very similar (Morris *et al.*, 2011). Although the CD spectra showed that these two

mutations did not dissipate the overall helical secondary structure of GSTM2C, significant changes in tryptophan fluorescence were observed indicating a modification in the fold in the proximity of tryptophan residues at positions 146 and/or 214. This apparent change in structure associated with both the F157A and Y160A substitutions parallels the loss of their capacity to inhibit Ca^{2+} release and RyR2 channels.

Morris *et al* also speculated that changes in structural stability may occur as a consequence of abolishing key protein intra-molecular interactions in these GSTM2C variants. The authors tested this possibility by performing denaturing experiments using CD and differential scanning fluorimetry (DSF). For CD experiments, the secondary structure profiles of GSTM2C and its mutants were monitored in the presence of the denaturant, guanidine HCl and molar elipticity was measured at 222 nm (Fig 4.14A). The free energy of unfolding was calculated mathematically using a model (two state unfolding model) and it was greatest for GSTM2C followed by F157A and Y160A (Table 4.3). DSF measures the temperature at which a protein unfolds, as an increase in the fluorescence of a dye with affinity for hydrophobic parts of the protein, which are exposed as the protein unfolds. The stability of the proteins was assessed by comparing the melting temperatures where Y160A showed the lowest at 35.7°C followed by the F157A at 38°C and GSTM2C at 46.3°C (Fig 4.14B). Combined with CD denaturation data, the authors concluded that F157 and Y160 are important in stabilizing the C-terminal domain of GSTM2 (Morris *et al.*, 2011).

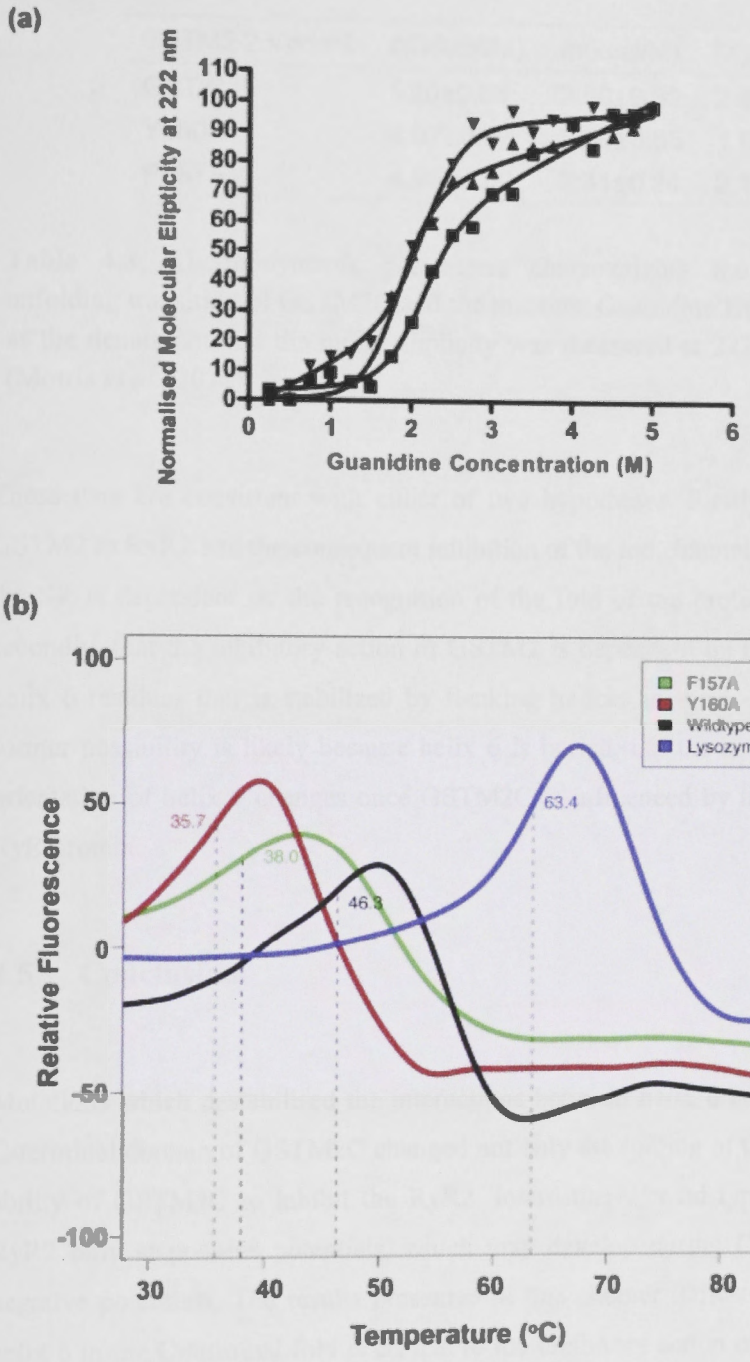

Fig 4.14: Determination of the stability of GSTM2C and its mutants, F157A and Y160A by circular dichroism and differential scanning fluorimetry. A) Normalized molecular elipticity measured at 222 nm in the presence of guanidine HCl. GSTM2C (■), Y160A (▼), F157A (▲) B) Differential scanning fluorimetry profiles for GSTM2C and its variants. Vertical lines indicate the melting temperatures. Figure adapted from (Morris *et al.*, 2011).

GSTM2-2 Variant	ΔG(kcal/M)	m(kcal/M)	$[X]_{half}$(M)
GST-C	5.20±0.88	2.50±0.39	2.08±0.04
Y160A	4.87±0.72	2.68±0.35	1.82±0.03
F157A	4.95±0.59	2.31±0.24	2.15±0.03

Table 4.3: Thermodynamic parameters characterizing the guanidine-induced unfolding transition of GSTM2C and the mutants. Guanidine HCl (0-5 M) was used as the denaturant and the molar elipticity was measured at 222 nm. Adapted from (Morris *et al.*, 2011).

These data are consistent with either of two hypotheses. Firstly, that the binding of GSTM2 to RyR2 and the consequent inhibition of the ion channel and Ca^{2+} release from the SR is dependent on the recognition of the fold of the protein around helix 6. Or secondly, that the inhibitory action of GSTM2 is dependent on the helical structure of helix 6 residues that is stabilized by flanking helices in the C-terminal domain. The former possibility is likely because helix 6 is buried, but the second is possible if the orientation of helix 6 changes once GSTM2C is influenced by the environment of the RyR protein.

4.5 Conclusion

Mutations which destabilised the interactions between helix 6 and other helices in the C-terminal domain of GSTM2C changed not only the folding of the protein but also the ability of GSTM2C to inhibit the RyR2. Interestingly, wild type GSTM2C inhibited RyR2 only at positive potentials, which may develop during Ca^{2+} efflux, but not at negative potentials. The results presented in this chapter indicate that the structure of helix 6 in the C-terminal fold is critical to the inhibitory action of GSTM2 and suggest that the therapeutics mimicking this structure may reduce excess Ca^{2+} release during diastole, which can lead to fatal arrhythmia.

Chapter 5 Identification of the region of cardiac ryanodine receptor that interacts with GSTM2.

5.1 Introduction

The ability of GSTM2/GSTM2C to inhibit RyR2 activity but not RyR1 activity is discussed in previous chapters. The difference in the mode of modulation of RyR1 and RyR2 suggests that the mechanisms and the binding sites of GSTM2 on RyR1 and RyR2 are different. As mentioned in chapter 3, cross linking experiments also showed that GSTM2C binds physically to RyR2 but not to RyR1. There are many endogenous compounds that bind to ryanodine receptors and regulate their activity. But only a few are isoform-specific. Therefore, it might be speculated that divergent regions in ryanodine receptors may be responsible for the isoform-specific action of some of the modulators. Thus far, only a few isoform-specific properties have been allocated to a particular divergent region. Therefore, it is very important to understand the mechanisms for the modulation of isoform-specific functions of RyR channels which would ultimately lead to the development of new therapeutic agents to specifically improve the cardiac and skeletal muscle function.

5.1.1 Divergent regions of ryanodine receptors

As mentioned in 1.2.2, the amino acid sequences of the three RyR isoforms share a high degree of sequence identity (66-70%) with their major variations occurring in three regions, known as divergent regions 1,2, and 3 (DR1, DR2 and DR3). DR1 region comprises residues 4254-4631 of RyR1 and residues 4210-4562 of RyR2. DR2 region includes residues 1342-1403 of RyR1 and residues 1353-1397 of RyR2. Residues 1872-1923 of RyR1 and residues 1852-1890 of RyR2 are denoted as the DR3 region (Sorrentino and Volpe, 1993). These regions are likely to be important for the isoform specific functions and have been the focus of many structural and functional studies. Sequence variations in the DR1 region between RyR1 and RyR2 have been shown to account for the different sensitivities of the isoforms to Ca^{2+} inactivation

(Du and MacLennan, 1999, Du *et al.*, 2000, Nakai *et al.*, 1999). The DR2 region, which is absent in RyR3, was found to be critical for skeletal muscle EC coupling, as the deletion of DR2 abolished EC coupling (Yamazawa *et al.*, 1997).

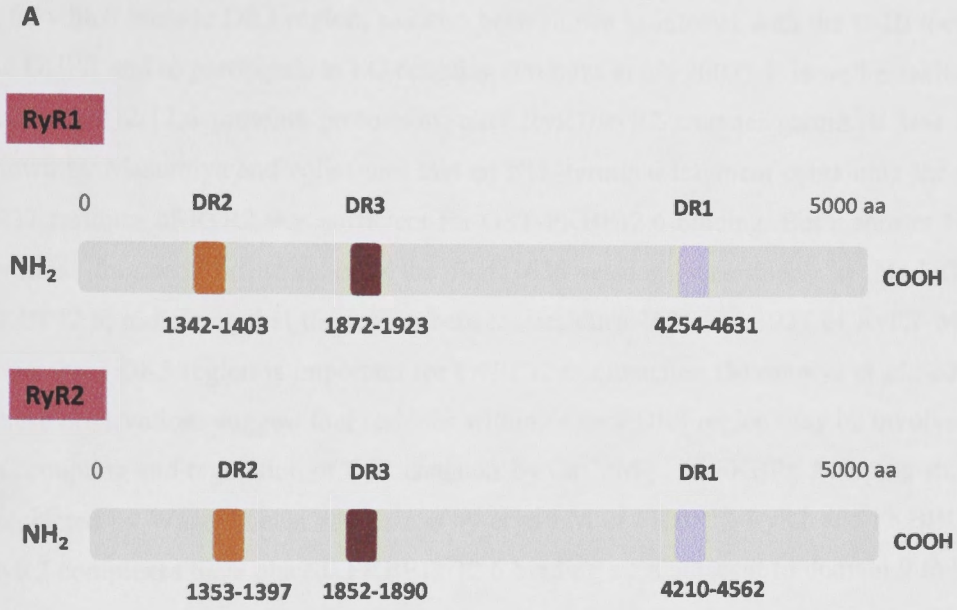

Fig 5.1: A comparison of the divergent regions of RyR1 and RyR2 (A) and residues in the DR3 region of RyR1 and RyR2 (B). Note that there are substantially fewer acidic residues in the DR3 of RyR2, and more basic and hydrophobic residues compared to the DR3 of RyR1.

As suggested in Zorzato *et al*, the DR3 region may have multiple roles in RyR channel function. In RyR1, DR3 consists of a stretch of ~30 negatively charged amino acid residues which constitute a low affinity Ca^{2+} binding site (Zorzato *et al.*, 1990).

Consistent with this hypothesis, deletion of DR3 region altered Ca^{2+} and Mg^{2+}-dependent regulation and conduction properties of the RyR channel (Bhat *et al.*, 1997b, Hayek *et al.*, 1999, Hayek *et al.*, 2000). A region of RyR1 between residues 1837 and 2168 which include DR3 region, has also been shown to interact with the II-III loop of the DHPR and to participate in EC coupling (Proenza *et al.*, 2002). It is well established that FKBP12/12.6 proteins profoundly alter RyR1/RyR2 channel gating. It was also shown by Masumiya and colleagues that an NH_2-terminal fragment containing the first 1937 residues of RyR2 was sufficient for GST-FKBP12.6 binding. But a shorter NH_2-terminal fragment including only the first 1636 residues was unable to bind GST-FKBP12.6, indicating that the region between residues 1636 and 1937 of RyR2 which encompass DR3 region is important for FKBP12.6 interaction (Masumiya *et al.*, 2003). These observations suggest that residues within or near DR3 region may be involved in EC coupling and regulation of RyR channels by Ca^{2+}, Mg^{2+} or FKBPs. Mapping studies conducted by Wagenknecht and Samso by cryo EM of FKBP12-RyR1 and FKBP12.6-RyR2 complexes have placed FKBP12/12.6 binding sites adjacent to domain 9 in both RyR isoforms. As suggested by the authors, three-dimentional reconstructions reported for the three RyR isoforms show strict conservation of the domain architecture of the cytoplasmic region and few significant differences at the 2-4 nm resolution (Wagenknecht and Samso, 2002). Therefore, the DR3 region maps to part of domain 9 in all three isoforms.

Domain 9 is one of the domains which comprise the clamp shaped structure which is substantially different in conformation in the open and closed channel structures. Therefore, there is a possibility that DR3 is involved in conformational changes in RyRs that are associated with channel gating. Comparison studies described earlier of the structure of RyR1 and RyR3 channels in closed and open states revealed structural differences in the vicinity of domain 9. Therefore, domain 9 may be important for EC coupling. The DR3 region appears to be involved not only in channel gating but also in channel conduction as the deletion of DR3 region altered the conduction properties of RyR1 (Hayek *et al.*, 2000). These studies therefore suggest that domain 9 might be an essential part of the macromolecular apparatus of RyRs that carry out EC coupling.

5.1.2 Binding of RyR modulators, CLIC2 and Dantrolene to RyR1 and RyR2

In the recent past, several groups made attempts to understand the mechanism of action of CLIC2 and dantrolene on the inhibitory effect of RyR activity. Therefore, it is interesting to note the similarities and differences of other modulators of RyR compared to GSTM2C. The action of CLIC2 on the skeletal RyR1 channel and its binding site on the RyR1 protein were investigated in detail by Meng *et al* using a range of functional techniques and cryo electron microscopy for structural localization (Meng *et al.*, 2009). As mentioned in the chapter 1, these results showed clearly that CLIC2 can interact with RyR1 and modulate its channel activity. Cryo electron microscopy reconstruction revealed that CLIC-2 bound to the surface of the cytoplasmic assembly of RyR1 that faces the T-tubular membrane, between domains 5 and 6 in the clamp shaped region of the protein (Fig 5.2). Interestingly, this binding caused a conformational change in a different part of the clamp region, with a marked separation of domains 9 and 10. The authors suggested that the structural changes in RyR1 seen when CLIC-2 binds is reminiscent of a separation of domains 9 and 10, which is seen in the "open' structure of the channel, but is not seen in the "closed" structure (Serysheva *et al.*, 1999). This suggests that CLIC-2 bound RyR1 clamp structure resembles the clamp structure in the "open" conformation of RyR1. According to the study by Serysheva *et al*, "open" structure of RyR1 as revealed by cryo electron microscopy had an opening in the central region of the RyR1 that was thought to indicate enhanced access to the channel pore region (Serysheva *et al.*, 1999). Surprisingly, this central opening is not observed in the CLIC2-RyR1 complex suggesting that the CLIC2 bound form of the RyR1 pore resembles the "closed" state of RyR1. Therefore, Meng *et al* suggested that inhibitory effect on Ca^{2+} release from SR and on the single channel lipid bilayer activity could be explained by CLIC-2 binding to the domains 5 and 6 of RyR1, which could strengthen the interaction between these two domains and thus stabilizing the closed state of the RyR1 channel. This would therefore limit access to the channel pore (Meng *et al.*, 2009). Studies have shown that the region around domain 5 and 6 contain "hotspots" which play an important role for the regulation of RyRs.

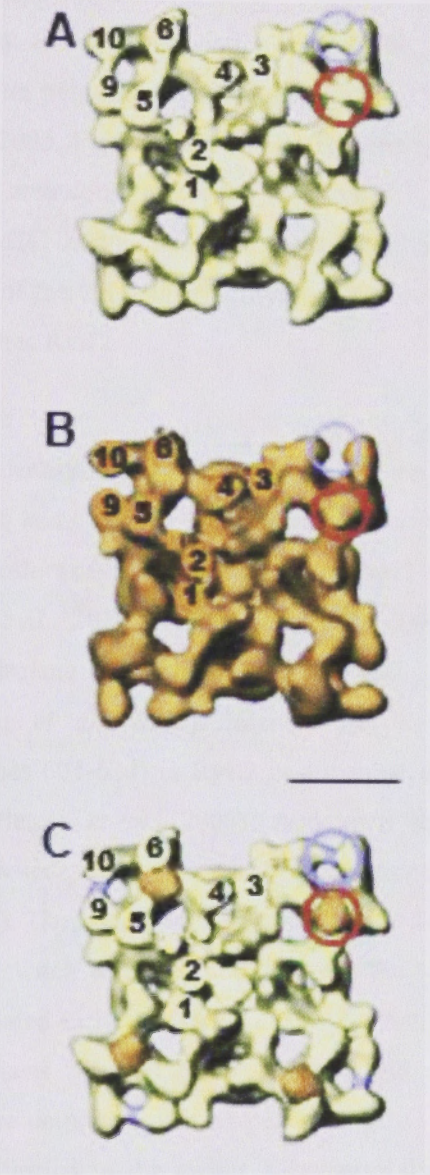

Fig 5.2: Three dimentional reconstruction of RyR1 from cryoelectron microscopic images of RyR1 obtained in the absence (A) and presence (B) of CLIC-2 and a 3D difference map (C). The view of the tetramer is from the cytoplasmic side facing the transverse tubular membrane. Note the difference between domains 5 and 6 (red circle) and domains 9 and 10 (blue circle) between A and B. Scale bar is 10 nm. Figure is modified from (Meng *et al.*, 2009).

These include the DR2 region, the phosphorylation site S2808, the central disease causing mutation region and one proposed coupling site for DHPR (Liu *et al.*, 2004, Meng *et al.*, 2007, Liu *et al.*, 2005, Perez *et al.*, 2003). Therefore, it is not surprising that binding of CLIC-2 to this area could affect the function of RyR1. Unfortunately, CLIC-2 binding site and GSTM2C binding site have not been determined for the same isoform of RyR. As a member of the GST superfamily, it would be interesting to know where CLIC-2 binds in the cardiac RyR2.

As mentioned in chapter 1, dantrolene, the primary drug used to treat malignant hyperthermia, is a known RyR antagonist. It has been shown to inhibit uncontrolled Ca^{2+} release by stabilizing inter-domain interactions between NH2-terminal and central regions of RyR (Kobayashi *et al.*, 2010, Kobayashi *et al.*, 2009). Further mapping studies also revealed that dantrolene binds to residues 590-609 in the NH2-terminal region of RyR1 (Paul-Pletzer *et al.*, 2002). Interestingly, it also binds to the corresponding sequence (residues 601-620) in RyR2 in a manner that is dependent on channel conformation (Paul-Pletzer *et al.*, 2005). According to Wang *et al*, the dantrolene binding sequence is located in domain 9 and adjacent to the FKBP12.6 binding site (Wang *et al.*, 2011). Their study further revealed that dantrolene is unlikely to bind directly to the domain switch that is formed between the NH2-terminal region and the central region as speculated earlier. Wang *et al* suggest that there could be more than one domain-domain contacts between NH2- terminal and central regions and dantrolene may bind near to the domain switch and allosterically stabilize it (Wang *et al.*, 2011). This has been confirmed in the recent X-ray crystal structure of the N-terminal part of RyR1 showing multiple contacts with other regions of the protein (Tung *et al.*, 2010).

5.1.3 GSTM2 binds to the DR3 region of RyR2

A series experiments were carried out by Dr Dan Liu of the Molecuar Genetics group (JCSMR, ANU) to elucidate the binding site of GSTM2C on RyR2. GSTM2C was cloned to the binding domain vector pGBKT7 (BD-GSTM2C) and used as bait in a GAL4 yeast two-hybrid screen (Liu D, 2011). A library containing 1-3 kb mouse RyR2 cDNA fragments were constructed in the activation domain prey vector, pGADT7. Four colonies grew on selective media. The plasmids were recovered from the yeast colonies and the RyR2 cDNA inserts sequenced. Three out of four plasmids contained a 1043 bp RyR2 sequence extending from nucleotide 5604-6646 of the mouse RyR2 cDNA, and was in frame with the GAL-4 activation domain which was named later as RyR2D3-1.

The cDNA fragment found to bind to GSTM2C, encodes a peptide of 347 amino acids between residues 1869-2215 in the mouse RyR2 amino acid sequence and includes most of the DR3 region at the N-terminal domain (residues 1869-1890). As mentioned above in 5.1.1, the sequence of the DR3 region is significantly different between RyR1 and RyR2. In order to define the binding site precisely, deletion constructs of the region identified (RyRD3-1) were made by digestion and relegation of the cDNA at the sites indicated in Fig 5.3. Further experiments on the yeast two-hybrid system revealed that deletion constructs AD-RyR2D3-2 and AD-RyR2D3-4 (Fig 5.3) supported the growth of yeast colonies and grew faster than the original positive fragment, AD-RyR2D3-1 indicating stronger binding. The fragment, AD-RyR2D3-4, which derived from the amino terminal of the original fragment consisted of 44 amino acids and included part of the D3 region. The results of this study therefore suggested that DR3 region of RyR2 is important for the specific binding of GSTM2C. The β-Galactosidase assay performed on these fragments also revealed that the binding between GSTM2C and RyR2D3-1 was weak and the comparatively smaller fragments showed stronger binding than the larger fragments. Cross linking studies performed on RyR2D3-2 provided further evidence that GSTM2C and RyR2D3-2 interacted *in vitro* and confirmed the observation obtained in the yeast two-hybrid analysis (Liu D, 2011).

As mentioned earlier, the RyR1 DR3 region contains more acidic amino acids, while there are more basic and hydrophobic amino acids in RyR2 DR3 region. In order to check whether these sequence differences determine the selective binding of GSTM2C to RyR2, a number of mutants were generated in the DR3 region of AD-RyR2D3-2 (I1871E, A1874D, K1875E, L1876E and K1883E).

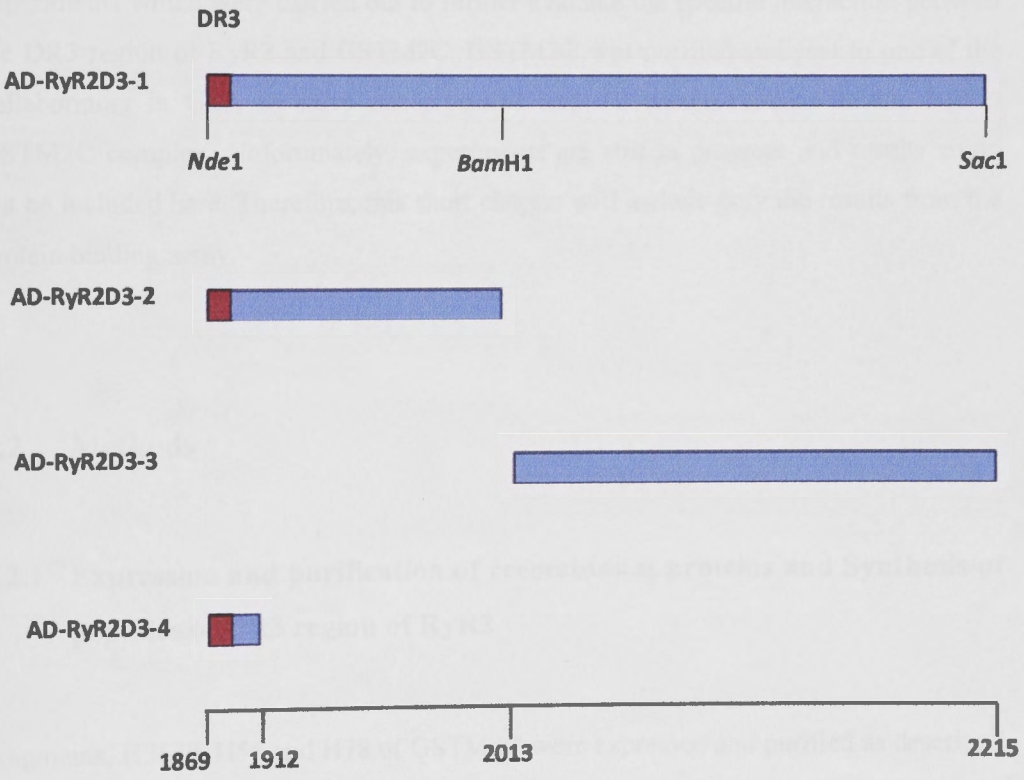

Fig 5.3: A schematic diagram showing the original clone, AD-RyR2D3-1 identified from yeast two-hybrid experiments and the subsequent deletion constructs. The restriction sites used for the creation of deletion fragments are also indicated with the respective amino acid sequence positions of the RyR2 clones.

Only K1875E caused a reduction in growth which was further confirmed by a 50% reduction in the β-galactosidase activity. An additional mutant containing five basic to acidic amino acid substitutions did not grow well and induced very little β-galactosidase activity. Therefore, this study which is under review to be published, confirmed the importance of K1875 and other positively charged amino acids, K1886, R1887, K1889 in the DR3 region of RyR2 for the binding of GSTM2C (Liu D, 2011).

The results presented in this chapter include intrinsic tryptophan fluorescence quenching experiments which were carried out to further evaluate the specific interaction between the DR3 region of RyR2 and GSTM2C. GSTM2C was purified and sent to one of the collaborators in USA to carry out cryo-EM and 3D reconstructions of the RyR2-GSTM2C complex. Unfortunately, experiments are still in progress and results could not be included here. Therefore, this short chapter will include only the results from the protein binding assay.

5.2 Methods

5.2.1 Expression and purification of recombinant proteins and Synthesis of peptides of DR3 region of RyR2

Fragments, H5678, H56 and H78 of GSTM2C were expressed and purified as described in 2.3.2. The AD-RyR2D3-2 region identified as a binding partner for GSTM2C by the yeast two-hybrid assay (5.1.3) was expressed and purified by Dr Dan Liu at the Molecular Genetics group, JCSMR, ANU. The RyR2D3-2 DNA fragment was sub-cloned from pGADT7-RyR2D3-1 into pQE30 vector using *Eco*R1/*Bam*H1 sites, and the N terminal His tag recombinant protein was expressed in *E.coli* strain BL21/DE3. The recombinant RyR2D3 protein was purified from the insoluble fraction of the lysate using Buffer A (50 mM phosphate buffer pH7 and 300 mM NaCl) with 8 M urea and

Ni-agarose affinity chromatography. The protein was refolded by rapid dilution of the purified protein (1:40) in Buffer B (50 mM HEPES pH 7.4, 200 mM KCl and 10%

glycerol) and the protein solution was concentrated to 1 mg/ml using a centrifugal filter device (Millipore, 290 Concord Road, Billerica, Massachusetts 01821). The RyR2 DR3 region, the DR3 mutant, the DR3 short peptide and the AS1(-) peptide were synthesized at the Biomolecular Resource Facility (BRF), JCSMR, ANU.

5.2.2 Intrinsic tryptophan fluorescence binding assay

Intrinsic tryptophan fluorescence experiments were performed as described in 2.3.4. The most active GSTM2C fragment identified in chapter 1, H5678 was placed in the cuvette at a 5 μM concentration. Different fragments of the RyR2 identified by the yeast two-hybrid system (Fig 5.4) or synthesized at BRF were titrated into the cuvette in 3 μl aliquots of 0.5 mM to change the concentration of the fragments in the solution from 3-50 μM. Equilibrium dissociation constants of the reaction between the fragments and H5678 were determined by fluorimetry. Titrations were performed at 25 °C using a Perkin Elmer LS50B luminescence spectrophotometer. GSTM2C fragments were excited at 280 nm and the fluorescence emission was monitored at 340 nm. Control experiments were also performed for each fragment of GSTM2C, RyR2 and AS1(-) construct of RyR1.

Binding of a double mutant identified in the DR3 region of RyR2 which is responsible for arrythmogenic right ventricular cardiomyopathy (ARVC) was also examined. The most active fragment identified from the RyR2 DR3 region was tested for binding affinity with two more fragments of GSTM2C which contain one tryptophan residue each. Measurements were corrected for dilution effects and the fluorescence arising from RyR2 fragments and D3 peptides were reduced from each test value. Each experiment was performed in triplicate and data were analysed using GraphPad Prism software and non linear regression.

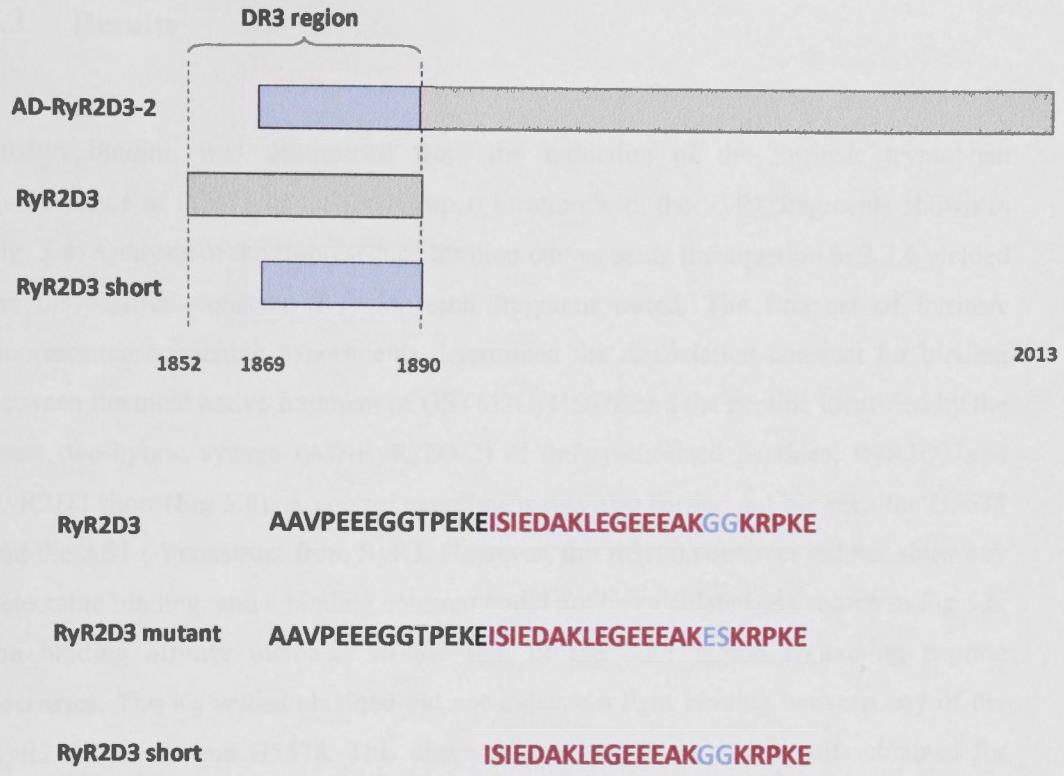

Fig 5.4: Peptide sequences used for the determination of dissociation constants for the binding of helix 5678 with RyR2D3 fragments. Peptide RyR2D3, encodes for the complete DR3 region of RyR2. Mutant peptide was derived from the amino acid replacement at G_{1885} and G_{1886} to E and S respectively. RyR2D3 short peptide encodes for the region of RyR2DR3 overlapped with the clone, AD-RyR2D3-2 identified by yeast two-hybrid experiments mentioned in 5.1.3.

5.3 Results

Protein binding was determined from the reduction of the intrinsic tryptophan fluorescence of H5678 of GSTM2C upon titration with the RyR2 fragments shown in Fig. 5.4. Analysis of the fluorescence titration curves using the equation in 2.3.4 yielded the dissociation constant (K_d) for each fragment tested. The first set of intrinsic fluorescence quenching experiments determined the dissociation constant for binding between the most active fragment of GSTM2C, H5678 and the peptide identified by the yeast two-hybrid system (AD-RyR2D3-2) or the synthesized peptides, RyR2D3 and RyR2D3 short (Fig 5.6). A control experiment was also carried out between the H5678 and the AS1 (-) construct from RyR1. However, the AS1(-) construct did not show any detectable binding, and a binding constant could not be calculated. As shown in Fig 5.6, the binding affinity increases as the size of the DR3 region containing peptide decreases. The K_d values obtained did not indicate a tight binding between any of the RyR2 fragments and H5678. This observation is consistent with results obtained for single channel lipid bilayer studies where the activity was reversed when the proteins were perfused from the *cis* chamber suggesting weaker binding. The region identified by the yeast two-hybrid assay, AD-RyR2D3-2 had a K_d of 89.0 ±4.4 μM while RyR2D3 and RyR2D3 short peptides obtained 57.8 ± 4.2 μM and 30.2 ± 5.8 μM respectively. The binding affinities of both the RyRD3 peptide and the RyR2D3 short peptide to H5678 were significantly different ($P<0.01$) from the binding affinity between AD-RyR2D3-2 and H5678. Therefore, the strongest binding was achieved by the shortest DR3 region fragment that occurs at the N-terminal of the AD-RyR2D3-2 fragment. These results are also consistent with the results obtained by the yeast two-hybrid assay described in 5.1.3.

Two single-nucleotide polymorphisms in RyR2 leading to the amino acid replacements G1885E and G1886S are associated with ARVC in patients who are carrying both of the corresponding RyR2 alleles (Milting *et al.*, 2006). In order to test whether these mutations affect the binding affinity between H5678 and the double mutant RyR2D3 peptide (Fig 5.4), another set of experiments were carried out. Interestingly, the binding affinity between the H5678 and the mutant peptide was significantly higher ($P<0.05$) than the affinity between the H5678 and RyR2D3 region with K_d of 43.4 ± 0.8 µM and 57.8 ± 4.2 µM respectively.

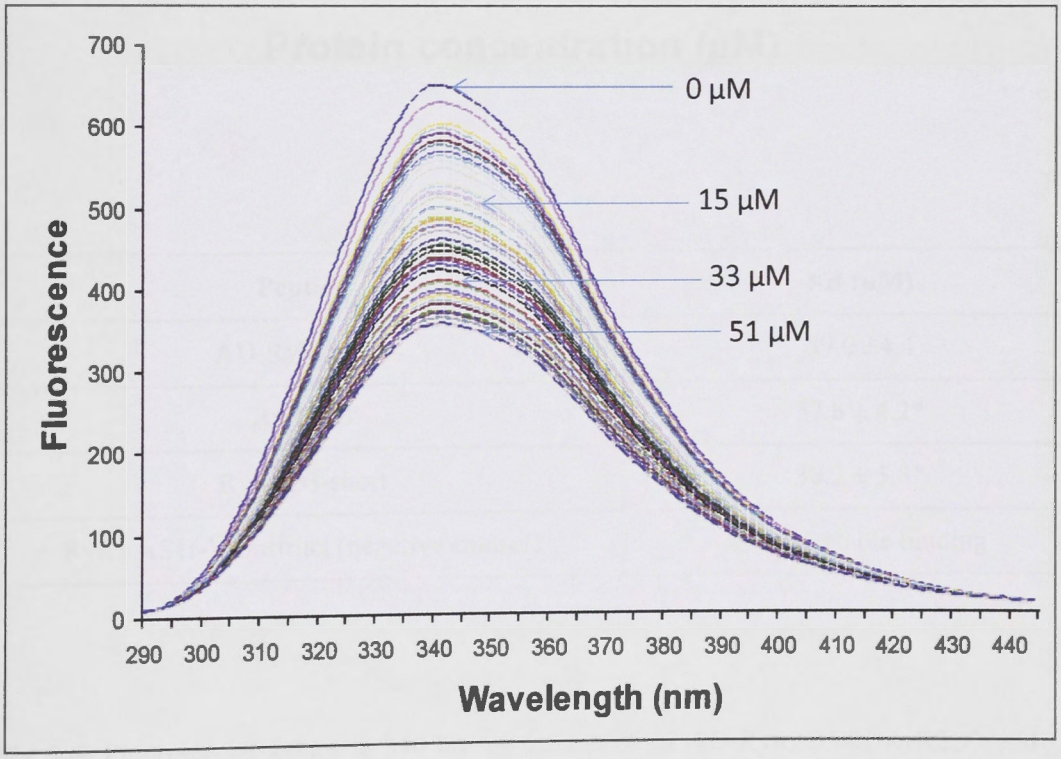

Fig 5.5: Affinity binding measurements using fluorescence spectroscopy: fluorescence spectra of GSTM2C H5678 (uppermost trace) with sequential 3 µl (0.5 mM) aliquot additions of RyR2D3 short peptide. Concentration of RyR2D3 peptide in the cuvette after several additions is shown on the graph.

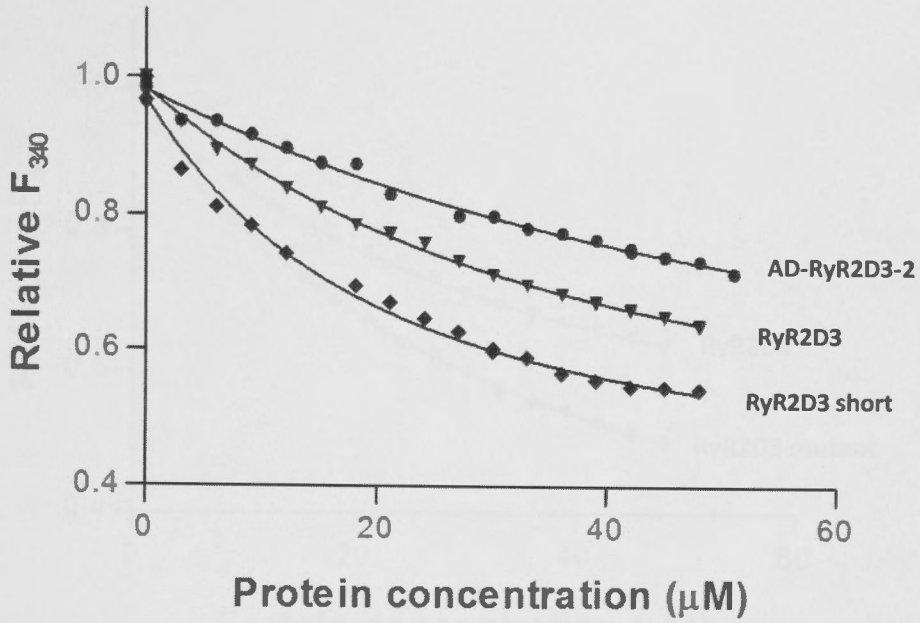

Peptide	Kd (μM)
AD-RyR2D3-2	89.0 ±4.4
RyR2D3	57.8 ± 4.2*
RyR2D3-short	30.2 ± 5.8*
RyR1 AS1(-) construct (negative control)	No detectable binding

Fig 5.6: Fluorescence values at 340 nm as a function of AD-RyR2D3-2, RyR2D3 and RyR2D3 short peptide concentration. The *Kd* values were derived using nonlinear regression analysis in the program GraphPad Prism and expressed as mean ± SEM from 3-4 fluorescence quenching experiments. Data from a representative experiment from each group is shown in the graph. RyR1 AS1(-) construct, which was the control didn't show any detectable binding. * Significantly different $P<0.01$ from AD-RyR2D3-2.

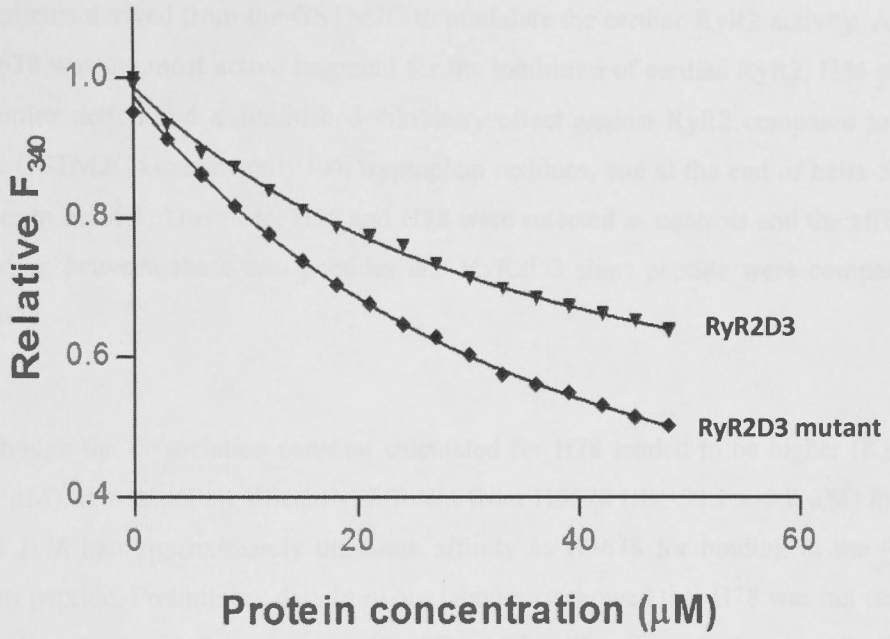

Peptide	Kd (μM)
RyR2D3	57.8 ± 4.2
RyRD3 (mutant)	43.4 ± 0.8*

Fig 5.7: Fluorescence values at 340 nm as a function of RyR2D3 and RyR2D3 double mutant (G1885E and G1886S) peptide concentration. The *Kd* values were derived using nonlinear regression analysis in the program GraphPad Prism and expressed as mean ± SEM from 3-4 fluorescence quenching experiments. Data from a representative experiment from each group is shown in the graph. * Significantly different $P<0.01$ from RyR2D3.

Results presented above in Chapter 3 showed a comparison of the ability of different fragments derived from the GSTM2C to modulate the cardiac RyR2 activity. Although, H5678 was the most active fragment for the inhibition of cardiac RyR2, H56 showed a complex action and a diminished inhibitory effect against RyR2 compared to H5678. The GSTM2C contains only two tryptophan residues, one at the end of helix 5 and the other in helix 8. Therefore, H56 and H78 were selected as controls and the affinities of binding between these two peptides and RyR2D3 short peptide were compared with H5678.

Although the dissociation constant calculated for H78 tended to be higher (K_d, 41.2 ± 7.1 μM), it was not significantly different from H5678 (K_d, 30.2 ± 5.8 μM) indicating that H78 had approximately the same affinity as H5678 for binding to the RyR2D3 short peptide. Preliminary data from our laboratory showed that H78 was not capable of reducing the Ca^{2+} release from cardiac SR vesicles. Therefore, further functional studies were not carried out. Interestingly, binding affinity between H56 and RyR2D3 short peptide (K_d, 134.3 ± 44.7 μM) was significantly less ($P<0.05$) compared to the binding affinity between H5678 and RyR2D3 short peptide (K_d, 30.2 ± 5.8 μM). Therefore, these results suggest that the helix 7 and 8 assist in the binding of the H5678 to the DR3 region of RyR2 but the inhibitory effect may be due to a cumulative effect of helices 5,6,7 and 8.

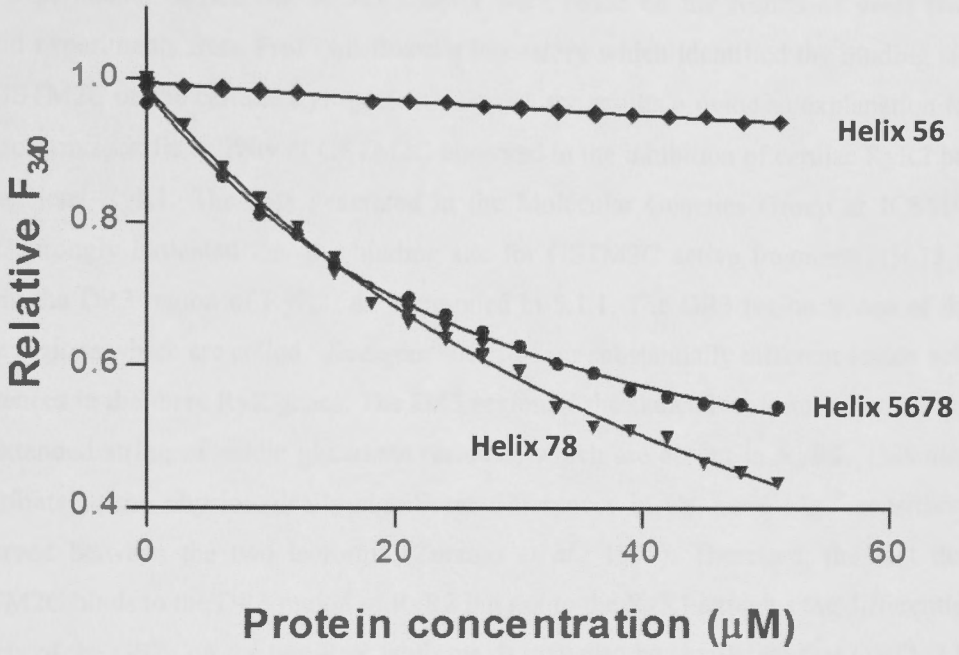

Peptides	Kd (μM)
RyR2D3 short & H5678	30.2± 5.8
RyR2D3 short & H56	134.3 ± 44.7*
RyR2D3 short & H78	41.2 ± 7.1

Fig 5.8: Fluorescence values at 340 nm as a function of RyR2D3 short peptide concentration with helix 5678, 56 and 78 of GSTM2C in the cuvette. The *K*d values were derived using nonlinear regression analysis in the program GraphPad Prism and expressed as mean ± SEM from 3-4 fluorescence quenching experiments. Data from a representative experiment from each group is shown in the graph * Significantly different P<0.01 from K_d value obtained for helix 5678.

5.4 Discussion

The experiments carried out in this chapter were based on the results of yeast two-hybrid experiments from Prof Phil Board's laboratory which identified the binding site for GSTM2C on the cardiac RyR protein. Overall, the results provide an explanation for the isoform specific activity of GSTM2C observed in the inhibition of cardiac RyR2 but not skeletal RyR1. The data generated in the Molecular Genetics Group at JCSMR, ANU strongly indicated that the binding site for GSTM2C active fragment H5678 is within the DR3 region of RyR2. As mentioned in 5.1.1, The DR3 region is one of the three regions which are called "divergent" due to their substantially different amino acid sequences in the three RyR genes. The DR3 region of the skeletal isoform is notable for its extended string of acidic glutamate residues, which are absent in RyR2. This may contribute to the physiologically significant differences in Ca^{2+} and Mg^{2+} sensitivity observed between the two isoforms (Zorzato *et al.*, 1990). Therefore, the fact that GSTM2C binds to the DR3 region of RyR2 but not to the RyR1 explains the differential effects of the GSTs on the two RyR isoforms. It may also be significant that GSTM2 is one of the few endogenous inhibitors of RyR2 and that it binds to a site on RyR2, that in RyR1, is a potential binding site for the major endogenous inhibitor of RyR1, Mg^{2+} (Zorzato *et al.*, 1990). This conclusion was based on the fact that acidic sequences in RyR1 DR3 region form a divalent cation binding site. However, some RyR1/RyR2 chimera studies suggest that it is not the major low-affinity Mg^{2+} binding site in RyR1 (Du and MacLennan, 1999). On the other hand, another study showed that the deletion of DR3 region in RyR1 affects both Ca^{2+} dependent activation/ inactivation and Mg^{2+} dependent inhibition of the channel (Bhat *et al.*, 1997a, Hayek *et al.*, 1999, Hayek *et al.*, 2000).

The results of the intrinsic tryptophan fluorescence spectroscopy experiments presented in this chapter revealed that the binding affinity between H5678 and RyR2D3 short was stronger than the region identified using the yeast two-hybrid system, AD-RyR2D3-2, or the full DR3 region. Consistent with results obtained for yeast two hybrid experiments and β galactosidase assay, dissociation constants calculated from the binding assay also showed weak binding between H5678 and the regions of RyR2 with the dissociation constants in the low micromolar (30-90 μM) range. These results are also consistent with functional studies presented in chapter 3 and 4 where GSTM2C inhibited RyR2 activity at concentrations between 5-30 μM, and the inhibitory effect

was easily reversed when GSTM2C fragments were perfused from the *cis* solution of the lipid bilayer experiments. The binding site on RyR2 was localised to a 22-amino acid fragment (1869-1890, Fig 5.4) within the DR3 region. As explained in 5.1.3, the mutagenesis of positively charged residues, I1871, A1874, K1875, L1876 and K1883 within this 22-amino acid region reduced binding between H5678 and RyR2. These results, therefore, confirm that the DR3 region is indeed the binding site of GSTM2C and also indicates that the interaction between the two proteins may be via electrostatic bonds.

As revealed by cryo electron microscopy, the three dimentional structure of RyR is shows two major components, a cytoplasmic assembly and a transmembrane assembly. The cytoplasmic assembly contains at least 10 domains (Radermacher *et al.*, 1994). The clamp shaped structure located at the corners of the cytoplasmic domain include domains 5,6, 9 and 10. Large conformational changes have been observed in the clamp region when the channel was switched from closed to the open states (Serysheva *et al.*, 1999, Orlova *et al.*, 1996). Cryo EM and three dimentional reconstruction studies done by Zhang *et al* mapped the DR3 region to a sub region within domain 9 (Fig 5.9) in the cytoplasmic assembly of the RyR2. As mentioned in 5.1.1, the authors suggest that the tertiary structure should be very similar among the three RyR isoforms due to the high degree of sequence identity (~70%) and that the DR3 region is likely to map to domain 9 in all three RyR isoforms (Zhang *et al.*, 2003). The presence of the DR3 region within the clamp region of RyR2 raises the possibility that the DR3 region is involved in the conformational changes associated with channel gating. This speculation was further supported by studies carried out on RyR1 and RyR3 on their open and closed states (Serysheva *et al.*, 1999, Hayek et al., 2000). The results revealed that structural differences occur between the open and closed states in the vicinity of domain 9 (Serysheva *et al.*, 1999, Orlova *et al.*, 1996, Sharma *et al.*, 2000). Therefore, it can be concluded that domain 9 is important for channel opening and perhaps for EC coupling.

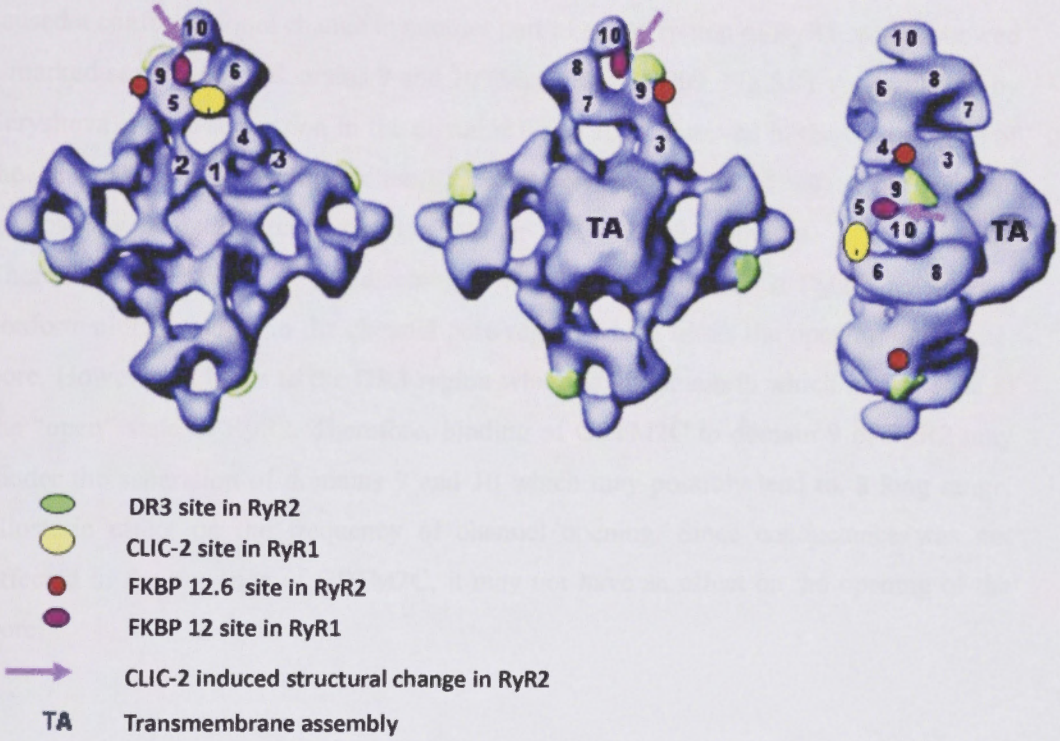

Fig 5.9: Three dimentional surface representation of RyR2 showing the location of DR3 region and binding sites for several modulators. Pink arrow points to the region between domains 9 and 10 that demonstrate structural separation upon CLIC-2 binding. Figure adapted from (Dulhunty *et al.*, 2011).

As mentioned in the introduction (5.1.2), a cryo electron microscopy study carried out on the binding of another member of GST super family, CLIC-2, to RyR1 revealed that the CLIC-2 binds to the upper surface of the cytoplasmic assembly, between domains 5 and 6 in the clamp region. Interestingly, this study revealed that binding of CLIC-2 caused a conformational change in another part of clamp region of RyR1, which showed a marked separation of domains 9 and 10 (Meng *et al.*, 2009, Fig 5.9). As explained by Serysheva *et al*, a separation in the domains 9 and 10 is observed in the "open" state of the channel, but not in the "closed" state (Serysheva *et al.*, 1999). Cryo electron microscopy and 3D reconstruction of GSTM2C-RyR2 complex is in progress. Therefore, we have not yet discovered whether binding of GSTM2C leads to a conformational change in the channel pore region which limits the opening of channel pore. However, it binds to the DR3 region which is in domain 9, which is displaced in the "open" state of RyR2. Therefore, binding of GSTM2C to domain 9 of RyR2 may hinder the separation of domains 9 and 10 which may possibly lead to, a long range, allosteric effect on the frequency of channel opening. Since conductance was not affected in the presence of GSTM2C, it may not have an effect on the opening of the pore.

The DR3 region of RyR2 which binds to GSTM2C, is located on the under surface of domain 9 (facing the SR membrane). If the location of DR3 region is similar in the 3D structure of RyR1 and RyR2, then the GSTM2C binding site on RyR1 is distinctly different from the CLIC-2 binding site. The GSTM2C binding site on RyR1 has not been established. But it is very unlikely to be the same as CLIC2 binding site or the binding site of RyR2. The GSTM2 and CLIC-2 proteins alter RyR1-channel function in different ways. GSTM2 increases RyR1-channel activity (Liu *et al.*, 2009, Abdellatif *et al.*, 2007), whereas CLIC-2 inhibits the RyR1 channel (Board *et al.*, 2004, Meng *et al.*, 2009). Therefore, the GSTM2-binding site on RyR1 can not be the same as the GSTM2-binding site on RyR2, as the active C-terminal half of GSTM2C can be cross-linked to RyR2, but not to RyR1 (Liu *et al.*, 2009). In addition, the C-terminal α-helical bundle of GSTM2 which inhibits RyR2 is inactive when applied to RyR1, implying that the residues in GSTM2 that activate RyR1 must include the N-terminal thioredoxin

domain. Thus, the binding site in RyR1 for the thioredoxin domain would, presumably, be structurally different from the binding site for the α-helical domain in RyR2. The GSTM2-binding site on RyR1 remains to be determined, also the CLIC-2- binding site on RyR2.

Although, the major target for dantrolene is RyR1, recent studies revealed that dantrolene suppresses the Ca^{2+} leak from the SR of failing cardiac myocytes or mutant myocytes expressing disease causing RyR2 mutation (Uchinoumi *et al.*, 2010, Kobayashi *et al.*, 2009). It is also interesting to note that the dantrolene binding sequence is also located in domain 9 near FKBP 12.6 binding site. The mechanism which leads to the inhibition of cardiac RyR2 is still not clear, but the authors assume that dantrolene binds to a region near the domain switch, for inter domain interactions between NH_2-terminal and central region of RyR1 which allosterically stabilize the closed state of the channel (Wang *et al.*, 2011). Although, the mechanism of action is not clear, it is important that two modulators which inhibit the cardiac ryanodine receptor activity and reduce the release of Ca^{2+} from the cardiac SR share a similar binding site on cardiac RyR2.

Preliminary results presented in this chapter also suggested that a double mutation associated with ARVC in the DR3 region of RyR2 increased the binding affinity of GSTM2C for RyR2. These experiments need to be repeated using different binding strategies. However, it is interesting to speculate GSTM2C might be used for the treatment of ARVC which causes sudden cardiac death due to stress-induced ventricular arrhythmias. If GSTM2C binds to the DR3 region of RyR2 with a higher affinity in patients suffering from ARVC related ventricular arrhythmias, there is a possibility of reducing the excessive release of Ca^{2+} from cardiac SR during diastole in the presence of GSTM2C. Further experiments will provide more insight into this specific activity of GSTM2C.

A comparison of the binding affinity of GSTM2C fragments, H56, H78 or H5678 to the RyR2D3 short peptide further confirmed that flanking helices of helix 6 are essential for the stability and binding of GSTM2C to RyR2. Fragment H56 alone did not facilitate binding of GSTM2C to RyR2. However, the affinity of binding of H78 to the RyR2D3 short peptide was not significantly different from that of H5678 and RyR2D3 short peptide. It can be assumed that H78 may play a role for the binding of GSTM2C to RyR2 but helices 5 and 6 are important for the inhibitory effect against RyR2.

5.5 Conclusion

Overall results obtained in our laboratory confirmed the binding of H5678 to the DR3 region of cardiac RyR2 which clearly explains the isoform specific inhibitory action of GSTM2C on RyR2. We identified the smallest fragment of RyR2 which binds to H5678, the most active fragment of GSTM2C using intrinsic tryptophan fluorescence spectroscopy. A 22 amino acid fragment (1869-1890) within DR3 region of RyR2 was identified and this shows the highest binding affinity to the H5678 fragment of GSTM2C. However, consistent with the results presented in chapter 3 and 4, binding between the two proteins was weak with dissociation constants in micro molar range. Considering the location of DR3 region in the clamp of RyR2, specific binding of GSTM2C to RyR2 could dramatically influence the gating of the channel. The isoform specificity of the GSTM2C interaction further suggests that this 22 amino acid region would be an ideal target for isoform specific drugs designed to modulate cardiac RyR2 activity.

Chapter 6 Effect of GSTM2C and its mutants on cardiomyocyte function

6.1 Introduction

Results presented in the previous chapters showed the importance of helix 6 and its flanking helices for the inhibition of cardiac RyR2. These results suggested that GSTM2 fragments have the potential to regulate RyR2 function. Single channel lipid bilayer experiments and Ca^{2+} release assays, used to determine the activity of GSTM2 proteins on RyR1 and RyR2, employed SR vesicles which contain the RyR receptors and other intracellular substances such as calsequestrin and RyR associated membrane proteins, triadin and junctin. However, these experiments did not provide insight into the mechanisms by which GSTM2 might influence excitation-contraction coupling and the factors which control the contractile status of the myocardium *in vivo*. Enzymatically isolated cardiomyocytes used as a model of cardiac function provide a useful preparation for use in probing the cardiac contractility in single cells. Therefore, neonatal cultured cardiomyocytes were used in this study. Another study conducted concurrently by Morris *et al* also provided useful information about the potential of GSTM2C to enter cells and carry cargo (Morris *et al.*, 2009). This study suggested that GSTM2C may be taken up to cardiomyocytes where it would be available to act directly on RyR2. Therefore, the first objective of the present investigation was to determine the ability of GSTM2C to enter neonatal cardiomyocytes. Then, the effect of GSTM2C and the mutants F157A, Y160A on the contractility of cardiomyocytes was determined.

6.1.1 Measurement of shortening as an index of contractility

The primary neonatal cardiomyocyte culture enables researchers to study and understand the morphological, biochemical and electrophysiological characteristics of the heart, by providing a valuable tool for pharmacological and toxicological studies.

The culture of neonatal murine cardiomyocytes was first described by Harary and Farley (Harary and Farley, 1963) and since then several modifications have been reported over the subsequent 40 years. Cultured neonatal cardiomyocytes have been used as a model for studying contraction, ischemia, hypoxia, and also to study the toxicology of drugs and their transport (Yamashita *et al.*, 1994, Bahi *et al.*, 2006, Limaye and Shaikh, 1999). RyR2 is expressed in embryonic and neonatal cardiomyocytes (Nakanishi *et al.*, 1088, Gorza *et al.*, 1997). Parameters of shortening and lengthening measured from isolated cardiomyocytes are indicative of "contractility" function. Indeed, the studies indicate that changes in cell length can be an adequate index of sarcomere dynamics if the data are obtained under carefully controlled conditions, where the entire cell is monitored to ensure minimal geometric or optical non-linearities. Information that is available regarding force development indicates that isolated cardiac myocytes retain at least some of the relatively high passive stiffness characteristic of cardiac muscle and that they are capable of active stress generation (Brady, 1991). Neonatal cardiomyocytes were used in this study. The best yields of viable dissociated cells are usually obtained from fetal or neonatal tissues. Spontaneous contraction in neonatal primary cultures is used as an indicator of cell viability. I established methods for isolation of neonatal cardiomyocytes and their maintenance in a primary culture in our laboratory. A method to measure contractility in the neonatal ventricular cardiomyocytes was also established and optimized. An investigation of the capacity of GSTM2C to enter cardiomyocytes and its impact on measurable aspect of contractility is presented in this chapter.

6.2 Methods

6.2.1 Isolation and culture of neonatal ventricular cardiomyocytes.

Isolation and culture of cardiomyocytes were carried out according to the method described in 2.3.8. Briefly, neonatal Wistar rats (1-2 days old) were sacrificed and the beating hearts were immediately removed into a solution of Hanks balanced salt

solution with 10% fetal calf serum. Ventricles were separated and cardiomyocytes were isolated as described in 2.3.8. At the end of the procedure, cells seeded on coverslips coated with collagen, were stored in complete DMEM media without serum in a dual chamber water jacketed incubator at 37 °C in an atmosphere of 5% CO_2 and 95% air. Culture medium was routinely changed every 2 days.

6.2.2 Observation of morphological and contractile properties of spontaneously beating cardiomocytes.

Morphological changes such as appearance, growth and overlapping of cardiomyocytes and appearance of dead, rounded cells were observed from the first day of the culture. After the culture procedure, cell viability was observed by tracking the spontaneous contraction of cardiomyocytes. Randomly selected areas (eight) in the cell culture dishes were selected to measure beating frequency and % beating cells. Several different cover slips (n=2-3) of the same culture were examined using a Nikon TE2000-U microscope at the Microscopy and Cytometry Resource Facility at JCSMR, ANU. This procedure was repeated for 4-5 different cultures. Cell beating frequency was evaluated for the control group treated with culture media and the test group treated with 15 μM GSTM2C by counting the number of cell contractions per min. All measurements were taken 2 h after treating the cells with either the culture media or GSTM2C. The optical fields were randomly chosen and observed for at least 3 min to ascertain the occurrence of spontaneous beats. The number of spontaneously beating cells in the selected field of view was counted in the control and GSTM2C treated groups.

6.2.3 Establishing a technique for the immunostaining of neonatal cardiomyocytes.

I established a method for the immunostaining of neonatal ventricular cardiomyocytes with anti α-actinin antibody as described in 2.3.9. This was done in some experiments to

identify cardiomyocytes as distinct from fibroblasts. An indirect immunostaining method was used in which cells were fixed with 4% paraformaldehyde for 20 min, permeabilized with 0.1% Triton-X-100 in PBS for 10 min and incubated for 1 h with monoclonal anti α-actinin (sarcomeric) primary antibody in 1:200 in dilution. Secondary antibody, Alexafluor 568 goat anti mouse IgG (excitation/emission maxima ~578/603 nm), was added in 1:100 dilution. Mounted cells were observed in Leica SP5 confocal microscope as explained in 2.3.11.

6.2.4 Determination of cellular uptake of GSTM2C into cardiomyocytes.

To establish whether GSTM2C enters cardiomyocytes, GSTM2C was fluorescently labelled with Oregon green dye (GSTM2C-OG) as described in 2.3.3. Cardiomyocytes which were 4 days old in culture were incubated with 1 μM GSTM2C-OG for 24 h period. This longer period (24 h) was selected to allow maximal uptake of GSTM2C-OG as the cell permeabilizing agent, Triton-X-100 was used during the immunostaining step which may remove some of the GSTM2C-OG from the cardiomyocytes. The procedure described in 6.2.3 was used to immunostain the cells to distinguish between cardiomyocytes and fibroblasts. Once cells were mounted on coverslips, they were observed under Leica SP5 confocal microscope by which a series of images were taken through the Z-plane.

6.2.5 Time course for the uptake of GSTM2C tagged with Oregon green dye into neonatal cardiomyocytes

GSTM2C was fluorescently labelled with Oregon green dye (GSTM2C-OG) as described in 2.3.3. Neonatal cardiomyocytes 4 days in culture were treated with 1 μM GSTM2C-OG and spontaneously beating cells were observed under Leica SP5 confocal microscope every half an hour (after thorough washing) up to 2.5 h to determine the maximal uptake of the protein into the cardiomyocytes. Fluorescence emission of oregon green dye was captured at 514 nm using an argon 488 nm laser line.

6.2.6 Measurement of contractility of spontaneously beating cardiomyocytes

I established a technique that had not previously been used in our laboratory to measure the contractility of neonatal cultured cardiomyocytes. Neonatal cardiomyocytes which are 4 days old in culture were used. They were placed on a heated stage in which the temperature was maintained at 37 °C and CO_2/air (5%/95%) was flowing over the cells. Cell contractions were recorded using a JVC video camera attached to a Nikon TE2000-U microscope for 5 min. Cells were kept on the stage without moving the field of view. Control images were captured initially. Then the media was exchanged with fresh media containing 15 μM GSTM2C. Two h later, cell contractions were recorded and images obtained during systole and diastole were frozen and analysed for both the control and the GSTM2C treated groups as described in 2.3.10.

6.2.7 Measurement of contractility in field stimulated cardiomyocytes

A procedure similar to that described in 6.2.6 was used. Instead of recording spontaneous contractions, contractions were measured in cells which were stimulated using a pair of Pt electrodes as described in 2.3.10, connected to a stimulator which delivered electrical stimuli of 1Hz for 2 ms duration and initially 3 V in amplitude. The polarity of the stimulating electrodes was reversed every fourth pulse to avoid build up of electrolyte by products. The distance between the electrodes was 2 mm. To optimize the pulse parameters, the stimulation voltage was slowly increased until contraction was observed. Cells were stimulated at a voltage 5% (in V/cm) higher than the threshold. Control contractions were recorded at the beginning of the experiment, after optimally adjusting the pulse parameters. Cells were then treated with 5,10 or 15 μM GSTM2C and kept on the stage for 2 h without changing the field of view. Cells were stimulated again and the contractions of the same set of cells were recorded after 2 h. Systolic and diastolic images were frozen (Fig 6.1) and analysed as described in 2.3.10. Distances

were measured along the axis of contraction between the same landmark points within the cell. The most contracted and relaxed images were selected and distances measured using Image Pro Plus 6.2 software and then the percentage shortening was calculated accordingly.

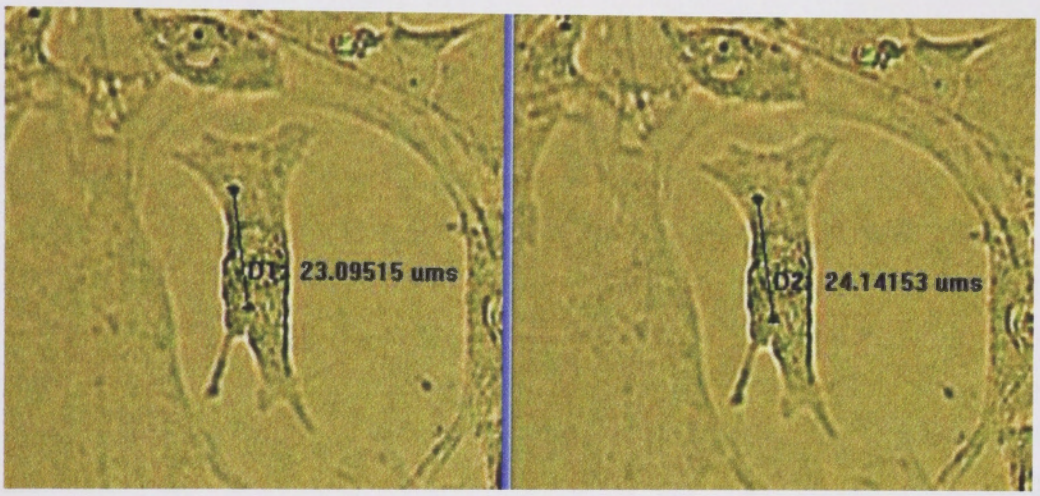

Fig 6.1: Frozen images obtained of the most contracted and relaxed states of the same cardiomyocyte. Distances between the same points were calculated using Image pro plus 6.2 software.

6.2.8 A comparison of the contractility of GSTM2C and mutants F157A and Y160A

Neonatal cardiomyocytes were treated with 15 μM of GSTM2C, F157A and Y160A and the experiment was repeated as described in 6.2.7. Contractility of each cardiomyocyte in each group was calculated.

6.3 Results

6.3.1 Morphological changes observed in cultured neonatal ventricular cardiomyocytes

The ventricular myocytes in this study were initially plated in DMEM supplemented with 10% fetal calf serum. After 3 h, medium was changed to serum free DMEM. The serum facilitates cell attachment to the coverslip, but also enhances the growth of fibroblasts which may outgrow cardiomyocytes if maintained in the serum for longer periods. Attachment of cardiomyocytes to the collagen coated cover slips occurred within the first day of culture. Cardiomyocytes lose their ability to proliferate shortly after birth. Growth of heart tissue is achieved by cell growth rather than by proliferation. The cells also spread out as they morphologically differentiate on day 1 in culture. On the second day, the myocytes are elongated. Most of them are uninucleate although some are binucleate. On day 3 *in vitro*, cell clusters were observed as cardiomyocytes overlapped each other with their growing pseudopodia. On day 6 in culture, a confluent monolayer of culture was observed. Some of the cardiomyocytes exhibited spontaneously beating activity from day 1 in culture. Most of the cardiomyocytes beat at a similar frequency when a monolayer is formed on the sixth day. The average beating rate was 42.5 ± 5.2 per min.

Fig 6.2: Cultured cardiomyocytes on day 3 in culture. Cardiomyocytes intercalated with each other to form a cluster by extending pseudopodia.

6.3.2 Immunostaining of neonatal cardiomyocytes with anti-α-actinin

Outgrowth of cardiomyocytes by contaminating fibroblasts is a persistent problem encountered in primary culturing of cardiomyocytes. Also, the fibroblasts can not be distinguished from cardiomyocytes by simply observing cells under the microscope. The cell morphology is similar and unless the cardiomyocyte is contracting, they can not be easily distinguished from fibroblasts. In the present study, precautions were taken by omitting fetal calf serum in the culture media. If fetal calf serum is included, fibroblasts outgrow the cardiomyocytes within a few days in culture. Although cultures maintained in fetal calf serum enriched media show more spontaneously beating cardiomyocytes, beating myocytes were still observed in the absence of serum. Although serum was omitted, fibroblasts were still present with the cardiomyocytes. Therefore, immunostaining was employed to distinguish between cardiomyocytes and fibroblasts.

Immunocytochemistry is the usual method used for locating an antigen to a particular structure or subcellular compartment provided that an antibody specific for the protein under study is available. Immunofluorescence is a sensitive method requiring only one available antigenic site on the protein. An indirect technique was used in this study where the primary antibody was unlabelled and can be made for a specific species (in this case mouse). After the primary antibody was bound to the antigen, a second antibody, against the IgGs in the species in which the first antibody was made and coupled to a fluorochrome, is added. In this study, cultured cardiomyocytes were immunostained with the primary antibody, which was a monoclonal anti-α-actinin antibody specific for skeletal and cardiac muscle α-actinins which are sarcomeric actin binding proteins. The anti-α-actinin antibody stains Z lines and stress fibers of myotubes in skeletal and cardiac muscle, but not in non-sarcomeric muscle elements such as connective tissues, epithelium, nerves and smooth muscle.

As shown in Fig 6.4, cultured, immunostained cardiomyocytes showed striations indicating muscle specific sarcomere formation. Therefore, cardiomyocytes were distinguished from fibroblasts using this immunostaining technique.

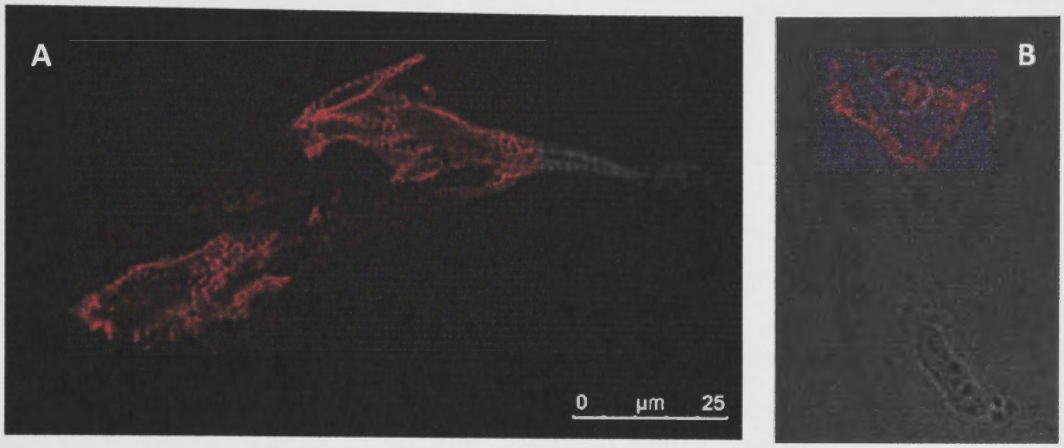

Fig 6.3: Neonatal ventricular cardiomyocytes immunostained with anti-α-actinin shows the typical striations characteristic of striated muscle fibers (A). Fig 6.3B shows a fibroblast and a cardiomyocyte in close proximity. Note that the fibroblast which is in close proximity to the cardiomyocyte is not stained with anti-α-actinin.

6.3.3 Confocal microscopy confirms the uptake of GSTM2C-OG into cardiomyocytes

As mentioned before, when GSTM2C-OG was incubated with neonatal cardiomyocyte culture, it is difficult to distinguish between cardiomyocytes and fibroblasts unless the cardiomyocytes are beating. Therefore, in an initial experiment, immunostaining of cardiomyocytes with anti-α-actinin was employed to accurately identify the cardiomyocytes. As shown in Fig 6.4 below, 24 h after the incubation of the cardiomyocytes with GSTM2C-OG, cardiomyocytes were immunostained with anti-α-actinin. Fig 6.4 A shows the striated appearance of cardiomyocytes specifically stained with anti-α-actinin and Fig 6.4 B shows the uptake of Oregon green tagged GSTM2C

characterised by the punctuate pattern of green fluorescence inside the cell. Cell overlay shown in Fig 6.4 C confirms the presence of GSTM2C-OG inside the cardiomyocytes. Transmission image of the cell is shown in Fig 6.4 D. These results confirm our hypothesis that GSTM2C enters neonatal cardiomyocytes without any cell penetrating peptides. Z stack analysis shown in Fig 6.5 confirms the presence of OG tagged GSTM2C inside the cardiomyocytes.

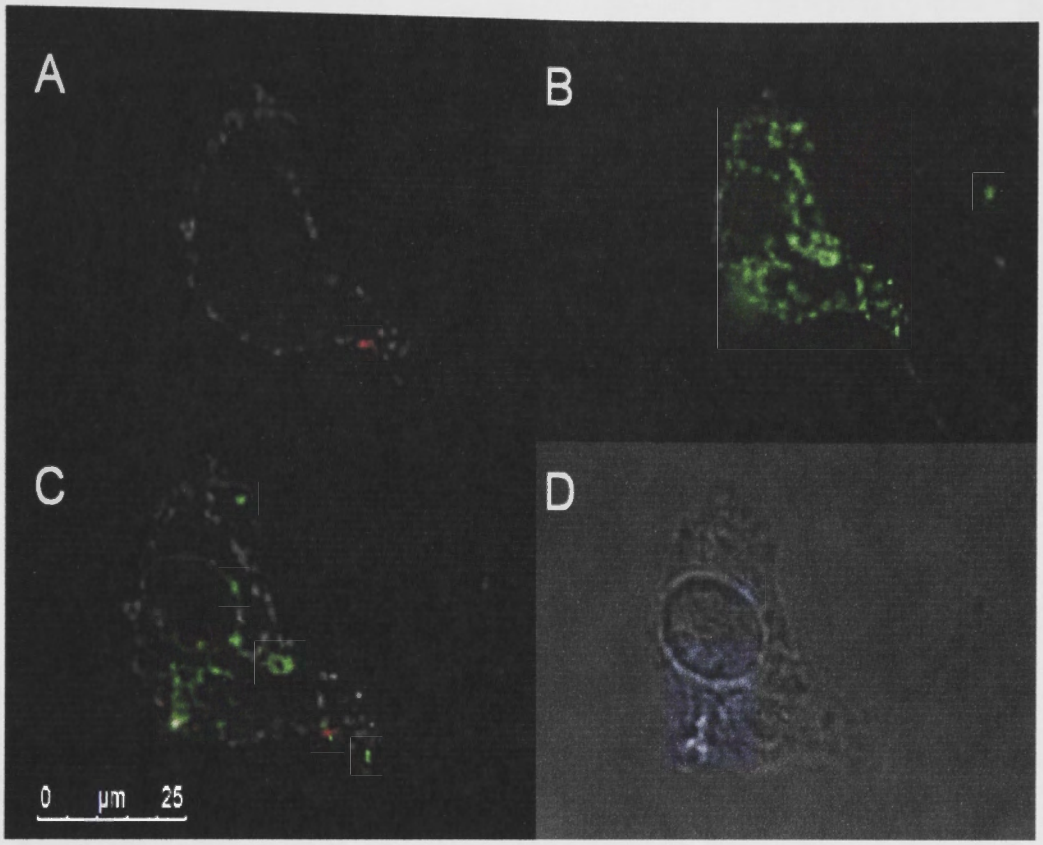

Fig 6.4: Confocal images confirm the uptake of GSTM2C-OG into neonatal cardiomyocytes. A: cardiomyocyte immunostained with striated muscle specific anti-α-actinin (sarcomeric) antibody. B: Punctuate pattern of GSTM2C-OG inside the cell. C: overlay of A and B confirms the uptake of GSTM2C-OG into cardiomyocytes. D: transmission image of the cardiomyocyte. In this experiment, the cells are fixed to allow immunostaining.

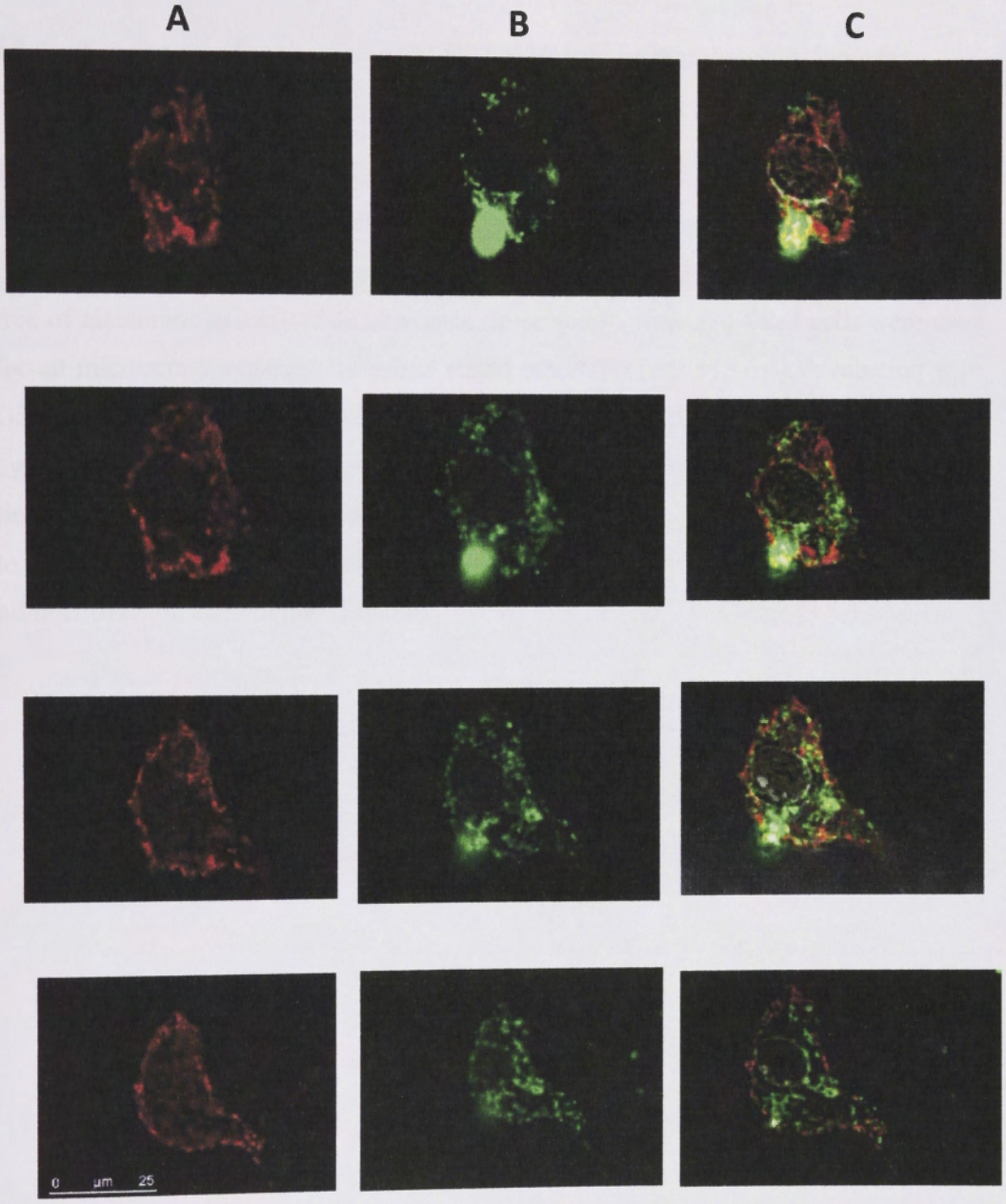

Fig 6.5: Z-stack analysis of confocal microscopy images shows clearly the presence of GSTM2C-OG in different Z planes of the neonatal cardiomyocyte. Column A: Identification of cardiomyocyte by the anti-α-actinin staining. B: Punctate pattern of GSTM2C-OG in cardiomyocytes. C: Overlay of A and B. Note a dead, rounded cell in contact with the cardiomyocyte stained in this study.

6.3.4 Time course for the uptake of GSTM2C into neonatal cardiomyocytes

To visualise the process of GSTM2C-OG entry into neonatal cardiomyocytes, a time course of incubation was conducted using a 1μM concentration of GSTM2C-OG. Confocal microscopy allowed an intracellular 'slice' of the cell to be viewed, which is free of membrane associated fluorescence. Importantly, live, non-fixed cells were used for all microscopy experiments unless stated otherwise (e.g. Fig 6.4). Incubation with GSTM2C-OG for 2.5 h produces a punctate pattern of intracellular fluorescence in the cytoplasm of neonatal cardiomyocytes. A central intracellular slice of cells from several time points is displayed in Figure 6.6. Punctate, vesicle-like fluorescent spheres began to appear 10 min after incubation with GSTM2C-OG, and continued to increase in number over the 2.5 h period (Fig 6.6).

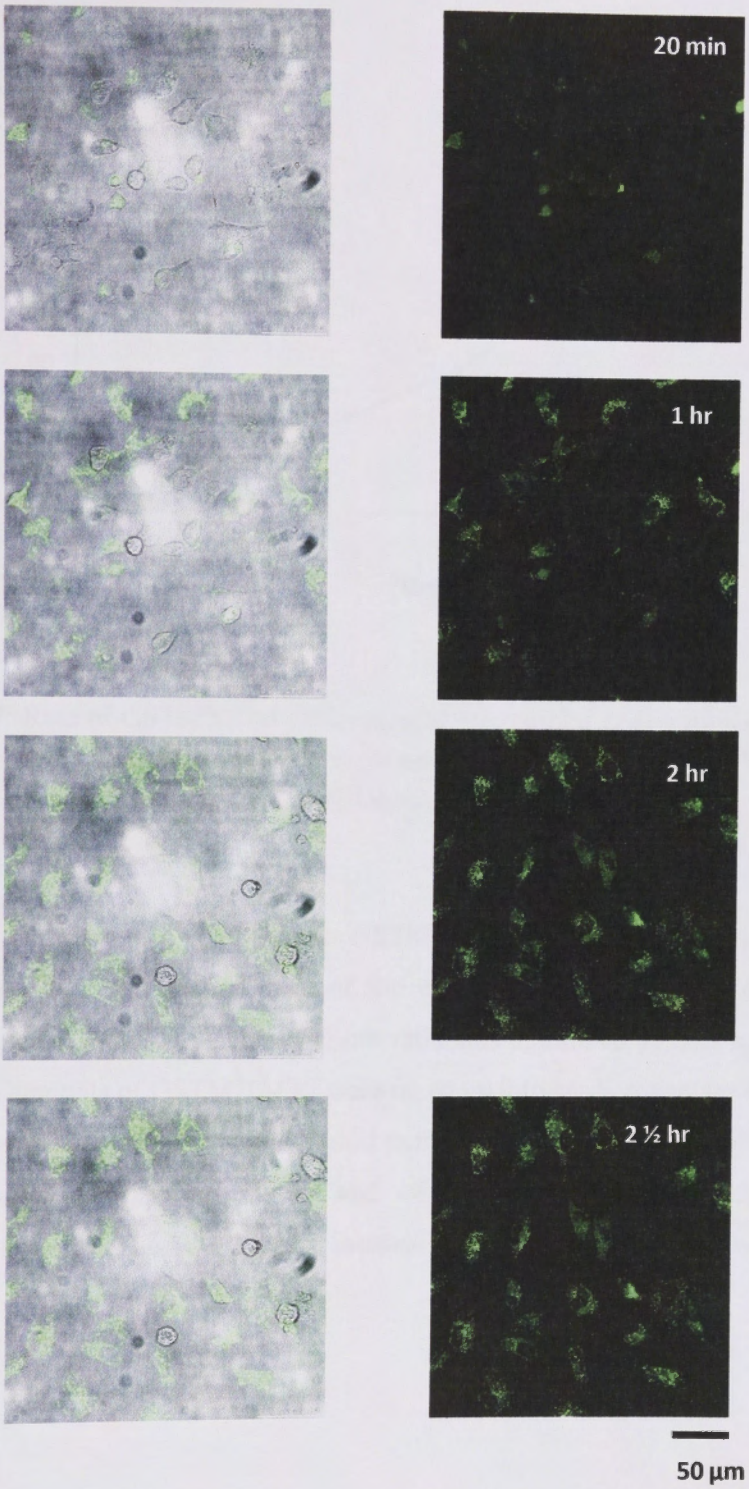

Figure 6.6: Visualising the uptake of GSTM2C in confocal microscopy. Individual cardiomyocyte cell coverslips were treated with 200 nM GSTM2C-OG for 2.5 hours, washed and visualised live by confocal microscopy. Representative central z-section transmission (left) and fluorescence (right) images at selected time intervals are presented and detector settings were maintained throughout all time points.

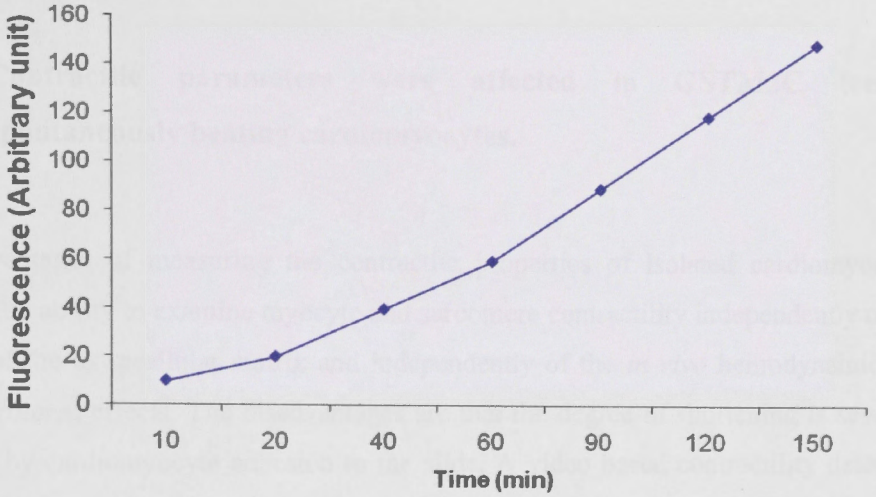

Fig 6.7: Rate of GSTM2C internalization at micromolar concentration. Mean cellular fluorescence of neonatal ventricular cardiomyocytes treated with 1 μM GSTM2C-OG over a 2 .5 h time period as measured by confocal microscopy.

The time of exposure of the cells to GSTM2C, the conditions of incubation on the microscope stage and maintenance of the cells on the microscopic stage with the desirable temperature (37 °C) and CO_2/air ratio was optimized by trial and error. Since significant amounts of GSTM2C-OG were taken up into cardiomyocytes in 2 hours (Fig 6.7), 2 h was chosen as an optimal period to maintain the cells on the microscope stage at the desired temperature (37°C) and CO_2/air ratio. Therefore, all contractility experiments were carried out 2 h after incubation of the cardiomyocytes with GSTM2C.

6.3.5 Contractile parameters were affected in GSTM2C treated spontaneously beating cardiomyocytes.

The advantages of measuring the contractile properties of isolated cardiomyocytes include the ability to examine myocyte and sarcomere contractility independently of the effects of the extracellular matrix and independently of the *in vivo* hemodynamic and neurohormonal effects. The disadvantages are that the degree of shortening is severely reduced by cardiomyocyte adhesion to the slide. A video based contractility detection system was optimized in this study which enabled the contractile parameters to be displayed in real time so that contractions could be visualized during the experiment and contracting cardiomyocyte aligned without much difficulty. The recorded images could then be analysed off line.

Data above (6.3.3) show clearly that GSTM2C enters neonatal cardiomyocytes without assistance of cell penetrating peptides. Since, results in chapters 3 and 4 showed that GSTM2C specifically inhibits cardiac RyR2 activity, the aim here was to investigate GSTM2C's action on the contractility of spontaneously beating cardiomyocytes. The presence of spontaneous beating is frequently used as an indicator of functionally intact cardiomyocytes. Cardiomyocytes which are 4 days old in culture were used for the study. The number of spontaneously beating cells observed in the control group (6.62±0.92%, n=10 coverslips) was significantly reduced to 1.9±0.28% ($P<0.001$, n=10 coverslips) in the GSTM2C treated group. Beating frequency (number of contractions per min) was also reduced significantly from 42.46±5.18/min in the control group to 6.89 ±0.92/min in the GSTM2C treated cells ($P<0.001$, Fig 6.8). To measure the effect of GSTM2C on the contraction in more detail, the degree of shortening in each beat was measured. As shown in Fig 6.8, the percentage shortening was significantly reduced from 7.48±0.9% in the control group of cardiomyocytes to 2.88±0.45%, after the GSTM2C treatment ($P<0.001$). This result is consistent with the previous observation where GSTM2C reduced the Ca^{2+} release from cardiac SR significantly (Chapter 3).

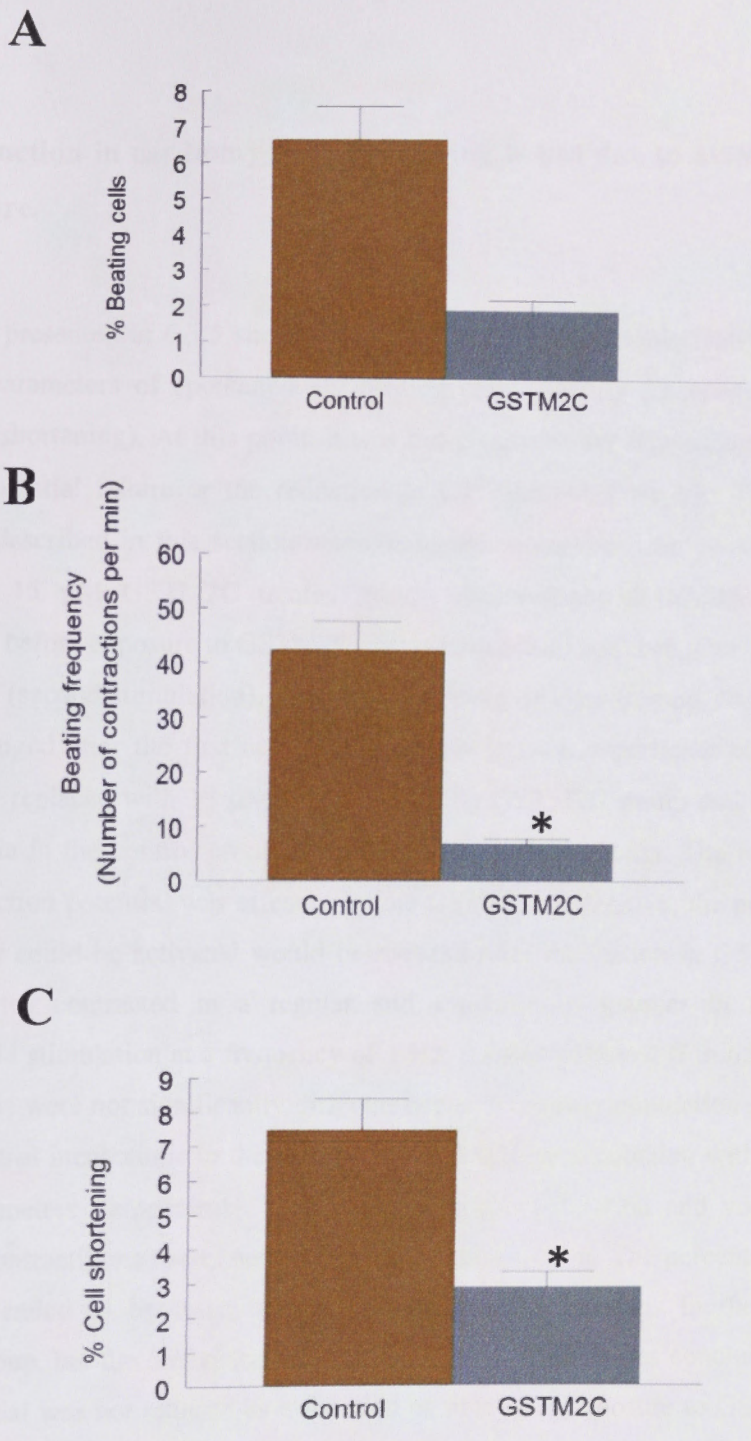

Fig 6.8: A comparison of the contractile parameters of spontaneously beating cardiomyocytes 2 h after the incubation with CDMEM media (control) and 1 μM GSTM2C. A: % beating cells B: Beating frequency and C: % cell shortening, all were reduced significantly ($P<0.001$) after the cardiomyocytes were treated with GSTM2C. The data is presented here as the mean±SEM from 10 different coverslips from 4-5 preparations.

6.3.6 Reduction in cardiomyocyte shortening is not due to action potential failure.

The Results presented in 6.3.5 showed clearly that GSTM2C significantly reduces the contractile parameters of spontaneously beating cells (beating frequency, % beating cells and % shortening). At this point, it was not clear whether this reduction is due to an action potential failure or the reduction in Ca^{2+} release from SR. Therefore, the experiment described in this section was conducted to compare the % of cells in the control and 15 μM GSTM2C treated groups that responded to field stimulation immediately before exposure to GSTM2C (first stimulation) and then after 2 h exposure to GSTM2C (second stimulation). Therefore, the field of view through the microscope was not changed after the first control stimulation in each experiment but the media solution was replaced with 15 μM GSTM2C in the GSTM2C group and kept for 2 h period. Media in the control group was replaced with fresh media. The rationale was that, if the action potential was affected by the GSTM2C derivative, the percentage of the cells that could be activated would be reduced after incubation in GSTM2C. The cardiomyocytes contracted in a regular and synchronous manner in response to electrical field stimulation at a frequency of 1 Hz. As shown below (Fig 6.9), the % of excitable cells were not significantly different between the two stimulation sessions 2 h apart, in control incubations in the absence of GSTM2C or incubation with GSTM2C. Similar parameters (temperarure, stimulation frequency, duration and voltage) were used in all contractility experiments carried out in this section. The percentage of cells responding tended to be lower during both stimulation sessions in the GSTM2C incubated group, but the difference was not significant. Thus, it was concluded that the action potential was not reduced as a function of time after exposure to GSTM2C (the second stimulation compared to the first stimulation).

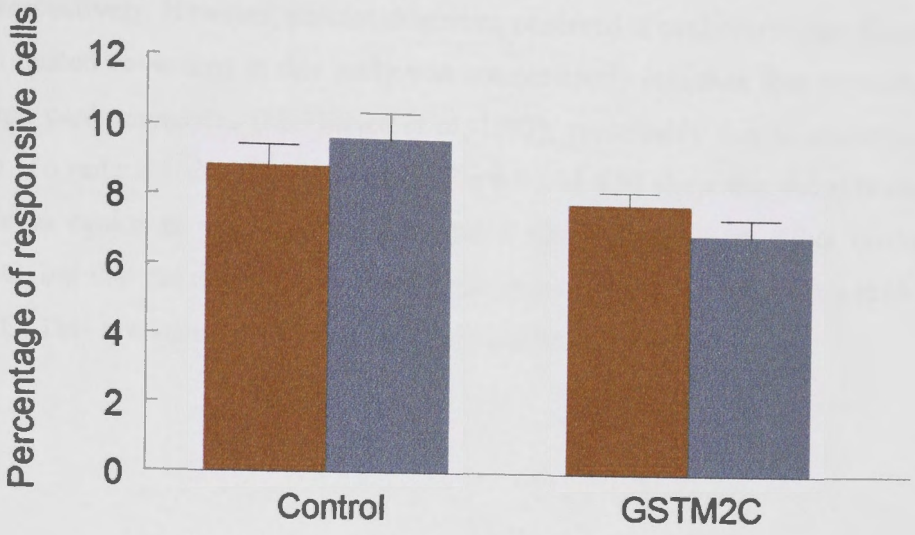

Fig 6.9: Excitability was not affected by the period of exposure to either media or GSTM2C (i.e. there was no difference between the % of responsive cells in the first and the second stimulation sessions). Figure shows the % beating cells in control and 15 μM GSTM2C treated cells after the first and second stimulations. Cells were stimulated for the second time while keeping the cells on the microscopic stage for 2 h without changing the field of view. The data presented here represent the mean±SEM from 10 (control) and 17 (GSTM2C) experiments.

6.3.7 Percentage shortening of field stimulated cardiomyocytes was reduced significantly by 15 μM GSTM2C

The effect of different concentrations of GSTM2C on the contractility of neonatal cardiomyocytes was determined in order to determine whether the inhibition of cardiac ryanodine receptor activity affects contraction. Previous results from single channel lipid bilayer experiments and SR Ca^{2+} release assay also showed comparable results in which a higher inhibition was observed in the presence of a higher concentration of GSTM2C, mostly 15 μM and 30 μM. As shown in Fig 6.10 below, the percentage shortening was reduced significantly in the presence of 15 μM of GSTM2C. A trend

towards a concentration-dependent reduction in contractility was observed between 5 μM, 10 μM to 15 μM, where the average shortening was 3.0%, 10.9% and 42.8% below control respectively. However, percent shortening observed in cardiomyocytes plated on collagen coated coverslips in this study was comparatively less than that measured in non-plated cardiomyocytes (Mukherjee *et al*, 1993), presumably due to anchoring of collagen. To reiterate, the results shown in Fig 6.9 and 6.10 show that the stimulation was able to evoke an action potential normally after incubation in either media or GSTM2C, but that the degree of shortening was reduced after 2 h incubation in15 μM GSTM2C. This is consistent with less Ca^{2+} released through RyR2.

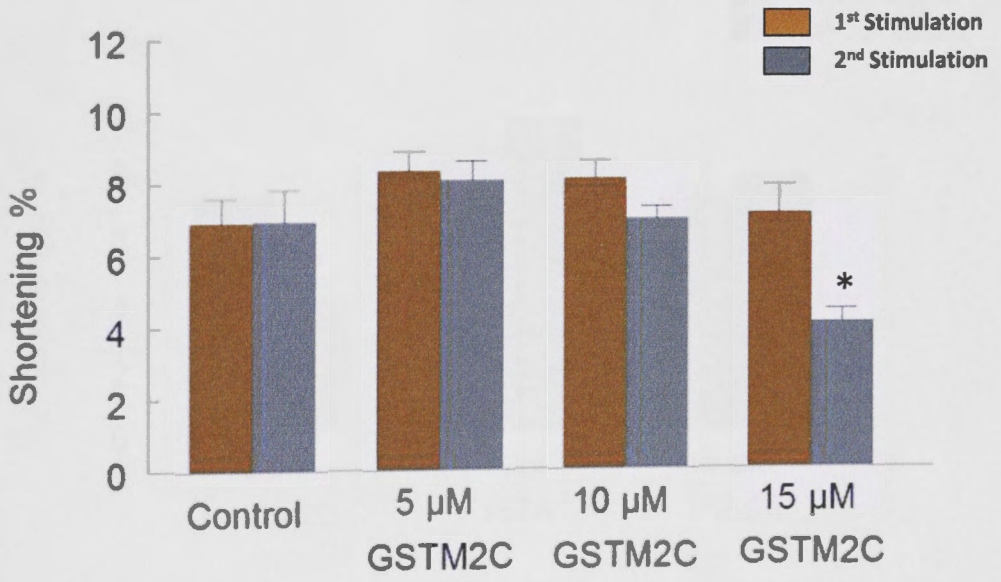

Fig 6.10: Concentration dependence of GSTM2C action on contractility of field stimulated cardiomyocytes. % shortening was calculated in the same set of neonatal cardiomyocytes after the first (control) stimulation and the second stimulation in the presence of 5,10 and 15 μM GSTM2C. A significant reduction in % shortening was observed only in the group treated with 15 μM GSTM2C ($P<0.001$). The data presented here represent the mean±SEM from 10 coverslips each.

6.3.8 Mutants (F157A, Y160A) that do not inhibit RyR2, do not reduce percentage shortening after field stimulation.

The study in this section was carried out to compare the activity of GSTM2C with its mutants, F157A and Y160A. In contrast to GSTM2C which significantly reduced the % shortening in the field stimulated cells (previous section), F157A and Y160A failed to reduce the % shortening. The results in Fig 6.11 showing a lack of effect of F157A and Y160A on contraction are consistent with our previous results where the cardiac RyR2 activity in single channel lipid bilayer experiments and Ca^{2+} release from cardiac SR were inhibited in the presence of GSTM2C but not with mutants.

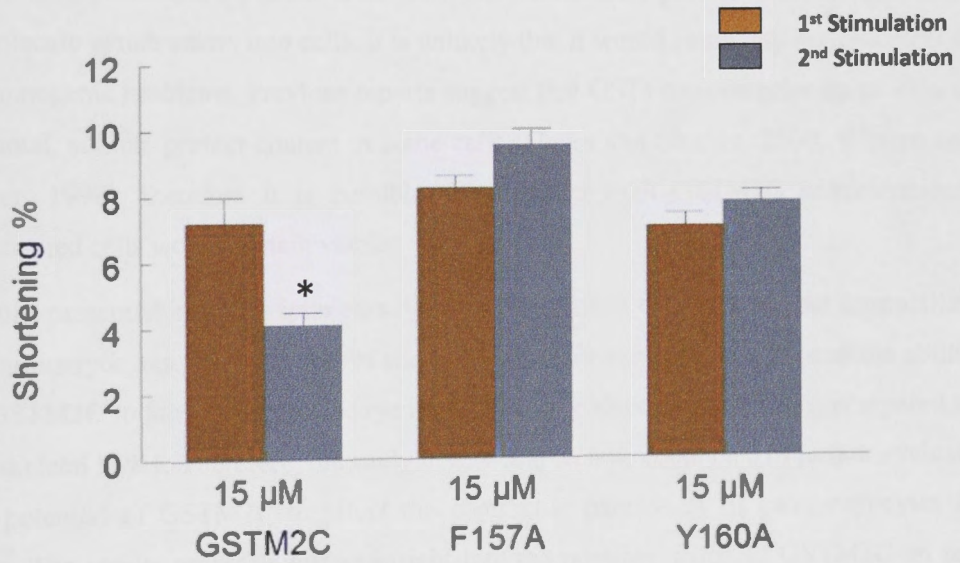

Fig 6.11: A comparison of the activity of GSTM2C constructs on contractility of electrically stimulated cardiomyocytes. A significant reduction in activity ($P<0.001$) was observed in the presence of the wild type protein only. Neither mutant altered the % shortening of neonatal cardiomyocytes significantly. The data presented here represent the mean±SEM from 22 (GSTM2C), 20 (F157A) and 27 (Y160A) experiments.

6.4 Discussion

As mentioned in the Introduction, GSTM2C enters cells in several cell lines as well as primary cells. In this chapter, the ability of GSTM2C to enter neonatal cardiomyocytes was investigated. The results shown in section 6.3.4 show that it enters cardiomyocytes without the assistance of any other endogenous carrier. The mode of entry was not investigated here, but as shown by Morris *et al* (Morris *et al.*, 2011) GSTM2C enters into many other cell lines and primary cells by endocytosis and it may be that the same mode of entry is employed in cardiomyocytes. Whatever the mode is, the entry alone increases the potential of GSTM2C for use as a therapeutic agent to reduce RyR2 activity in diastole.

Since GST proteins are present in humans, if a human GST protein could be utilised as a molecule which enters into cells, it is unlikely that it would cause any toxicological or immunogenic problems. Previous reports suggest that GSTs can comprise up to 10% of the total, soluble protein content in some cells (Hayes and Strange, 2000, Whalen and Boyer, 1998), therefore it is possible that even at high GSTM2C concentrations, transfected cells would remain viable.

Results presented in this chapter clearly show the effect of GSTM2C on the contractility of cardiomyocytes. Previous results shown in chapters 3 and 4 demonstrated the ability of GSTM2C to inhibit the cardiac ryanodine receptor activity specifically, compared to the skeletal RyR1. Therefore, the study in this chapter was conducted to further evaluate the potential of GSTM2C to affect the contractile parameters of cardiomyocytes *in vitro*. The results provided further insight into the possible action of GSTM2C on the cardiac contraction mechanism and suggested that the reduced release of Ca^{2+} from cardiac SR due to the inhibition of RyR2 affects the contractility of cardiomyocytes.

The studies conducted on spontaneously beating cardiomyocytes and field stimulated cardiomyocytes both revealed the ability of GSTM2C to inhibit the contractile parameters significantly. However, the mutants of the GSTM2C, F157A and Y160A failed to reduce the % shortening of cardiomyocytes. These results are in agreement with our previous results that the predicted destabilization of helix 6 of the GSTM2C affects the inhibition of RyR2. Consistent with our previous results in single channel lipid bilayer experiments, 15 μM GSTM2C reduced the contractility of cardiomyocytes

significantly. Lower concentration of the protein failed to inhibit the RyR2 and similarly did not cause a reduction in % shortening.

6.4.1 Possible effects of helix 6 of GSTM2C on cell translocation

Although experiments were not conducted to compare the effect of mutations on the ability of GSTM2C to enter neonatal cardiomyocytes, it can be speculated that it might be different from that of the wild type protein. Other results presented in this study provided evidence that the mutations in the helix 6 region of GSTM2C may destabilize the structure of the molecule. Interestingly, Morris *et al* also identified helix 6 as playing a structurally important role in the ability of GSTM2C to enter cells. They suggest that the destabilization would most likely expose the hydrophobic helix 6 region more compared to the wild type molecule. Therefore, it is possible that this exposure would enhance the ability of the mutants to enter cells. Results presented by Morris *et al*, (2011) confirmed this hypothesis when GSTM2C constructs were compared for their ability to affect the entry into L-929 cells. The figure adapted from their study (Fig 6.12), shows that two destabilizing mutations, F157A and Y160A, were taken up into L-929 cells by 45% and 85% more compared to the wild type GSTM2C (Morris *et al.*, 2011).

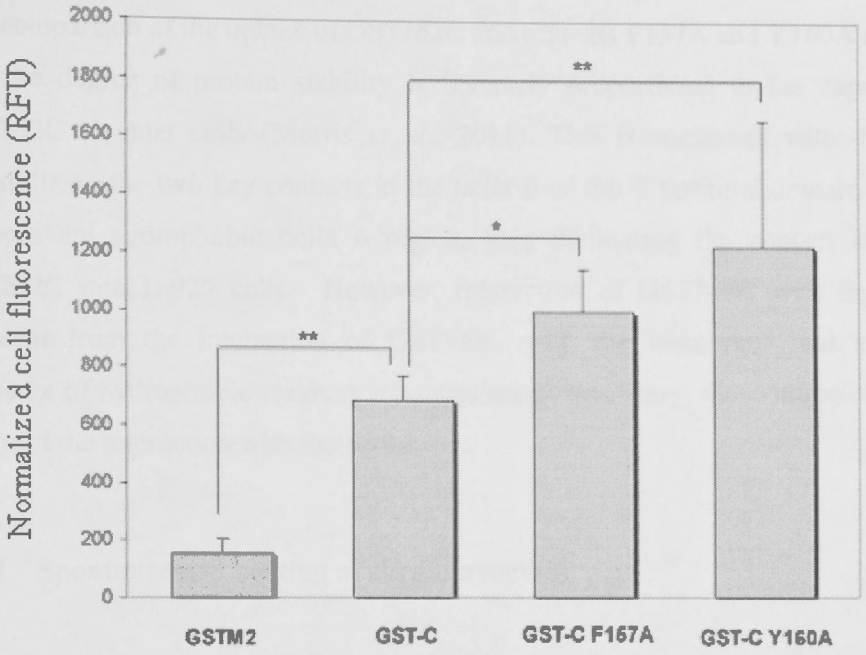

Fig 6.12: Effect of substitution mutations within the GSTM2 α-6 helix upon cellular translocation of the C-terminal domain (GST-C).L-929 cells were treated for 2 h with 200 nM Oregon Green-labelled GST-C variants and GST-C wildtype. The mean cellular fluorescence of each sample was normalised for the degree of fluorescent labeling of that protein. Data represents the average of four to six independent experiments 6 SEM. Significantly changed translocation efficiency (as determined by student's paired t-Test; one-tailed) is indicated by an asterisk (* = $P<0.05$; ** = $P<0.01$). Adapted from (Morris *et al.*, 2011)

The comparison of the uptake of GSTM2C and mutants F157A and Y160A also showed that the degree of protein stability is inversely proportional to the capacity of the GSTM2C to enter cells (Morris *et al.*, 2011). This is consistent with the idea that destabilizing the two key contacts in the helix 6 of the C terminal domain of GSTM2, exposes the hydrophobic helix 6 region, thus facilitating the contact and entry of GSTM2C into L-929 cells. However, interaction of GSTM2C with RyR2 is very different from the interaction of GSTM2C with the membrane and although the exposure of hydrophobic residues enhances membrane entry, these mutations appear to interrupt the interaction with the RyR2.

6.4.2 Spontaneously beating of cardiomyocytes

Spontaneous contractions or "beating" is commonly observed in cultured neonatal ventricular myocytes. Contraction in ventricular myocytes depends on synchronized intracellular Ca^{2+} oscillations that are initiated by an action potential in response to excitation of the cell membrane from an external source. This can be referred to as a "duty cycle". As discussed in Chapter 1, in normal myocardium *in vivo*, the source of the rhythmic excitation is the sinoatrial node. In experimentally isolated cardiac ventricular muscle or single cells, the external source is the electrical stimulation that produces inward current to trigger an action potential. Since the cardiac SR is "wired" to physiologically oscillate between Ca^{2+} release and uptake, the potential for spontaneous Ca^{2+} release is inherent in the organelle. When disconnected from the surface membrane, ventricular myocyte SR is no longer co-ordinated by rhythmic action potentials, but becomes a "free running" Ca^{2+} oscillator or "clock" which generates spontaneous, roughly periodic Ca^{2+} releases even in the context of physiological intracellular [Ca^{2+}] (Fabiato and Fabiato, 1978, Capogrossi *et al.*, 1987).

Maltsev *et al* in 2006 presented a model for the normal pacemaker function where they showed an interaction between a "membrane clock" (external loop) and intracellular "Ca^{2+} clock" (internal loop) which results in robust normal automaticity. $I_{Ca,L}$ activation was shown as the common step for both loops (Fig 6.13) (Maltsev *et al.*, 2006).

As explained before, electric automaticity in any type of cell requires the presence of particular conductance's, which progressively depolarize the cell membrane during the diastolic phase and bring the voltage to the threshold for the generation of the next action potential. The amplitude of the current responsible for this slow diastolic depolarization directly controls the duration of the period between consecutive action potentials and, therefore, the action potential frequency. In the membrane clock, two distinct classes of ionic channels are putatively responsible for this inward current: the hyperpolarization-activated cyclic nucleotide-gated channels (HCN) (Barbuti *et al.*, 2007), responsible for the so called "funny" current (I_f) observed in pacemaker cells, and low-threshold voltage-activated, T-type Ca^{2+} channels (Vassort *et al.*, 2006). Interestingly, both channels are normally poorly expressed in adult ventricular myocytes but strongly expressed or upregulated in these cells in pathological conditions such as cardiac infarction, heart failure, or hypertrophy (Hoppe *et al.*, 1998, Huang *et al.*, 2000, Beuckelmann *et al.*, 1991). Because of this "fetal" re-expression program in pathological conditions, embryonic or neonatal cardiomyocytes appear as a relevant model for this kind of study.

A study published by Er *et al* showed for the first time that HCN genes transcribe the major molecular component of native cardiac I_f. Their results clearly indicated that HCN channels are critical for the generation of spontaneous action potentials in neonatal cardiomyocytes (Er *et al.*, 2003). There has been a great deal of controversy about the functional contribution of I_f to cardiac pacing. Some authors speculate that I_f is essential for spontaneous diastolic depolarization, whereas others postulate that I_f only modulates the beating frequency of autonomic cardiac cells (DiFrancesco, 1993, Noma, 1996, Campbell *et al.*, 1992). Overexpression of HCN2 and HCN4 markedly accelerated the spontaneous beating rate of neonatal cardiomyocyte monolayers, demonstrating that HCN channels modify pacing frequency.

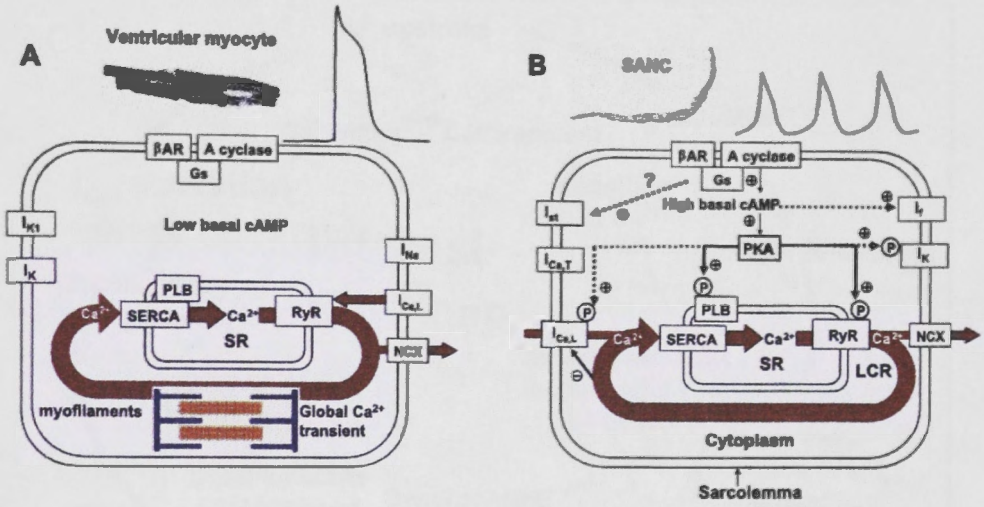

Fig 6.13a: Duty cycles for ventricular myocyte and sino atrial node. In A and B, thick red lines indicate spontaneous Ca^{2+} cycling and the spontaneous local Ca^{2+} releases from SR is linked to diastolic depolarization via Ca^{2+} activation of inward NCX current. RyR: Ryanodine receptor, SERCA: SR Ca^{2+} ATPase, PLB: phospholamban, SR: sarcoplasmic reticulum, NCX: Na^{+}/Ca^{2+} exchanger, $I_{Ca,L}$: L-type Ca^{2+} current, I_{Na}: Na current, I_K: K current, $I_{Ca,T}$: T-type Ca^{2+} current , β-AR: β-adrenergic receptors, A cyclise: Adenyl cyclase. (Maltsev *et al.*, 2006)

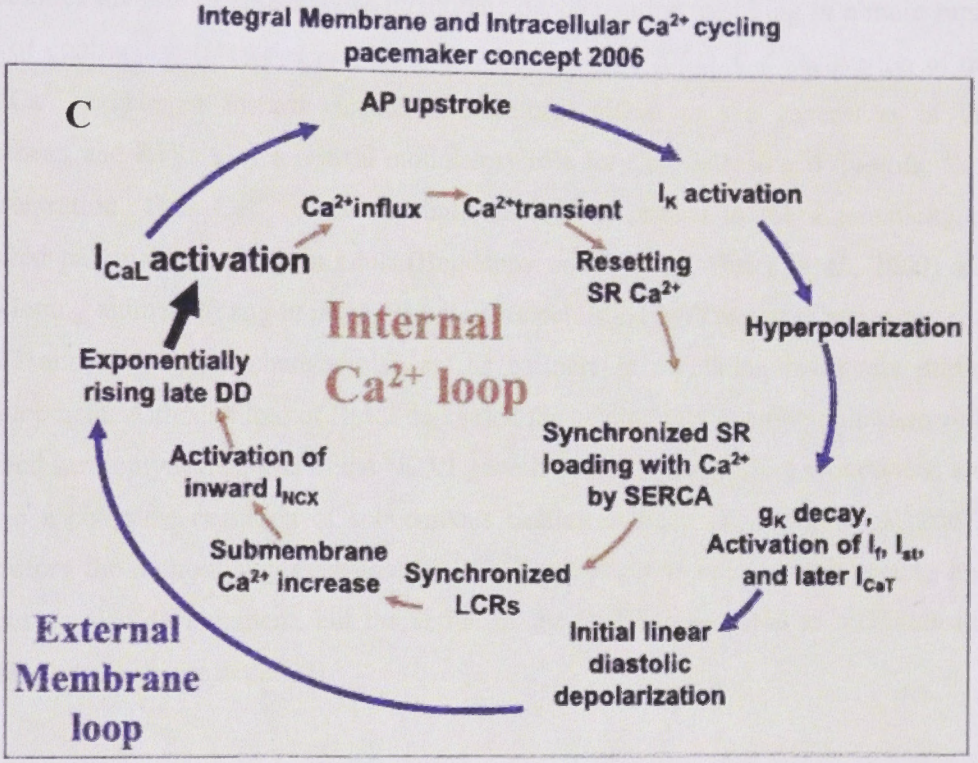

Fig 6.13b: A novel mechanism proposed for the normal pacemaker function. C indicates the interactions of membrane clock" (external loop) and intracellular "Ca^{2+} clock" (internal loop) which results in robust normal automaticity. $I_{Ca,L}$ activation is the common step for both loops. AP: Action potential, SERCA: SR Ca^{2+} ATPase, SR: sarcoplasmic reticulum, NCX: Na^{+}/Ca^{2+} exchanger, $I_{Ca,L}$: L-type Ca^{2+} current, I_{Na}: Na current, I_K: K current, $I_{Ca,T}$: T-type Ca^{2+} current , I_F: funny current, LCR: local Ca^{2+} releases, DD: diastolic depolarization (Maltsev *et al.*, 2006).

As mentioned in Fig 6.13b, in the Ca^{2+} loop, calcium released from the SR of pacemaker cells via RyR during diastolic depolarization and before an action potential also activates the Na^+/Ca^{2+} exchanger rhythmically to produce an inward current that accelerates the rate of spontaneous membrane depolarization, resulting in a more rapid rate of contraction (Huser *et al.*, 2000, Bogdanov *et al.*, 2001). Ca^{2+} activation of the Na^+/Ca^{2+} exchanger inward current is therefore critical to the generation of the heartbeat, and RyRs play a critical modulatory role for Ca^{2+} release and diastolic Ca^{2+} concentration. Thus Ca^{2+} release through the RyR is critical in the automaticity of isolated pacemaker cells from adult (Bogdanov *et al.*, 2001, Huser *et al.*, 2000) and developing animals (Yang *et al.*, 2002). Results published by Yang *et al* suggested that RyR2 and Na^+/Ca^{2+} exchanger also act as partners in regulating heart rate during development. Although loss of RyR2 decreased the beating rate in embryonic stem cell-derived cardiomyocytes, loss of the NCX1 gene is phenotypically more pronounced and led to a complete cessation of spontaneous beating in heart (Koushik *et al.*, 2001). Therefore the authors suggested that Na^+/Ca^{2+} exchanger is required for beating and proper cardiac development, but the action of the RyR2 is essential to modulate the beating rate (Yang *et al.*, 2002).

6.4.3 Field stimulation of cardiomyocytes

In order to study contraction parameters and EC coupling in isolated cardiomyocytes, various methods are employed to trigger cell shortening. Normal cell shortening is initiated by the Na^+ current (I_{Na}). The subsequent depolarization activates the L-type Ca^{2+} current ($I_{Ca,L}$), which triggers Ca^{2+} release from the SR. In addition, the combination of depolarization and Na^+ accumulation in the cell facilitates reverse mode Na^+/ Ca^{2+} exchange, which also might contribute to Ca^{2+} induced Ca^{2+} release. Experimentally, the action potential and cell shortening is triggered by either current clamp or field stimulation. During current clamp experiments a small current is injected into the cell through a microelectrode and a normal action potential is generated. In field stimulation, a brief electric field is used to induce an inward current which again triggers an action potential and cell shortening. Biphasic pulses are usually used to

minimize electrolysis. As mentioned in Bokenes *et al*, cell shortening was reduced only by 60% in field stimulated cells in the presence of Cd^{2+} which blocks the L-type Ca^{2+} channels. When the Na^{+}/Ca^{2+} exchanger was blocked selectively by the isothiouria derivative KB, there was no effect on cell shortening but Cd^{+} and KB together abolished the cell shortening. Their study strongly suggested that cell shortening in field stimulated cells is primarily triggered by L type Ca^{2+} current which is directly triggered by the electric field, but reverse mode Na^{+}/Ca^{2+} exchanger can add to activation of Ca^{2+} release provided that the $I_{Ca,L}$ is reduced (Bokenes *et al.*, 2005).

6.4.4 Inhibition of RyR2 by GSTM2C affects contractile parameters of neonatal Cardiomyocytes

As discussed in the General Introduction and in 6.4.2, there is a strong relationship between intracellular Ca^{2+} concentration and the contractility of cardiomyocytes. Results presented in previous chapters provided evidence that GSTM2C inhibits cardiac RyR2 activity, therefore has the potential to reduce the intracellular Ca^{2+} concentration during both systole and diastole. An effect of GSTM2C on spontaneous contractility would most likely depend on an effect on Ca^{2+} release (leak) during diastole as cardiomyocytes alter their Ca^{2+} regulatory function in a manner that compensates for changes in RyR activity and ensures Ca^{2+} release from the SR during systole remains constant (Trafford *et al.*, 2000). Thus any effect of GSTM2C on spontaneous contractility is most likely to be an effect on the diastolic Ca^{2+} concentration. On the other hand, effects on the infrequent field evoked contractions may be due to changes in Ca^{2+} released during the contraction phase as time was not allowed for adaptation and the action potential was not dependent on diastolic depolarization.

It is established that Ca^{2+} release from RyR2 affects the electrogenic Na^{+}/Ca^{2+} exchanger (NCX) and the electrogenic Na^{+}/Ca^{2+} exchanger activity can produce an exponential increase in diastolic depolarization (6.4.2). Results presented in (Eisner and Cerbai, 2009) and (Koushik *et al.*, 2001) both stressed the importance of NCX activity

for the maintenance of the heart beat as removal of Na^+ from the culture medium and loss of the NCX1 gene completely abolished spontaneous beating of cardiomyocytes.

In this study, the effect of GSTM2C on NCX activity was not investigated, therefore, it is assumed that the only effect of GSTM2C is on the RyR2. Maltsev *et al* also suggest that both Ca^{2+} clock and membrane clock are essential for the maintenance of the contractility of beating cardiomyocytes. During spontaneous beating, local Ca^{2+} releases (LCR's) occur beneath the cell membrane during late diastolic delolarization in the form of sub membrane Ca^{2+} sparks or small Ca^{2+} wavelets. These LCR's ignite significant NCX inward current which cause an exponential increase to the later part of diastolic depolarization leading to the activation of L-type Ca^{2+} channels to initiate an action potential. (Maltsev *et al.*, 2006). Inhibition of RyR2 by GSTM2C would reduce Ca^{2+} leak during diastole and thus reduce diastolic cytoplasmic Ca^{2+} concentration. This would reduce NCX activity and diastolic depolarization. Therefore, this could explain the observation that spontaneous beating frequency and % of beating cells was reduced in the presence of GSTM2C and inhibition of RyR2.

Spontaneously beating in cardiomyocytes can be likened to free running Ca^{2+} clocks. Therefore, unless externally stimulated, they are not co-ordinated by rhythmic action potentials. There is always an individual variation among the spontaneously beating cardiomyocytes when contractility parameters are measured (Maltsev *et al.*, 2006). Therefore, external stimulation is essential in order to provide a uniform, rhythmic action potential to minimize individual variability. External stimulation, in this case field stimulation, provides a more accurate protocol for testing the effect of GSTM2C constructs on the contractility of neonatal cardiomyocytes. Since the contractility was measured as a result of the stimulation, it can be assumed that the results obtained for field stimulated cardiomyocytes reflect the scenario during systole.

As mentioned in chapter 1, the concentration of intracellular Ca^{2+}, hence the Ca^{2+} released from RyR2, is directly related to the extent of contraction generated by the

contractile apparatus. Therefore, the inhibition of RyR2 by GSTM2C would release less Ca^{2+}, which is evident by the Ca^{2+} release data presented in chapter 3 and 4. Therefore, the reduced % shortening observed in the presence of GSTM2C is consistent with the reduced Ca^{2+} release from the SR. However, action potential in the presence of

GSTM2C was not directly measured in this study. Therefore, any activity of GSTM2C on the action potential can not be totally disregarded. The inability of the mutants,

F157A and Y160A to reduce the % shortening of cardiomyocytes significantly, can be explained by their inability to inhibit the cardiac RyR2. This provides further evidence that mutations in GSTM2C prevented the molecule from binding to and inhibiting the cardiac RyR2. Therefore, our hypothesis that helix 6 is essential for the inhibitory action of GSTM2C is further justified. Our future studies to determine the Ca^{2+} transients and Ca^{2+} sparks in the presence of GSTM2C constructs would provide further insight into the actual mechanism of action.

6.5 Conclusion

Results presented in this chapter further confirmed the ability of GSTM2C to inhibit the cardiac ryanodine receptor, hence reducing the contractility of neonatal ventricular cardiomyoctes. Our hypothesis that helix 6 is important for the capacity of GSTM2C to inhibit RyR2 is also supported as the mutants F157A and Y160A which destabilized the interactions between helix 6 and flanking helices in the C terminal domain of GSTM2 produced a construct that failed to reduce the contractility of cardiomyocytes. The ability of GSTM2C to enter neonatal cardiomyocytes without a carrier protein was also confirmed. This opens up the development of GSTM2C as a self delivering agent to reduce cardiac ryanodine receptor activity when it is overly active during diastole.

Chapter 7 : General Discussion

Glutathione transferases are generally recognized for their role in phase II detoxification reactions, but recent publications indicate a diverse range of other functions which are unrelated to detoxification. One such action was discussed in detail here; specific inhibition of the cardiac isoform of ryanodine recepter intracellular calcium release channel by GSTM2 which was initially reported by Abdellatif *et al* (Abdellatif *et al.*, 2007).

The results presented in chapter 3 discussed the importance of helix 6 which is located in the centre of the predicted structure of the GSTM2C terminal domain. However, helix 6 alone was unstructured and was unable to inhibit cardiac RyR2 channel activity and Ca^{2+} release from cardiac SR. Substitution mutations (F157A, Y160A) in helix 6 of GSTM2C were predicted to destabilize the interaction between helix 6 and other helices, and the mutant GSTM2C was unable to inhibit RyR2 channel activity and Ca^{2+} release from cardiac SR. This loss of function indicates the importance of helix 6 and its flanking helices for the stability of the region and hence the inhibitory action. This was further confirmed in the neonatal ventricular cardiomyocyte cultures where the contractility in spontaneously beating and field stimulated cardiomyocytes was significantly reduced in the presence of GSTM2C but not in the presence of F157A and Y160A, confirming that the reduced Ca^{2+} release from cardiac SR required the normal structural stability of the region. An attempt was also made to identify the region of RyR2 responsible for GSTM2 binding and results showed that H5678, the most active fragment of GSTM2C is capable of binding to the DR3 region of RyR2. The binding site was further localized to a 22 amino acid fragment. Therefore, the study presented here provides the first basic structural information about the RyR isoform specific inhibitory action of the endogenous protein, GSTM2.

7.1 Rynodine receptor: Potential therapeutic drug target

It is important to emphasize the fact that RyR2 is essential for Ca^{2+} release from cardiac SR and cardiac contraction is very sensitive to changes in RyR2 activity. As mentioned

before, this is in contrast to other tissues, where there appear to be redundancies in the sources of Ca^{2+}, as more than one isoform of RyR is often expressed and IP3 sensitive Ca^{2+} stores are present in the same cells (Liu *et al.*, 2009, Van Den Bosch *et al.*, 1999, Vallot *et al.*, 2000). The importance of the RyR in striated muscle has also been proven by the fact that their knockout is lethal, with death at birth. In addition, point mutations in the ion channel protein can cause severe disability and potentially death, in disorders such as malignant hyperthermia (MH) and central core disease (CCD) in skeletal muscle and stress-induced catecholaminergic polymorphic ventricular tachycardia (CPVT) and arrhythmogenic right ventricular cardiomyopathy type 2 (ARVC 2) in the heart (Dulhunty *et al.*, 2007). More than 70 mutations in the RyR2 that lead to CPVT were identified by 2007 (Mohamed *et al.*, 2007). It is interesting to note that these mutations are generally located in regions of RyR2 which are equivalent to regions in RyR1 that harbour MH and CCD mutations (Fig 7.1).

Abnormal intracellular Ca^{2+} handling by the SR is a critical factor in the development of heart failure. Not only decreased Ca^{2+} uptake, but also uncoordinated Ca^{2+} release, plays a significant role in contraction and relaxation dysfunction. As discussed in chapter 5, spontaneous Ca^{2+} release through RyR2 during diastole leads to a decrease in SR Ca^{2+} content, and also triggers delayed after depolarisations which cause lethal arrhythmias. Therefore, the essential nature of the RyR macromolecular complex and its role in Ca^{2+} handling, make it a logical target for therapeutic agents which might be used to alleviate the effects of cardiac disorders.

As mentioned in chapter 6, a higher binding affinity of the DR3 mutant associated with ARVC to H5678 indicated the possibility of using GSTM2 derived compound for the treatment of ARVC. Although the current data are not sufficient to conclude that the DR3 mutant binds with higher affinity to GSTM2C, this possibility is worth further investigation.

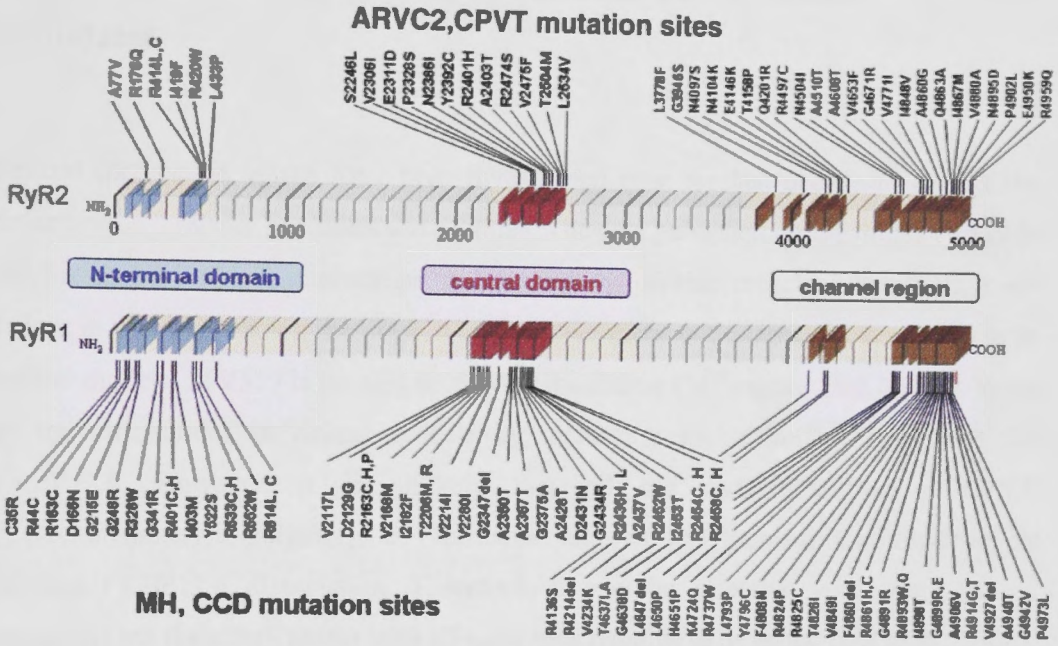

Fig 7.1: Schematic diagram of the reported mutation sites on RyR1 and RyR2. The 3 hotspot regions and the RyR mutations found in these regions are indicated. The 3 regions encompass the amino acid residues as indicated: N-terminal domain (amino-acids 0–600), central domain (amino-acids 2,100–2,500), channel region (amino-acids 4,100–5,000). ARVC2, (arrhythmogenic right ventricular cardiomyopathy type 2), CPVT, (catecholaminergic polymorphic ventricular tachycardia), MH (malignant hyperthermia) and CCD (central core disease) mutation sites are shown. Figure adapted from (Yano *et al.*, 2005).

7.2 Therapeutic potential of GSTM2-2C compared to other candidates

Several therapeutic agents have been investigated over the last decade to correct the defective Ca^{2+} release in cardiac arrhythmias. The data published on the drug JTV519 in stabilizing FKBP/RyR interactions and improving cardiac muscle function in heart failure in mice has shown that RyR is an effective therapeutic target for heart failure in animal models. JTV519 is thought to prevent the excess Ca^{2+} release that leads to some of the arrhythmias in animal models by increasing the affinity of the RyR for FKBP12.6. However, it is unlikely that all the mutations causing CPVT (Catecholaminergic polymorphic ventricular tachycardia) increase Ca^{2+} release by causing FKBP12.6 dissociation. Therefore, it may be effective with some of the mutations but the effectiveness with all mutations remains to be tested (Liu *et al.*, 2006).

While many compounds are known to inhibit RyR2 activity, relatively few of them have been studied at the single channel level. Anti-arrhthmic drug, flecainide and the local anaesthetic, tetracaine are two molecules recently studied in detail. Flecainide is a non-specific blocker of the RyR2 as it is also effective in blocking Na^{+} channels. It inhibits RyR2 channels by reducing RyR2 channel open duration. On the other hand tetracaine, which is also a non-specific RyR2 ihibitor, blocks RyR2 channels by reducing the rate of RyR2 channel openings, but has no effect on RyR2 channel open times (Hilliard *et al.*, 2010, Watanabe *et al.*, 2009). However, tetracaine causes a rebound increase in sarcoplasmic reticulum Ca^{2+} release events during prolonged exposure (Gyorke *et al.*, 1997), effective inhibitory concentrations are too high for clinical use (Shoshan-Barmatz and Zchut, 1993) and systemic administration is contradicted in humans. GSTM2 which also reduces the open probability of cardiac RyR, rather than blocking the channel and reducing its conductance, acts in a similar manner to flecainide as it reduces Po by abbreviating channel open times (Abdellatif *et al.*, 2007). It is likely that drugs based on the structure of the RyR binding domain in

GSTM2 would be more specific and safer than drugs such as JTV519, flecainide or tetracaine. An active peptide or a peptide mimetic derived from GSTM2C may be effective in the presence of endogenous GSTM2, since it could displace the endogenous protein and exaggerate its inhibitory action. It is also significant that an active peptide based on the endogenous GSTM2 would be less immunogenic.

7.3 Physiological significance of GSTM2C activity

There are in fact several mechanisms which ensure that skeletal RyRs are minimally active when muscle is not contracting. These include channel inhibition by Mg^{2+}, which is ubiquitously present in the cytoplasm of muscle cells. RyR1 is strongly inhibited under resting conditions by the millimolar concentrations of Mg^{2+} (Lamb and Stephenson, 1991, Lamb and Stephenson, 1994, Laver *et al.*, 1997a). Although the inhibition site has similar affinity for Ca^{2+} and Mg^{2+} ions, it is occupied mainly by Mg^{2+} which is present in the cytoplasm in substantially higher concentrations than Ca^{2+}. Therefore, part of the EC coupling process in skeletal muscle is the relief of Mg^{2+} inhibition to allow the channel to open (Lamb and Stephenson, 1994).

Although there are only a few endogenous inhibitors of RyR2, low RyR2 activity during diastole is vitally important for normal cardiac myocyte function. The cardiac RyR has a lower affinity for Mg^{2+} inhibition (Laver *et al.*, 1997b), thus it requires other endogenous inhibitors to prevent excess Ca^{2+} release from the SR during diastole. Mg^{2+} is not recruited to carry out the job as 10-fold higher concentrations of Mg^{2+} ions would be required and that would be a substantially higher concentration than that found in the cytoplasm. Maintenance of low channel activity during diastole is essential in cardiac muscle to allow the SR to accumulate sufficient Ca^{2+} for the next heart beat and to reduce the cytosolic Ca^{2+} concentration during diastole to prevent delayed after depolarizations. GSTM2 is a potential candidate to fulfil this role in the heart. It is also worth noting that the difference between RyR1 and RyR2 in the inhibition by Mg^{2+} is thought by some authors to be dependent on the sequence differences in DR3 region

(Hayek *et al.*, 1999). As mentioned in chapter 06, the DR3 region is highly acidic in RyR1 compared to RyR2 and thus is a potential Ca^{2+}/Mg^{2+} binding site. Previous reports also suggest that binding of Mg^{2+} to domain 9 may also affect binding of FKBP, which binds adjacent to domain 9 (Wagenknecht *et al.*, 1997). It is very interesting and significant that the binding site identified in RyR2 for GSTM2C is also within this DR3 region.

7.4 Overall effect of GSTM2C on the striated muscle

As mentioned in Chapter 3, GSTM2 has very different mechanisms of actions on skeletal and cardiac RyRs. Despite these differences, the overall context is similar as they regulate RyR activity in a manner that would conserve the Ca^{2+} stores in SR. In comparison to other GST isoforms, physiological action of GSTM2 in the heart is also similar as it reduces RyR2 channel activity in lipid bilayers and depresses Ca^{2+} release from cardiac SR vesicles in a manner that would enhance Ca^{2+} accumulation in the SR and the lowering of cytoplasmic Ca^{2+} during diastole.

Although GSTM2 enhances the RyR1 activity physiologically when the channel activity is low, it is unlikely that it would deplete the SR store. As mentioned in Chapter 1, GSTM2 inactivates the channel when the activity is too high when it could lead to depletion of SR store, through an activation dependent inactivation process. Therefore, ultimately GSTM2 would conserve the SR store in RyR1. Results presented in chapter 3 showed extensively that the C-terminal domain of GSTM2 molecule which interacts with RyR2 is distinctly different in sequence and structure from the N-terminal domain of GSTM2 which interacts with RyR1. The implication of this fact is that the structure of GSTM2 required to interact with skeletal and cardiac isoforms of RyR are very different. This is very important as the drugs designed to inhibit Ca^{2+} release in cardiac muscle, based on the structure of the RyR2-active site of the GSTM2C molecule would not influence RyR1 channel activity. This was further confirmed in chapter 6, as the

binding site for GSTM2C on RyR2 was identified as DR3 region which is distinctly different in sequence from that of RyR1.

7.5 Specific action of GSTM2C on the cardiac muscle

The results presented in this study suggested that compounds based on the structure of the interacting segment of GSTM2 would be more effective in modifying contraction in the heart than in modifying function in any other tissues. Firstly, the compounds would not be active in skeletal muscle, therefore would not influence skeletal muscle contractility. Secondly, since RyR2 is essential for Ca^{2+} release from SR, cardiac contraction is exquisitely sensitive to changes in the RyR2 activity. This is in contrast to other tissues where more than one isoform of RyR is expressed and there are other sources of Ca^{2+} with IP3 sensitive Ca^{2+} stores often present in the same cell (Van Den Bosch *et al.*, 1999, Vallot *et al.*, 2000). Thirdly, the GSTM2C terminal domain does not have enzymatic activity as the active site is located in the N-terminal domain which is not responsible for the inhibitory effect of GSTM2. Thus the selective inhibition of RyR2 by the C-terminal half of the GSTM2 has significant clinical potential in the treatment of chronic heart failure where RyR2 channels can become abnormally active, inducing arrhythmias and reducing Ca^{2+} store filling during diastole and contractility.

7.6 A comparison with CLIC-2, another member of GST structural family

Results presented in Chapter 6 provided evidence that GSTM2 may bind to two different sites on the cardiac and skeletal ryanodine receptor. In contrast to GST proteins, CLIC-2 may bind to a similar domain on RyR1 and RyR2 channels. Although CLIC-2 belongs to the same structural family as GSTs, its action on both RyR1 and RyR2 is a simple inhibition. The complex activation dependent inhibition of RyR1

observed in GSTM2 is not seen with CLIC-2. CLIC-2 also showed some additional actions of substantial biophysical interest, as it increases the fraction and duration of RyR2 opening to substate levels, defined conductance levels that are less than the maximum conductance (Dulhunty *et al*, 2011). It also enhanced coupled gating, which enable several RyR2 channels to open synchronously (Dulhunty *et al*., 2005c). This is not observed with any other member of the GST structural family. The mechanism by which CLIC-2 interact with the RyR is still not clear. Whatever it may turn out to be, the results indicate that CLIC-2 binds to a site on RyR2 that profoundly influence the gating machinery of the ion channel (Dulhunty *et al*, 2011). Jalilian *et al* discussed the fact that both RyR2 and CLIC-2 also contains redox sensors (Jalilian *et al*., 2008). Approximately one quarter of the 80-100 cysteines in each RyR subunit contain free –SH groups, many of which are available to sense redox potential ((Dulhunty *et al*., 2000). The addition of CLIC-2 to the cytoplasmic solution inhibited RyR2 when the cytoplasmic redox potential was oxidizing, but had no effect on RyR2 when the cytoplamic redox environment was more reducing. Any effect of a regulated redox potential on the ability of GSTM2 to inhibit RyR2 is yet to be explored.

7.7 H5678: The minimal region of GSTM2 capable of inhibiting RyR2

Results presented here show clearly that the ability of GSTM2 to specifically inhibit cardiac RyR2 channels depends on the structural integrity of the C-terminal domain of the protein with helix 6 playing a critical role in the inhibition of ryanodine receptors. Mutations in the helix 6 region, F157A and Y160A which presumably destabilized the interaction between helix 6 and flanking helices, disrupted the ability of GSTM2C to inhibit RyR2. Cross linking studies and tryptophan fluorescence binding experiments also confirmed the ability of H5678 to bind to the RyR2 or its fragments physically. Yeast two-hybrid experiments performed between H5678 with mutations in the helix 6

region and the DR3 region fragment of RyR2 failed to produce yeast colonies on selective media. These results further emphasized the future possibility of using H5678, which showed the highest inhibitory effect against RyR2, as a template for drugs to depress RyR2 function when the Ca^{2+} channel is hyperactive in arrhythmias in heart failure and CPVT. Therefore, these observations provide the first basic structural information on the specific interaction between GSTM2 and RyR2.

7.8 Therapeutic advantage of a voltage-dependent action of GSTM2C

As discussed in detail in Chapter 4, the voltage dependent action of the GSTM2C, coupled with the systolic autocorrection (Trafford *et al.*, 1998) suggests that GSTM2C would be primarily active on the RyR2 channels which are leaky during diastole. Results observed in single channel lipid bilayer experiments were further confirmed in contractility measurements where GSTM2C was capable of reducing the percent contractility of spontaneously beating cardiomyocytes (61.49%, represent a diastolic scenario) to a greater degree than field stimulated cells (42.8%, represent systolic scenario). It is interesting to speculate on the mechanism of the voltage-dependent effect of GSTM2C on RyR2. The conformation of the binding site in the DR3 region of RyR2, may be influenced by the membrane field through long range allosteric influences which arise in the transmembrane regions of RyR2. According to Zhang *et al*, the DR3 region of RyR2 is located in domain 9 which belongs to the clamp region (Zhang *et al.*, 2003). However, cryo- electron microscopy reconstructions indicate that the DR3 region is well outside the influence of the membrane field (Carnie and McLaughlin, 1983). Samso *et al* speculated that an electrical field dependent conformational change in the transmembrane domain of the ryanodine receptor protein, near the membrane surface or within the transmembrane parts, could be transmitted along connecting pillars to distant cytoplasmic domains (Samso *et al.*, 2006). Therefore, it can be assumed that the effect of GSTM2C binding to the DR3 region of RyR2 in

inhibiting the channel might cause a similar but reversed scenario, since the binding of GSTM2C must be transmitted to residues within the transmembrane region which regulate channel gating. This kind of a transmission might occur via long range allosteric interactions through structures such as pillars which connect the DR3 rgion of RyR2 to the transmembrane assembly. Our cryo electron microscopy experiments which are in progress will shed more light on the orientation of GSTM2C on the DR3 region of RyR2 and subsequent changes which could occur in the transmembrane region of the protein.

7.9 Possible mechanism of action of GSTM2 on RyR2

Overall the results presented here identify H5678 as the minimal structural fragment of GSTM2 capable of inhibition of RyR2. Therefore, H5678 may bind to the D3 short region (22 amino acid fragment of DR3 region identified in intrinsic tryptophan fluorescence spectroscopy experiments) of RyR2 via the helix 6 and helices 5, 7 and 8 may be arranged in a manner which facilitates binding. Binding to domain 9 of RyR2 (located in the clamp region) may initiate long range allosteric interactions via pillars connecting the cytoplasmic and transmembrane regions and limit opening of the channel pore. As domain 9 and 10 are separated when the channel opens, binding of H5678 to domain 9 may also limit this separation which may cause a negative feedback effect on channel opening. This scenario would take place when the outside of SR membrane tend to be positively charged if there is excess Ca^{2+} release during diastole.

It is also interesting to note that GSTM2C binding site on RyR2 is located, on the 3D structure, in close proximity to the FKBP12/12.6 binding site. It is well established that FKBP12/12.6 proteins profoundly alter RyR1/RyR2 activity and channel gating and since their binding site is remote from the channel pore, their binding must also be communicated to the channel through long range effects. Therefore, the possibility cannot be dismissed that GSTM2C alters the gating properties of RyR2 by interacting with or altering the binding between FKBP12/12.6 proteins and RyR2 and this

alteration is transmitted to the pore region to alter RyR2 channel gating. This possibility deserves further exploration.

7.10 Conclusion

A very specific action of the GSTM2 C terminal domain on the cardiac RyR2 is discussed here. The activity depends on its binding to the DR3 region containing residues that are found only in the RyR2 isoform of the protein. Helix 6 of the GSTM2 C terminal domain played a major role, with its flanking helices stabilizing the structure of the molecule, to bind to the DR3 region of RyR2. The ability of GSTM2C to reduce the contractility of neonatal cardiomyocytes provided further evidence that it affects the contraction mechanism of the cardiac cells, due to the reduced release of Ca^{2+} from cardiac SR. Also, the C-terminal half of the GSTM2 that interacts with RyR2 has no enzyme activity; thus its introduction to the cell would not have unwanted side effects which might be associated with altering the normal balance of GSTs within the cytosol. It is also physiologically significant that it is one of the endogenous modulators of RyR2 which is capable of maintaining low levels of Ca^{2+} leak through RyR2 during diastole, to prevent delayed after depolarizations that cause arrhythmias and sudden cardiac death. Also, the delivery of GSTM2C would not require a cell penetrating peptide as it is capable of entering into cardiomyocytes itself. Therefore, GSTM2C has a higher therapeutic potential as a self delivering agent to specifically reduce RyR2 activity during diastole. As explained in 7.2 and 7.3, findings of this thesis will have a significant impact on the advancement of GST mediated drug therapy and a drug based on the GSTM2C structure may displace endogenous GSTs and inhibit cardiac RyR2 during abnormal Ca2+ release. As far as I am aware, GSTM2C is the only isoform specific, endogenous inhibitor of cardiac RyR2 activity that has been reported so far. Therefore, it is believed that these findings contributed immensely for the advancement of the research field.

7.11 Future directions

- The results presented here indicate the importance of helix 6 in the C terminal domain of GSTM2 for the inhibition of RyR2. However, the helix 6 sequence alone was found to be unstructured and was unable to inhibit RyR2 on its own. Therefore, it is worth investigating whether the helix 6 sequence in an α helical conformation is capable of inhibiting RyR2 without the involvement of flanking helices.

- It would also be useful to know the structure of the H5678 construct which showed the highest activity in single channel lipid bilayer experiments and Ca^{2+} release assays. Also, the structure of GSTM2 C terminal domain is unknown and it was predicted from the crystal structure of GSTM2 full length protein. X-ray crystallography will be employed to determine the structure of the C terminal domain and H5678 construct. The knowledge of any changes in structure of these important fragments of GSTM2 will provide insight into the mechanism of action.

- In this study, contractility of cardiomyocytes was determined in the presence of the C terminal domain of GSTM2. A repetition of experiments with H5678 construct will also provide a better understanding of the action of the minimal active fragment of GSTM2.

- Determination of Ca^{2+} transients and measurement of Ca^{2+} sparks are under investigation. These experiments will provide further insight into the handling of Ca^{2+} by neonatal cardiomyocytes in the presence of GSTM2C terminal domain and its mutants.

- It will also be worth measuring the cardiac output of isolated perfused hearts in the presence of GSTM2C terminal domain, its mutants (F157A, Y160A) and H5678.

- As mentioned in chapter 6, the H5678 construct binding site on RyR2 has already been localized to be the DR3 region. Experiments are in progress to determine the 3D location using cryo electron microscopy and 3D reconstruction. This will provide further evidence for the obtained yeast two-hybrid results indicating binding to the DR3 region.

References

ABDELLATIF, Y., LIU, D., GALLANT, E. M., GAGE, P. W., BOARD, P. G. & DULHUNTY, A. F. 2007. The Mu class glutathione transferase is abundant in striated muscle and is an isoform-specific regulator of ryanodine receptor calcium channels. *Cell Calcium,* 41, 429-40.

ACETO, A., DRAGANI, B., MELINO, S., ALLOCATI, N., MASULLI, M., DI ILIO, C. & PETRUZZELLI, R. 1997. Identification of an N-capping box that affects the alpha 6-helix propensity in glutathione S-transferase superfamily proteins: a role for an invariant aspartic residue. *Biochem J,* 322 (Pt 1), 229-34.

ADLER, V., YIN, Z., FUCHS, S. Y., BENEZRA, M., ROSARIO, L., TEW, K. D., PINCUS, M. R., SARDANA, M., HENDERSON, C. J., WOLF, C. R., DAVIS, R. J. & RONAI, Z. 1999. Regulation of JNK signaling by GSTp. *EMBO J,* 18, 1321-34.

AHERN, G. P., JUNANKAR, P. R. & DULHUNTY, A. F. 1994. Single channel activity of the ryanodine receptor calcium release channel is modulated by FK-506. *FEBS Lett,* 352, 369-74.

AHERN, G. P., JUNANKAR, P. R. & DULHUNTY, A. F. 1997. Subconductance states in single-channel activity of skeletal muscle ryanodine receptors after removal of FKBP12. *Biophys J,* 72, 146-62.

AMADOR, F. J., LIU, S., ISHIYAMA, N., PLEVIN, M. J., WILSON, A., MACLENNAN, D. H. & IKURA, M. 2009. Crystal structure of type I ryanodine receptor amino-terminal beta-trefoil domain reveals a disease-associated mutation "hot spot" loop. *Proc Natl Acad Sci U S A,* 106, 11040-4.

ANDERSON, A. A., ALTAFAJ, X., ZHENG, Z., WANG, Z. M., DELBONO, O., RONJAT, M., TREVES, S. & ZORZATO, F. 2006. The junctional SR protein JP-45 affects the functional expression of the voltage-dependent Ca2+ channel Cav1.1. *J Cell Sci,* 119, 2145-55.

ANGO, F., PREZEAU, L., MULLER, T., TU, J. C., XIAO, B., WORLEY, P. F., PIN, J. P., BOCKAERT, J. & FAGNI, L. 2001. Agonist-independent activation of metabotropic glutamate receptors by the intracellular protein Homer. *Nature,* 411, 962-5.

ANTIC, S., MAJOR, G., ZECEVIC, D.1999. Fast optical recordings of membrane potential changes from dendrites of pyramidal neurons. *J Neurophysiol*, 82(3):1615-21.

ARACENA, P., TANG, W., HAMILTON, S. L. & HIDALGO, C. 2005. Effects of S-glutathionylation and S-nitrosylation on calmodulin binding to triads and FKBP12 binding to type 1 calcium release channels. *Antioxid Redox Signal,* 7, 870-81.

ARMSTRONG, R. N. 1997. Structure, catalytic mechanism, and evolution of the glutathione transferases. *Chem Res Toxicol,* 10, 2-18.

ARMSTRONG, R. N. 2000. Mechanistic diversity in a metalloenzyme superfamily. *Biochemistry,* 39, 13625-32.

ASHLEY, R. H. & WILLIAMS, A. J. 1990. Divalent cation activation and inhibition of single calcium release channels from sheep cardiac sarcoplasmic reticulum. *J Gen Physiol,* 95, 981-1005.

ATKINS, W. M., WANG, R. W., BIRD, A. W., NEWTON, D. J. & LU, A. Y. 1993. The catalytic mechanism of glutathione S-transferase (GST). Spectroscopic determination of the pKa of Tyr-9 in rat alpha 1-1 GST. *J Biol Chem,* 268, 19188-91.

BAHI, N., ZHANG, J., LLOVERA, M., BALLESTER, M., COMELLA, J. X. & SANCHIS, D. 2006. Switch from caspase-dependent to caspase-independent death during heart development: essential role of endonuclease G in ischemia-induced DNA processing of differentiated cardiomyocytes. *J Biol Chem,* 281, 22943-52.

BAILEY, K. 1942. Myosin and adenosinetriphosphatase. *Biochem J,* 36, 121-39.

BAKER, R. T., CATANZARITI, A. M., KARUNASEKARA, Y., SOBOLEVA, T. A., SHARWOOD, R., WHITNEY, S. & BOARD, P. G. 2005. Using deubiquitylating enzymes as research tools. *Methods Enzymol,* 398, 540-54.

BARBUTI, A., BARUSCOTTI, M. & DIFRANCESCO, D. 2007. The pacemaker current: from basics to the clinics. *J Cardiovasc Electrophysiol,* 18, 342-7.

BARG, S., COPELLO, J. A. & FLEISCHER, S. 1997. Different interactions of cardiac and skeletal muscle ryanodine receptors with FK-506 binding protein isoforms. *Am J Physiol,* 272, C1726-33.

BAYLOR, SM., CHANDLER, WK., MARSHALL, MW.1984. Calcium release and sarcoplasmic reticulum membrane potential in frog skeletal muscle fibers. *J. Physiol*, 348, 209-238.

BEARD, N. A., CASAROTTO, M. G., WEI, L., VARSANYI, M., LAVER, D. R. & DULHUNTY, A. F. 2005. Regulation of ryanodine receptors by calsequestrin: effect of high luminal Ca2+ and phosphorylation. *Biophys J,* 88, 3444-54.

BEARD, N. A., LAVER, D. R. & DULHUNTY, A. F. 2004. Calsequestrin and the calcium release channel of skeletal and cardiac muscle. *Prog Biophys Mol Biol,* 85, 33-69.

BEARD, N. A., SAKOWSKA, M. M., DULHUNTY, A. F. & LAVER, D. R. 2002. Calsequestrin is an inhibitor of skeletal muscle ryanodine receptor calcium release channels. *Biophys J,* 82, 310-20.

BEARD, N. A., WEI, L. & DULHUNTY, A. F. 2009. Ca(2+) signaling in striated muscle: the elusive roles of triadin, junctin, and calsequestrin. *Eur Biophys J,* 39, 27-36.

BELCH, J. J., BRIDGES, A. B., SCOTT, N. & CHOPRA, M. 1991. Oxygen free radicals and congestive heart failure. *Br Heart J,* 65, 245-8.

BENSLER, J. M., FRANK, C. M., RAZAVI, M., RASEKH, A., SAEED, M., HAAS, P. C., NAZERI, A. & MASSUMI, A. 2010. Tachycardia-mediated cardiomyopathy and the permanent form of junctional reciprocating tachycardia. *Tex Heart Inst J,* 37, 695-8.

BERS, D. M. 2001. *Excitation-contraction coupling and cardiac contractile force,* The Netherlands, Kluwer Academic Publishers.

BERS, D. M. 2004. Macromolecular complexes regulating cardiac ryanodine receptor function. *J Mol Cell Cardiol,* 37, 417-29.

BERTOCCHINI, F., OVITT, C. E., CONTI, A., BARONE, V., SCHOLER, H. R., BOTTINELLI, R., REGGIANI, C. & SORRENTINO, V. 1997. Requirement for the ryanodine receptor type 3 for efficient contraction in neonatal skeletal muscles. *EMBO J,* 16, 6956-63.

BETZENHAUSER, M. J. & MARKS, A. R. 2010. Ryanodine receptor channelopathies. *Pflugers Arch,* 460, 467-80.

BEUCKELMANN, D. J., NABAUER, M. & ERDMANN, E. 1991. Characteristics of calcium-current in isolated human ventricular myocytes from patients with terminal heart failure. *J Mol Cell Cardiol,* 23, 929-37.

BEZPROZVANNY, I. 2005. The inositol 1,4,5-trisphosphate receptors. *Cell Calcium,* 38, 261-72.

BHAT, M. B., ZHAO, J., HAYEK, S., FREEMAN, E. C., TAKESHIMA, H. & MA, J. 1997. Deletion of amino acids 1641-2437 from the foot region of skeletal muscle ryanodine receptor alters the conduction properties of the Ca release channel. *Biophys J,* 73, 1320-8.

BHAT, M. B., ZHAO, J., TAKESHIMA, H. & MA, J. 1997a. Functional calcium release channel formed by the carboxyl-terminal portion of ryanodine receptor. *Biophys J,* 73, 1329-36.

BLACKBURN, A. C., WOOLLATT, E., SUTHERLAND, G. R. & BOARD, P. G. 1998. Characterization and chromosome location of the gene GSTZ1 encoding the human Zeta class glutathione transferase and maleylacetoacetate isomerase. *Cytogenet Cell Genet,* 83, 109-14.

BOARD, P. G., BAKER, R. T., CHELVANAYAGAM, G. & JERMIIN, L. S. 1997. Zeta, a novel class of glutathione transferases in a range of species from plants to humans. *Biochem J,* 328 (Pt 3), 929-35.

BOARD, P. G., CHELVANAYAGAM, G., JERMIIN, L. S., TETLOW, N., TZENG, H. F., ANDERS, M. W. & BLACKBURN, A. C. 2001. Identification of novel glutathione transferases and polymorphic variants by expressed sequence tag database analysis. *Drug Metab Dispos,* 29, 544-7.

BOARD, P. G., COGGAN, M., CHELVANAYAGAM, G., EASTEAL, S., JERMIIN, L. S., SCHULTE, G. K., DANLEY, D. E., HOTH, L. R., GRIFFOR, M. C., KAMATH, A. V., ROSNER, M. H., CHRUNYK, B. A., PERREGAUX, D. E., GABEL, C. A., GEOGHEGAN, K. F. & PANDIT, J. 2000. Identification, characterization, and crystal structure of the Omega class glutathione transferases. *J Biol Chem,* 275, 24798-806.

BOARD, P. G., COGGAN, M., WATSON, S., GAGE, P. W. & DULHUNTY, A. F.

2004. CLIC-2 modulates cardiac ryanodine receptor Ca2+ release channels. *Int J Biochem Cell Biol,* 36, 1599-612.

BOARD, P. G., SUZUKI, T. & SHAW, D. C. 1988. Human muscle glutathione S-transferase (GST-4) shows close homology to human liver GST-1. *Biochim Biophys Acta,* 953, 214-7.

BOGDANOV, K. Y., VINOGRADOVA, T. M. & LAKATTA, E. G. 2001. Sinoatrial nodal cell ryanodine receptor and Na(+)-Ca(2+) exchanger: molecular partners in pacemaker regulation. *Circ Res,* 88, 1254-8.

BOKENES, J., SJAASTAD, I. & SEJERSTED, O. M. 2005. Artifactual contractions triggered by field stimulation of cardiomyocytes. *J Appl Physiol,* 98, 1712-9.

BOKHARI, M. B., PATEL, C. B., RAMOS-VALADEZ, D. I., RAGUPATHI, M. & HAAS, E. M. 2011. Learning curve for robotic-assisted laparoscopic colorectal surgery. *Surg Endosc,* 25, 855-60.

BORCHMAN, D., SIMON, R. & BICKNELL-BROWN, E. 1982. Variation in the lipid composition of rabbit muscle sarcoplasmic reticulum membrane with muscle type. *J Biol Chem,* 257, 14136-9.

BRADY, A. J. 1991. Mechanical properties of isolated cardiac myocytes. *Physiol Rev,* 71, 413-28.

BREWIS, N., PHELAN, A., WEBB, J., DREW, J., ELLIOTT, G. & O'HARE, P. 2000. Evaluation of VP22 spread in tissue culture. *J Virol,* 74, 1051-6.

BRILLANTES, A. B., ONDRIAS, K., SCOTT, A., KOBRINSKY, E., ONDRIASOVA, E., MOSCHELLA, M. C., JAYARAMAN, T., LANDERS, M., EHRLICH, B. E. & MARKS, A. R. 1994. Stabilization of calcium release channel (ryanodine receptor) function by FK506-binding protein. *Cell,* 77, 513-23.

BRILLANTES, A. M., BEZPROZVANNAYA, S. & MARKS, A. R. 1994. Developmental and tissue-specific regulation of rabbit skeletal and cardiac muscle calcium channels involved in excitation-contraction coupling. *Circ Res,* 75, 503-10.

BRUNS, C. M., HUBATSCH, I., RIDDERSTROM, M., MANNERVIK, B. & TAINER, J. A. 1999. Human glutathione transferase A4-4 crystal structures and mutagenesis reveal the basis of high catalytic efficiency with toxic lipid peroxidation products. *J Mol Biol,* 288, 427-39.

CALA, S. E., SCOTT, B. T. & JONES, L. R. 1990. Intralumenal sarcoplasmic reticulum Ca(2+)-binding proteins. *Semin Cell Biol,* 1, 265-75.

CALLAWAY, C., SERYSHEV, A., WANG, J. P., SLAVIK, K. J., NEEDLEMAN, D. H., CANTU, C., 3RD, WU, Y., JAYARAMAN, T., MARKS, A. R. & HAMILTON, S. L. 1994. Localization of the high and low affinity [3H]ryanodine binding sites on the skeletal muscle Ca2+ release channel. *J Biol Chem,* 269, 15876-84.

CAMPBELL, D. L., RASMUSSON, R. L. & STRAUSS, H. C. 1992. Ionic current mechanisms generating vertebrate primary cardiac pacemaker activity at the single cell level: an integrative view. *Annu Rev Physiol,* 54, 279-302.

CAMPBELL, K. P., MACLENNAN, D. H., JORGENSEN, A. O. & MINTZER, M. C. 1983. Purification and characterization of calsequestrin from canine cardiac sarcoplasmic reticulum and identification of the 53,000 dalton glycoprotein. *J Biol Chem,* 258, 1197-204.

CAPOGROSSI, M. C., HOUSER, S. R., BAHINSKI, A. & LAKATTA, E. G. 1987. Synchronous occurrence of spontaneous localized calcium release from the sarcoplasmic reticulum generates action potentials in rat cardiac ventricular myocytes at normal resting membrane potential. *Circ Res,* 61, 498-503.

CARAFOLI, E. 2005. Calcium--a universal carrier of biological signals. Delivered on 3 July 2003 at the Special FEBS Meeting in Brussels. *FEBS J,* 272, 1073-89.

CARNIE, S. & MCLAUGHLIN, S. 1983. Large divalent cations and electrostatic potentials adjacent to membranes. A theoretical calculation. *Biophys J,* 44, 325-32.

CATANZARITI, A. M., SOBOLEVA, T. A., JANS, D. A., BOARD, P. G. & BAKER, R. T. 2004. An efficient system for high-level expression and easy purification of authentic recombinant proteins. *Protein Sci,* 13, 1331-9.

CESSELLI, D., JAKONIUK, I., BARLUCCHI, L., BELTRAMI, A. P., HINTZE, T. H., NADAL-GINARD, B., KAJSTURA, J., LERI, A. & ANVERSA, P. 2001. Oxidative stress-mediated cardiac cell death is a major determinant of ventricular dysfunction and failure in dog dilated cardiomyopathy. *Circ Res,* 89, 279-86.

CHAMBERLAIN, B. K. & FLEISCHER, S. 1988. Isolation of canine cardiac sarcoplasmic reticulum. *Methods Enzymol,* 157, 91-9.

CHAN, W. M., WELCH, W. & SITSAPESAN, R. 2000. Structural factors that determine the ability of adenosine and related compounds to activate the cardiac ryanodine receptor. *Br J Pharmacol,* 130, 1618-26.

CHEN, S. R., LI, P., ZHAO, M., LI, X. & ZHANG, L. 2002. Role of the proposed pore-forming segment of the Ca2+ release channel (ryanodine receptor) in ryanodine interaction. *Biophys J,* 82, 2436-47.

CHEN, S. R., LI, X., EBISAWA, K. & ZHANG, L. 1997. Functional characterization of the recombinant type 3 Ca2+ release channel (ryanodine receptor) expressed in HEK293 cells. *J Biol Chem,* 272, 24234-46.

CHEN, S. R. & MACLENNAN, D. H. 1994. Identification of calmodulin-, Ca(2+)-, and ruthenium red-binding domains in the Ca2+ release channel (ryanodine receptor) of rabbit skeletal muscle sarcoplasmic reticulum. *J Biol Chem,* 269, 22698-704.

CHEN, Z., LI, Z., WEI, B., YIN, W., XU, T., KOTLIKOFF, M. I. & JI, G. 2010. FKBP12.6-knockout mice display hyperinsulinemia and resistance to high-fat diet-induced hyperglycemia. *FASEB J,* 24, 357-63.

CHO, S. G., LEE, Y. H., PARK, H. S., RYOO, K., KANG, K. W., PARK, J.,

EOM, S. J., KIM, M. J., CHANG, T. S., CHOI, S. Y., SHIM, J., KIM, Y., DONG, M. S., LEE, M. J., KIM, S. G., ICHIJO, H. & CHOI, E. J. 2001. Glutathione S-transferase mu modulates the stress-activated signals by suppressing apoptosis signal-regulating kinase 1. *J Biol Chem,* 276, 12749-55.

COPELLO, J. A., BARG, S., ONOUE, H. & FLEISCHER, S. 1997. Heterogeneity of Ca2+ gating of skeletal muscle and cardiac ryanodine receptors. *Biophys J,* 73, 141-56.

COPELLO, J. A., BARG, S., SONNLEITNER, A., PORTA, M., DIAZ-SYLVESTER, P., FILL, M., SCHINDLER, H. & FLEISCHER, S. 2002. Differential activation by Ca2+, ATP and caffeine of cardiac and skeletal muscle ryanodine receptors after block by Mg2+. *J Membr Biol,* 187, 51-64.

CORNU, J. N., CHANU, T., BELEY, S., SEBE, P., PEYRAT, L., CIOFU, C. & HAAB, F. 2011. [Initial experience combinating transobturator male sling and penile implant after radical prostatectomy]. *Prog Urol,* 21, 349-53.

CORNU, J. N., MERLET, B., CIOFU, C., MOULY, S., PEYRAT, L., SEBE, P., YIOU, R., VALLANCIEN, G., DEBRIX, I., LARIBI, K., CUSSENOT, O. & HAAB, F. 2011. Duloxetine for mild to moderate postprostatectomy incontinence: preliminary results of a randomised, placebo-controlled trial. *Eur Urol,* 59, 148-54.

CORONADO, R., AHERN, C. A., SHERIDAN, D. C., CHENG, W., CARBONNEAU, L. & BHATTACHARYA, D. 2004. Functional equivalence of dihydropyridine receptor alpha1S and beta1a subunits in triggering excitation-contraction coupling in skeletal muscle. *Biol Res,* 37, 565-75.

CORONADO, R., KAWANO, S., LEE, C. J., VALDIVIA, C. & VALDIVIA, H. H. 1992. Planar bilayer recording of ryanodine receptors of sarcoplasmic reticulum. *Methods Enzymol,* 207, 699-707.

CORONADO, R., MORRISSETTE, J., SUKHAREVA, M. & VAUGHAN, D. M. 1994. Structure and function of ryanodine receptors. *Am J Physiol,* 266, C1485-504.

CROMER, B. A., GORMAN, M. A., HANSEN, G., ADAMS, J. J., COGGAN, M., LITTLER, D. R., BROWN, L. J., MAZZANTI, M., BREIT, S. N., CURMI, P. M., DULHUNTY, A. F., BOARD, P. G. & PARKER, M. W. 2007. Structure of the Janus protein human CLIC2. *J Mol Biol,* 374, 719-31.

CROMER, B. A., MORTON, C. J., BOARD, P. G. & PARKER, M. W. 2002. From glutathione transferase to pore in a CLIC. *Eur Biophys J,* 31, 356-64.

CULMAN, J., DAS, G., OHLENDORF, C., HAASS, M., MASER-GLUTH, C., ZUHAYRA, M., ZHAO, Y. & ITOI, K. 2010. Blockade of tachykinin NK1/NK2 receptors in the brain attenuates the activation of corticotrophin-releasing hormone neurones in the hypothalamic paraventricular nucleus and the sympathoadrenal and pituitary-adrenal responses to formalin-induced pain in the rat. *J Neuroendocrinol,* 22,

467-76.

DIFRANCESCO, D. 1993. Pacemaker mechanisms in cardiac tissue. *Annu Rev Physiol,* 55, 455-72.

DIFRANCESCO, D. 2006. Funny channels in the control of cardiac rhythm and mode of action of selective blockers. *Pharmacol Res,* 53, 399-406.

DIRR, H., REINEMER, P. & HUBER, R. 1994. X-ray crystal structures of cytosolic glutathione S-transferases. Implications for protein architecture, substrate recognition and catalytic function. *Eur J Biochem,* 220, 645-61.

DO CARMO, P. L., ZAPATA-SUDO, G., TRACHEZ, M. M., DAS GRACAS FERNANDES SALES, M. & SUDO, R. T. 2010. Toxicological evaluation of azumolene after repeated intraperitoneal administration in rats. *Fundam Clin Pharmacol,* 24, 491-500.

DONOSO, P., SANCHEZ, G., BULL, R. & HIDALGO, C. 2011. Modulation of cardiac ryanodine receptor activity by ROS and RNS. *Front Biosci,* 16, 553-67.

DU, G. G., KHANNA, V. K. & MACLENNAN, D. H. 2000. Mutation of divergent region 1 alters caffeine and Ca(2+) sensitivity of the skeletal muscle Ca(2+) release channel (ryanodine receptor). *J Biol Chem,* 275, 11778-83.

DU, G. G. & MACLENNAN, D. H. 1999. Ca(2+) inactivation sites are located in the COOH-terminal quarter of recombinant rabbit skeletal muscle Ca(2+) release channels (ryanodine receptors). *J Biol Chem,* 274, 26120-6.

DULHUNTY, A., GAGE, P., CURTIS, S., CHELVANAYAGAM, G. & BOARD, P. 2001. The glutathione transferase structural family includes a nuclear chloride channel and a ryanodine receptor calcium release channel modulator. *J Biol Chem,* 276, 3319-23.

DULHUNTY, A., HAARMANN, C., GREEN, D. & HART, J. 2000. How many cysteine residues regulate ryanodine receptor channel activity? *Antioxid Redox Signal,* 2, 27-34.

DULHUNTY, A. F., BEARD, N. A., POULIQUIN, P. & CASAROTTO, M. G. 2007. Agonists and antagonists of the cardiac ryanodine receptor: potential therapeutic agents? *Pharmacol Ther,* 113, 247-63.

DULHUNTY, A. F., HAARMANN, C. S., GREEN, D., LAVER, D. R., BOARD, P. G. & CASAROTTO, M. G. 2002. Interactions between dihydropyridine receptors and ryanodine receptors in striated muscle. *Prog Biophys Mol Biol,* 79, 45-75.

DULHUNTY, A. F., HEWAWASAM, R., LIU, D., CASAROTTO, M. G. & BOARD, P. G. 2011. Regulation of the cardiac muscle ryanodine receptor by glutathione transferases. *Drug Metab Rev.*

DULHUNTY, A. F., KARUNASEKARA, Y., CURTIS, S. M., HARVEY, P. J., BOARD, P. G. & CASAROTTO, M. G. 2005. The recombinant dihydropyridine receptor II-III loop and partly structured 'C' region peptides modify cardiac ryanodine receptor activity. *Biochem J,* 385, 803-13.

DULHUNTY, A. F., KARUNASEKARA, Y., CURTIS, S. M., HARVEY, P. J., BOARD, P. G. & CASAROTTO, M. G. 2005. Role of some unconserved residues in the "C" region of the skeletal DHPR II-III loop. *Front Biosci,* 10, 1368-81.

DULHUNTY, A. F., LAVER, D., CURTIS, S. M., PACE, S., HAARMANN, C. & GALLANT, E. M. 2001. Characteristics of irreversible ATP activation suggest that native skeletal ryanodine receptors can be phosphorylated via an endogenous CaMKII. *Biophys J,* 81, 3240-52.

DULHUNTY, A. F., LAVER, D. R., GALLANT, E. M., CASAROTTO, M. G., PACE, S. M. & CURTIS, S. 1999. Activation and inhibition of skeletal RyR channels by a part of the skeletal DHPR II-III loop: effects of DHPR Ser687 and FKBP12. *Biophys J,* 77, 189-203.

DULHUNTY, A. F., POULIQUIN, P., COGGAN, M., GAGE, P. W. & BOARD, P. G. 2005. A recently identified member of the glutathione transferase structural family modifies cardiac RyR2 substate activity, coupled gating and activation by Ca2+ and ATP. *Biochem J,* 390, 333-43.

EAGER, K. R. & DULHUNTY, A. F. 1999. Cardiac ryanodine receptor activity is altered by oxidizing reagents in either the luminal or cytoplasmic solution. *J Membr Biol,* 167, 205-14.

EBASHI, F. & EBASHI, S. 1962. Removal of calcium and relaxation in actomyosin systems. *Nature,* 194, 378-9.

EBASHI, S. 1961. Calcium binding activity of vesicular relaxing factor. *J Chir (Paris),* 50, 236-44.

EBASHI, S. & ENDO, M. 1968. Ca ion and muscle contraction. *Progr Biophys Mol Biol* 18, 123–83

EISNER, D. A. & CERBAI, E. 2009. Beating to time: calcium clocks, voltage clocks, and cardiac pacemaker activity. *Am J Physiol Heart Circ Physiol,* 296, H561-2.

ELISON, C. & JENDEN, D. J. 1967. The effects of ryanodine on model systems derived from muscle. 3. Reconstituted actomyosin. *Biochem Pharmacol,* 16, 1355-63.

ENDO, M., TANAKA, M., OGAWA, Y. 1970. Calcium induced release of calcium from sarcoplasmic reticulum of skinned skeletal muscle fibres. *Nature*, 228, 34–6.

ER, F., LARBIG, R., LUDWIG, A., BIEL, M., HOFMANN, F., BEUCKELMANN, D. J. & HOPPE, U. C. 2003. Dominant-negative suppression of HCN channels markedly reduces the native pacemaker current I(f) and undermines spontaneous beating of neonatal cardiomyocytes. *Circulation,* 107, 485-9.

FABIATO, A. & FABIATO, F. 1978. Calcium-induced release of calcium from the sarcoplasmic reticulum of skinned cells from adult human, dog, cat, rabbit, rat, and frog hearts and from fetal and new-born rat ventricles. *Ann N Y Acad Sci,* 307, 491-522.

FAIRHURST, A. S. 1973. Effect of ryanodine on skeletal muscle reticulum

calcium adenosine triphosphatase (CaATPase). *Biochem Pharmacol,* 22, 2815-27.

FEHER, J. J., MANSON, N. H. & POLAND, J. L. 1988. The rate and capacity of calcium uptake by sarcoplasmic reticulum in fast, slow, and cardiac muscle: effects of ryanodine and ruthenium red. *Arch Biochem Biophys,* 265, 171-82.

FELDER, E. & FRANZINI-ARMSTRONG, C. 2002. Type 3 ryanodine receptors of skeletal muscle are segregated in a parajunctional position. *Proc Natl Acad Sci U S A,* 99, 1695-700.

FENG, W., TU, J., YANG, T., VERNON, P. S., ALLEN, P. D., WORLEY, P. F. & PESSAH, I. N. 2002. Homer regulates gain of ryanodine receptor type 1 channel complex. *J Biol Chem,* 277, 44722-30.

FERNANDEZ-CANON, J. M., HEJNA, J., REIFSTECK, C., OLSON, S. & GROMPE, M. 1999. Gene structure, chromosomal location, and expression pattern of maleylacetoacetate isomerase. *Genomics,* 58, 263-9.

FIELD, A. C., HILL, C. & LAMB, G. D. 1988. Asymmetric charge movement and calcium currents in ventricular myocytes of neonatal rat. *J Physiol,* 406, 277-97.

FILL, M. & COPELLO, J. A. 2002. Ryanodine receptor calcium release channels. *Physiol Rev,* 82, 893-922.

FILL, M. & CORONADO, R. 1988. Ryanodine receptor channel of sarcoplasmic reticulum. *Trends Neurosci,* 11, 453-7.

FLEISCHER, S., OGUNBUNMI, E. M., DIXON, M. C. & FLEER, E. A. 1985. Localization of Ca2+ release channels with ryanodine in junctional terminal cisternae of sarcoplasmic reticulum of fast skeletal muscle. *Proc Natl Acad Sci U S A,* 82, 7256-9.

FOSKETT, J. K., WHITE, C., CHEUNG, K. H. & MAK, D. O. 2007. Inositol trisphosphate receptor Ca2+ release channels. *Physiol Rev,* 87, 593-658.

FREDJ, S., BESCOND, J., LOUAULT, C. & POTREAU, D. 2005. Interactions between cardiac cells enhance cardiomyocyte hypertrophy and increase fibroblast proliferation. *J Cell Physiol,* 202, 891-9.

FRITZ, N., MOREL, J. L., JEYAKUMAR, L. H., FLEISCHER, S., ALLEN, P. D., MIRONNEAU, J. & MACREZ, N. 2007. RyR1-specific requirement for depolarization-induced Ca2+ sparks in urinary bladder smooth muscle. *J Cell Sci,* 120, 3784-91.

FRYER, M. W. & STEPHENSON, D. G. 1996. Total and sarcoplasmic reticulum calcium contents of skinned fibres from rat skeletal muscle. *J Physiol,* 493 (Pt 2), 357-70.

GELLEN, B., FERNANDEZ-VELASCO, M., BRIEC, F., VINET, L., LEQUANG, K., ROUET-BENZINEB, P., BENITAH, J. P., PEZET, M., PALAIS, G., PELLEGRIN, N., ZHANG, A., PERRIER, R., ESCOUBET, B., MARNIQUET, X., RICHARD, S., JAISSER, F., GOMEZ, A. M.,

CHARPENTIER, F. & MERCADIER, J. J. 2008. Conditional FKBP12.6 overexpression in mouse cardiac myocytes prevents triggered ventricular tachycardia through specific alterations in excitation-contraction coupling. *Circulation,* 117, 1778-86.

GERMANN WJ, S. C. 2005. *principles of human physiology,* Sanfrancisco, USA, Pearson education Inc.

GIANNINI, G., CONTI, A., MAMMARELLA, S., SCROBOGNA, M. & SORRENTINO, V. 1995. The ryanodine receptor/calcium channel genes are widely and differentially expressed in murine brain and peripheral tissues. *J Cell Biol,* 128, 893-904.

GIORDANO, F. J. 2005. Oxygen, oxidative stress, hypoxia, and heart failure. *J Clin Invest,* 115, 500-8.

GOONASEKERA, S. A., BEARD, N. A., GROOM, L., KIMURA, T., LYFENKO, A. D., ROSENFELD, A., MARTY, I., DULHUNTY, A. F. & DIRKSEN, R. T. 2007. Triadin binding to the C-terminal luminal loop of the ryanodine receptor is important for skeletal muscle excitation contraction coupling. *J Gen Physiol,* 130, 365-78.

GOONASEKERA, S. A., BEARD, N. A., GROOM, L., KIMURA, T., LYFENKO, A. D., ROSENFELD, A., MARTY, I., DULHUNTY, A. F. & DIRKSEN, R. T. 2007. Triadin binding to the C-terminal luminal loop of the ryanodine receptor is important for skeletal muscle excitation contraction coupling. *J Gen Physiol,* 130, 365-78.

GORZA, L., VETTORE, S., TESSARO, A., SORRENTINO, V. & VITADELLO, M. 1997. Regional and age-related differences in mRNA composition of intracellular Ca(2+)-release channels of rat cardiac myocytes. *J Mol Cell Cardiol,* 29, 1023-36.

GOTHEL, S. F. & MARAHIEL, M. A. 1999. Peptidyl-prolyl cis-trans isomerases, a superfamily of ubiquitous folding catalysts. *Cell Mol Life Sci,* 55, 423-36.

GYORKE, I. & GYORKE, S. 1998. Regulation of the cardiac ryanodine receptor channel by luminal Ca2+ involves luminal Ca2+ sensing sites. *Biophys J,* 75, 2801-10.

GYORKE, S. 2009. Molecular basis of catecholaminergic polymorphic ventricular tachycardia. *Heart Rhythm,* 6, 123-9.

GYORKE, S., LUKYANENKO, V. & GYORKE, I. 1997. Dual effects of tetracaine on spontaneous calcium release in rat ventricular myocytes. *J Physiol,* 500 (Pt 2), 297-309.

HA, J. W., SCHWAHN, A. B. & DOWNARD, K. M. 2010. Ability of N-acetylcarnosine to protect lens crystallins from oxidation and oxidative damage by radical probe mass spectrometry (RP-MS). *Rapid Commun Mass Spectrom,* 24, 2900-8.

HAIN, J., NATH, S., MAYRLEITNER, M., FLEISCHER, S. & SCHINDLER, H. 1994. Phosphorylation modulates the function of the calcium release channel of sarcoplasmic reticulum from skeletal muscle. *Biophys J,* 67,

1823-33.

HAIN, J., ONOUE, H., MAYRLEITNER, M., FLEISCHER, S. & SCHINDLER, H. 1995. Phosphorylation modulates the function of the calcium release channel of sarcoplasmic reticulum from cardiac muscle. *J Biol Chem,* 270, 2074-81.

HAKAMATA, Y., NAKAI, J., TAKESHIMA, H. & IMOTO, K. 1992. Primary structure and distribution of a novel ryanodine receptor/calcium release channel from rabbit brain. *FEBS Lett,* 312, 229-35.

HARARY, I. & FARLEY, B. 1963. In vitro studies on single beating rat heart cells. II. Intercellular communication. *Exp Cell Res,* 29, 466-74.

HARROP, S. J., DEMAERE, M. Z., FAIRLIE, W. D., REZTSOVA, T., VALENZUELA, S. M., MAZZANTI, M., TONINI, R., QIU, M. R., JANKOVA, L., WARTON, K., BAUSKIN, A. R., WU, W. M., PANKHURST, S., CAMPBELL, T. J., BREIT, S. N. & CURMI, P. M. 2001. Crystal structure of a soluble form of the intracellular chloride ion channel CLIC1 (NCC27) at 1.4-A resolution. *J Biol Chem,* 276, 44993-5000.

HAYEK, S. M., ZHAO, J., BHAT, M., XU, X., NAGARAJ, R., PAN, Z., TAKESHIMA, H. & MA, J. 1999. A negatively charged region of the skeletal muscle ryanodine receptor is involved in Ca(2+)-dependent regulation of the Ca(2+) release channel. *FEBS Lett,* 461, 157-64.

HAYEK, S. M., ZHU, X., BHAT, M. B., ZHAO, J., TAKESHIMA, H., VALDIVIA, H. H. & MA, J. 2000. Characterization of a calcium-regulation domain of the skeletal-muscle ryanodine receptor. *Biochem J,* 351, 57-65.

HAYES, J. D. & MCLELLAN, L. I. 1999. Glutathione and glutathione-dependent enzymes represent a co-ordinately regulated defence against oxidative stress. *Free Radic Res,* 31, 273-300.

HAYES, J. D. & PULFORD, D. J. 1995. The glutathione S-transferase supergene family: regulation of GST and the contribution of the isoenzymes to cancer chemoprotection and drug resistance. *Crit Rev Biochem Mol Biol,* 30, 445-600.

HAYES, J. D. & STRANGE, R. C. 2000. Glutathione S-transferase polymorphisms and their biological consequences. *Pharmacology,* 61, 154-66.

HEILBRUNN, L. V., HARRIS, D. L. & ET AL. 1946. Heat death, heat injury, and toxic factor. *Physiol Zool,* 19, 404-29.

HEISS, N. S. & POUSTKA, A. 1997. Genomic structure of a novel chloride channel gene, CLIC2, in Xq28. *Genomics,* 45, 224-8.

HERRMANN-FRANK, A. & VARSANYI, M. 1993. Enhancement of Ca2+ release channel activity by phosphorylation of the skeletal muscle ryanodine receptor. *FEBS Lett,* 332, 237-42.

HERZOG, A., SZEGEDI, C., JONA, I., HERBERG, F. W. & VARSANYI, M. 2000. Surface plasmon resonance studies prove the interaction of skeletal muscle sarcoplasmic reticular Ca(2+) release channel/ryanodine

receptor with calsequestrin. *FEBS Lett,* 472, 73-7.

HEWAWASAM, R., LIU, D., CASAROTTO, M. G., DULHUNTY, A. F. & BOARD, P. G. 2010. The structure of the C-terminal helical bundle in glutathione transferase M2-2 determines its ability to inhibit the cardiac ryanodine receptor. *Biochem Pharmacol,* 80, 381-8.

HIDALGO, C., ARACENA, P., SANCHEZ, G. & DONOSO, P. 2002. Redox regulation of calcium release in skeletal and cardiac muscle. *Biol Res,* 35, 183-93.

HILLIARD, F. A., STEELE, D. S., LAVER, D., YANG, Z., LE MARCHAND, S. J., CHOPRA, N., PISTON, D. W., HUKE, S. & KNOLLMANN, B. C. 2010. Flecainide inhibits arrhythmogenic Ca2+ waves by open state block of ryanodine receptor Ca2+ release channels and reduction of Ca2+ spark mass. *J Mol Cell Cardiol,* 48, 293-301.

HIROTA, A. & ITO, S. 2006. A Long-time, hgh spatiotemporal resolution optical recording system for membrane potential activity via real-time writing to the hard disk. *J Physiol Sci,* 56(3), 263-66.

HOPPE, U. C., JANSEN, E., SUDKAMP, M. & BEUCKELMANN, D. J. 1998. Hyperpolarization-activated inward current in ventricular myocytes from normal and failing human hearts. *Circulation,* 97, 55-65.

HU, S. T., SHEN, Y. F., LIU, G. S., LEI, C. H., TANG, Y., WANG, J. F. & YANG, Y. J. 2010. Altered intracellular Ca2+ regulation in chronic rat heart failure. *J Physiol Sci,* 60, 85-94.

HUANG, B., QIN, D., DENG, L., BOUTJDIR, M. & N, E.-S. 2000. Reexpression of T-type Ca2+ channel gene and current in post-infarction remodeled rat left ventricle. *Cardiovasc Res,* 46, 442-9.

HUANG, F., SHAN, J., REIKEN, S., WEHRENS, X. H. & MARKS, A. R. 2006. Analysis of calstabin2 (FKBP12.6)-ryanodine receptor interactions: rescue of heart failure by calstabin2 in mice. *Proc Natl Acad Sci U S A,* 103, 3456-61.

HUSER, J., BLATTER, L. A. & LIPSIUS, S. L. 2000. Intracellular Ca2+ release contributes to automaticity in cat atrial pacemaker cells. *J Physiol,* 524 Pt 2, 415-22.

HUSSEY, A. J. & HAYES, J. D. 1992. Characterization of a human class-Theta glutathione S-transferase with activity towards 1-menaphthyl sulphate. *Biochem J,* 286 (Pt 3), 929-35.

HUSSEY, A. J., KERR, L. A., CRONSHAW, A. D., HARRISON, D. J. & HAYES, J. D. 1991. Variation in the expression of Mu-class glutathione S-transferase isoenzymes from human skeletal muscle. Evidence for the existence of heterodimers. *Biochem J,* 273(Pt 2), 323-32.

HUXLEY, H.E. & HANSON, J. 1954. Changes in the cross-striations of muscle during contraction and stretch and their structural interpretation. *Nature,* 173, 973–76.

HUXLEY, A.F. & NIEDERGERKE, R. (1954) Structural changes in muscle

during contraction. Interference microscopy of living muscle fibres. *Nature,* 173, 971–73.

HYMEL, L., INUI, M., FLEISCHER, S. & SCHINDLER, H. 1988. Purified ryanodine receptor of skeletal muscle sarcoplasmic reticulum forms Ca2+-activated oligomeric Ca2+ channels in planar bilayers. *Proc Natl Acad Sci U S A,* 85, 441-5.

INUI, M., SAITO, A. & FLEISCHER, S. 1987. Purification of the ryanodine receptor and identity with feet structures of junctional terminal cisternae of sarcoplasmic reticulum from fast skeletal muscle. *J Biol Chem,* 262, 1740-7.

JAKOBSSON, P. J., MORGENSTERN, R., MANCINI, J., FORD-HUTCHINSON, A. & PERSSON, B. 1999. Common structural features of MAPEG -- a widespread superfamily of membrane associated proteins with highly divergent functions in eicosanoid and glutathione metabolism. *Protein Sci,* 8, 689-92.

JALILIAN, C., GALLANT, E. M., BOARD, P. G. & DULHUNTY, A. F. 2008. Redox potential and the response of cardiac ryanodine receptors to CLIC-2, a member of the glutathione S-transferase structural family. *Antioxid Redox Signal,* 10, 1675-86.

JAYARAMAN, T., BRILLANTES, A. M., TIMERMAN, A. P., FLEISCHER, S., ERDJUMENT-BROMAGE, H., TEMPST, P. & MARKS, A. R. 1992. FK506 binding protein associated with the calcium release channel (ryanodine receptor). *J Biol Chem,* 267, 9474-7.

JENDEN, D. J. & FAIRHURST, A. S. 1969. The pharmacology of ryanodine. *Pharmacol Rev,* 21, 1-25.

JEYAKUMAR, L. H., COPELLO, J. A., O'MALLEY, A. M., WU, G. M., GRASSUCCI, R., WAGENKNECHT, T. & FLEISCHER, S. 1998. Purification and characterization of ryanodine receptor 3 from mammalian tissue. *J Biol Chem,* 273, 16011-20.

JI, X., ZHANG, P., ARMSTRONG, R. N. & GILLILAND, G. L. 1992. The three-dimensional structure of a glutathione S-transferase from the mu gene class. Structural analysis of the binary complex of isoenzyme 3-3 and glutathione at 2.2-A resolution. *Biochemistry,* 31, 10169-84.

JOHANSSON, A. S. & MANNERVIK, B. 2001. Human glutathione transferase A3-3, a highly efficient catalyst of double-bond isomerization in the biosynthetic pathway of steroid hormones. *J Biol Chem,* 276, 33061-5.

JOHNSON, W. C., JR. 1990. Protein secondary structure and circular dichroism: a practical guide. *Proteins,* 7, 205-14.

JOWSEY, I. R., THOMSON, R. E., ORTON, T. C., ELCOMBE, C. R. & HAYES, J. D. 2003. Biochemical and genetic characterization of a murine class Kappa glutathione S-transferase. *Biochem J,* 373, 559-69.

KAFTAN, E., MARKS, A. R. & EHRLICH, B. E. 1996. Effects of rapamycin on ryanodine receptor/Ca(2+)-release channels from cardiac muscle. *Circ Res,* 78, 990-7.

KARGACIN, G. J., ASCHAR-SOBBI, R. & KARGACIN, M. E. 2005. Inhibition of SERCA2 Ca(2+)-ATPases by Cs(+). *Pflugers Arch,* 449, 356-63.

KATZ, A. M. 2006. *Physiology of the heart,* Philadelphia, USA, Lippincott, Williams and Wilkins.

KAWAKAMI, M. & OKABE, E. 1998. Superoxide anion radical-triggered Ca2+ release from cardiac sarcoplasmic reticulum through ryanodine receptor Ca2+ channel. *Mol Pharmacol,* 53, 497-503.

KEEN, J. H. & JAKOBY, W. B. 1978. Glutathione transferases. Catalysis of nucleophilic reactions of glutathione. *J Biol Chem,* 253, 5654-7.

KERMODE, H., WILLIAMS, A. J. & SITSAPESAN, R. 1998. The interactions of ATP, ADP, and inorganic phosphate with the sheep cardiac ryanodine receptor. *Biophys J,* 74, 1296-304.

KIMURA, T., NAKAMORI, M., LUECK, J. D., POULIQUIN, P., AOIKE, F., FUJIMURA, H., DIRKSEN, R. T., TAKAHASHI, M. P., DULHUNTY, A. F. & SAKODA, S. 2005. Altered mRNA splicing of the skeletal muscle ryanodine receptor and sarcoplasmic/endoplasmic reticulum Ca2+-ATPase in myotonic dystrophy type 1. *Hum Mol Genet,* 14, 2189-200.

KIRCHHEFER, U., NEUMANN, J., BERS, D. M., BUCHWALOW, I. B., FABRITZ, L., HANSKE, G., JUSTUS, I., RIEMANN, B., SCHMITZ, W. & JONES, L. R. 2003. Impaired relaxation in transgenic mice overexpressing junctin. *Cardiovasc Res,* 59, 369-79.

KIRCHHOF, P., KLIMAS, J., FABRITZ, L., ZWIENER, M., JONES, L. R., SCHAFERS, M., HERMANN, S., BOKNIK, P., SCHMITZ, W., BREITHARDT, G., KIRCHHEFER, U. & NEUMANN, J. 2007. Stress and high heart rate provoke ventricular tachycardia in mice expressing triadin. *J Mol Cell Cardiol,* 42, 962-71.

KLABUNDE, R. E. 2005. *Cardiovascular physiology concepts* Lippincott Williams & Wilkins.

KOBAYASHI, S., BANNISTER, M. L., GANGOPADHYAY, J. P., HAMADA, T., PARNESS, J. & IKEMOTO, N. 2005. Dantrolene stabilizes domain interactions within the ryanodine receptor. *J Biol Chem,* 280, 6580-7.

KOBAYASHI, S., VOLDEN, P., TIMM, D., MAO, K., XU, X. & LIANG, Q. 2010. Transcription factor GATA4 inhibits doxorubicin-induced autophagy and cardiomyocyte death. *J Biol Chem,* 285, 793-804.

KOBAYASHI, S., YANO, M., SUETOMI, T., ONO, M., TATEISHI, H., MOCHIZUKI, M., XU, X., UCHINOUMI, H., OKUDA, S., YAMAMOTO, T., KOSEKI, N., KYUSHIKI, H., IKEMOTO, N. & MATSUZAKI, M. 2009. Dantrolene, a therapeutic agent for malignant hyperthermia, markedly improves the function of failing cardiomyocytes by stabilizing interdomain interactions within the ryanodine receptor. *J Am Coll Cardiol,* 53, 1993-2005.

KOULEN, P. & THROWER, E. C. 2001. Pharmacological modulation of intracellular Ca(2+) channels at the single-channel level. *Mol Neurobiol,* 24, 65-86.

KOUSHIK, S. V., WANG, J., ROGERS, R., MOSKOPHIDIS, D., LAMBERT, N. A., CREAZZO, T. L. & CONWAY, S. J. 2001. Targeted inactivation of the sodium-calcium exchanger (Ncx1) results in the lack of a heartbeat and abnormal myofibrillar organization. *FASEB J,* 15, 1209-11.

KRAUSE, T., GERBERSHAGEN, M. U., FIEGE, M., WEISSHORN, R. & WAPPLER, F. 2004. Dantrolene--a review of its pharmacology, therapeutic use and new developments. *Anaesthesia,* 59, 364-73.

KUGLER, G., WEISS, R. G., FLUCHER, B. E. & GRABNER, M. 2004. Structural requirements of the dihydropyridine receptor alpha1S II-III loop for skeletal-type excitation-contraction coupling. *J Biol Chem,* 279, 4721-8.

KUSHNIR, A., BETZENHAUSER, M. J. & MARKS, A. R. 2010. Ryanodine receptor studies using genetically engineered mice. *FEBS Lett,* 584, 1956-65.

KUSHNIR, A. & MARKS, A. R. 2010. The ryanodine receptor in cardiac physiology and disease. *Adv Pharmacol,* 59, 1-30.

KUSHNIR, A., SHAN, J., BETZENHAUSER, M. J., REIKEN, S. & MARKS, A. R. 2010. Role of CaMKIIdelta phosphorylation of the cardiac ryanodine receptor in the force frequency relationship and heart failure. *Proc Natl Acad Sci U S A,* 107, 10274-9.

KUWAJIMA, G., FUTATSUGI, A., NIINOBE, M., NAKANISHI, S. & MIKOSHIBA, K. 1992. Two types of ryanodine receptors in mouse brain: skeletal muscle type exclusively in Purkinje cells and cardiac muscle type in various neurons. *Neuron,* 9, 1133-42.

LADNER, J. E., PARSONS, J. F., RIFE, C. L., GILLILAND, G. L. & ARMSTRONG, R. N. 2004. Parallel evolutionary pathways for glutathione transferases: structure and mechanism of the mitochondrial class kappa enzyme rGSTK1-1. *Biochemistry,* 43, 352-61.

LAHAT, H., PRAS, E., OLENDER, T., AVIDAN, N., BEN-ASHER, E., MAN, O., LEVY-NISSENBAUM, E., KHOURY, A., LORBER, A., GOLDMAN, B., LANCET, D. & ELDAR, M. 2001. A missense mutation in a highly conserved region of CASQ2 is associated with autosomal recessive catecholamine-induced polymorphic ventricular tachycardia in Bedouin families from Israel. *Am J Hum Genet,* 69, 1378-84.

LAI, F. A., ERICKSON, H. P., ROUSSEAU, E., LIU, Q. Y. & MEISSNER, G. 1988. Purification and reconstitution of the calcium release channel from skeletal muscle. *Nature,* 331, 315-9.

LAI, F. A. & MEISSNER, G. 1989. The muscle ryanodine receptor and its intrinsic Ca2+ channel activity. *J Bioenerg Biomembr,* 21, 227-46.

LAI, F. A., MISRA, M., XU, L., SMITH, H. A. & MEISSNER, G. 1989. The ryanodine receptor-Ca2+ release channel complex of skeletal muscle sarcoplasmic reticulum. Evidence for a cooperatively coupled, negatively charged homotetramer. *J Biol Chem,* 264, 16776-85.

LAKATTA, E. G. & DIFRANCESCO, D. 2009. What keeps us ticking: a funny

current, a calcium clock, or both? *J Mol Cell Cardiol,* 47, 157-70.

LALIBERTE, R. E., PERREGAUX, D. G., HOTH, L. R., ROSNER, P. J., JORDAN, C. K., PEESE, K. M., EGGLER, J. F., DOMBROSKI, M. A., GEOGHEGAN, K. F. & GABEL, C. A. 2003. Glutathione s-transferase omega 1-1 is a target of cytokine release inhibitory drugs and may be responsible for their effect on interleukin-1beta posttranslational processing. *J Biol Chem,* 278, 16567-78.

LAMB, G. D., CELLINI, M. A. & STEPHENSON, D. G. 2001. Different Ca2+ releasing action of caffeine and depolarisation in skeletal muscle fibres of the rat. *J Physiol,* 531, 715-28.

LAMB, G. D. & STEPHENSON, D. G. 1991. Effect of Mg2+ on the control of Ca2+ release in skeletal muscle fibres of the toad. *J Physiol,* 434, 507-28.

LAMB, G. D. & STEPHENSON, D. G. 1994. Effects of intracellular pH and [Mg2+] on excitation-contraction coupling in skeletal muscle fibres of the rat. *J Physiol,* 478 (Pt 2), 331-9.

LAMB, G. D. & STEPHENSON, D. G. 1996. Effects of FK506 and rapamycin on excitation-contraction coupling in skeletal muscle fibres of the rat. *J Physiol,* 494 (Pt 2), 569-76.

LAUNIKONIS, B. S., ZHOU, J., SANTIAGO, D., BRUM, G. & RIOS, E. 2006. The changes in Ca2+ sparks associated with measured modifications of intra-store Ca2+ concentration in skeletal muscle. *J Gen Physiol,* 128, 45-54.

LAVER, D. 2001. The power of single channel recording and analysis: its application to ryanodine receptors in lipid bilayers. *Clin Exp Pharmacol Physiol,* 28, 675-86.

LAVER, D. R. 2007. Ca2+ stores regulate ryanodine receptor Ca2+ release channels via luminal and cytosolic Ca2+ sites. *Biophys J,* 92, 3541-55.

LAVER, D. R. 2009. Luminal Ca(2+) activation of cardiac ryanodine receptors by luminal and cytoplasmic domains. *Eur Biophys J,* 39, 19-26.

LAVER, D. R., BAYNES, T. M. & DULHUNTY, A. F. 1997. Magnesium inhibition of ryanodine-receptor calcium channels: evidence for two independent mechanisms. *J Membr Biol,* 156, 213-29.

LAVER, D. R. & LAMB, G. D. 1998. Inactivation of Ca2+ release channels (ryanodine receptors RyR1 and RyR2) with rapid steps in [Ca2+] and voltage. *Biophys J,* 74, 2352-64.

LAVER, D. R., LENZ, G. K. & LAMB, G. D. 2001. Regulation of the calcium release channel from rabbit skeletal muscle by the nucleotides ATP, AMP, IMP and adenosine. *J Physiol,* 537, 763-78.

LAVER, D. R., OWEN, V. J., JUNANKAR, P. R., TASKE, N. L., DULHUNTY, A. F. & LAMB, G. D. 1997. Reduced inhibitory effect of Mg2+ on ryanodine receptor-Ca2+ release channels in malignant hyperthermia. *Biophys J,* 73, 1913-24.

LAVER, D. R., RODEN, L. D., AHERN, G. P., EAGER, K. R., JUNANKAR, P. R. & DULHUNTY, A. F. 1995. Cytoplasmic Ca2+ inhibits the ryanodine receptor from cardiac muscle. *J Membr Biol,* 147, 7-22.

LI, J., XIA, Z. & DING, J. 2005. Thioredoxin-like domain of human kappa class glutathione transferase reveals sequence homology and structure similarity to the theta class enzyme. *Protein Sci,* 14, 2361-9.

LI, X. Q., ZHENG, Y. M., RATHORE, R., MA, J., TAKESHIMA, H. & WANG, Y. X. 2009. Genetic evidence for functional role of ryanodine receptor 1 in pulmonary artery smooth muscle cells. *Pflugers Arch,* 457, 771-83.

LI, Y., LI, D., ZENG, Z. & WANG, D. 2006. Trimeric structure of the wild soluble chloride intracellular ion channel CLIC4 observed in crystals. *Biochem Biophys Res Commun,* 343, 1272-8.

LIMAYE, D. A. & SHAIKH, Z. A. 1999. Cytotoxicity of cadmium and characteristics of its transport in cardiomyocytes. *Toxicol Appl Pharmacol,* 154, 59-66.

LINDSAY, M. A. 2002. Peptide-mediated cell delivery: application in protein target validation. *Curr Opin Pharmacol,* 2, 587-94.

LITTLER, D. R., ASSAAD, N. N., HARROP, S. J., BROWN, L. J., PANKHURST, G. J., LUCIANI, P., AGUILAR, M. I., MAZZANTI, M., BERRYMAN, M. A., BREIT, S. N. & CURMI, P. M. 2005. Crystal structure of the soluble form of the redox-regulated chloride ion channel protein CLIC4. *FEBS J,* 272, 4996-5007.

LITTLER, D. R., HARROP, S. J., FAIRLIE, W. D., BROWN, L. J., PANKHURST, G. J., PANKHURST, S., DEMAERE, M. Z., CAMPBELL, T. J., BAUSKIN, A. R., TONINI, R., MAZZANTI, M., BREIT, S. N. & CURMI, P. M. 2004. The intracellular chloride ion channel protein CLIC1 undergoes a redox-controlled structural transition. *J Biol Chem,* 279, 9298-305.

LIU, D., HEWAWASAM, R., PACE, S. M., GALLANT, E. M., CASAROTTO, M. G., DULHUNTY, A. F. & BOARD, P. G. 2009. Dissection of the inhibition of cardiac ryanodine receptors by human glutathione transferase GSTM2-2. *Biochem Pharmacol,* 77, 1181-93.

LIU D, H. R., CASAROTTO M, DULHUNTY AF, BOARD PG 2011. The inhibitory GSTM2-2 binding site is located in divergent region 3 of the cardiac ryanodine receptor. *J Biol Chem,* Under review.

LIU, N., COLOMBI, B., MEMMI, M., ZISSIMOPOULOS, S., RIZZI, N., NEGRI, S., IMBRIANI, M., NAPOLITANO, C., LAI, F. A. & PRIORI, S. G. 2006. Arrhythmogenesis in catecholaminergic polymorphic ventricular tachycardia: insights from a RyR2 R4496C knock-in mouse model. *Circ Res,* 99, 292-8.

LIU, S., ZHANG, P., JI, X., JOHNSON, W. W., GILLILAND, G. L. & ARMSTRONG, R. N. 1992. Contribution of tyrosine 6 to the catalytic mechanism of isoenzyme 3-3 of glutathione S-transferase. *J Biol Chem,* 267, 4296-9.

LIU, Z., WANG, R., ZHANG, J., CHEN, S. R. & WAGENKNECHT, T. 2005. Localization of a disease-associated mutation site in the three-dimensional structure of the cardiac muscle ryanodine receptor. *J Biol Chem,* 280, 37941-7.

LIU, Z., ZHANG, J., LI, P., CHEN, S. R. & WAGENKNECHT, T. 2002. Three-dimensional reconstruction of the recombinant type 2 ryanodine receptor and localization of its divergent region 1. *J Biol Chem,* 277, 46712-9.

LIU, Z., ZHANG, J., WANG, R., WAYNE CHEN, S. R. & WAGENKNECHT, T. 2004. Location of divergent region 2 on the three-dimensional structure of cardiac muscle ryanodine receptor/calcium release channel. *J Mol Biol,* 338, 533-45.

LOBO, P. A. & VAN PETEGEM, F. 2009. Crystal structures of the N-terminal domains of cardiac and skeletal muscle ryanodine receptors: insights into disease mutations. *Structure,* 17, 1505-14.

LU, X., XU, L. & MEISSNER, G. 1994. Activation of the skeletal muscle calcium release channel by a cytoplasmic loop of the dihydropyridine receptor. *J Biol Chem,* 269, 6511-6.

LUDTKE, S. J., SERYSHEVA, II, HAMILTON, S. L. & CHIU, W. 2005. The pore structure of the closed RyR1 channel. *Structure,* 13, 1203-11.

LUKYANENKO, V., SUBRAMANIAN, S., GYORKE, I., WIESNER, T. F. & GYORKE, S. 1999. The role of luminal Ca2+ in the generation of Ca2+ waves in rat ventricular myocytes. *J Physiol,* 518 (Pt 1), 173-86.

MA, J. 1993. Block by ruthenium red of the ryanodine-activated calcium release channel of skeletal muscle. *J Gen Physiol,* 102, 1031-56.

MA, J. 1995. Desensitization of the skeletal muscle ryanodine receptor: evidence for heterogeneity of calcium release channels. *Biophys J,* 68, 893-9.

MACKRILL, J. J. 2010. Ryanodine receptor calcium channels and their partners as drug targets. *Biochem Pharmacol,* 79, 1535-43.

MALTSEV, V. A., VINOGRADOVA, T. M. & LAKATTA, E. G. 2006. The emergence of a general theory of the initiation and strength of the heartbeat. *J Pharmacol Sci,* 100, 338-69.

MANNERVIK, B., ALIN, P., GUTHENBERG, C., JENSSON, H., TAHIR, M. K., WARHOLM, M. & JORNVALL, H. 1985. Identification of three classes of cytosolic glutathione transferase common to several mammalian species: correlation between structural data and enzymatic properties. *Proc Natl Acad Sci U S A,* 82, 7202-6.

MANNERVIK, B., AWASTHI, Y. C., BOARD, P. G., HAYES, J. D., DI ILIO, C., KETTERER, B., LISTOWSKY, I., MORGENSTERN, R., MURAMATSU, M., PEARSON, W. R. & ET AL. 1992. Nomenclature for human glutathione transferases. *Biochem J,* 282 (Pt 1), 305-6.

MANNERVIK, B. & DANIELSON, U. H. 1988. Glutathione transferases--structure and catalytic activity. *CRC Crit Rev Biochem,* 23, 283-337.

MARIEB EM, H. K. 2010. *Human Anatomy and Physiology,* Sanfrancisco, USA, Pearson Education, Inc.

MARKS, A. R. 1996. Cellular functions of immunophilins. *Physiol Rev,* 76, 631-49.

MARKS, A. R. 2001. Ryanodine receptors/calcium release channels in heart failure and sudden cardiac death. *J Mol Cell Cardiol,* 33, 615-24.

MARKS, A. R., TEMPST, P., HWANG, K. S., TAUBMAN, M. B., INUI, M., CHADWICK, C., FLEISCHER, S. & NADAL-GINARD, B. 1989. Molecular cloning and characterization of the ryanodine receptor/junctional channel complex cDNA from skeletal muscle sarcoplasmic reticulum. *Proc Natl Acad Sci U S A,* 86, 8683-7.

MARX, S. O., GABURJAKOVA, J., GABURJAKOVA, M., HENRIKSON, C., ONDRIAS, K. & MARKS, A. R. 2001. Coupled gating between cardiac calcium release channels (ryanodine receptors). *Circ Res,* 88, 1151-8.

MARX, S. O., ONDRIAS, K. & MARKS, A. R. 1998. Coupled gating between individual skeletal muscle Ca2+ release channels (ryanodine receptors). *Science,* 281, 818-21.

MARX, S. O., REIKEN, S., HISAMATSU, Y., JAYARAMAN, T., BURKHOFF, D., ROSEMBLIT, N. & MARKS, A. R. 2000. PKA phosphorylation dissociates FKBP12.6 from the calcium release channel (ryanodine receptor): defective regulation in failing hearts. *Cell,* 101, 365-76.

MASUMIYA, H., WANG, R., ZHANG, J., XIAO, B. & CHEN, S. R. 2003. Localization of the 12.6-kDa FK506-binding protein (FKBP12.6) binding site to the NH2-terminal domain of the cardiac Ca2+ release channel (ryanodine receptor). *J Biol Chem,* 278, 3786-92.

MCCALL, E., LI, L., SATOH, H., SHANNON, T. R., BLATTER, L. A. & BERS, D. M. 1996. Effects of FK-506 on contraction and Ca2+ transients in rat cardiac myocytes. *Circ Res,* 79, 1110-21.

MCGREW, S. G., WOLLEBEN, C., SIEGL, P., INUI, M. & FLEISCHER, S. 1989. Positive cooperativity of ryanodine binding to the calcium release channel of sarcoplasmic reticulum from heart and skeletal muscle. *Biochemistry,* 28, 1686-91.

MEISSNER, G. 1984. Adenine nucleotide stimulation of Ca2+-induced Ca2+ release in sarcoplasmic reticulum. *J Biol Chem,* 259, 2365-74.

MEISSNER, G. 1986. Ryanodine activation and inhibition of the Ca2+ release channel of sarcoplasmic reticulum. *J Biol Chem,* 261, 6300-6.

MEISSNER, G. 2002. Regulation of mammalian ryanodine receptors. *Front Biosci,* 7, d2072-80.

MEISSNER, G., DARLING, E. & EVELETH, J. 1986. Kinetics of rapid Ca2+ release by sarcoplasmic reticulum. Effects of Ca2+, Mg2+, and adenine nucleotides. *Biochemistry,* 25, 236-44.

MEISSNER, G. & HENDERSON, J. S. 1987. Rapid calcium release from cardiac sarcoplasmic reticulum vesicles is dependent on Ca2+ and is

modulated by Mg2+, adenine nucleotide, and calmodulin. *J Biol Chem,* 262, 3065-73.

MEISSNER, G., RIOS, E., TRIPATHY, A. & PASEK, D. A. 1997. Regulation of skeletal muscle Ca2+ release channel (ryanodine receptor) by Ca2+ and monovalent cations and anions. *J Biol Chem,* 272, 1628-38.

MENG, X., WANG, G., VIERO, C., WANG, Q., MI, W., SU, X. D., WAGENKNECHT, T., WILLIAMS, A. J., LIU, Z. & YIN, C. C. 2009. CLIC2-RyR1 interaction and structural characterization by cryo-electron microscopy. *J Mol Biol,* 387, 320-34.

MENG, X., XIAO, B., CAI, S., HUANG, X., LI, F., BOLSTAD, J., TRUJILLO, R., AIREY, J., CHEN, S. R., WAGENKNECHT, T. & LIU, Z. 2007. Three-dimensional localization of serine 2808, a phosphorylation site in cardiac ryanodine receptor. *J Biol Chem,* 282, 25929-39.

MIKOSHIBA, K. 2007. IP3 receptor/Ca2+ channel: from discovery to new signaling concepts. *J Neurochem,* 102, 1426-46.

MILLER, C. & RACKER, E. 1976. Ca++-induced fusion of fragmented sarcoplasmic reticulum with artificial planar bilayers. *J Membr Biol,* 30, 283-300.

MILTING, H., LUKAS, N., KLAUKE, B., KORFER, R., PERROT, A., OSTERZIEL, K. J., VOGT, J., PETERS, S., THIELECZEK, R. & VARSANYI, M. 2006. Composite polymorphisms in the ryanodine receptor 2 gene associated with arrhythmogenic right ventricular cardiomyopathy. *Cardiovasc Res,* 71, 496-505.

MOHAMED, U., NAPOLITANO, C. & PRIORI, S. G. 2007. Molecular and electrophysiological bases of catecholaminergic polymorphic ventricular tachycardia. *J Cardiovasc Electrophysiol,* 18, 791-7.

MOREL, F., RAUCH, C., PETIT, E., PITON, A., THERET, N., COLES, B. & GUILLOUZO, A. 2004. Gene and protein characterization of the human glutathione S-transferase kappa and evidence for a peroxisomal localization. *J Biol Chem,* 279, 16246-53.

MORI, F., FUKAYA, M., ABE, H., WAKABAYASHI, K. & WATANABE, M. 2000. Developmental changes in expression of the three ryanodine receptor mRNAs in the mouse brain. *Neurosci Lett,* 285, 57-60.

MORRIS, M. J., CRAIG, S. J., SUTHERLAND, T. M., BOARD, P. G. & CASAROTTO, M. G. 2009. Transport of glutathione transferase-fold structured proteins into living cells. *Biochim Biophys Acta,* 1788, 676-85.

MORRIS, M. J., LIU, D., WEAVER, L. M., BOARD, P. G. & CASAROTTO, M. G. 2011. A structural basis for cellular uptake of GST-fold proteins. *PLoS One,* 6, e17864.

MUKHERJEE, R., CRAWFORD, F. A., HEWETT, K. W. & SPINALE, F. G. 1993. Cell and sarcomere contractile performance from the same cardiocyte using video microscopy. *J Appl Physiol,* 74, 2023-33.

MURPHY, R. M., MOLLICA, J. P., BEARD, N. A., KNOLLMANN, B. C. & LAMB, G. D. 2010. Quantification of calsequestrin 2 (CSQ2) in sheep cardiac

muscle and Ca2+-binding protein changes in CSQ2-knockout mice. *Am J Physiol Heart Circ Physiol.*

MURRAY, B. E. & OHLENDIECK, K. 1997. Cross-linking analysis of the ryanodine receptor and alpha1-dihydropyridine receptor in rabbit skeletal muscle triads. *Biochem J,* 324 (Pt 2), 689-96.

NAKAI, J., GAO, L., XU, L., XIN, C., PASEK, D. A. & MEISSNER, G. 1999. Evidence for a role of C-terminus in Ca(2+) inactivation of skeletal muscle Ca(2+) release channel (ryanodine receptor). *FEBS Lett,* 459, 154-8.

NAKAI, J., IMAGAWA, T., HAKAMAT, Y., SHIGEKAWA, M., TAKESHIMA, H. & NUMA, S. 1990. Primary structure and functional expression from cDNA of the cardiac ryanodine receptor/calcium release channel. *FEBS Lett,* 271, 169-77.

NAKAI, J., SEKIGUCHI, N., RANDO, T. A., ALLEN, P. D. & BEAM, K. G. 1998. Two regions of the ryanodine receptor involved in coupling with L-type Ca2+ channels. *J Biol Chem,* 273, 13403-6.

NAKAI, J., TANABE, T., KONNO, T., ADAMS, B. & BEAM, K. G. 1998. Localization in the II-III loop of the dihydropyridine receptor of a sequence critical for excitation-contraction coupling. *J Biol Chem,* 273, 24983-6.

NAKANISHI, T., SEGUCHI, M. & TAKAO, A. 1988. Development of the myocardial contractile system. *Experientia,* 44, 936-44.

NAYLER, W. G., DAILE, P., CHIPPERFIELD, D. & GAN, K. 1970. Effect of ryanodine on calcium in cardiac muscle. *Am J Physiol,* 219, 1620-6.

NELSON, T. E. 1987. Ryanodine: antithetical calcium channel effects in skeletal muscle sarcoplasmic reticulum. *J Pharmacol Exp Ther,* 242, 56-61.

NISHIE, I., ANZAI, K., YAMAMOTO, T. & KIRINO, Y. 1990. Measurement of steady-state Ca2+ pump current caused by purified Ca2(+)-ATPase of sarcoplasmic reticulum incorporated into a planar bilayer lipid membrane. *J Biol Chem,* 265, 2488-91.

NOGUCHI, N., YOSHIKAWA, T., IKEDA, T., TAKAHASHI, I., SHERVANI, N. J., URUNO, A., YAMAUCHI, A., NATA, K., TAKASAWA, S., OKAMOTO, H. & SUGAWARA, A. 2008. FKBP12.6 disruption impairs glucose-induced insulin secretion. *Biochem Biophys Res Commun,* 371, 735-40.

NOMA, A. 1996. Ionic mechanisms of the cardiac pacemaker potential. *Jpn Heart J,* 37, 673-82.

OETLIKER, H. 1982. An appraisal of the evidence for a sarcoplasmic reticulum membrane potential and its relation to calcium release in skeletal muscle. *J Muscle Res Cell Motil,* 3, 247-72.

OGAWA, Y., KUREBAYASHI, N. & MURAYAMA, T. 2000. Putative roles of type 3 ryanodine receptor isoforms (RyR3). *Trends Cardiovasc Med,* 10, 65-70.

ORLOVA, E. V., SERYSHEVA, II, VAN HEEL, M., HAMILTON, S. L. & CHIU,

W. 1996. Two structural configurations of the skeletal muscle calcium release channel. *Nat Struct Biol,* 3, 547-52.

OTSU, K., WILLARD, H. F., KHANNA, V. K., ZORZATO, F., GREEN, N. M. & MACLENNAN, D. H. 1990. Molecular cloning of cDNA encoding the Ca2+ release channel (ryanodine receptor) of rabbit cardiac muscle sarcoplasmic reticulum. *J Biol Chem,* 265, 13472-83.

PARK, H., PARK, I. Y., KIM, E., YOUN, B., FIELDS, K., DUNKER, A. K. & KANG, C. 2004. Comparing skeletal and cardiac calsequestrin structures and their calcium binding: a proposed mechanism for coupled calcium binding and protein polymerization. *J Biol Chem,* 279, 18026-33.

PATSKOVSKY, Y. V., PATSKOVSKA, L. N. & LISTOWSKY, I. 1999. An asparagine-phenylalanine substitution accounts for catalytic differences between hGSTM3-3 and other human class mu glutathione S-transferases. *Biochemistry,* 38, 16187-94.

PATSKOVSKY, Y. V., PATSKOVSKA, L. N. & LISTOWSKY, I. 1999. Functions of His107 in the catalytic mechanism of human glutathione S-transferase hGSTM1a-1a. *Biochemistry,* 38, 1193-202.

PAUL-PLETZER, K., YAMAMOTO, T., BHAT, M. B., MA, J., IKEMOTO, N., JIMENEZ, L. S., MORIMOTO, H., WILLIAMS, P. G. & PARNESS, J. 2002. Identification of a dantrolene-binding sequence on the skeletal muscle ryanodine receptor. *J Biol Chem,* 277, 34918-23.

PAUL-PLETZER, K., YAMAMOTO, T., IKEMOTO, N., JIMENEZ, L. S., MORIMOTO, H., WILLIAMS, P. G., MA, J. & PARNESS, J. 2005. Probing a putative dantrolene-binding site on the cardiac ryanodine receptor. *Biochem J,* 387, 905-9.

PEMBLE, S. E., WARDLE, A. F. & TAYLOR, J. B. 1996. Glutathione S-transferase class Kappa: characterization by the cloning of rat mitochondrial GST and identification of a human homologue. *Biochem J,* 319 (Pt 3), 749-54.

PENINGTON, C. J. & RULE, G. S. 1992. Application of site-directed mutagenesis in nuclear magnetic resonance spectroscopy. *Biophys J,* 62, 116-8.

PENINGTON, C. J. & RULE, G. S. 1992. Use of petroleum jelly for sealing coverslips in crystallization trials. *Biotechniques,* 12, 833.

PENPARGKUL, S. 1979. Effects of adenine nucleotides on calcium binding by rat heart sarcoplasmic reticulum. *Cardiovasc Res,* 13, 243-53.

PEREZ, C. F., MUKHERJEE, S. & ALLEN, P. D. 2003. Amino acids 1-1,680 of ryanodine receptor type 1 hold critical determinants of skeletal type for excitation-contraction coupling. Role of divergence domain D2. *J Biol Chem,* 278, 39644-52.

POLEKHINA, G., BOARD, P. G., BLACKBURN, A. C. & PARKER, M. W. 2001. Crystal structure of maleylacetoacetate isomerase/glutathione transferase zeta reveals the molecular basis for its remarkable catalytic promiscuity. *Biochemistry,* 40, 1567-76.

POULIQUIN, P., PACE, S. M., CURTIS, S. M., HARVEY, P. J., GALLANT, E. M., ZORZATO, F., CASAROTTO, M. G. & DULHUNTY, A. F. 2006. Effects of an alpha-helical ryanodine receptor C-terminal tail peptide on ryanodine receptor activity: modulation by Homer. *Int J Biochem Cell Biol,* 38, 1700-15.

POWERS, S. K., MURLASITS, Z., WU, M. & KAVAZIS, A. N. 2007. Ischemia-reperfusion-induced cardiac injury: a brief review. *Med Sci Sports Exerc,* 39, 1529-36.

PROENZA, C., O'BRIEN, J., NAKAI, J., MUKHERJEE, S., ALLEN, P. D. & BEAM, K. G. 2002. Identification of a region of RyR1 that participates in allosteric coupling with the alpha(1S) (Ca(V)1.1) II-III loop. *J Biol Chem,* 277, 6530-5.

RADERMACHER, M., RAO, V., GRASSUCCI, R., FRANK, J., TIMERMAN, A. P., FLEISCHER, S. & WAGENKNECHT, T. 1994. Cryo-electron microscopy and three-dimensional reconstruction of the calcium release channel/ryanodine receptor from skeletal muscle. *J Cell Biol,* 127, 411-23.

RAGHUNATHAN, S., CHANDROSS, R. J., KRETSINGER, R. H., ALLISON, T. J., PENINGTON, C. J. & RULE, G. S. 1994. Crystal structure of human class mu glutathione transferase GSTM2-2. Effects of lattice packing on conformational heterogeneity. *J Mol Biol,* 238, 815-32.

RAGUPATHI, M., PATEL, C. B., RAMOS-VALADEZ, D. I. & HAAS, E. M. 2010. Robotic-assisted laparoscopic "salvage" rectopexy for recurrent ileoanal J-pouch prolapse. *Gastroenterol Res Pract,* 2010, 790462.

REINEMER, P., DIRR, H. W., LADENSTEIN, R., HUBER, R., LO BELLO, M., FEDERICI, G. & PARKER, M. W. 1992. Three-dimensional structure of class pi glutathione S-transferase from human placenta in complex with S-hexylglutathione at 2.8 A resolution. *J Mol Biol,* 227, 214-26.

REINEMER, P., DIRR, H. W., LADENSTEIN, R., SCHAFFER, J., GALLAY, O. & HUBER, R. 1991. The three-dimensional structure of class pi glutathione S-transferase in complex with glutathione sulfonate at 2.3 A resolution. *EMBO J,* 10, 1997-2005.

RINGER, S. 1883. A further Contribution regarding the influence of the different Constituents of the Blood on the Contraction of the Heart. *J Physiol,* 4, 29-42 3.

RINGER, S. 1883. A third contribution regarding the Influence of the Inorganic Constituents of the Blood on the Ventricular Contraction. *J Physiol,* 4, 222-5.

RIOS, E., LAUNIKONIS, B. S., ROYER, L., BRUM, G. & ZHOU, J. 2006. The elusive role of store depletion in the control of intracellular calcium release. *J Muscle Res Cell Motil,* 27, 337-50.

ROBERT, B., LEVY,M., KOEPPEN,B., STANTON,B 2004. *Physiology*, Elsevier Mosby.

ROBINSON, A., HUTTLEY, G. A., BOOTH, H. S. & BOARD, P. G. 2004.

Modelling and bioinformatics studies of the human Kappa-class glutathione transferase predict a novel third glutathione transferase family with similarity to prokaryotic 2-hydroxychromene-2-carboxylate isomerases. *Biochem J,* 379, 541-52.

ROSS, V. L. & BOARD, P. G. 1993. Molecular cloning and heterologous expression of an alternatively spliced human Mu class glutathione S-transferase transcript. *Biochem J,* 294 (Pt 2), 373-80.

ROSSJOHN, J., MCKINSTRY, W. J., OAKLEY, A. J., VERGER, D., FLANAGAN, J., CHELVANAYAGAM, G., TAN, K. L., BOARD, P. G. & PARKER, M. W. 1998. Human theta class glutathione transferase: the crystal structure reveals a sulfate-binding pocket within a buried active site. *Structure,* 6, 309-22.

ROUSSEAU, E., MICHAUD, C., LEFEBVRE, D., PROTEAU, S. & DECROUY, A. 1996. Reconstitution of ionic channels from inner and outer membranes of mammalian cardiac nuclei. *Biophys J,* 70, 703-14.

ROUSSEAU, E., PINKOS, J. & SAVARIA, D. 1992. Functional sensitivity of the native skeletal Ca(2+)-release channel to divalent cations and the Mg-ATP complex. *Can J Physiol Pharmacol,* 70, 394-402.

ROWE, J. D., PATSKOVSKY, Y. V., PATSKOVSKA, L. N., NOVIKOVA, E. & LISTOWSKY, I. 1998. Rationale for reclassification of a distinctive subdivision of mammalian class Mu glutathione S-transferases that are primarily expressed in testis. *J Biol Chem,* 273, 9593-601.

RYCHKOV, G. Y., PUSCH, M., ROBERTS, M. L., JENTSCH, T. J. & BRETAG, A. H. 1998. Permeation and block of the skeletal muscle chloride channel, CIC-1, by foreign anions. *J Gen Physiol,* 111, 653-65.

SAITO, A., SEILER, S., CHU, A. & FLEISCHER, S. 1984. Preparation and morphology of sarcoplasmic reticulum terminal cisternae from rabbit skeletal muscle. *J Cell Biol,* 99, 875-85.

SAMBROOK, J., FRITSCH,EF., MANIATIS,T 1989. *Molecular cloning: A laboratory manual,* New York, Cold Spring Harbour Laboratory.

SAMSO, M., SHEN, X. & ALLEN, P. D. 2006. Structural characterization of the RyR1-FKBP12 interaction. *J Mol Biol,* 356, 917-27.

SAMSO, M. & WAGENKNECHT, T. 2002. Apocalmodulin and Ca2+-calmodulin bind to neighboring locations on the ryanodine receptor. *J Biol Chem,* 277, 1349-53.

SAMSO, M., WAGENKNECHT, T. & ALLEN, P. D. 2005. Internal structure and visualization of transmembrane domains of the RyR1 calcium release channel by cryo-EM. *Nat Struct Mol Biol,* 12, 539-44.

SANDERS, L., RAKOVIC, S., LOWE, M., MATTICK, P. A. & TERRAR, D. A. 2006. Fundamental importance of Na+-Ca2+ exchange for the pacemaking mechanism in guinea-pig sino-atrial node. *J Physiol,* 571, 639-49.

SAWYER, D. B., SIWIK, D. A., XIAO, L., PIMENTEL, D. R., SINGH, K. & COLUCCI, W. S. 2002. Role of oxidative stress in myocardial

hypertrophy and failure. *J Mol Cell Cardiol,* 34, 379-88.

SCHIENE-FISCHER, C. & YU, C. 2001. Receptor accessory folding helper enzymes: the functional role of peptidyl prolyl cis/trans isomerases. *FEBS Lett,* 495, 1-6.

SERYSHEVA, II, HAMILTON, S. L., CHIU, W. & LUDTKE, S. J. 2005. Structure of Ca2+ release channel at 14 A resolution. *J Mol Biol,* 345, 427-31.

SERYSHEVA, II, SCHATZ, M., VAN HEEL, M., CHIU, W. & HAMILTON, S. L. 1999. Structure of the skeletal muscle calcium release channel activated with Ca2+ and AMP-PCP. *Biophys J,* 77, 1936-44.

SHARMA, M. R., JEYAKUMAR, L. H., FLEISCHER, S. & WAGENKNECHT, T. 2000. Three-dimensional structure of ryanodine receptor isoform three in two conformational states as visualized by cryo-electron microscopy. *J Biol Chem,* 275, 9485-91.

SHARMA, M. R., PENCZEK, P., GRASSUCCI, R., XIN, H. B., FLEISCHER, S. & WAGENKNECHT, T. 1998. Cryoelectron microscopy and image analysis of the cardiac ryanodine receptor. *J Biol Chem,* 273, 18429-34.

SHEEHAN, D., MEADE, G., FOLEY, V. M. & DOWD, C. A. 2001. Structure, function and evolution of glutathione transferases: implications for classification of non-mammalian members of an ancient enzyme superfamily. *Biochem J,* 360, 1-16.

SHOSHAN-BARMATZ, V., HADAD-HALFON, N. & OSTERSETZER, O. 1995. Cross-linking of the ryanodine receptor/Ca2+ release channel from skeletal muscle. *Biochim Biophys Acta,* 1237, 151-61.

SHOSHAN-BARMATZ, V. & ZCHUT, S. 1993. The interaction of local anesthetics with the ryanodine receptor of the sarcoplasmic reticulum. *J Membr Biol,* 133, 171-81.

SINGHAL, A. K., CHIEN, K. Y., WU, W. G. & RULE, G. S. 1993. Solution structure of cardiotoxin V from Naja naja atra. *Biochemistry,* 32, 8036-44.

SINNING, I., KLEYWEGT, G. J., COWAN, S. W., REINEMER, P., DIRR, H. W., HUBER, R., GILLILAND, G. L., ARMSTRONG, R. N., JI, X., BOARD, P. G. & ET AL. 1993. Structure determination and refinement of human alpha class glutathione transferase A1-1, and a comparison with the Mu and Pi class enzymes. *J Mol Biol,* 232, 192-212.

SITSAPESAN, R. & WILLIAMS, A. J. 1995. The gating of the sheep skeletal sarcoplasmic reticulum Ca(2+)-release channel is regulated by luminal Ca2+. *J Membr Biol,* 146, 133-44.

SITSAPESAN, R. & WILLIAMS, A. J. 1997. Regulation of current flow through ryanodine receptors by luminal Ca2+. *J Membr Biol,* 159, 179-85.

SMITH, J. S., CORONADO, R. & MEISSNER, G. 1985. Sarcoplasmic reticulum contains adenine nucleotide-activated calcium channels. *Nature,* 316, 446-9.

SMITH, J. S., IMAGAWA, T., MA, J., FILL, M., CAMPBELL, K. P. & CORONADO, R. 1988. Purified ryanodine receptor from rabbit skeletal

muscle is the calcium-release channel of sarcoplasmic reticulum. *J Gen Physiol,* 92, 1-26.

SMITH, P. K., KROHN, R. I., HERMANSON, G. T., MALLIA, A. K., GARTNER, F. H., PROVENZANO, M. D., FUJIMOTO, E. K., GOEKE, N. M., OLSON, B. J. & KLENK, D. C. 1985. Measurement of protein using bicinchoninic acid. *Anal Biochem,* 150, 76-85.

SONG, D. W., LEE, J. G., YOUN, H. S., EOM, S. H. & KIM DO, H. 2011. Ryanodine receptor assembly: a novel systems biology approach to 3D mapping. *Prog Biophys Mol Biol,* 105, 145-61.

SONNLEITNER, A., FLEISCHER, S. & SCHINDLER, H. 1997. Gating of the skeletal calcium release channel by ATP is inhibited by protein phosphatase 1 but not by Mg2+. *Cell Calcium,* 21, 283-90.

SORRENTINO, V. & VOLPE, P. 1993. Ryanodine receptors: how many, where and why? *Trends Pharmacol Sci,* 14, 98-103.

STOKES, D. L. & WAGENKNECHT, T. 2000. Calcium transport across the sarcoplasmic reticulum: structure and function of Ca2+-ATPase and the ryanodine receptor. *Eur J Biochem,* 267, 5274-9.

STRANGE, R. C., HOWIE, A. F., HUME, R., MATHAROO, B., BELL, J., HILEY, C., JONES, P. & BECKETT, G. J. 1989. The development expression of alpha-, mu- and pi-class glutathione S-transferases in human liver. *Biochim Biophys Acta,* 993, 186-90.

SUKO, J., MAURER-FOGY, I., PLANK, B., BERTEL, O., WYSKOVSKY, W., HOHENEGGER, M. & HELLMANN, G. 1993. Phosphorylation of serine 2843 in ryanodine receptor-calcium release channel of skeletal muscle by cAMP-, cGMP- and CaM-dependent protein kinase. *Biochim Biophys Acta,* 1175, 193-206.

SUN, X. H., PROTASI, F., TAKAHASHI, M., TAKESHIMA, H., FERGUSON, D. G. & FRANZINI-ARMSTRONG, C. 1995. Molecular architecture of membranes involved in excitation-contraction coupling of cardiac muscle. *J Cell Biol,* 129, 659-71.

SUZUKI, T., COGGAN, M., SHAW, D. C. & BOARD, P. G. 1987. Electrophoretic and immunological analysis of human glutathione S-transferase isozymes. *Ann Hum Genet,* 51, 95-106.

SZEGEDI, C., SARKOZI, S., HERZOG, A., JONA, I. & VARSANYI, M. 1999. Calsequestrin: more than 'only' a luminal Ca2+ buffer inside the sarcoplasmic reticulum. *Biochem J,* 337 (Pt 1), 19-22.

TAKASAGO, T., IMAGAWA, T., FURUKAWA, K., OGURUSU, T. & SHIGEKAWA, M. 1991. Regulation of the cardiac ryanodine receptor by protein kinase-dependent phosphorylation. *J Biochem,* 109, 163-70.

TAKESHIMA, H. 1993. Primary structure and expression from cDNAs of the ryanodine receptor. *Ann N Y Acad Sci,* 707, 165-77.

TAKESHIMA, H., NISHIMURA, S., MATSUMOTO, T., ISHIDA, H., KANGAWA, K., MINAMINO, N., MATSUO, H., UEDA, M., HANAOKA, M., HIROSE, T. & ET AL. 1989. Primary structure and expression from complementary

DNA of skeletal muscle ryanodine receptor. *Nature,* 339, 439-45.

TAKESHIMA, H., YAMAZAWA, T., IKEMOTO, T., TAKEKURA, H., NISHI, M., NODA, T. & IINO, M. 1995. Ca(2+)-induced Ca2+ release in myocytes from dyspedic mice lacking the type-1 ryanodine receptor. *EMBO J,* 14, 2999-3006.

TANABE, T., BEAM, K. G., ADAMS, B. A., NIIDOME, T. & NUMA, S. 1990. Regions of the skeletal muscle dihydropyridine receptor critical for excitation-contraction coupling. *Nature,* 346, 567-9.

TERENTYEV, D., CALA, S. E., HOULE, T. D., VIATCHENKO-KARPINSKI, S., GYORKE, I., TERENTYEVA, R., WILLIAMS, S. C. & GYORKE, S. 2005. Triadin overexpression stimulates excitation-contraction coupling and increases predisposition to cellular arrhythmia in cardiac myocytes. *Circ Res,* 96, 651-8.

TERENTYEV, D., GYORKE, I., BELEVYCH, A. E., TERENTYEVA, R., SRIDHAR, A., NISHIJIMA, Y., DE BLANCO, E. C., KHANNA, S., SEN, C. K., CARDOUNEL, A. J., CARNES, C. A. & GYORKE, S. 2008. Redox modification of ryanodine receptors contributes to sarcoplasmic reticulum Ca2+ leak in chronic heart failure. *Circ Res,* 103, 1466-72.

TERENTYEV, D., NORI, A., SANTORO, M., VIATCHENKO-KARPINSKI, S., KUBALOVA, Z., GYORKE, I., TERENTYEVA, R., VEDAMOORTHYRAO, S., BLOM, N. A., VALLE, G., NAPOLITANO, C., WILLIAMS, S. C., VOLPE, P., PRIORI, S. G. & GYORKE, S. 2006. Abnormal interactions of calsequestrin with the ryanodine receptor calcium release channel complex linked to exercise-induced sudden cardiac death. *Circ Res,* 98, 1151-8.

TERENTYEV, D., VIATCHENKO-KARPINSKI, S., GYORKE, I., VOLPE, P., WILLIAMS, S. C. & GYORKE, S. 2003. Calsequestrin determines the functional size and stability of cardiac intracellular calcium stores: Mechanism for hereditary arrhythmia. *Proc Natl Acad Sci U S A,* 100, 11759-64.

TIMERMAN, A. P., JAYARAMAN, T., WIEDERRECHT, G., ONOUE, H., MARKS, A. R. & FLEISCHER, S. 1994. The ryanodine receptor from canine heart sarcoplasmic reticulum is associated with a novel FK-506 binding protein. *Biochem Biophys Res Commun,* 198, 701-6.

TIMERMAN, A. P., OGUNBUMNI, E., FREUND, E., WIEDERRECHT, G., MARKS, A. R. & FLEISCHER, S. 1993. The calcium release channel of sarcoplasmic reticulum is modulated by FK-506-binding protein. Dissociation and reconstitution of FKBP-12 to the calcium release channel of skeletal muscle sarcoplasmic reticulum. *J Biol Chem,* 268, 22992-9.

TIMERMAN, A. P., ONOUE, H., XIN, H. B., BARG, S., COPELLO, J., WIEDERRECHT, G. & FLEISCHER, S. 1996. Selective binding of FKBP12.6 by the cardiac ryanodine receptor. *J Biol Chem,* 271, 20385-91.

TINKER, A., LINDSAY, A. R. & WILLIAMS, A. J. 1992. A model for ionic

conduction in the ryanodine receptor channel of sheep cardiac muscle sarcoplasmic reticulum. *J Gen Physiol,* 100, 495-517.

TONINI, R., FERRONI, A., VALENZUELA, S. M., WARTON, K., CAMPBELL, T. J., BREIT, S. N. & MAZZANTI, M. 2000. Functional characterization of the NCC27 nuclear protein in stable transfected CHO-K1 cells. *FASEB J,* 14, 1171-8.

TRAFFORD, A. W., DIAZ, M. E. & EISNER, D. A. 1998. Stimulation of Ca-induced Ca release only transiently increases the systolic Ca transient: measurements of Ca fluxes and sarcoplasmic reticulum Ca. *Cardiovasc Res,* 37, 710-7.

TRAFFORD, A. W., SIBBRING, G. C., DIAZ, M. E. & EISNER, D. A. 2000. The effects of low concentrations of caffeine on spontaneous Ca release in isolated rat ventricular myocytes. *Cell Calcium,* 28, 269-76.

TU, J. C., XIAO, B., YUAN, J. P., LANAHAN, A. A., LEOFFERT, K., LI, M., LINDEN, D. J. & WORLEY, P. F. 1998. Homer binds a novel proline-rich motif and links group 1 metabotropic glutamate receptors with IP3 receptors. *Neuron,* 21, 717-26.

TUNG, C. C., LOBO, P. A., KIMLICKA, L. & VAN PETEGEM, F. 2010. The amino-terminal disease hotspot of ryanodine receptors forms a cytoplasmic vestibule. *Nature,* 468, 585-8.

UCHINOUMI, H., YANO, M., SUETOMI, T., ONO, M., XU, X., TATEISHI, H., ODA, T., OKUDA, S., DOI, M., KOBAYASHI, S., YAMAMOTO, T., IKEDA, Y., OHKUSA, T., IKEMOTO, N. & MATSUZAKI, M. 2010. Catecholaminergic polymorphic ventricular tachycardia is caused by mutation-linked defective conformational regulation of the ryanodine receptor. *Circ Res,* 106, 1413-24.

UEMURA, Y., LIU, T. Y., NARITA, Y., SUZUKI, M., OHSHIMA, S., MIZUKAMI, S., ICHIHARA, Y., KIKUCHI, H. & MATSUSHITA, S. 2007. Identification of functional type 1 ryanodine receptors in human dendritic cells. *Biochem Biophys Res Commun,* 362, 510-5.

VALDIVIA, H. H., KAPLAN, J. H., ELLIS-DAVIES, G. C. & LEDERER, W. J. 1995. Rapid adaptation of cardiac ryanodine receptors: modulation by Mg2+ and phosphorylation. *Science,* 267, 1997-2000.

VALENZUELA, S. M., MAZZANTI, M., TONINI, R., QIU, M. R., WARTON, K., MUSGROVE, E. A., CAMPBELL, T. J. & BREIT, S. N. 2000. The nuclear chloride ion channel NCC27 is involved in regulation of the cell cycle. *J Physiol,* 529 Pt 3, 541-52.

VALLOT, O., COMBETTES, L., JOURDON, P., INAMO, J., MARTY, I., CLARET, M. & LOMPRE, A. M. 2000. Intracellular Ca(2+) handling in vascular smooth muscle cells is affected by proliferation. *Arterioscler Thromb Vasc Biol,* 20, 1225-35.

VAN DEN BOSCH, L., VERHOEVEN, K., DE SMEDT, H., WUYTACK, F., MISSIAEN, L. & ROBBERECHT, W. 1999. Calcium handling proteins in isolated spinal motoneurons. *Life Sci,* 65, 1597-606.

VAN DER WERF, F., BALJET, B., PRINS, M., TIMMERMAN, A. & OTTO, J. A. 1993. Innervation of the superior tarsal (Muller's) muscle in the cynomolgus monkey: a retrograde tracing study. *Invest Ophthalmol Vis Sci,* 34, 2333-40.

VARSANYI, M. & MEYER, H. E. 1995. Sarcoplasmic reticular Ca2+ release channel is phosphorylated at serine 2843 in intact rabbit skeletal muscle. *Biol Chem Hoppe Seyler,* 376, 45-9.

VASSILOPOULOS, S., THEVENON, D., REZGUI, S. S., BROCARD, J., CHAPEL, A., LACAMPAGNE, A., LUNARDI, J., DEWAARD, M. & MARTY, I. 2005. Triadins are not triad-specific proteins: two new skeletal muscle triadins possibly involved in the architecture of sarcoplasmic reticulum. *J Biol Chem,* 280, 28601-9.

VASSORT, G., TALAVERA, K. & ALVAREZ, J. L. 2006. Role of T-type Ca2+ channels in the heart. *Cell Calcium,* 40, 205-20.

VERKERK, A. O., WILDERS, R., VAN BORREN, M. M., PETERS, R. J., BROEKHUIS, E., LAM, K., CORONEL, R., DE BAKKER, J. M. & TAN, H. L. 2007. Pacemaker current (I(f)) in the human sinoatrial node. *Eur Heart J,* 28, 2472-8.

VIATCHENKO-KARPINSKI, S., TERENTYEV, D., GYORKE, I., TERENTYEVA, R., VOLPE, P., PRIORI, S. G., NAPOLITANO, C., NORI, A., WILLIAMS, S. C. & GYORKE, S. 2004. Abnormal calcium signaling and sudden cardiac death associated with mutation of calsequestrin. *Circ Res,* 94, 471-7.

WAGENKNECHT, T., GRASSUCCI, R., BERKOWITZ, J., WIEDERRECHT, G. J., XIN, H. B. & FLEISCHER, S. 1996. Cryoelectron microscopy resolves FK506-binding protein sites on the skeletal muscle ryanodine receptor. *Biophys J,* 70, 1709-15.

WAGENKNECHT, T., HSIEH, C. E., RATH, B. K., FLEISCHER, S. & MARKO, M. 2002. Electron tomography of frozen-hydrated isolated triad junctions. *Biophys J,* 83, 2491-501.

WAGENKNECHT, T., RADERMACHER, M., GRASSUCCI, R., BERKOWITZ, J., XIN, H. B. & FLEISCHER, S. 1997. Locations of calmodulin and FK506-binding protein on the three-dimensional architecture of the skeletal muscle ryanodine receptor. *J Biol Chem,* 272, 32463-71.

WANG, H., VIATCHENKO-KARPINSKI, S., SUN, J., GYORKE, I., BENKUSKY, N. A., KOHR, M. J., VALDIVIA, H. H., MURPHY, E., GYORKE, S. & ZIOLO, M. T. 2010. Regulation of myocyte contraction via neuronal nitric oxide synthase: role of ryanodine receptor S-nitrosylation. *J Physiol,* 588, 2905-17.

WANG, J. & BEST, P. M. 1992. Inactivation of the sarcoplasmic reticulum calcium channel by protein kinase. *Nature,* 359, 739-41.

WANG, R., ZHONG, X., MENG, X., KOOP, A., TIAN, X., JONES, P. P., FRUEN, B. R., WAGENKNECHT, T., LIU, Z. & CHEN, S. R. 2011. Localization of the dantrolene-binding sequence near the FK506-binding protein-binding site in the three-dimensional structure of the ryanodine

receptor. *J Biol Chem,* 286, 12202-12.

WANG, Y., LI, X., DUAN, H., FULTON, T. R., EU, J. P. & MEISSNER, G. 2009. Altered stored calcium release in skeletal myotubes deficient of triadin and junctin. *Cell Calcium,* 45, 29-37.

WARTON, K., TONINI, R., FAIRLIE, W. D., MATTHEWS, J. M., VALENZUELA, S. M., QIU, M. R., WU, W. M., PANKHURST, S., BAUSKIN, A. R., HARROP, S. J., CAMPBELL, T. J., CURMI, P. M., BREIT, S. N. & MAZZANTI, M. 2002. Recombinant CLIC1 (NCC27) assembles in lipid bilayers via a pH-dependent two-state process to form chloride ion channels with identical characteristics to those observed in Chinese hamster ovary cells expressing CLIC1. *J Biol Chem,* 277, 26003-11.

WATANABE, H., CHOPRA, N., LAVER, D., HWANG, H. S., DAVIES, S. S., ROACH, D. E., DUFF, H. J., RODEN, D. M., WILDE, A. A. & KNOLLMANN, B. C. 2009. Flecainide prevents catecholaminergic polymorphic ventricular tachycardia in mice and humans. *Nat Med,* 15, 380-3.

WEHRENS, X. H., LEHNART, S. E., HUANG, F., VEST, J. A., REIKEN, S. R., MOHLER, P. J., SUN, J., GUATIMOSIM, S., SONG, L. S., ROSEMBLIT, N., D'ARMIENTO, J. M., NAPOLITANO, C., MEMMI, M., PRIORI, S. G., LEDERER, W. J. & MARKS, A. R. 2003. FKBP12.6 deficiency and defective calcium release channel (ryanodine receptor) function linked to exercise-induced sudden cardiac death. *Cell,* 113, 829-40.

WEHRENS, X. H., LEHNART, S. E., REIKEN, S., VEST, J. A., WRONSKA, A. & MARKS, A. R. 2006. Ryanodine receptor/calcium release channel PKA phosphorylation: a critical mediator of heart failure progression. *Proc Natl Acad Sci U S A,* 103, 511-8.

WEHRENS, X. H., LEHNART, S. E., REIKEN, S. R., DENG, S. X., VEST, J. A., CERVANTES, D., COROMILAS, J., LANDRY, D. W. & MARKS, A. R. 2004. Protection from cardiac arrhythmia through ryanodine receptor-stabilizing protein calstabin2. *Science,* 304, 292-6.

WEHRENS, X. H., LEHNART, S. E., REIKEN, S. R. & MARKS, A. R. 2004. Ca2+/calmodulin-dependent protein kinase II phosphorylation regulates the cardiac ryanodine receptor. *Circ Res,* 94, e61-70.

WEHRENS, X. H. & MARKS, A. R. 2003. Altered function and regulation of cardiac ryanodine receptors in cardiac disease. *Trends Biochem Sci,* 28, 671-8.

WEHRENS, X. H. & MARKS, A. R. 2004. Novel therapeutic approaches for heart failure by normalizing calcium cycling. *Nat Rev Drug Discov,* 3, 565-73.

WEI, L., GALLANT, E. M., DULHUNTY, A. F. & BEARD, N. A. 2009. Junctin and triadin each activate skeletal ryanodine receptors but junctin alone mediates functional interactions with calsequestrin. *Int J Biochem Cell Biol,* 41, 2214-24.

WEI, L., HANNA, A. D., BEARD, N. A. & DULHUNTY, A. F. 2009. Unique isoform-specific properties of calsequestrin in the heart and skeletal

muscle. *Cell Calcium,* 45, 474-84.

WEI, L., VARSANYI, M., DULHUNTY, A. F. & BEARD, N. A. 2006. The conformation of calsequestrin determines its ability to regulate skeletal ryanodine receptors. *Biophys J,* 91, 1288-301.

WESTHOFF, J. H., HWANG, S. Y., DUNCAN, R. S., OZAWA, F., VOLPE, P., INOKUCHI, K. & KOULEN, P. 2003. Vesl/Homer proteins regulate ryanodine receptor type 2 function and intracellular calcium signaling. *Cell Calcium,* 34, 261-9.

WHALEN, R. & BOYER, T. D. 1998. Human glutathione S-transferases. *Semin Liver Dis,* 18, 345-58.

WHITE, M. A., HABER, G. P., AUTORINO, R., KHANNA, R., FOREST, S., YANG, B., ALTUNRENDE, F., STEIN, R. J. & KAOUK, J. H. 2010. Robotic laparoendoscopic single-site radical prostatectomy: technique and early outcomes. *Eur Urol,* 58, 544-50.

WILCE, M. C. & PARKER, M. W. 1994. Structure and function of glutathione S-transferases. *Biochim Biophys Acta,* 1205, 1-18.

WU, Y., FAN, Y., XUE, B., LUO, L., SHEN, J., ZHANG, S., JIANG, Y. & YIN, Z. 2006. Human glutathione S-transferase P1-1 interacts with TRAF2 and regulates TRAF2-ASK1 signals. *Oncogene,* 25, 5787-800.

XIAO, B., TU, J. C. & WORLEY, P. F. 2000. Homer: a link between neural activity and glutamate receptor function. *Curr Opin Neurobiol,* 10, 370-4.

XIAO, J., TIAN, X., JONES, P. P., BOLSTAD, J., KONG, H., WANG, R., ZHANG, L., DUFF, H. J., GILLIS, A. M., FLEISCHER, S., KOTLIKOFF, M., COPELLO, J. A. & CHEN, S. R. 2007. Removal of FKBP12.6 does not alter the conductance and activation of the cardiac ryanodine receptor or the susceptibility to stress-induced ventricular arrhythmias. *J Biol Chem,* 282, 34828-38.

XIAO, R. P., VALDIVIA, H. H., BOGDANOV, K., VALDIVIA, C., LAKATTA, E. G. & CHENG, H. 1997. The immunophilin FK506-binding protein modulates Ca2+ release channel closure in rat heart. *J Physiol,* 500 (Pt 2), 343-54.

XIN, H. B., SENBONMATSU, T., CHENG, D. S., WANG, Y. X., COPELLO, J. A., JI, G. J., COLLIER, M. L., DENG, K. Y., JEYAKUMAR, L. H., MAGNUSON, M. A., INAGAMI, T., KOTLIKOFF, M. I. & FLEISCHER, S. 2002. Oestrogen protects FKBP12.6 null mice from cardiac hypertrophy. *Nature,* 416, 334-8.

XU, L., EU, J. P., MEISSNER, G. & STAMLER, J. S. 1998. Activation of the cardiac calcium release channel (ryanodine receptor) by poly-S-nitrosylation. *Science,* 279, 234-7.

XU, L., MANN, G. & MEISSNER, G. 1996. Regulation of cardiac Ca2+ release channel (ryanodine receptor) by Ca2+, H+, Mg2+, and adenine nucleotides under normal and simulated ischemic conditions. *Circ Res,* 79, 1100-9.

XU, L. & MEISSNER, G. 1998. Regulation of cardiac muscle Ca2+ release channel by sarcoplasmic reticulum lumenal Ca2+. *Biophys J,* 75, 2302-

12.

XU, L. & MEISSNER, G. 2004. Mechanism of calmodulin inhibition of cardiac sarcoplasmic reticulum Ca2+ release channel (ryanodine receptor). *Biophys J,* 86, 797-804.

XU, L., TRIPATHY, A., PASEK, D. A. & MEISSNER, G. 1999. Ruthenium red modifies the cardiac and skeletal muscle Ca(2+) release channels (ryanodine receptors) by multiple mechanisms. *J Biol Chem,* 274, 32680-91.

YAMAGUCHI, N., TAKAHASHI, N., XU, L., SMITHIES, O. & MEISSNER, G. 2007. Early cardiac hypertrophy in mice with impaired calmodulin regulation of cardiac muscle Ca release channel. *J Clin Invest,* 117, 1344-53.

YAMAGUCHI, N., XU, L., PASEK, D. A., EVANS, K. E. & MEISSNER, G. 2003. Molecular basis of calmodulin binding to cardiac muscle Ca(2+) release channel (ryanodine receptor). *J Biol Chem,* 278, 23480-6.

YAMASHITA, N., NISHIDA, M., HOSHIDA, S., KUZUYA, T., HORI, M., TANIGUCHI, N., KAMADA, T. & TADA, M. 1994. Induction of manganese superoxide dismutase in rat cardiac myocytes increases tolerance to hypoxia 24 hours after preconditioning. *J Clin Invest,* 94, 2193-9.

YAMAZAWA, T., TAKESHIMA, H., SHIMUTA, M. & IINO, M. 1997. A region of the ryanodine receptor critical for excitation-contraction coupling in skeletal muscle. *J Biol Chem,* 272, 8161-4.

YANG, H. T., TWEEDIE, D., WANG, S., GUIA, A., VINOGRADOVA, T., BOGDANOV, K., ALLEN, P. D., STERN, M. D., LAKATTA, E. G. & BOHELER, K. R. 2002. The ryanodine receptor modulates the spontaneous beating rate of cardiomyocytes during development. *Proc Natl Acad Sci U S A,* 99, 9225-30.

YANO, M., ONO, K., OHKUSA, T., SUETSUGU, M., KOHNO, M., HISAOKA, T., KOBAYASHI, S., HISAMATSU, Y., YAMAMOTO, T., NOGUCHI, N., TAKASAWA, S., OKAMOTO, H. & MATSUZAKI, M. 2000. Altered stoichiometry of FKBP12.6 versus ryanodine receptor as a cause of abnormal Ca(2+) leak through ryanodine receptor in heart failure. *Circulation,* 102, 2131-6.

YANO, M., YAMAMOTO, T., IKEDA, Y. & MATSUZAKI, M. 2006. Mechanisms of Disease: ryanodine receptor defects in heart failure and fatal arrhythmia. *Nat Clin Pract Cardiovasc Med,* 3, 43-52.

YANO, M., YAMAMOTO, T., IKEMOTO, N. & MATSUZAKI, M. 2005. Abnormal ryanodine receptor function in heart failure. *Pharmacol Ther,* 107, 377-91.

YUAN, Q., FAN, G. C., DONG, M., ALTSCHAFL, B., DIWAN, A., REN, X., HAHN, H. H., ZHAO, W., WAGGONER, J. R., JONES, L. R., JONES, W. K., BERS, D. M., DORN, G. W., 2ND, WANG, H. S., VALDIVIA, H. H., CHU, G. & KRANIAS, E. G. 2007. Sarcoplasmic reticulum calcium overloading in junctin deficiency enhances cardiac contractility but

increases ventricular automaticity. *Circulation,* 115, 300-9.

ZHANG, J., LIU, Z., MASUMIYA, H., WANG, R., JIANG, D., LI, F., WAGENKNECHT, T. & CHEN, S. R. 2003. Three-dimensional localization of divergent region 3 of the ryanodine receptor to the clamp-shaped structures adjacent to the FKBP binding sites. *J Biol Chem,* 278, 14211-8.

ZHANG, J. Z., WU, Y., WILLIAMS, B. Y., RODNEY, G., MANDEL, F., STRASBURG, G. M. & HAMILTON, S. L. 1999. Oxidation of the skeletal muscle Ca2+ release channel alters calmodulin binding. *Am J Physiol,* 276, C46-53.

ZHANG, X., TALLINI, Y. N., CHEN, Z., GAN, L., WEI, B., DORAN, R., MIAO, L., XIN, H. B., KOTLIKOFF, M. I. & JI, G. 2009. Dissociation of FKBP12.6 from ryanodine receptor type 2 is regulated by cyclic ADP-ribose but not beta-adrenergic stimulation in mouse cardiomyocytes. *Cardiovasc Res,* 84, 253-62.

ZHANG, Y., HUANG, Z. J., DAI, D. Z., FENG, Y., NA, T., TANG, X. Y. & DAI, Y. 2008. Downregulated FKBP12.6 expression and upregulated endothelin signaling contribute to elevated diastolic calcium and arrhythmogenesis in rat cardiomyopathy produced by l-thyroxin. *Int J Cardiol,* 130, 463-71.

ZHOU, Q., XIAO, J., JIANG, D., WANG, R., VEMBAIYAN, K., WANG, A., SMITH, CD., XIE, C., CHEN, W., ZHANG, J., TIAN, X., JONES, PP., ZHONG, X., GUO, A., CHEN, H., ZHANG, L., ZHU, W., YANG, D., LI, X., CHEN, J., GILLIS, AM., DUFF, HJ., CHENG, H., FELDMAN, AM., SONG, LS., FILL, M., BACK, TG., CHEN, SR. 2011. Carvedilol and its new analogs suppress arrhythmogenic store overload-induced Ca^{2+} release. *Nat Med.* 17(8), 1003-9.

ZIMA, A. V. & BLATTER, L. A. 2006. Redox regulation of cardiac calcium channels and transporters. *Cardiovasc Res,* 71, 310-21.

ZORZATO, F., FUJII, J., OTSU, K., PHILLIPS, M., GREEN, N. M., LAI, F. A., MEISSNER, G. & MACLENNAN, D. H. 1990. Molecular cloning of cDNA encoding human and rabbit forms of the Ca2+ release channel (ryanodine receptor) of skeletal muscle sarcoplasmic reticulum. *J Biol Chem,* 265, 2244-56.

ZUCCHI, R. & RONCA-TESTONI, S. 1997. The sarcoplasmic reticulum Ca2+ channel/ryanodine receptor: modulation by endogenous effectors, drugs and disease states. *Pharmacol Rev,* 49, 1-51.